Assessing Impacts of Climate Change on Vulnerability of Brook Trout in Lake Superior's Tributary Streams of Minnesota

Lucinda B. Johnson, Natural Resources Research Institute, University of Minnesota Duluth
William Herb, St. Anthony Falls Laboratory, University of Minnesota, Minneapolis
Meijun Cai, Natural Resources Research Institute, University of Minnesota Duluth

Report to Minnesota Department of Natural Resources, upon completion of contract # MN DNR/1229G WO 47578

Natural Resources Research Institute technical report number NRRI/TR-2013/05

Executive Summary

Water temperature is generally considered one of the primary physical habitat parameter determining the suitability of stream habitat for fish species, with effects on the mortality, metabolism, growth, behavior, and reproduction of individuals. In this study we assessed the potential threats of climate change on stream temperatures and flow regimes in Lake Superior tributary streams in Minnesota, USA. The study included deterministic models for stream flow and temperature of three study streams (Amity Creek, Baptism River, Knife River), and regional (empirical) models for specific flow and temperature parameters to give better spatial coverage of the region. Information on stream flow, stream temperature, and land cover was used to develop a brook trout presence/absence model to understand the current pattern of distribution of brook trout and predict future distributions under future climate.

The hydrology of north shore streams is mainly driven by air temperature and precipitation. Historical air temperatures in the region have a significant upward trend, particularly since 1980. Global climate model (GCM) outputs project a continued increasing trend in air temperature, with an increase in mean annual air temperature of 2 to 3 °C by 2089. The historical precipitation data shows an increasing trend for total annual precipitation at Duluth and Two Harbors between 1900 and 2010, whereas Grand Marais and Grand Portage do not have a clear trend. Based on an analysis of daily precipitation totals, there is some indication of an increasing trend in the number of days in summer with high precipitation (10-20 cm). Both the GENMOM and the ECHAM5 GCMs project overall increases in precipitation of about 15%, but differ with respect to the seasonal distribution of the precipitation changes. A significant and relatively certain impact of climate change is a projected shift in precipitation from snowfall to rainfall.

While an increasing trend in precipitation leads to increasing streamflow, the increasing trend in spring and summer air temperature tends to reduce streamflow (by increasing evapotranspiration). Available streamflow records for north shore streams suggest there may be a decreasing trend in mean annual flow and summer low flow, but the trends are not statistically significant. Future projections of streamflow based on the GCM output were mixed, with the deterministic models projecting moderate increases in average stream flow and summer low flow, while the regression models for project a moderate decrease in low flow.

Stream temperature analyses for the three study streams based on GCM climate output give the result of fairly uniform seasonal increases in stream temperature to 2089 ranging from 1.3 to 1.9 °C for the GENMOM model to 2.2 to 3.5°C for the ECHAM5 model. Application of the GENMOM climate data to the deterministic stream temperature models produced fairly similar stream temperature changes for the three study sites. The empirical stream temperature study found stream temperature in the north shore region to be influenced by air temperature, catchment size, percentage of woody wetlands, latitude, and soil permeability rate. In response

to climate change projected by the GENMOM GCM, the regional stream temperature model projects July mean water temperature to rapidly increase by approximately 1.2^{o}C from 1990s to 2060s, followed by a slight decrease to 2089. The temperature increase was predicted to be the largest in the coastal area of middle north shore region.

The brook trout presence/absence model found water temperature to have the strongest influence on trout presence. Brook trout were predicted to be at risk for water temperatures above 18.7^{o}C and be extirpated from streams for temperatures over 20^{o}C. Stream flow was shown to have a negative effect on trout presence, though not as strong as water temperature. Overall, these data predict that brook trout may be extirpated from lower shore area, be exposed to increasing risk in middle shore region, and remain present in upper shore streams from the present to 2089.

This work would benefit greatly from a number of modifications to the GCM's, the spatial data used in the development of both the deterministic and empirical models, and implementation of a more detailed, spatially explicit, hydrologic model. Finally, additional fish data, including cool and warm water assemblage data, along with descriptors of landscape structure (i.e., connectivity) would allow us to assess the areas where cold water species may be threatened by the presence or potential presence of coolwater competitors.

1. Introduction

Water temperature is generally considered one of the primary physical habitat parameter determining the suitability of stream habitat for fish species (Magnuson et al. 1979). Stream temperature affects individuals throughout their life cycle, with impacts on mortality, metabolism, growth, behavior, and reproduction (Magnuson et al. 1979, Hughes et al. 2006, Ficke et al 2007). Many studies have implicated maximum seasonal stream temperature as the cause of lethal and sub-lethal effects (e.g., Fry 1967, Raleigh 1982, Bisson et al. 1985). The upper temperature limits for trout has been measured variously as the maximum weekly average temperature, (e.g., highest single value of a 7-day moving average), an instantaneous maximum, or the maximum weekly maximum temperature (Brungs and Jones 1977). In a Midwestern study, Wehrly et al. (2007) found the upper temperature limits for trout to depend systematically on the number of consecutive days of exposure to high temperature. In addition to stream temperature, summer or autumn low flow conditions and groundwater inflows have also been found to be a limiting factor in trout survival (Chu et al. 2008, Arismendi et al. 2012, Grantham et al. 2012,). In addition, other stressors, such as the presence of urban development in a watershed, can interact with climate to influence flow, temperature, and water quality factors—all of which influence fish distributions (e.g., Nelson et al. 2009).

Salmonids are particularly sensitive to temperate extremes and have therefore been the topic of numerous studies addressing impacts of climate change on fish communities (e.g., Eaton and Scheller 1996, Mantua et al. 2009, Lyons et al. 2010, Wenger et al. 2011, Arismendi et al. 2012). In North America, study of climate change impacts on salmonoid populations has included studies of trout streams in Appalachia (Clark et al. 2001, Flebbe et al. 2006), southern Ontario (Meisner 1990, Chu et al. 2008), Upper Midwest (Deitchman and Loheide 2012), Rocky mountains (Rahel et al. 1996, Isaac et al. 2010), salmon rivers in the Pacific Northwest (Crozier and Zabel 2006, Crozier et al. 2008, Yates et al. 2008, Mantua et al. 2010), and the Arctic fish populations (Reist et al. 2006). Several more generalized fish studies have considered climate change impacts on coldwater fishes, including studies of fish populations in the Upper Midwest (Magnuson et al. 1990, Lyons et al. 2010). In Europe, climate change studies have considered salmonoids (Hari et al. 2006, Hrachowitz et al. 2010) and more generalized fish populations (Daufresne and Boët 2007, Buisson et al. 2008, Graham and Harrod 2009). The combined effects of land use and climate change also have been examined in the Piedmont streams in the eastern U.S. (Nelson et al. 2009).

A number of studies have focused on Pacific Northwest salmon habitat (Crozier et al. 2008). In the Salmon River basin in Idaho the survival of juvenile salmon was found to be controlled by summer water temperatures and autumn low flows. These relationships were clarified by considering four separate population models rather than treating the entire basin with one model (Crozier and Zabel 2006). Populations with higher temperature sensitivity were projected to be more sensitive to climate change scenarios compared to flow-sensitive populations, suggesting

that the different population sensitivities could act as a buffer to large-scale extinction in the basin.

In a study of Appalachian trout streams using individual-based models for brook and rainbow trout, the response of brook trout was found to be spatially complex (Clark et al. 2001). A projected increase in stream temperature of 1.5 to 2.5°C alone led to a projected increase in the trout populations, while the temperature increase combined with a reduction in baseflow and an increase in peak flows lead to spatially heterogeneous response of increased and decreased trout populations, with minimal overall changes in trout density for the region. However, another study of southern Appalachian trout streams projected 53 – 97% habitat loss by 2090 (Flebbe et al. 2006). This study differs from previous work in that suitable trout habitat is linked to temperature via elevation.

Groundwater and thermal refugia are widely documented as a primary factor in determining the response of coldwater habitat to climate change (Chu et al. 2008, Meisner et al. 2008). In a study of southern Ontario streams, Chu et al. found that, along with air temperature, baseflow index was a primary factor determining the distribution of cold-, cool-, and warm-water fish species. Coldwater streams with more groundwater input were projected to be more resilient to climate change. Localized inputs of groundwater and other thermal refugia that help trout survive extreme flow and temperature conditions (Petty et al. 2012), while land development activities such as forestry may have the opposite effect (Curry et al. 2002). The addition of urbanization to climate change scenarios generally resulted in reduced adult growth of all fish species and loss of diversity also was predicted (Nelson et al. 2009).

In this study we assessed the potential threats of climate change on stream temperatures and flow regimes in Lake Superior tributary streams in Minnesota, USA. In this region, temperatures are predicted to increase, and precipitation patterns are expected to shift seasonally, with great precipitation occurring during the winter and spring (when ground is frozen) and less precipitation falling during the summer months (Kling et al. 2003; S. Hostetler, personal communication). Summer rainfall is expected to fall in the form of large storms, with the potential for long periods of dry weather. In this scenario, coldwater fish communities are expected to decline as a function of reduced thermal habitat resulting from the convergence of increasing air and water temperatures and low flow conditions. We considered potential limiting factors including flow, gradient, Quaternary geology, land use, and land cover to understand the current pattern of distribution of brook trout and predict future distributions under future climate.

References

Arismendi I., Safeeq M., Johnson S.L., Dunham J.B. and Haggerty R. 2012. Increasing synchrony of high temperature and low flow in western North American streams: double trouble for coldwater biota? Hydrobiologia, doi: 10.1007/s10750-012-1327-2.

Brungs, W.A., and B.R. Jones. 1977. Temperature criteria for freshwater fish: protocol and procedures. Environmental Research Laboratory, Duluth, MN. U.S. Environmental Protection Agency. EPA-600/3-77-061. 136pp.

Buisson, L., Thuiller, W., Lek, S., Lim, P., Grenouillet, G., 2008. Climate change hastens the turnover of stream fish assemblages. Global Change Biology 14, 2232–2248.

Chu, C., Jones, N.E., Mandrak, N.E., Piggott, A.R., Minns, C.K., 2008. The influence of air temperature, groundwater discharge, and climate change on the thermal diversity of stream fishes in southern Ontario watersheds. Canadian Journal of Fisheries and Aquatic Sciences 65, 297–308.oi:10.1111/j.1365-2486.2008.01657.x

Clark, M.E., Rose, K.A., Levine, D.A., Hargrove, W.W., 2001. Predicting climate change effects on Appalachian trout: combining GIS and individual-based modeling. Ecological Applications 11, 161–178.

Crozier, L., Zabel, R.W., 2006. Climate impacts at multiple scales: evidence for differential population responses in juvenile Chinook salmon. The Journal of Animal Ecology 75, 1100–9.

Crozier, L.G., Zabel, R.W., Hamlet, A.F., 2008. Predicting differential effects of climate change at the population level with life-cycle models of spring Chinook salmon. Global Change Biology 14, 236–249.

Curry, R.A., Scruton, D.A., Clarke, K.D., 2002. The thermal regimes of brook trout incubation habitats and evidence of changes during forestry operations. Canadian Journal of Forest Research 32, 1200–1207.

Daufresne, M., Boët, P., 2007. Climate change impacts on structure and diversity of fish communities in rivers. Global Change Biology 13, 2467–2478.

Deitchman, R., Loheide, S.P., 2012. Sensitivity of thermal habitat of a trout stream to potential climate change, Wisconsin, United States. JAWRA Journal of the American Water Resources Association 48, 1091–1103.

Eaton, J.G., and Scheller, R.M. 1996. Effects of climate warming on fish thermal habitat in streams of the United States. Limnology and Oceanography 41, 1109-1115.

Ficke, A.D., Myrick, C.A., and Hansen, L.J. 2007. Potential impacts of global climate change on freshwater fisheries. Reviews in Fish Biology and Fisheries 17, 581-613.

Flebbe, P.A., Roghair, L.D., Bruggink, J.L., 2006. Spatial modeling to project southern Appalachian trout distribution in a warmer climate. Transactions of the American Fisheries Society 135, 1371–1382.

Fry, F.E.J. 1967. Responses of vertebrate poikilotherms to temperature. In A.H. Rose (ed). Thermobiology. P 375 – 409. Academic Press, London.

Grantham, T.E., Newburn, D. a., McCarthy, M. A., Merenlender, A.M., 2012. The role of streamflow and land use in limiting oversummer survival of juvenile steelhead in California streams. Transactions of the American Fisheries Society 141, 585–598.

Graham, C.T., Harrod, C., 2009. Implications of climate change for the fishes of the British Isles. Journal of Fish Biology 74, 1143–205.

Hari, R.E., Livingstone, D.M., Siber, R., Burkhardt-Holm, P., Guttinger, H., 2006. Consequences of climatic change for water temperature and brown trout populations in Alpine rivers and streams. Global Change Biology 12, 10–26.

Hrachowitz, M., Soulsby, C., Imholt, C., Malcolm, I. a., Tetzlaff, D., 2010. Thermal regimes in a large upland salmon river: a simple model to identify the influence of landscape controls and climate change on maximum temperatures. Hydrological Processes 24, 3374–3391.

Hughes, R.M., Wang, L., and Seelbach, P.W. (eds) 2006. Landscape influences on stream habitats and biological assemblages. Bethesda, MD. American Fisheries Society.

Lyons, J., Stewart, J.S., Mitro, M., 2010. Predicted effects of climate warming on the distribution of 50 stream fishes in Wisconsin, USA. Journal of Fish Biology 77, 1867–98.

Magnuson, J. J., L. B. Crowder, and P. A. Medvick. 1979. Temperature as an ecological resource. American Zoologist 19:331-343.

Magnuson, J.J., Meisner, J.D., Hill, D.K., 1990. Potential changes in the thermal habitat of Great Lakes fish after global climate warming. Transactions of the American Fisheries Society 119, 254–264.

McDermid, J.L., Fischer, F. a., Al-Shamlih, M., Sloan, W.N., Jones, N.E., Wilson, C.C., 2012. Variation in acute thermal tolerance within and among hatchery strains of brook trout. Transactions of the American Fisheries Society 141, 1230–1235.

Meisner, J.D., Rosenfeld, J.S., Regier, H. a., 1988. The role of groundwater in the impact of climate warming on stream salmonines. Fisheries 13, 2–8.

Petty, J.T., Hansbarger, J.L., Huntsman, B.M., Mazik, P.M., 2012. Brook trout movement in response to temperature, flow, and thermal refugia within a complex Appalachian riverscape. Transactions of the American Fisheries Society 141, 1060–1073.

Picard, C.R., Bozek, M.A., Momot, W.T., 2003. Effectiveness of using summer thermal indices to classify and protect brook trout streams in northern Ontario. North American Journal of Fisheries Management 23, 206–215.

Rahel, F.J., Keleher, C.J., Anderson, J.L., 1996. Potential habitat loss and population fragmentation for cold water fish in the North Platte River drainage of the Rocky Mountains: Response to climate warming. Limnology and Oceanography 41, 1116–1123.

Raleigh, R.F. 1982. Habitat suitability index models: brook trout. U.S.D.I. Fish and Wildlife Service. FWS/OBS-82/10.24.

Reist, J.D., Wrona, F.J., Prowse, T.D., Power, M., Dempson, J.B., King, J.R., Beamish, R.J., 2006. An overview of effects of climate change on selected arctic freshwater and anadromous fishes. Ambio 35, 381–7.

Wehrly, K.E., Wang, L., Mitro, M., 2007. Field-based estimates of thermal tolerance limits for trout: incorporating exposure time and temperature fluctuation. Transactions of the American Fisheries Society 136, 365–374.

Yates, D., Galbraith, H., Purkey, D., Huber-Lee, A., Sieber, J., West, J., Herrod-Julius, S., Joyce, B., 2008. Climate warming, water storage, and Chinook salmon in California's Sacramento Valley. Climatic Change 91, 335–350.

2. Analysis of Climate and Hydrologic Data for the Minnesota Lake Superior North Shore Region

Here we review and summarize climate and hydrologic data relevant to analyses of climate and landscape characteristics of Lake Superior basin streams in Minnesota, including air temperature, precipitation, stream flow, soils, elevation, and land cover.

2.1 Available data

Streamflow data were compiled for the nine north shore trout streams in Minnesota with the longest history of flow records (Table 2.1). In addition to flow, GIS spatial data sets compiled for this study included the 2001 national land cover data set (NLCD), the National Wetlands Inventory data set, the USGS quaternary geology layer, the STATSGO soil data, and a lithology data layer assembled by the USGS Rocky Mountain Geographic Science Center. Land cover from 2001 was chosen to reflect a period that best represents the midpoint of the flow records for these nine streams, since the majority of streams have records with fewer than 10 years of data.

The precipitation data assembled for this study (Figure 2.1) included: hourly National Weather Service (NWS) airport data from Duluth, Two Harbors, and Grand Marais, daily data from the Minnesota high-density network, and monthly PRISM data. For predicting monthly averaged streamflow, the PRISM precipitation data (http://www.prism.oregonstate.edu/) were found to be comparable to NWS and high-density daily data. The PRISM data set was also used to supply monthly air temperature inputs. Precipitation from the high-density network were compiled, but were used relatively little in this study due to their shorter and/or discontinuous records.

Table 2.1. Summary of available stream flow data for nine north shore trout streams plus the Pigeon River.

Stream	First year of data	Number of years, total	Number of years, 1981-2010
Amity	2002	8	8
Brule	2002	8	8
Poplar	2002	9	9
Sucker	2001	8	8
Talmadge	2001	8	8
Knife	1974	36	30
Baptism	1928	68	16
Miller	1997	5	5
Pigeon	1921	89	30

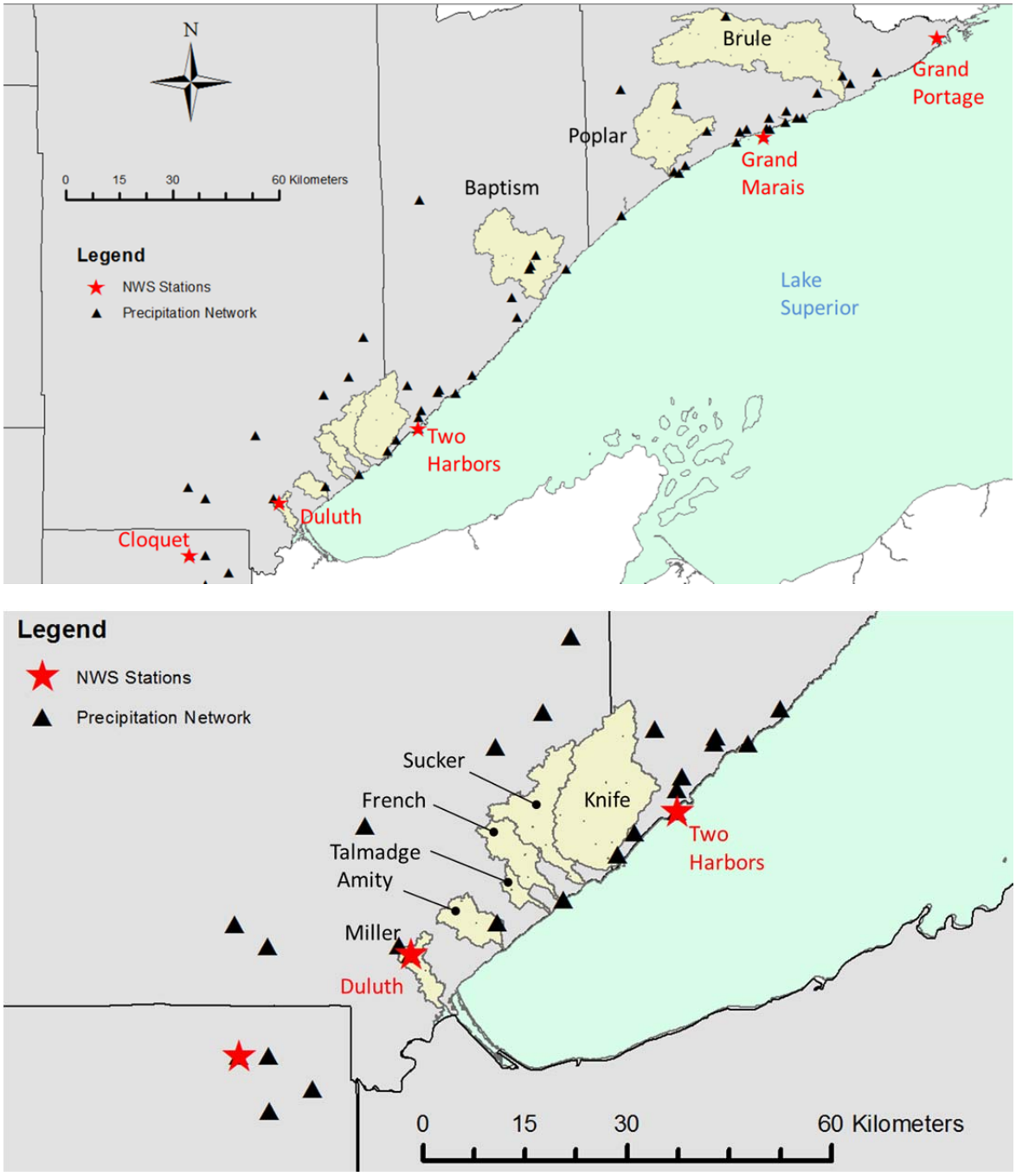

Figure 2.1. Map of NWS climate stations and gaged stream catchments for the study. Upper panel shows the entire study area, and the lower panel provides some detail of the Duluth area.

2.2 Trends in north shore precipitation

Precipitation data from NWS stations with the longest record lengths (Duluth, Two Harbors, Grand Marais, and Grand Portage) were analyzed for trends in annual and seasonal precipitation

depth. Annual precipitation time series for the four NWS stations are given in Figure 2.2, including locally weighted scatterplot smoothing (LOWESS) trend lines. Seasonal precipitation time series for Duluth are given in Figure 2.3 and Grand Marais in Figure 2.4.

Table 2.2 Tau and p-values from the Mann-Kendall trend test for the full record of annual and seasonal precipitation in Duluth, Two Harbors, Grand Marais, and Grand Portage. Highlighted text indicates significant trends.

	Duluth		Two Harbors		Grand Marais		Grand Portage	
	Tau	p-value	Tau	p-value	Tau	p-value	Tau	p-value
Annual	0.22	<0.001	0.23	<0.001	-0.085	0.26	-0.11	0.21
Winter	0.078	0.226	0.21	0.0010	-0.25	<0.001	-0.002	0.98
Spring	0.14	0.031	0.19	0.003	-0.043	0.55	0.023	0.77
Summer	0.087	0.177	0.04	0.53	0.015	0.83	-0.089	0.24
Autumn	0.13	0.040	0.12	0.055	0.033	0.64	-0.051	0.52

Table 2.3. Tau and p-values from the Mann-Kendall trend test for the 30 years (1980-2010) of annual and seasonal precipitation in Duluth, Two Harbors, Grand Marais, and Grand Portage. Highlighted text indicates a significant trend.

	Duluth		Two Harbors		Grand Marais		Grand Portage	
	Tau	p-value	Tau	p-value	Tau	p-value	Tau	p-value
Annual	-0.030	0.83	-0.048	0.72	-0.071	0.57	0.054	0.71
Winter	0.17	0.18	0.23	0.066	0.15	0.25	0.17	0.21
Spring	0.043	0.75	0.13	0.32	0.11	0.41	0.22	0.090
Summer	-0.032	0.81	-0.33	0.0089	-0.27	0.032	-0.19	0.14
Autumn	0.13	0.040	0.12	0.055	0.033	0.64	-0.050	0.52

The Mann-Kendall trend test (Burn and Elnur 2002) was used to identify the statistical significance of the annual and seasonal precipitation trends. The Mann-Kendall Tau parameter varies from -1 to 1 for negative to positive trends. The closer the tau value is to 1 (or -1), the stronger is the likelihood that a trend exists. The significance (p-values) of the trends is also summarized in Tables 2.1 and 2.2. A p-value less than 0.05 (95% confidence interval) was used a criteria for a statistically significant tend. For the entire 111-year record (1910-2010), Duluth and Two Harbors have significant positive trends in annual precipitation, while Grand Marais and Grand Portage have no significant negative trend (Figure 2.2, Table 2.2).

Breaking annual precipitation down to seasons, spring (March-May) and autumn (Sept-Oct) precipitation shows positive trends in Duluth and spring precipitation in Two Harbors (Table 2.1). During a more recent 30-year period (1980-2010), Two Harbors and Grand Marais show (March-May) significant negative trends for summer precipitation (Jun-Aug), while Duluth shows a positive trend in autumn precipitation (Table 2.3).

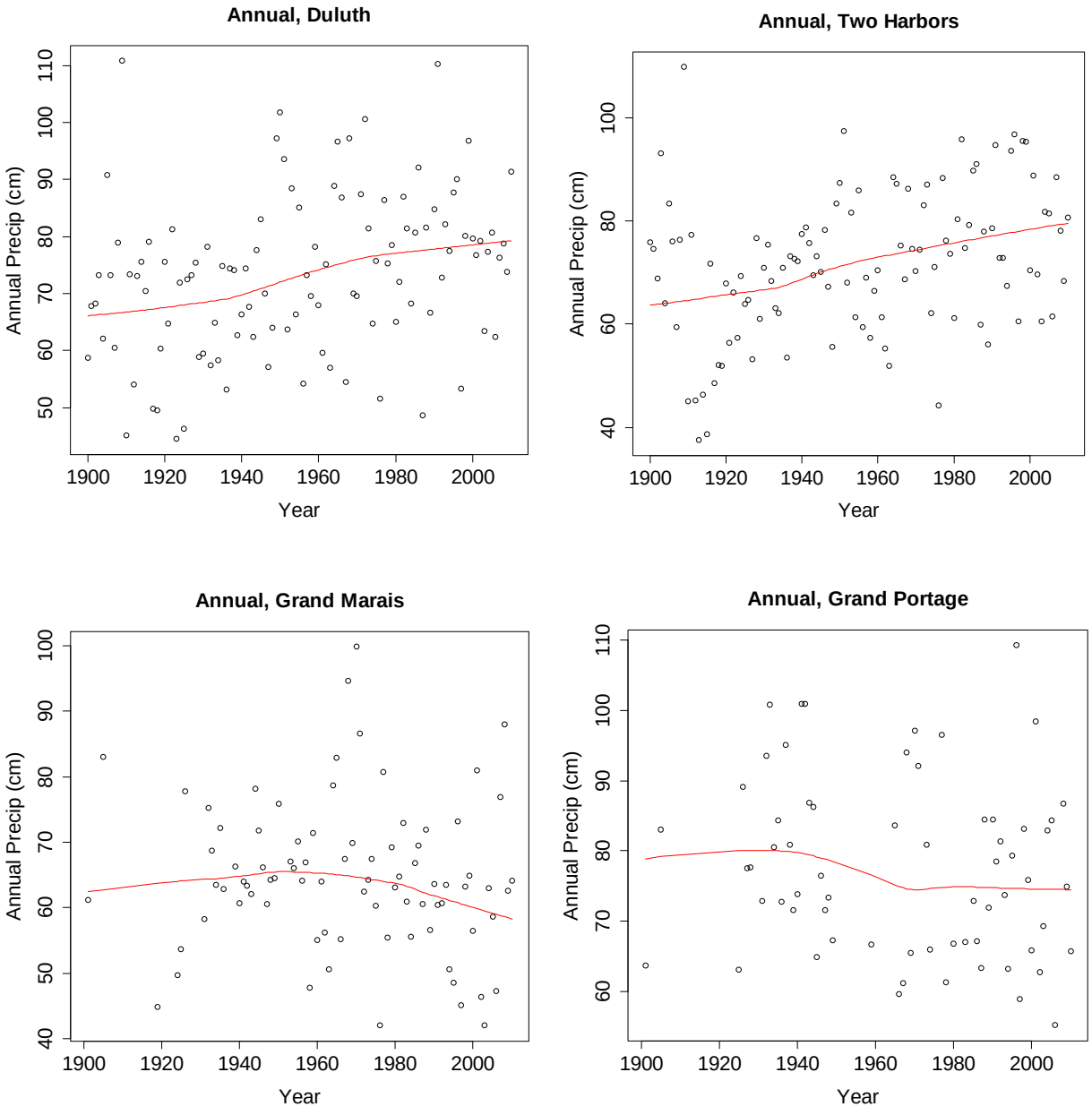

Figure 2.2. Time series (1910 – 2010) of total annual precipitation for Duluth, Two Harbors, Grand Marais, and Grand Portage, MN along with LOWESS trend lines.

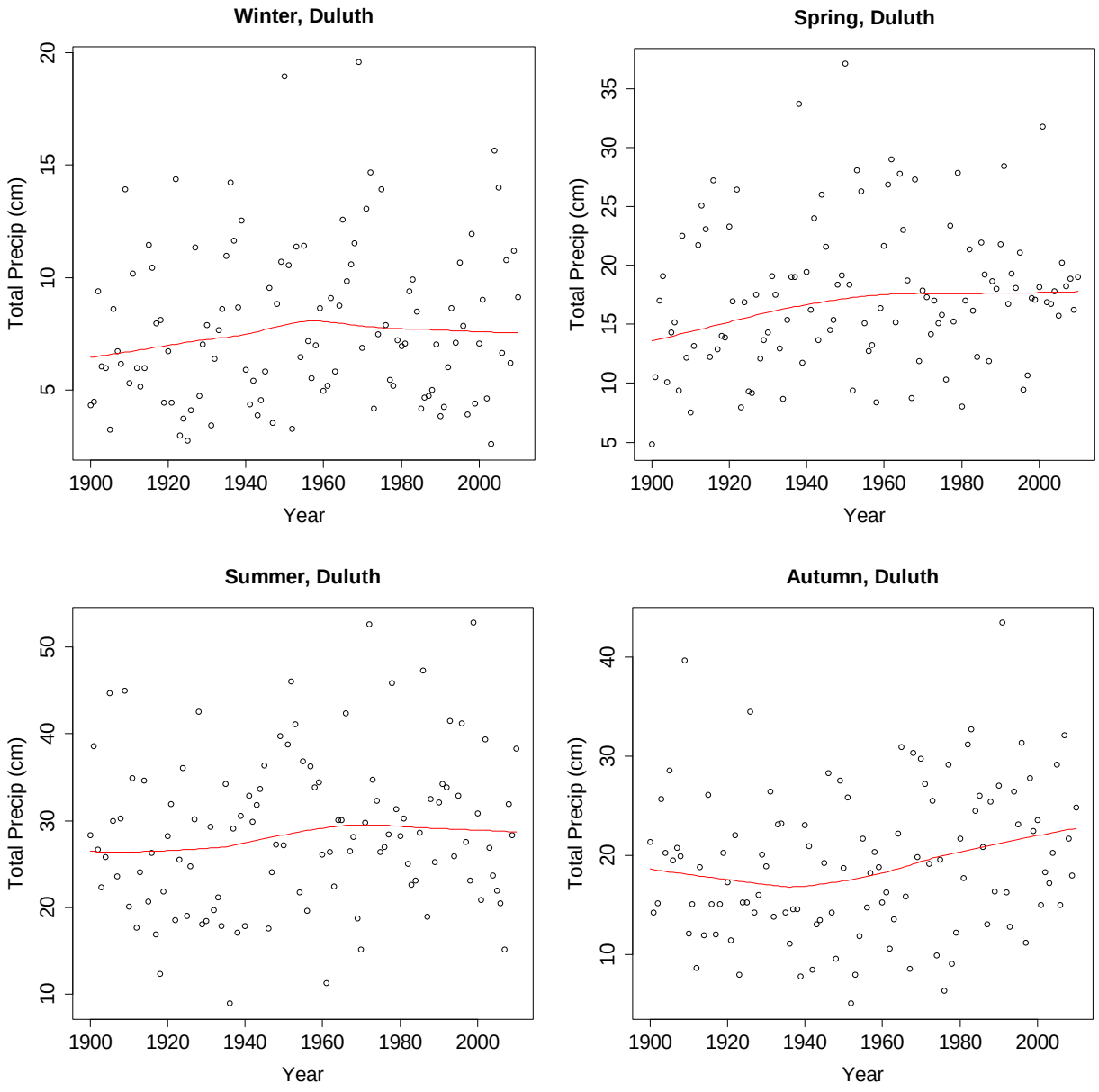

Figure 2.3. Time series (1910 – 2010) of seasonal precipitation for Duluth, MN along with LOWESS trend lines. Winter = Dec-Feb, spring = Mar-May, summer = Jun-Aug, autumn = Sep-Nov.

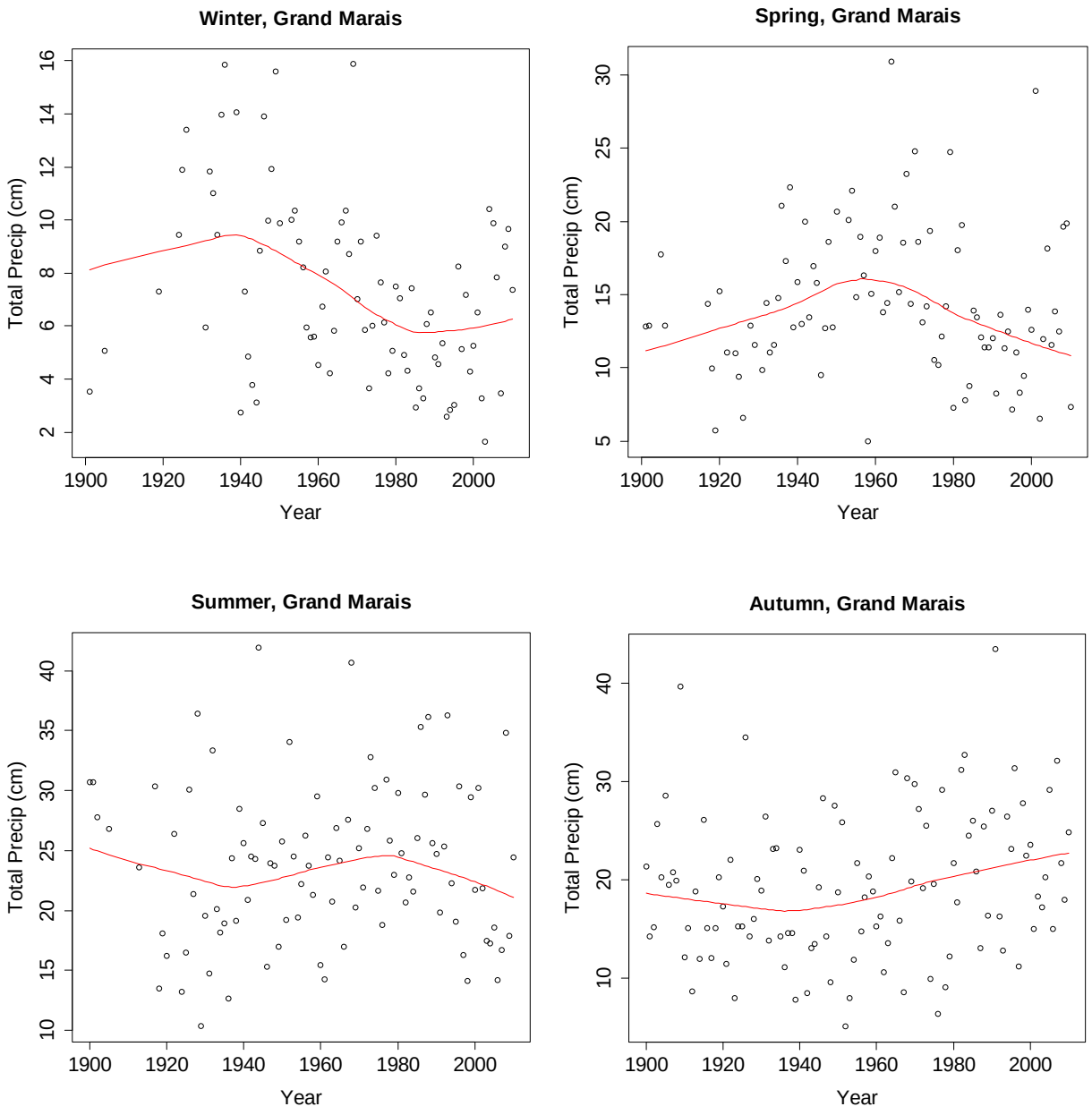

Figure 2.4. Time series (1919 – 2010) of seasonal precipitation for Grand Marais, MN along with LOWESS trend lines. Winter = Dec-Feb, spring = Mar-May, summer = Jun-Aug, autumn = Sep-Nov.

2.3 Trends in air temperature

Historical air temperature data (1900 – 2010) from NWS stations with the longest record lengths (Duluth, Two Harbors, Grand Marais) were analyzed for trends in mean annual and mean seasonal air temperatures. As with the precipitation data, the statistical significance of observed trends was tested using the Mann-Kendall analysis methods. Overall, mean annual air

temperature has a significant increasing trend at Two Harbors and Grand Marais (Figure 2.5, Table 2.3) from 1900 to 2010. Although the Duluth station also appears to have an increasing trend, the trend is not statistically significant, with the Mann-Kendall p-value slightly above 0.05 (Table 2.3). Breaking down air temperatures into seasonal values, Duluth has a significant increasing trend only in spring (Figure 2.6, Table 2.3), whereas Two Harbors has significant increasing trends in autumn and winter, and Grand Marais has significant increasing trends in spring, summer and winter (Figure 2.7, Table 2.4).

For the more recent 30-year time period analyzed (1981-2010), the air temperature trends were more consistent across the three north shore stations. Duluth, Two Harbors, and Grand Marais air temperatures did not show a significant trend for annual averages, but did show significant increasing trends for winter and summer (Table 2.4). In Duluth, the trends in mean average, mean daily maximum, and mean daily minimum air temperature are fairly similar (Figure 2.6). In Grand Marais (1981-2010), mean daily maximum air temperature has a stronger trend than mean daily minimum (Figure 2.7, Table 2.5).

Table 2.4. Tau and p-values from the Mann-Kendall trend test for the full record of annual and seasonal air temperature at Duluth, Two Harbors, and Grand Marais. Significant trends ($p<0.05$) are highlighted in bold.

	Duluth		Two Harbors		Grand Marais	
	Tau	p-value	Tau	p-value	Tau	p-value
Annual	0.13	0.055	**0.20**	**0.0015**	**0.33**	**<0.001**
Winter	0.089	0.17	**0.23**	**<0.001**	**0.20**	**0.009**
Spring	**0.25**	**<0.001**	0.065	0.31	**0.22**	**0.003**
Summer	0.067	0.30	0.11	0.10	**0.25**	**<0.001**
Autumn	-0.050	0.40	**0.14**	**0.029**	0.13	0.075

Table 2.5. Tau and p-values from the Mann-Kendall trend test for the 30 years (1980-2010) of annual and seasonal air temperature at Duluth, Two Harbors, and Grand Marais. Significant trends ($p<0.05$) are highlighted in bold.

		Duluth		Two Harbors		Grand Marais	
Parameter	Season	Tau	p-value	Tau	p-value	Tau	p-value
Tave	Annual	0.17	0.20	0.12	0.34	0.19	0.14
	Winter	**0.29**	**0.009**	0.015	0.92	0.028	0.84
	Spring	0.12	0.27	-0.011	0.95	0.14	0.29
	Summer	**0.27**	**0.014**	0.13	0.31	**0.29**	**0.023**
	Autumn	0.19	0.082	0.18	0.15	0.16	0.23
Tmax	Annual	0.17	0.17	0.15	0.25	**0.43**	**0.001**
	Winter	**0.30**	**0.006**	0.045	0.73	0.14	0.28
	Spring	0.066	0.55	-0.0086	0.96	**0.27**	**0.032**
	Summer	0.15	0.18	0.22	0.089	**0.50**	**<0.001**
	Autumn	0.18	0.094	0.20	0.12	**0.29**	**0.025**
Tmin	Annual	0.2	0.12	0.10	0.43	-0.081	0.54
	Winter	**0.24**	**0.027**	0.0022	1.0	-0.028	0.84
	Spring	0.22	0.047	0.028	0.84	-0.037	0.79
	Summer	**0.39**	**<0.001**	0.045	0.731	-0.067	0.61
	Autumn	0.18	0.099	0.16	0.22	0.040	0.78

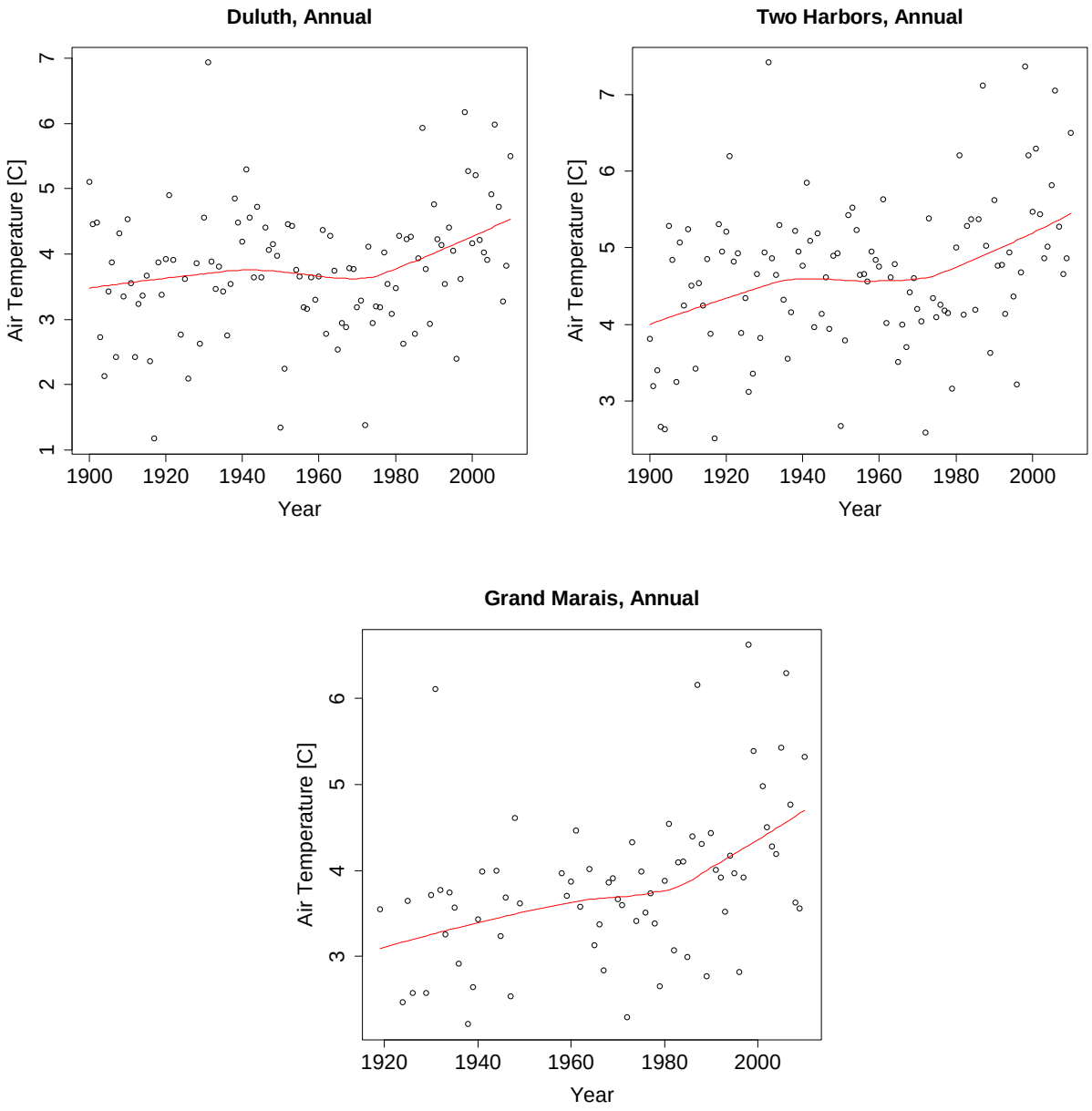

Figure 2.5. Time series (1900 –2010) of mean annual air temperature for Duluth, Two Harbors,and Grand Marais along with LOWESS trend lines.

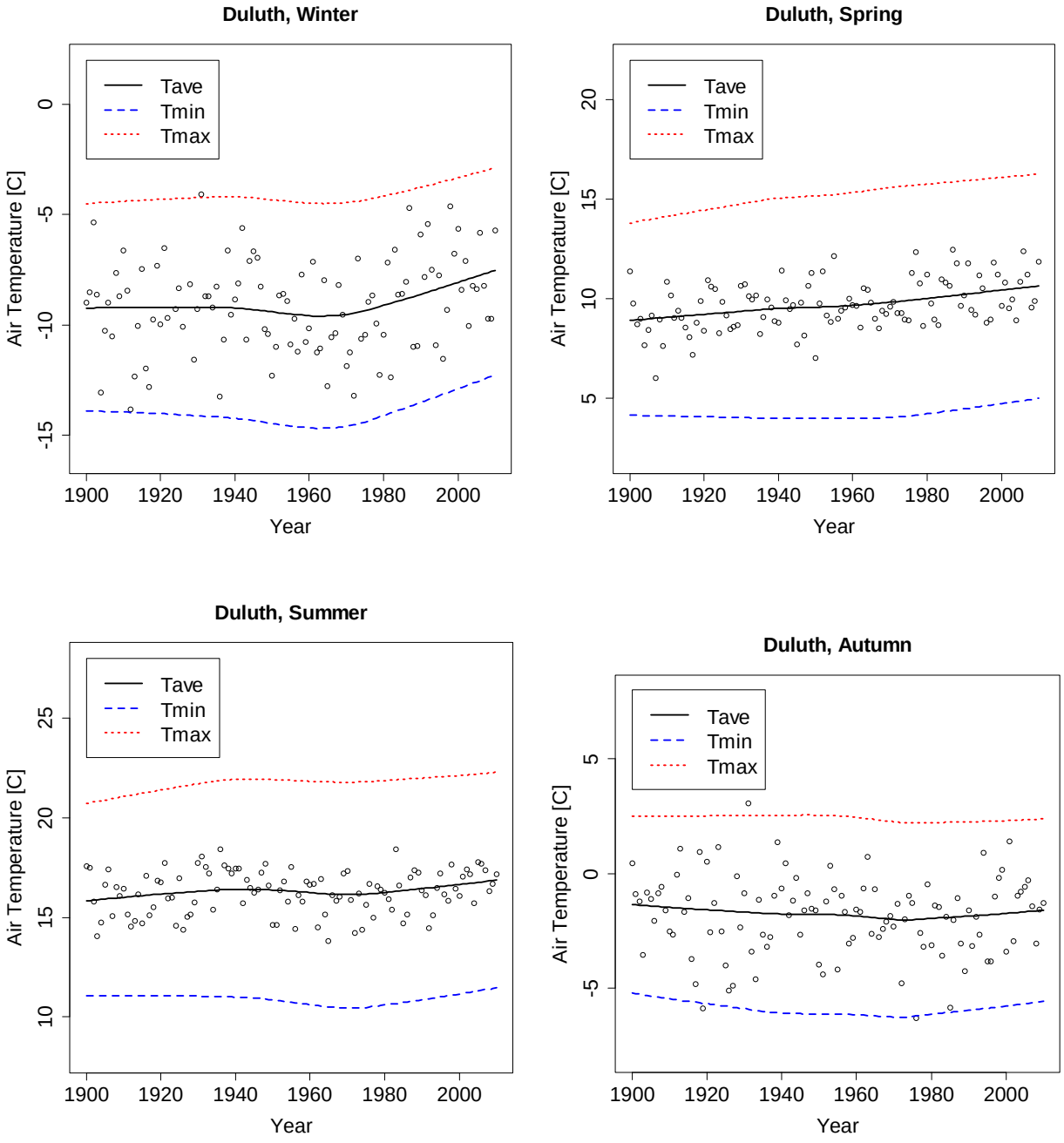

Figure 2.6. Time series (1900 –2010) of mean seasonal air temperature (Tave) for Duluth, MN along with LOWESS trend lines for Tave, Tmax (mean daily max air temperature) and Tmin (mean daily minimum air temperature) . Winter = Dec-Feb, spring = Mar-May, summer = Jun-Aug, autumn = Sep-Nov.

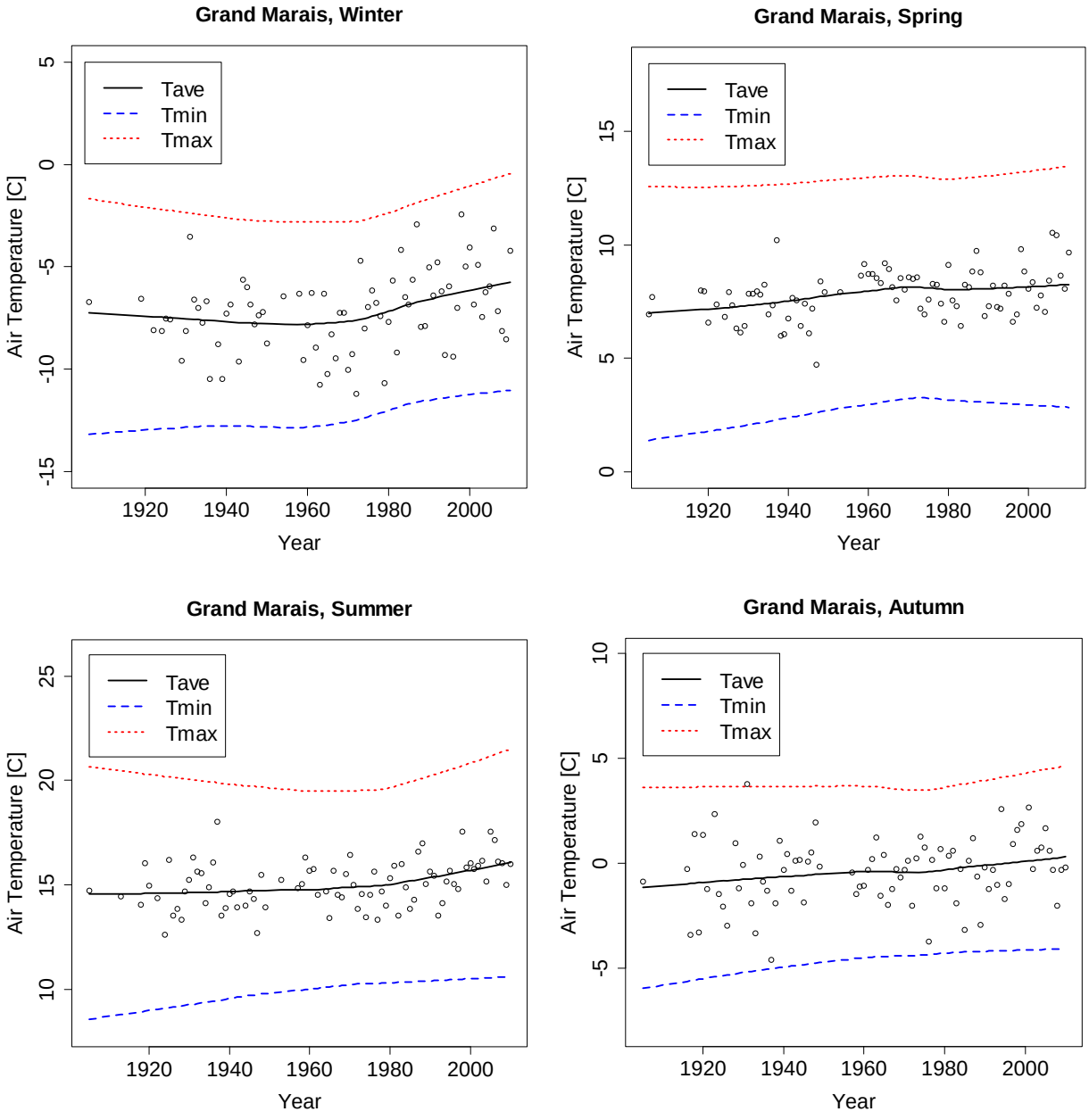

Figure 2.7. Time series (1900 –2010) of mean seasonal air temperature (Tave) for Grand Marais, MN along with LOWESS trend lines for Tave, Tmax (mean daily max air temperature) and Tmin (mean daily minimum air temperature)

2.4 Historical trends in streamflow

Long-term trend analysis of north shore trout stream flows is limited by the availability of longflow records. Of the eight flow gages used in the study, only the Baptism river gage has a record length longer than 50 years (Table 2.1), and only two stations (Baptism, Knife) have gage records of at least 30 years. The gage records at other north shore sites are less than 10 years and typically don't include winter data. For the purposes of trend analysis, the gage at the Pigeon

River was also included, although this river is substantially larger than the other gages sites and is not a trout stream.

Visual inspection of the flow time series with a LOWESS fit suggest a decreasing trend in annual flows in the Baptism, Knife, and Pigeon after about 1980 (Figure 2.8). Analysis of the time period 1981-2010 with the Mann-Kendall trend test did not give statistically significant trends, although the tau parameter was negative for all three gages (Tables 2.6, 2.7). Summer (May-Aug) low flows also may have decreasing trends (Figure 2.9), particularly in the Pigeon River, but these trends are not statistically significant with a 95% confidence interval (Tables 2.6, 2.7). Spring high flows appear to be decreasing in the Pigeon and Baptism, and increasing in the Knife (Figure 2.10). Again none of the apparent trends in high flow are statistically significant (Table 2.6, 2.7).

Table 2.6. Tau and p-values from the Mann-Kendall trend test for the annual and seasonal streamflow at the Pigeon, Baptism, and Knife Rivers, MN (full record).

	Pigeon (1922-2010)		Baptism (1928-2010)		Knife (1974-2010)	
Flow parameter	Tau	p-value	Tau	p-value	Tau	p-value
Annual	-0.027	0.71	0.16	0.056	0.036	0.76
Summer low flow	-0.036	0.62	**0.17**	**0.043**	0.069	0.56
Spring high flow	-0.13	0.064	-0.057	0.52	0.079	0.50

Table 2.7. Tau and p-values from the Mann-Kendall trend test for the annual and seasonal streamflow, 1981-2010, at the Pigeon, Baptism, and Knife rivers.

	Pigeon		Baptism		Knife	
Flow parameter	Tau	p-value	Tau	p-value	Tau	p-value
Annual	-0.21	0.12	-0.12	0.56	-0.08	0.54
Summer low flow	-0.22	0.094	-0.15	0.46	-0.15	0.24
Spring high flow	-0.081	0.54	-0.24	0.23	0.12	0.37

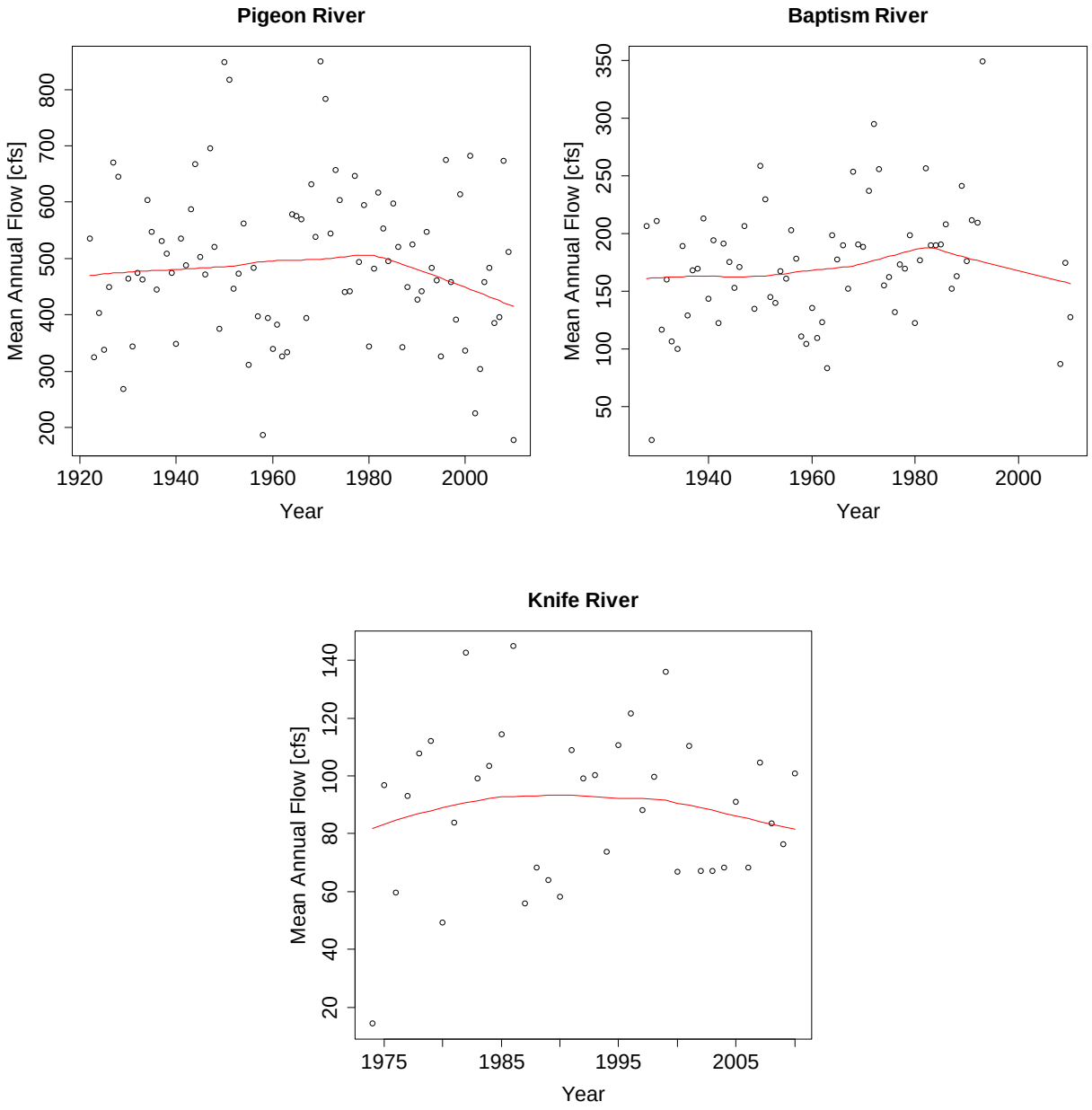

Figure 2.8. Time series of mean annual streamflow for the Pigeon (1922-2010), Knife (1974-2010), and Baptism (1928-2010) rivers, MN along with LOWESS trend lines.

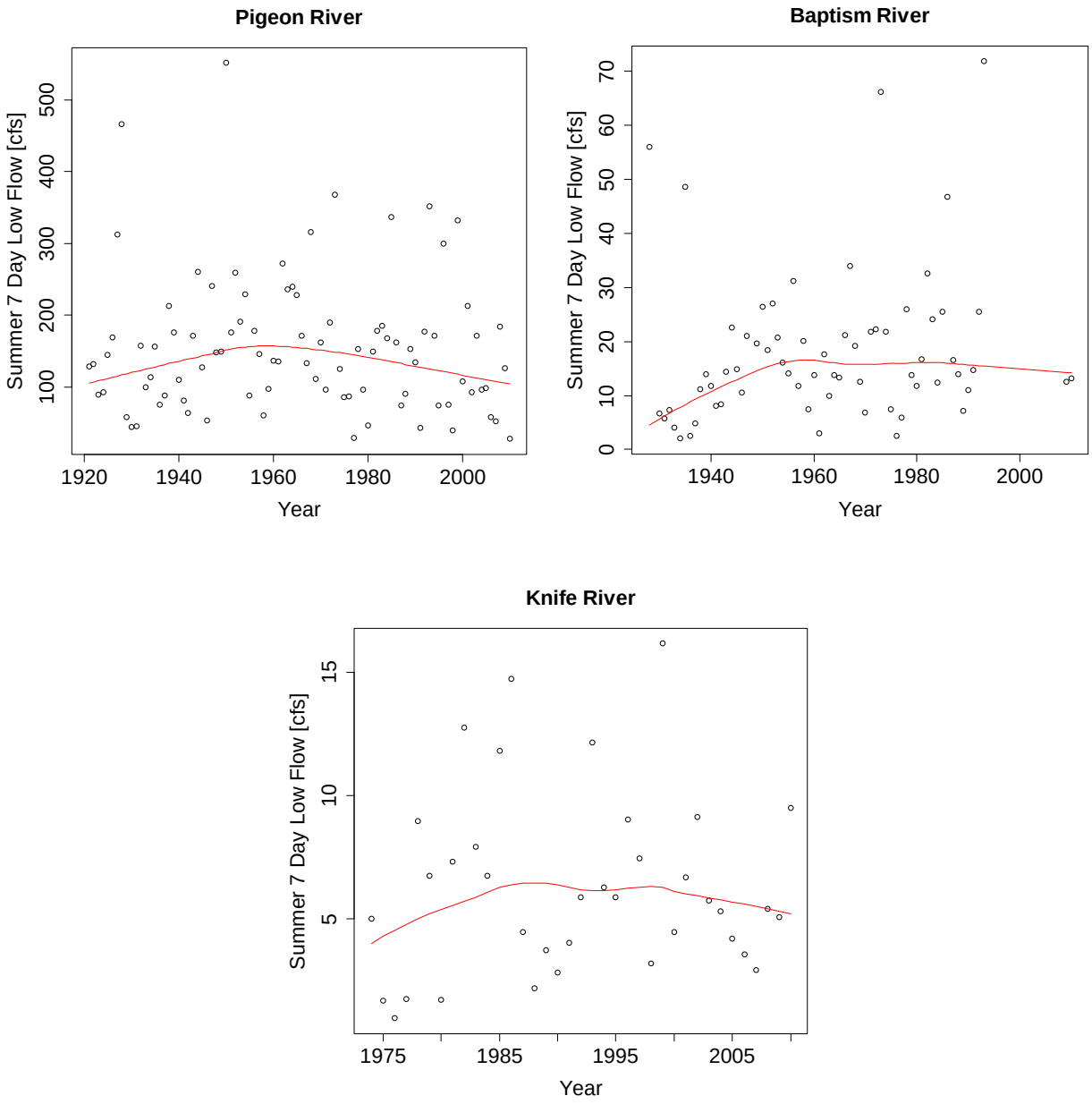

Figure 2.9. Time series of summer 7-day low flow for the Pigeon (1922-2010), Knife (1974-2010), and Baptism (1928-2010) rivers, MN along with LOWESS trend lines.

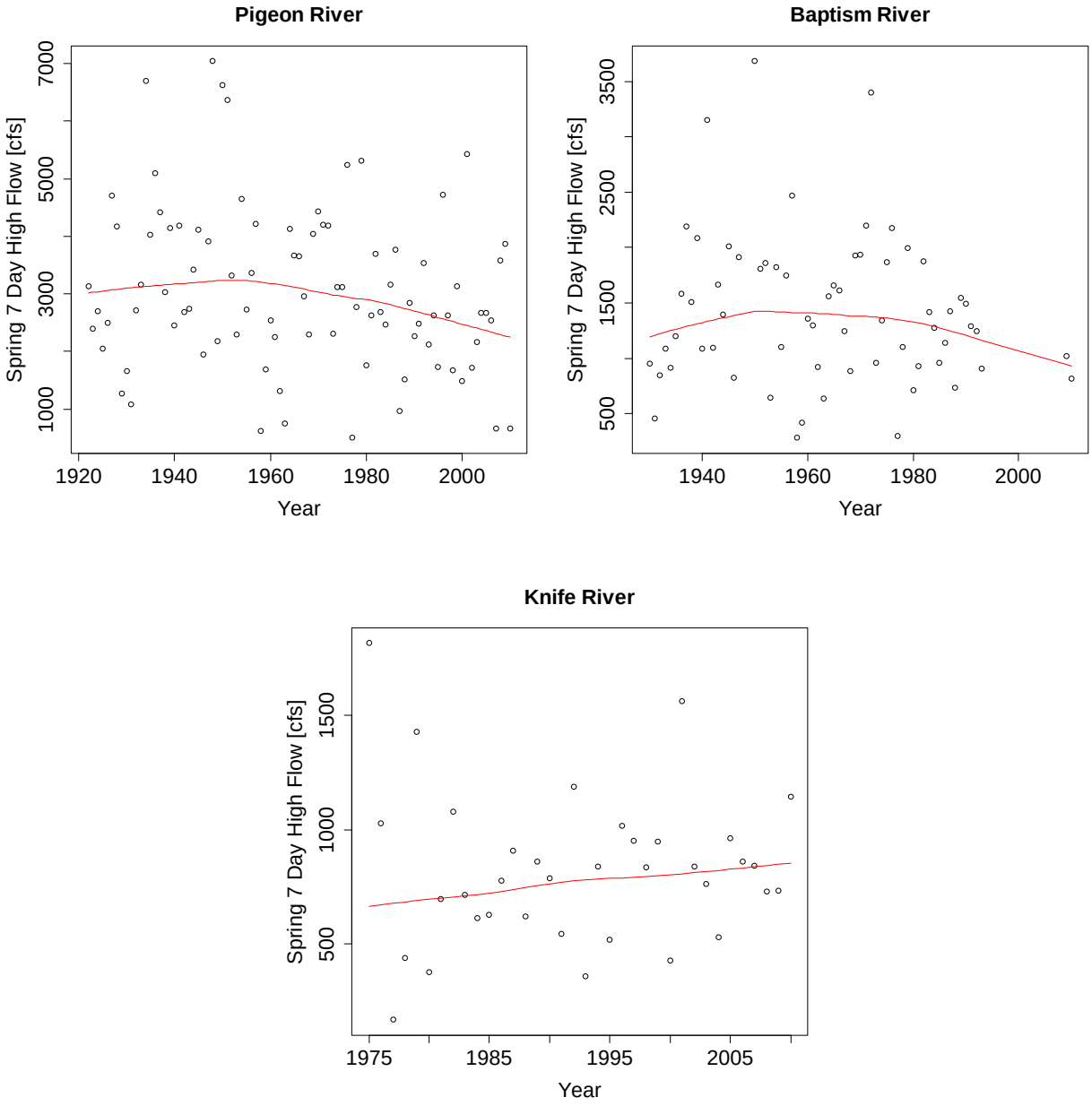

Figure 2.10. Time series of spring 7-day high flow for the Pigeon (1922-2010), Knife (1974-2010), and Baptism (1928-2010) rivers, MN along with LOWESS trend lines.

2.5 Relationships between observed precipitation and streamflow

To help characterize the available streamflow and precipitation data, and to select the best precipitation gages for deterministic hydrology models, yearly streamflow was plotted against annual precipitation for May through November totals. For each stream gaging site, streamflow was plotted against precipitation data from a number of the closest gages, and the precipitation gage giving the best relationship (highest R^2) was recorded (Table 2.8). Precipitation data from both NWS stations and from the high-density network stations were considered. For the Baptism River, a non-NWS precipitation gage at Isabella gave the best results, and for the Brule River, a non-NWS precipitation gage at Sawbill gave the best results. For the other stream gages, NWS precipitation data gave the best results (Table 2.8).

The streamflow-precipitation relationships are plotted in Figures 2.11a-2.11c. It is evident that the R^2 of the relationships varies drastically, from fairly good (Knife River R^2= 0.74) to poor (Sucker River R^2= 0.06). This variation in R^2 is likely due to a number of factors, including the flow record length, the streamflow and precipitation data quality, the proximity of the precipitation gage to the watershed, and the watershed characteristics.

Table 2.8. Summary of stream gages and the precipitation station with the highest correlation to stream flow for annual averaged data (May –November). NWS = National Weather Service, HD = High Density Network station.

Stream Gage	Precipitation Station	Station Type	Number of Years	R^2
Amity	Duluth	NWS	7	0.34
Baptism	Isabella	HD	45	0.33
Brule	Sawbill	HD	3	0.76
Knife	Two Harbors	NWS	36	0.74
Miller	Duluth	NWS	4	0.6
Poplar	Duluth	NWS	6	0.59
Sucker	Duluth	NWS	7	0.062

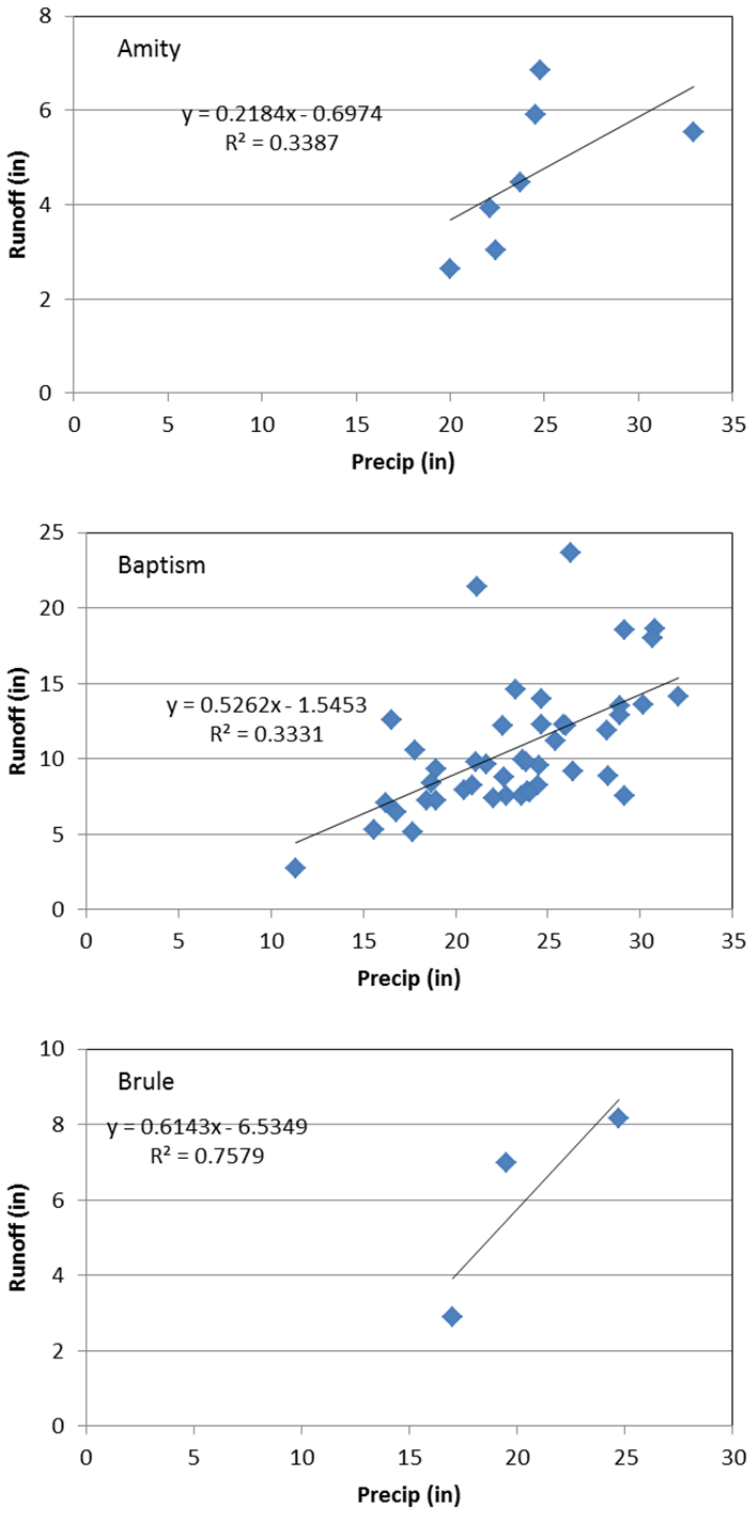

Figure 2.11a. Observed runoff depth versus observed precipitation depth, for May through November for the Amity Creek, Baptism River, and Brule River gages. The precipitation gages used for each stream gage are listed in Table 2.8.

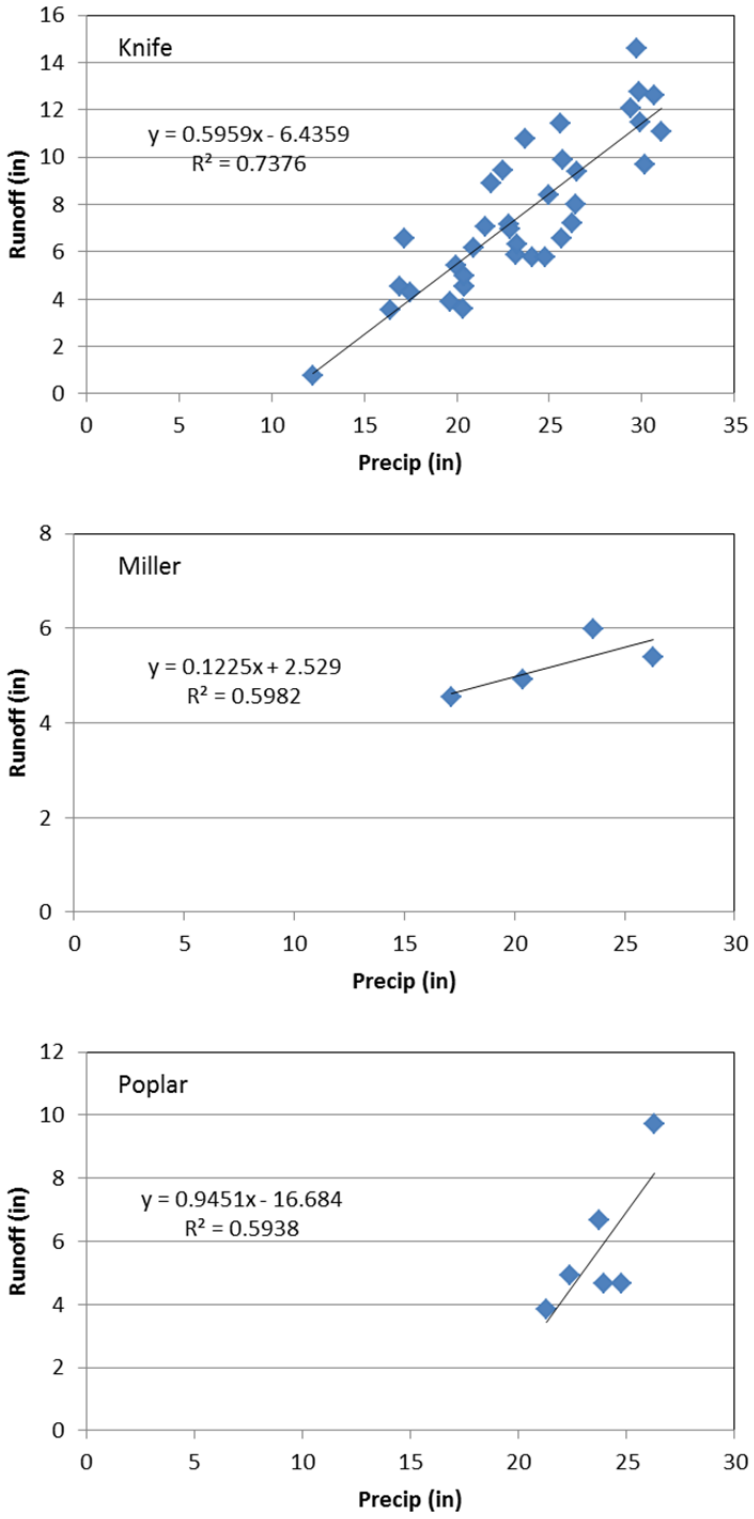

Figure 2.11b. Observed runoff depth versus observed precipitation depth, for May through November for the Knife River, Miller Creek, and the Poplar River gages. The precipitation gages used for each stream gage are listed in Table 2.8.

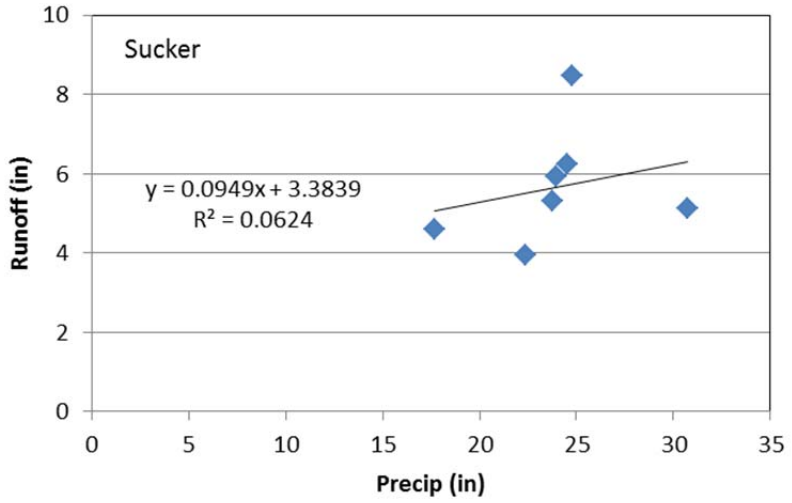

Figure 2.11c. Observed runoff depth versus observed precipitation depth, for May through November for the Sucker River gage. The precipitation gages used for each stream gage are listed in Table 2.7.

2.6 Relationships between observed stream temperature and air temperature

In general, stream temperature is strongly correlated to air temperature, and regression relationships between the two are the simplest form of a stream temperature model (Mohseni and Stefan 1998), which have been used to project the response of stream temperature to climate change (e.g. Mohseni et al. 1999). The water temperature of north shore trout streams can be expected to have particularly strong correlations to air temperature because of low groundwater inputs. In fact, for the three north shore streams used as study cases in the project, very strong correlations between stream temperature and air temperature were found (Figure 2.12), with R^2 above 0.90 for all three streams. Air temperatures from Duluth International Airport were used in all cases. From Figure 12, Amity Creek can be seen to have the lowest stream temperature / air temperature slope (0.89), while the Baptism river has the highest (0.95).

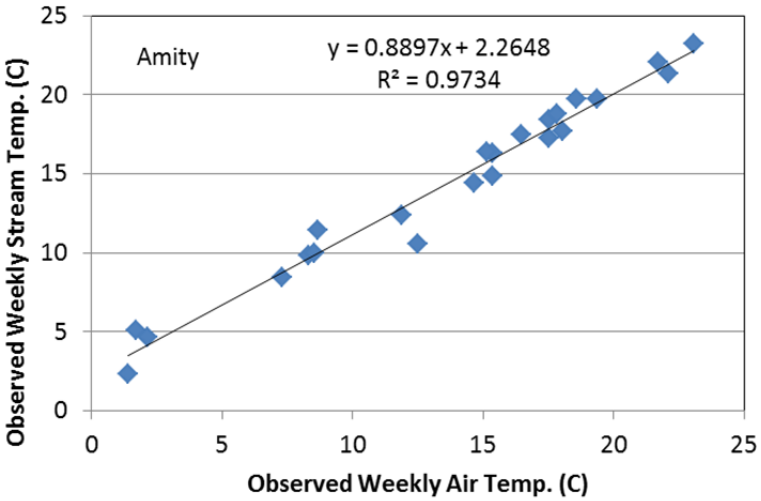

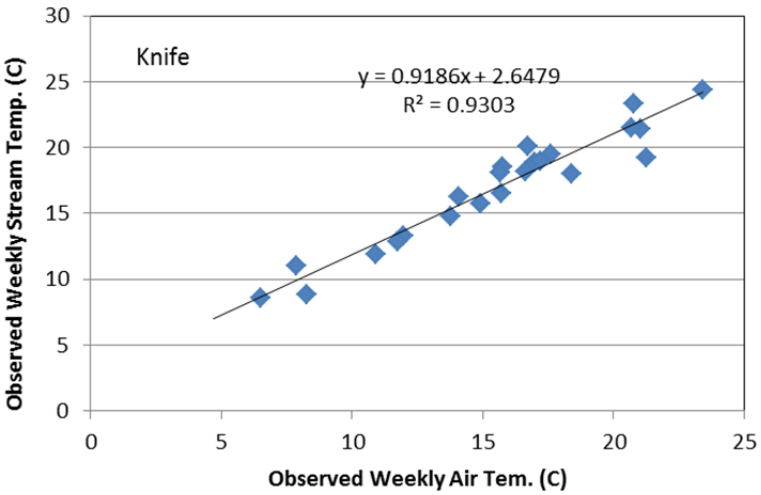

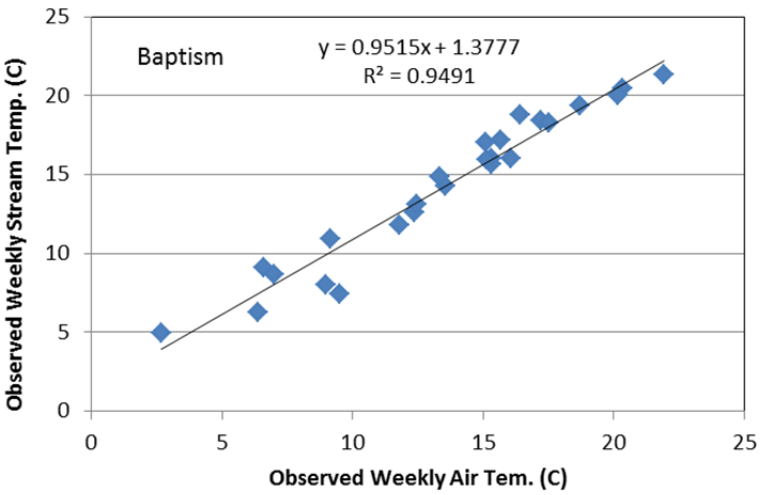

Figure 2.12. Weekly average stream temperature versus weekly average air temperature for May-October in Amity Creek (2006), the Baptism River (1981), and the Knife River (2005).

References

Burn, D.H., Elnur, M.A.H., 2002. Detection of hydrologic trends and variability. Journal of Hydrology 255, 107-122.

Mohseni, O. and H.G. Stefan (1998), A non-linear regression model for weekly stream temperatures. Water Resour. Res., 34(10): 2685-2692.

Mohseni, O., Erickson, T.R., and H.G. Stefan (1999), Sensitivity of stream temperatures in the U.S. to air temperatures projected under a global warming scenario, Water Resour. Res., 35(12), 3723-3733.

3. Climate Change Projections for the Lake Superior North Shore Region

A key task in this project was to project future changes in hydrological conditions of north shore trout streams using projected global climate model (GCM) data as input to the deterministic and empirical hydrologic models. Specific questions to be addressed include:

- What are the projected changes in flow statistics?
- How much do the results differ for the different GCMs?
- How much difference does it make using the monthly increments or the daily projections, i.e., how well do monthly increments represent the projected changes, particularly precipitation?

3.1 Available climate projections

Several GCM projections were available for this study. Dynamically downscaled GCM output (15 km grid spacing) made by Oregon State University for the USGS National Fish Habitat Assessment Project, were available for three GCMs: GENMOM, GFDL, ECHAM5. All of the GCM data described in this report were regionally downscaled using the RegCM3 model(Hostetler et al. 2011). The downscaled climate projections are based on the A2 emissions scenario, which has a doubling in CO_2 concentration by the end of the century (IPCC, 2007).

The available downscaled GCM data were used to calculate monthly increments to historical climate for 2020-2039, 2040-2059, 2060-2079, 2070-2089. Daily time step downscaled GCM output were also available for the GENMOM GCM only, for 2020-2089. These data were used to calculate weekly-averaged climate, and run directly in the hydrologic models. A full suite of climate variables was available; for the hydrologic model, air temperature, humidity, precipitation, wind speed, and solar radiation data were used.

The downscaled GCM data were downloaded, converted to regional raster files, and attributed to the north shore stream catchments. There are approximately 20 GCM nodes in the north shore trout stream catchment region (Figure 3.1). The monthly GCM outputs were used to determine future increments for the climate variables, by finding the difference, or ratio, between future projections and the GCM output for the historical period (1980-1999). For air temperature, an additive increment was determined for each of the 3 GCM and each 20-year time period, so future air temperature conditions were determined as:

$$TA_{i,future} = TA_{i,\,NWS} + TA_{inc,m} \quad (3.1)$$

$$TA_{inc,m} = TA_{GCM,\,future,m} - TA_{GCM,\,historical,m} \quad (3.2)$$

where $TA_{i,\,future}$ is an air temperature value at, e.g. weekly time step for some future period, $TA_{i,\,NWS}$ is an observed weekly air temperature from the historical record, $TA_{inc,m}$ is the monthly air temperature increment calculated as the difference between the GCM mean monthly air temperature for the future period ($TA_{GCM,\,future,m}$) and the GCM mean monthly air temperature for

the historical period ($TA_{GCM,\ historical,m}$). For creating future, weekly climate input for the hydrologic model, an increment is added to the weekly values based on what month they fall in.

For the remaining variables (precipitation, humidity, wind speed, solar radiation), a multiplicative increment was used, as exemplified for precipitation in Equations 3.3 and 3.4:

$$PR_{i,future} = PR_{i,\ NWS} \cdot PR_{inc,m} \quad (3.3)$$

$$PR_{inc,m} = PR_{GCM,\ future,m} / PR_{GCM,\ historical,m} \quad (3.4)$$

For precipitation, in particular, using a multiplicative increment avoids negative future precipitation values when precipitation is projected to decrease, and weeks with no precipitation are maintained as zero. A complete listing of the calculated increments for Duluth is given in Appendix 3.1. For the GFDL GCM, model output was available only for 2040-2069, so only one future increment was calculated (2040-2059).

The monthly wind speed increments calculated using Eqs. 3.3 and 3.4 were found to be highly variable, with multiplicative increments of up to 3.0. Investigation revealed that the monthly average wind speeds supplied as GCM outputs were calculated as using separate, scalar averages of daily east-west and north-south wind components, rather than as a monthly average of daily wind velocity. As a result, daily variability in wind direction leads to small values in the monthly average wind components. For the purposes of this study, monthly wind speed increments were subsequently recalculated using the daily GENMOM output.

Figure 3.2 summarizes the air temperature and precipitation increments associated with the GENMOM model. The monthly increments were aggregated to seasons for the figure (winter = Dec, Jan, Feb; spring = Mar, Apr, May; summer = Jun, Jul, Aug; autumn = Sept, Oct, Nov). The systematic increase in air temperature for all four seasons is evident, approaching 3°C for winter air temperatures by 2070-2089, but less than 2 °C for summer air temperatures. The precipitation multiplier varies from 0.92 to 1.24, but the relative seasonal values vary between time periods.

Figure 3.3 compares the monthly increments for air temperature, precipitation, and humidity for the three GCMs in the period 2040-2059. Both the GFDL and ECHAM5 models gives air temperature increments somewhat higher than GENMOM, but no monthly increment exceeds 3 °C for this period. Precipitation multipliers appear to vary somewhat randomly by month for each of the three models, with the range of values similar between models. All three models project increases in humidity of up to 20%.

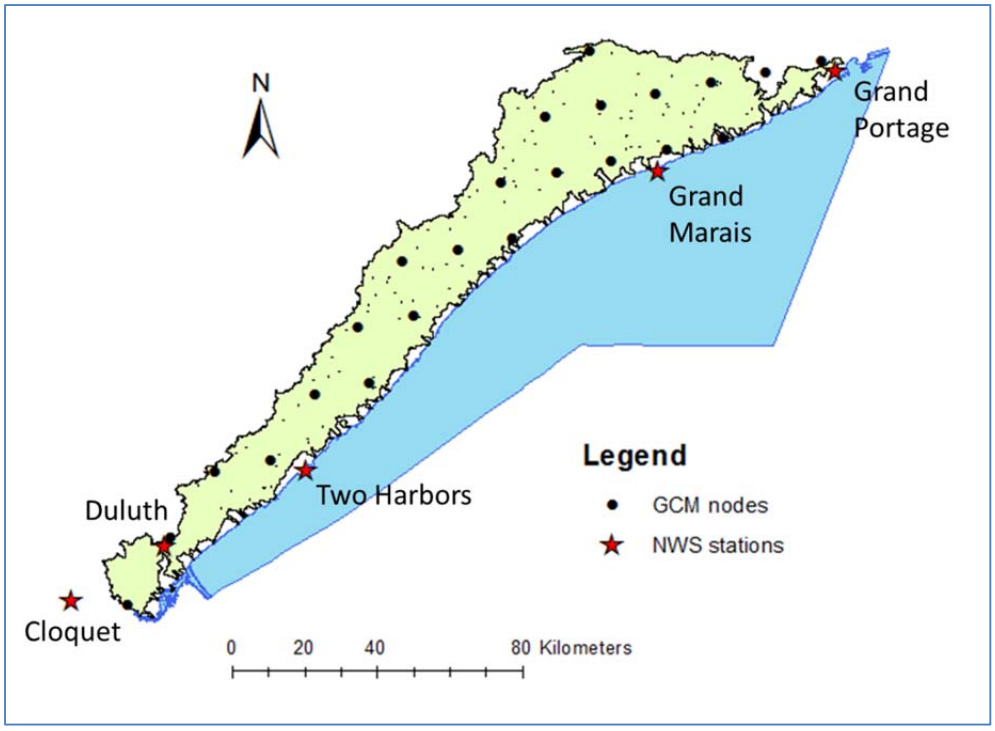

Figure 3.1. Location of GCM nodes for the available downscaled climate data used in this study, along with National Weather Service (NWS) station locations.

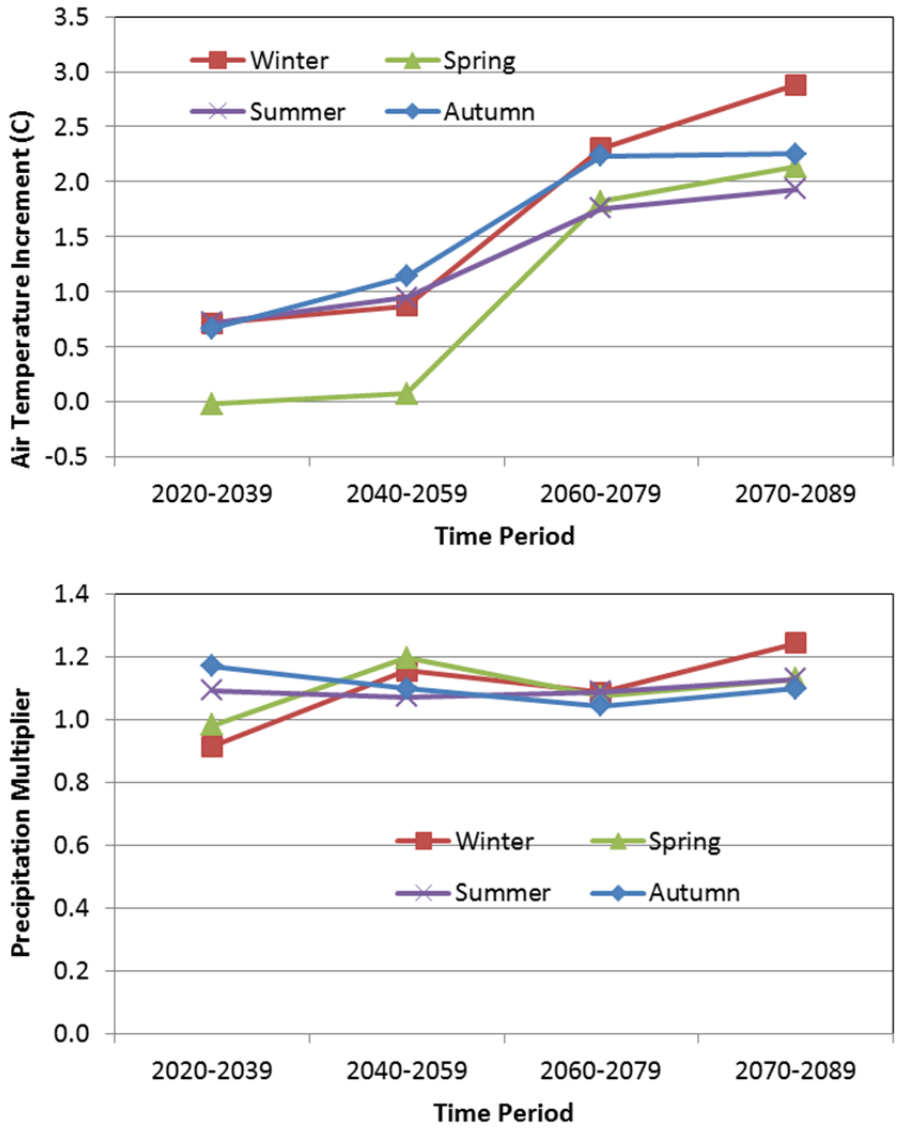

Figure 3.2. GENMOM increments for air temperature, precipitation, and humidity for the 5 future time periods.

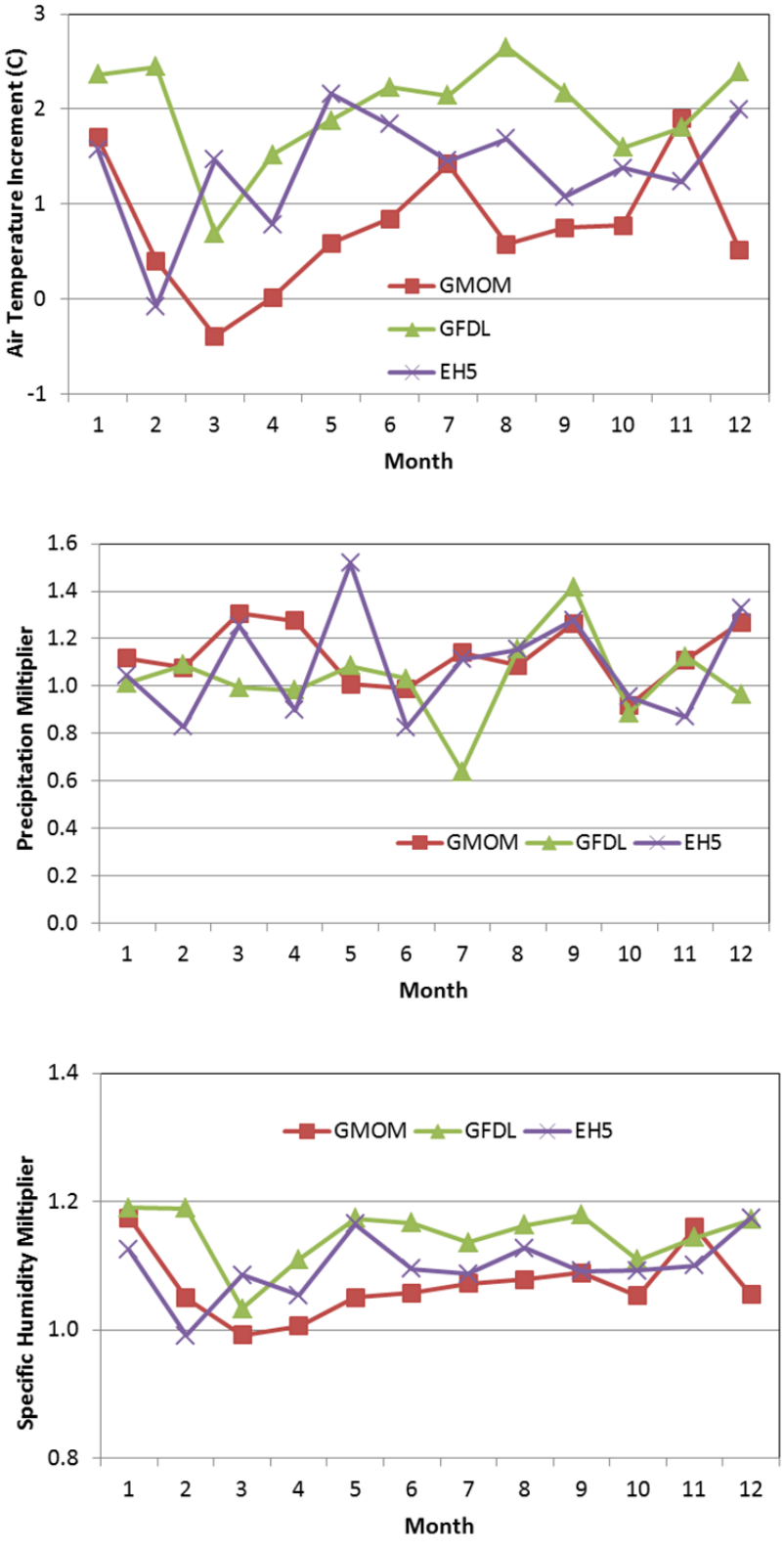

Figure 3.3. GENMOM, GFDL, and ECHAM5 GCM increments for air temperature, precipitation, and humidity for the 2040-2069 time period.

3.2 Characterization of GENMOM projected daily air temperature and precipitation.
The monthly increments described in the previous section describe future changes in mean monthly values, but do not address inter-annual and daily variability of air temperature and precipitation. Characterizing the available time series of daily and monthly values of air temperature and precipitation can provide additional insight on 1) how well the GCM matches the dynamics of historical, local climate, and 2) how variability of these climate parameters could change in the future.

Figures 3.4 and 3.5 examine the present and future variability of seasonal air temperature. Figure 3.4 plots the GENMOM time series for mean seasonal air temperature with LOWESS trend lines, while Figure 3.5 gives box plots of the seasonal air temperature statistics in 20-year blocks. Overall, inter-annual variability of air temperature changes little as the mean values increase. The trends in annual precipitation were fairly similar for other north shore GCM nodes, including nodes near Schroeder, Grand Marais, and Grand Portage (Figure 3.6 and 3.7).

To help evaluate the ability of the GENMOM model to match historical precipitation observations, the GENMOM monthly simulations for the historical period were compared to observations at Duluth International Airport (DLH). Overall, the GENMOM model captures the seasonal variation of precipitation quite well (Figure 3.8). The monthly precipitation biases (errors) vary from a factor of 0.63 to 1.38, but the overall annual bias only 1.05. Figure 3.9 gives the spatial variation of mean annual precipitation along a line from Duluth to Grand Portage for NWS observations and for the GEMOM nodes (Figure 3.1). Both data sets suggest a decreasing trend in annual precipitation towards Grand Portage.

The downscaled daily precipitation time series obtained for the GENMOM model provide an opportunity to examine how well the downscaled data match observed daily precipitation statistics, and to see how these statistics could change in the future. The precipitation data are daily, rather than storm-based, so that characterization focused on the statistics of daily precipitation depth.

National Weather Service daily precipitation observations for Duluth International Airport (DLH) were obtained from the Minnesota State Climatology Office (http://climate.umn.edu/hidradius/radius.asp). Simulated daily precipitation data for the downscaled GENMOM model were extracted for the closest node to DLH for the calibration period (1980-1999) and for future projections (2020-2089) using Matlab. The historical and future GENMOM daily precipitation data were debiased, by month, using multiplicative factors based on the calibration period (1980-1999), as given in the previous section of this report. The goals of the analysis in this section were 1) determine how well the GENMOM model reproduces the statistics of observed daily precipitation data and 2) characterize the future daily precipitation statistics projected by the GENMOM model.

Figure 3.10 compares the distribution of simulated and observed precipitation depth over all months for the calibration period (1980-1999). The GENMOM daily precipitation data is skewed towards lower daily precipitation values compared to the NWS observations, with the GENMOM peaking in the 10-20 mm range while the NWS distribution peaks at 20-50 mm. The daily precipitation distributions are broken down by season in Figures 3.11 and 3.12. The differences between the GENMOM and NWS data are most apparent in summer (June-August), with the GENMOM output significantly under-predicting the number of days with 50-100 mm of precipitation, but also predicting some higher values (100-200 mm) not present in the NWS observations.

The GENMOM future precipitation statistics for Duluth (2020-2089) are summarized for 20-year blocks in Figures 3.13 – 3.17, with Figure 3.13 giving the full year statistics and Figures 3.14-3.17 breaking down the precipitation statistics by season. NWS observations from 1930-2010 are also shown for comparison. The full year GENMOM precipitation statistics show minimal changes from 2020 to 2089, with the most variability in the large events (daily depth > 100 mm). Breaking the data down by season (Figures 3.14-3.17), there is a somewhat more systematic increase in day with precipitation greater than 100 mm in summer (June – August) and a corresponding decrease in days with between 50 and 100 mm precipitation after an initial increase to 2020-2039 (Figure 3.16).

The long-term changes in days with high precipitation were also examined by calculating percentiles on the daily precipitation depths. Note that these are not storm depth percentiles, since the data are daily totals, not storm totals, and include many days with little or no precipitation. Figure 3.18 gives the 95th, 99th, and 99.9th percentile daily precipitation depth for 20-year blocks of historical NWS data and GENMOM projections. The daily precipitation percentiles are fairly consistent from the historical to projected time periods, and show a moderate upward trend in the 99.9th percentile precipitation depth. The 99.9th percentile, i.e. a daily precipitation depth expected to occur about once every 3 years, increases from about 50 mm around 1900-20 to a projected 70 mm by 2070-89.

Overall, the future climate projections align with the historical trends in climate for the region. GCM outputs project a continued increasing trend in air temperature, with an increase in mean annual air temperature of 2 to 3 °C by 2089. Precipitation trends are less clear. The historical precipitation data shows an increasing trend for total annual precipitation at Duluth and Two Harbors between 1900 and 2010, whereas Grand Marais and Grand Portage do not have a clear trend. Based on an analysis of daily precipitation totals, there is some indication of an increasing trend in the number of days in summer with high precipitation (10-20 cm). The daily GCM output projects further increases in these larger summer precipitation events, however, these results are based on the analysis of only one GCM output (GENMOM). Both the GENMOM and the ECHAM5 GCMs project overall increases in precipitation of about 15%, but differ on the seasonal distribution of the precipitation changes.

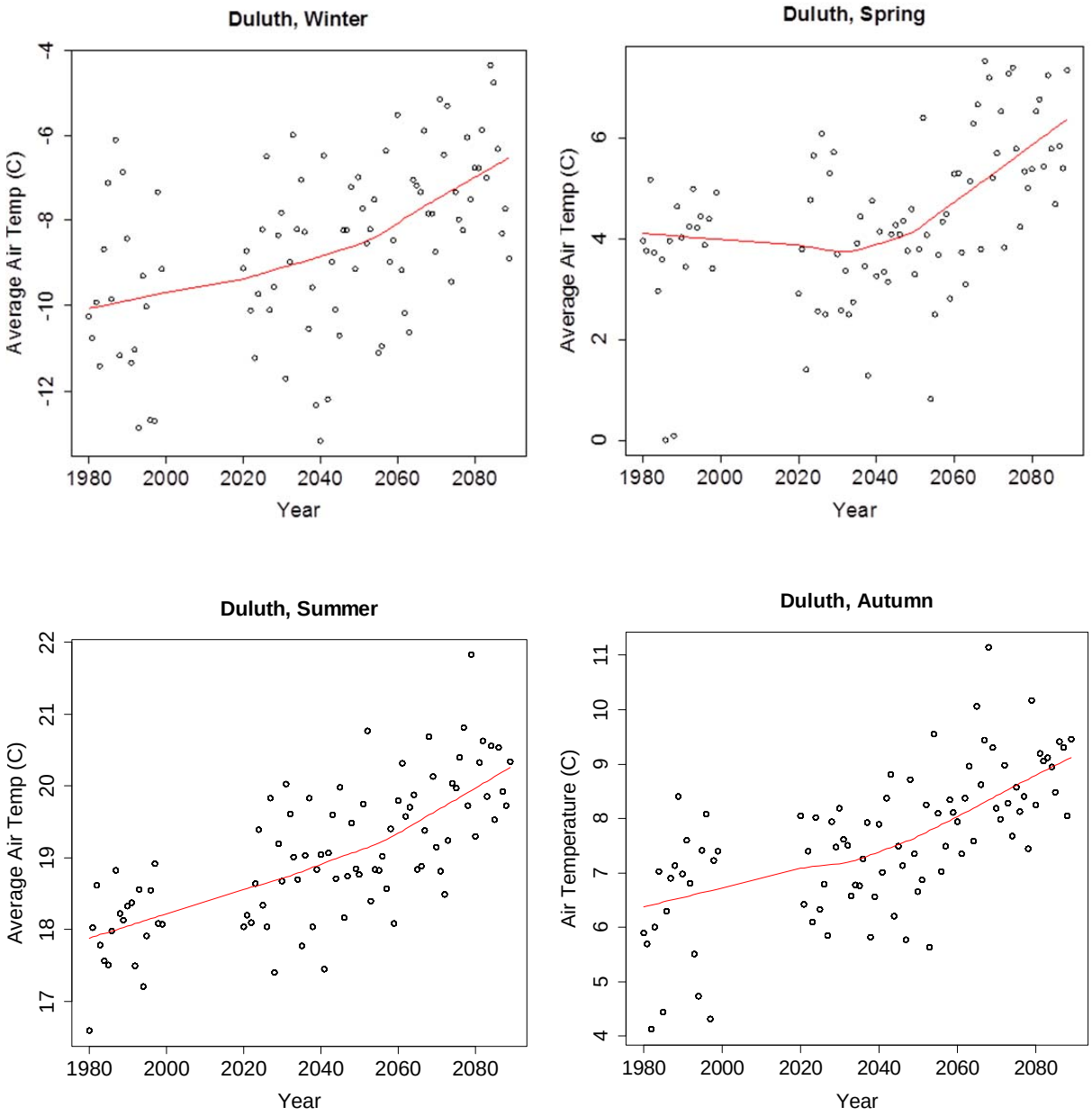

Figure 3.4. Time series of projected seasonal air temperatures at Duluth, MN from the GENMOM model, along with LOWESS trend lines.

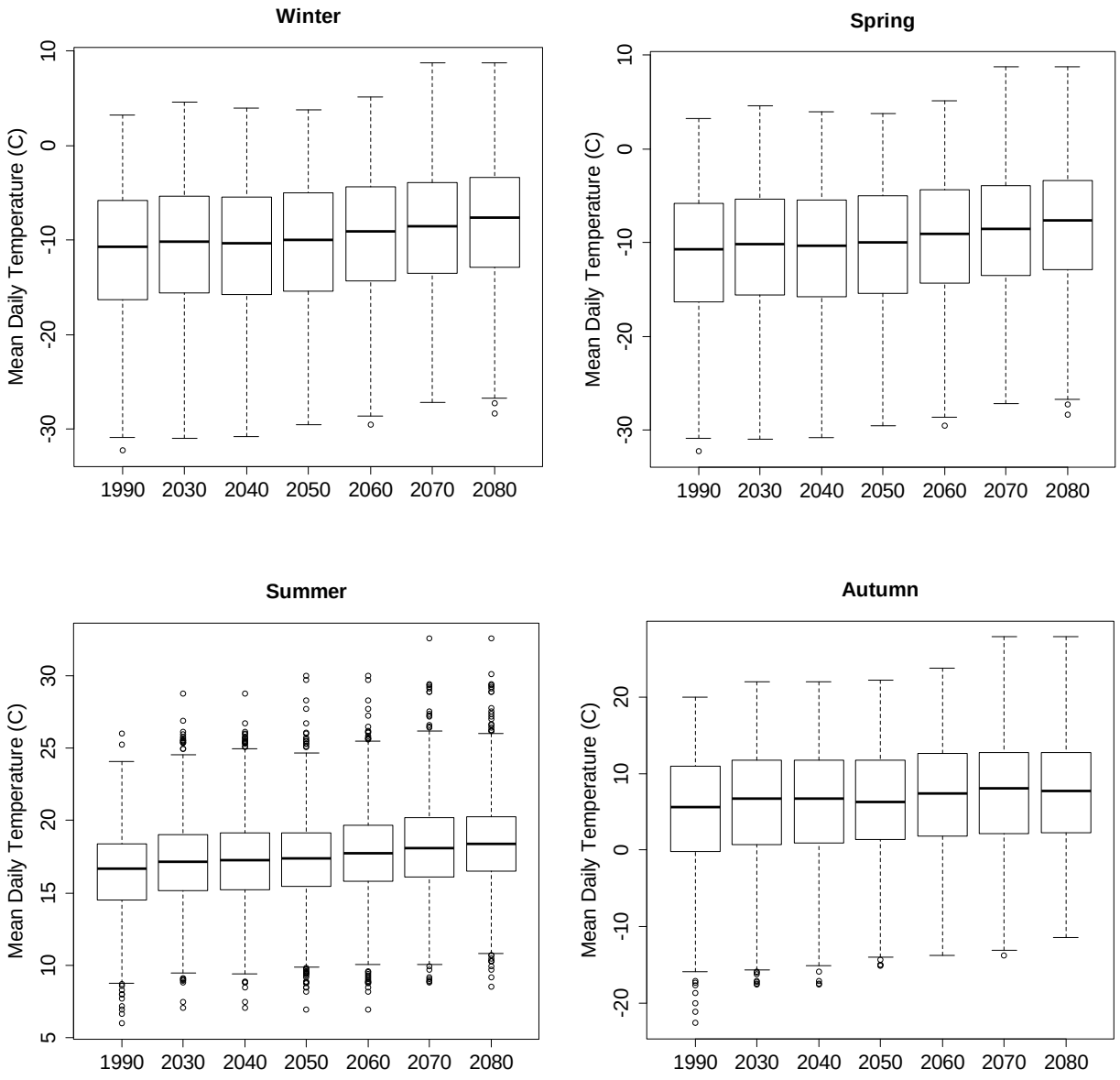

Figure 3.5. Statistics of projected seasonal air temperatures, in 20-year blocks, at Duluth, MN from the GENMOM model.

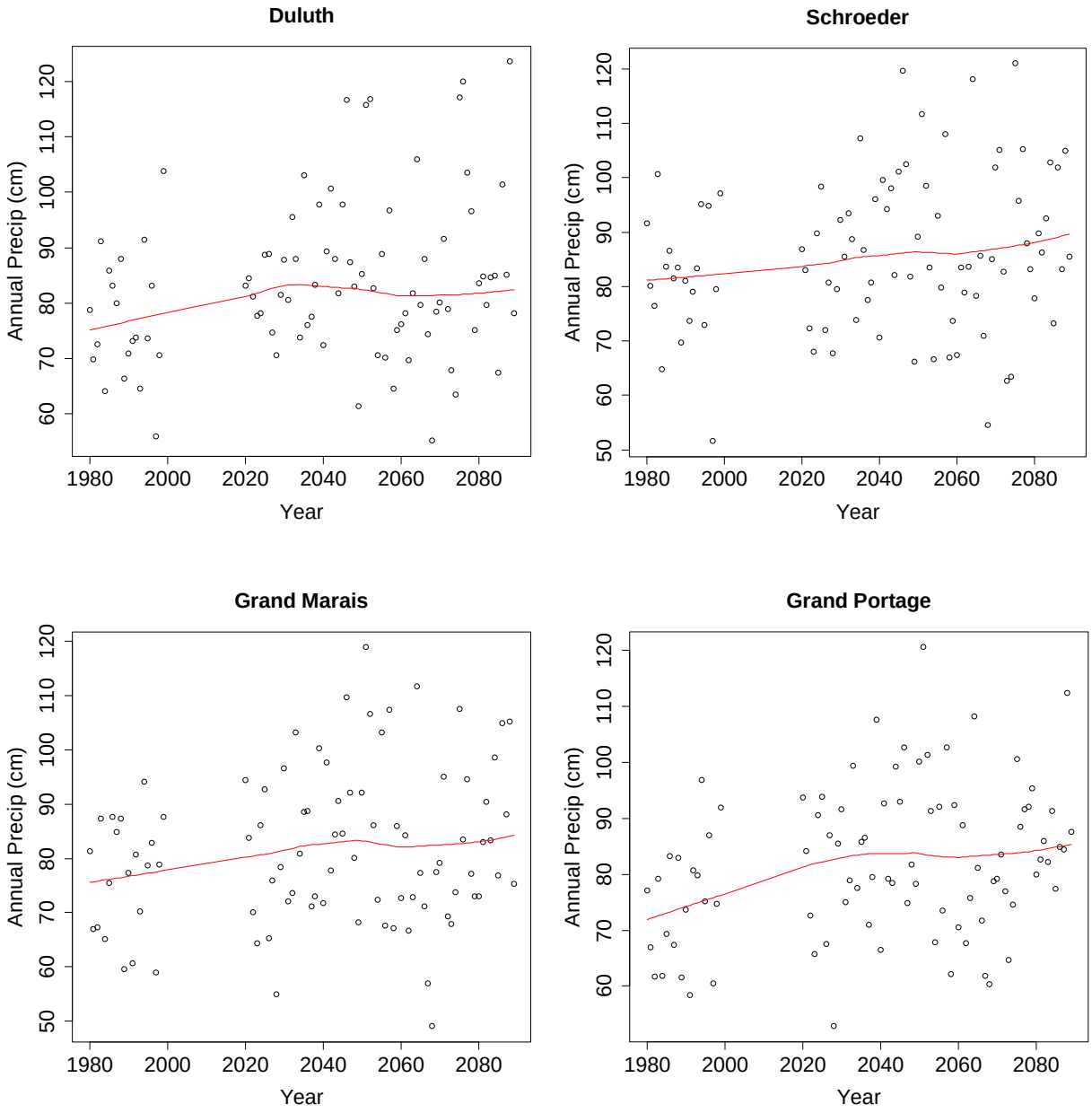

Figure 3.6. Projected annual precipitation for Duluth, Schroeder, Grand Marais, and Grand Portage, MN from GENMOM model, with lowess trend lines in red (1980 – 2089).

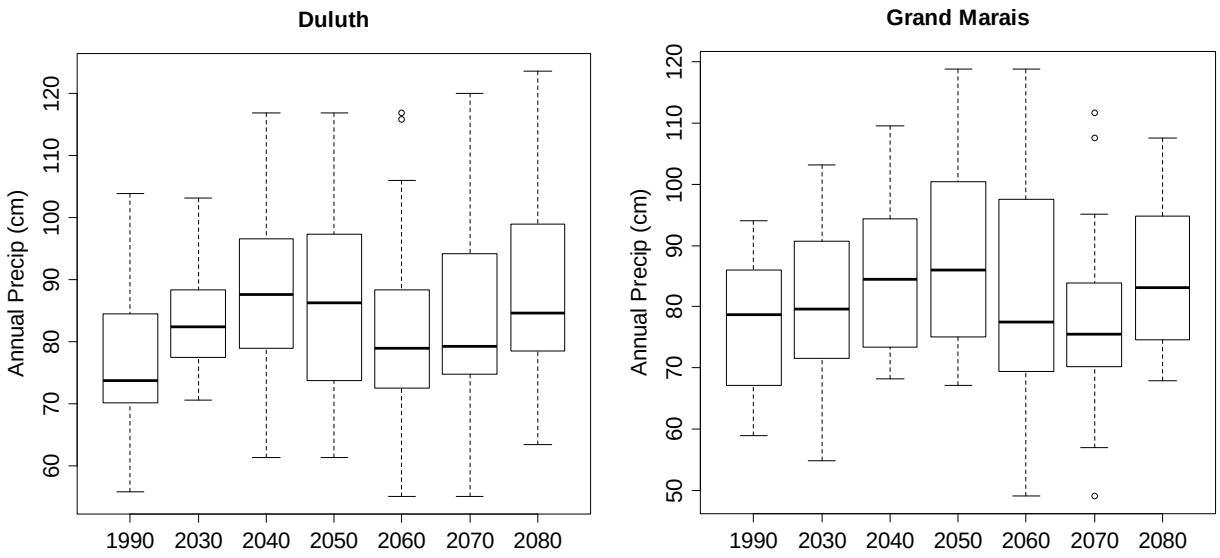

Figure 3.7. Projected annual precipitation for Duluth and Grand Marais, MN. Each boxplot gives the distribution of 20-year blocks of annual precipitation centered on the year given on the x-axis.

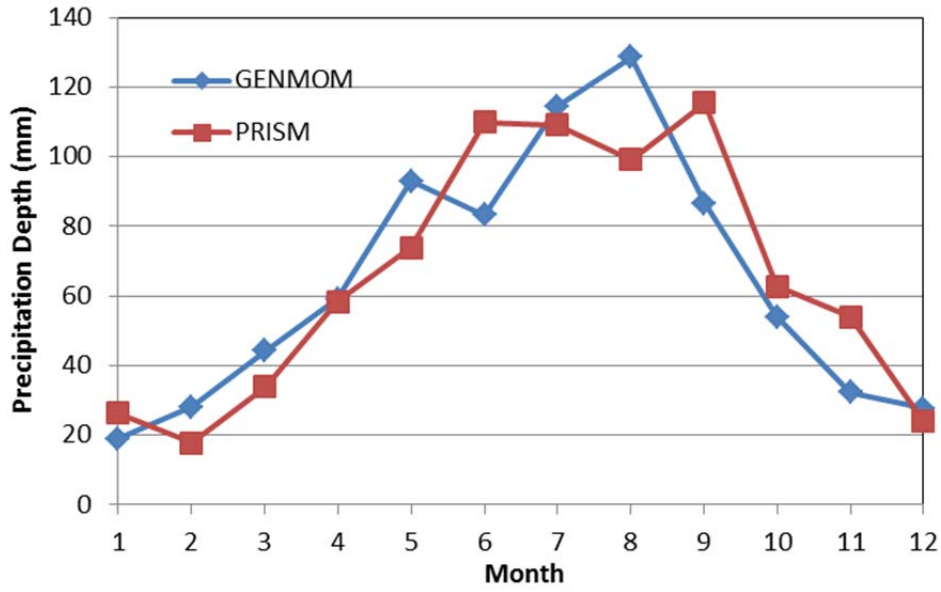

Figure 3.8. Monthly average precipitation for the period 1980-1999 for NWS observations in Duluth and GENMOM simulations for the same location and period.

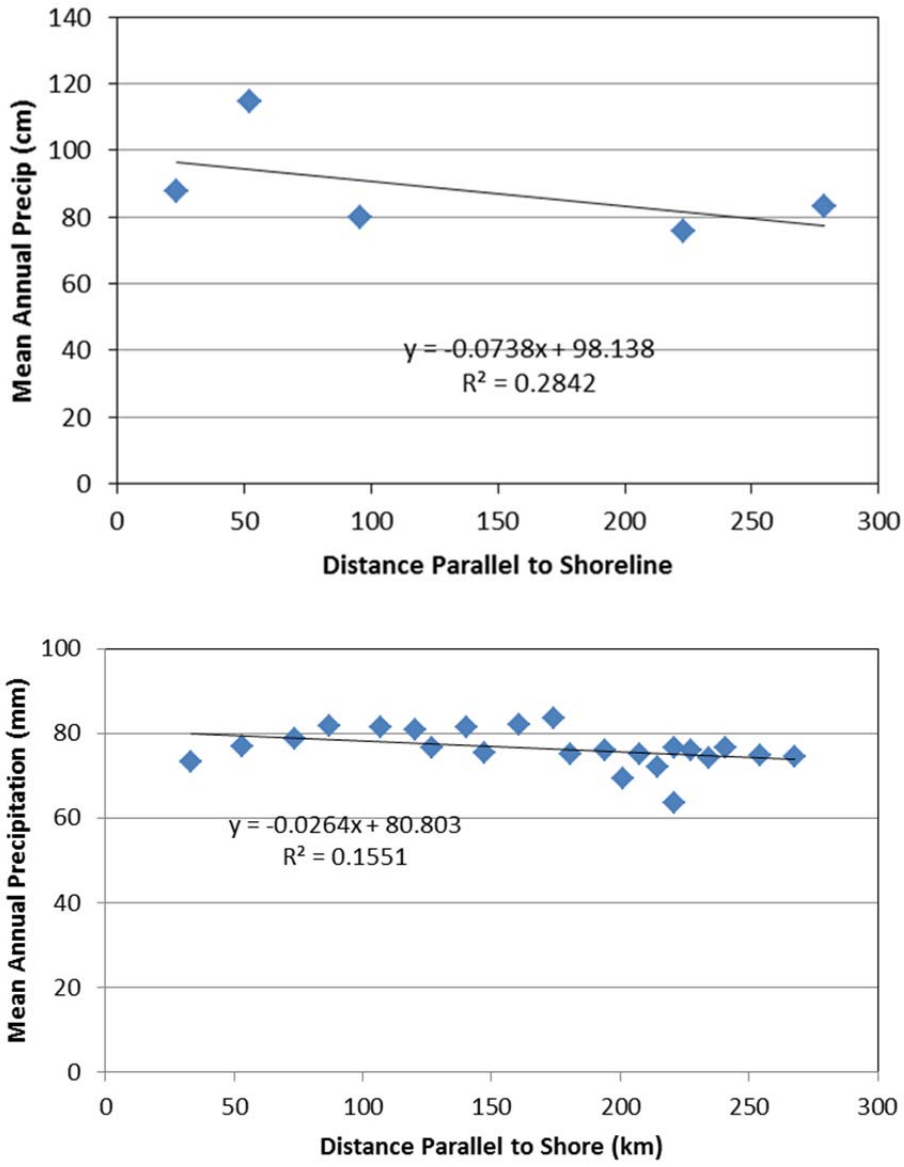

Figure 3.9. Longshore gradient of 1980-1999 mean annual precipitation for NWS observations (upper panel) and GENMOM simulations (lower panel).

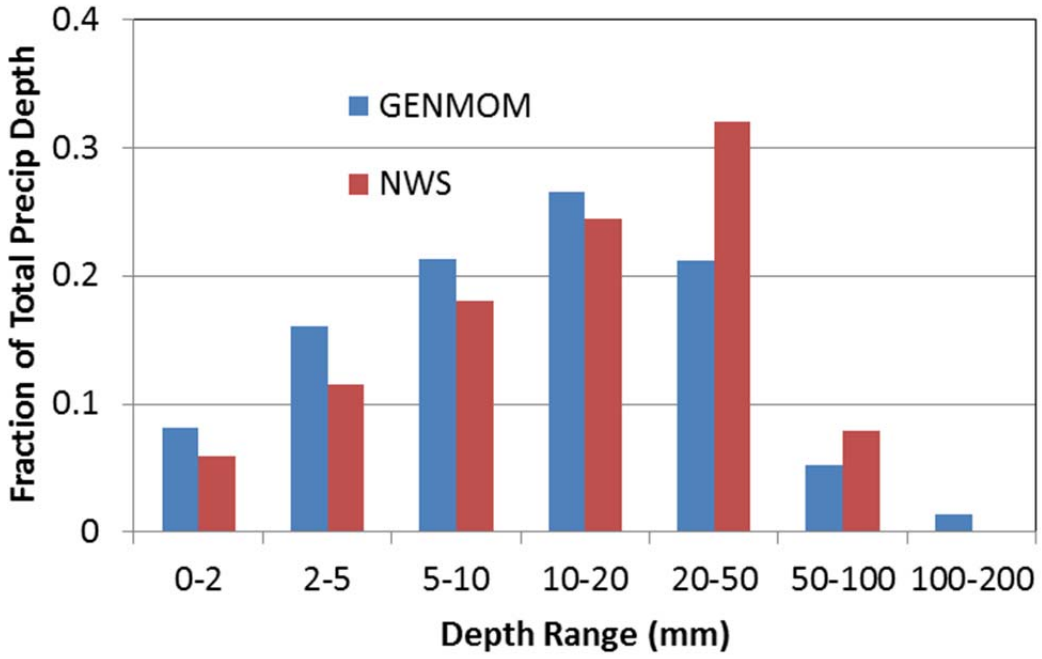

Figure 3.10. Historical (1980-1999) average number of counts per year of daily precipitation depth in ranges from 0-1 mm to 100-200 mm, for NWS observations at DLH and downscaled GENMOM output for the same location.

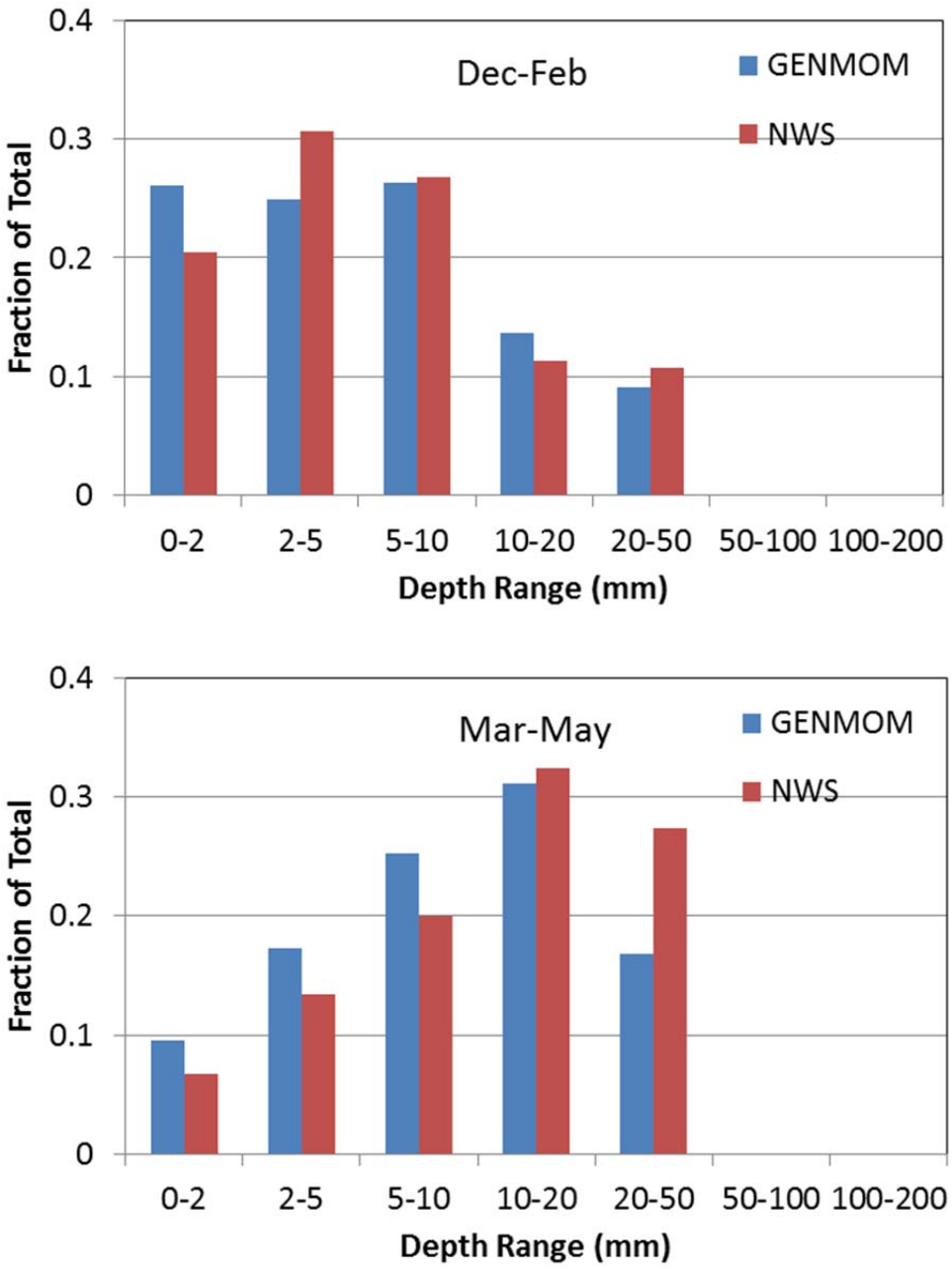

Figure 3.11. Seasonal distribution of seasonal precipitation fraction in ranges from 0-2 mm to 100-200 mm, for NWS observations at DLH and downscaled GENMOM output for the same location, 1980-1999, December–February (upper panel) and March-May (lower panel).

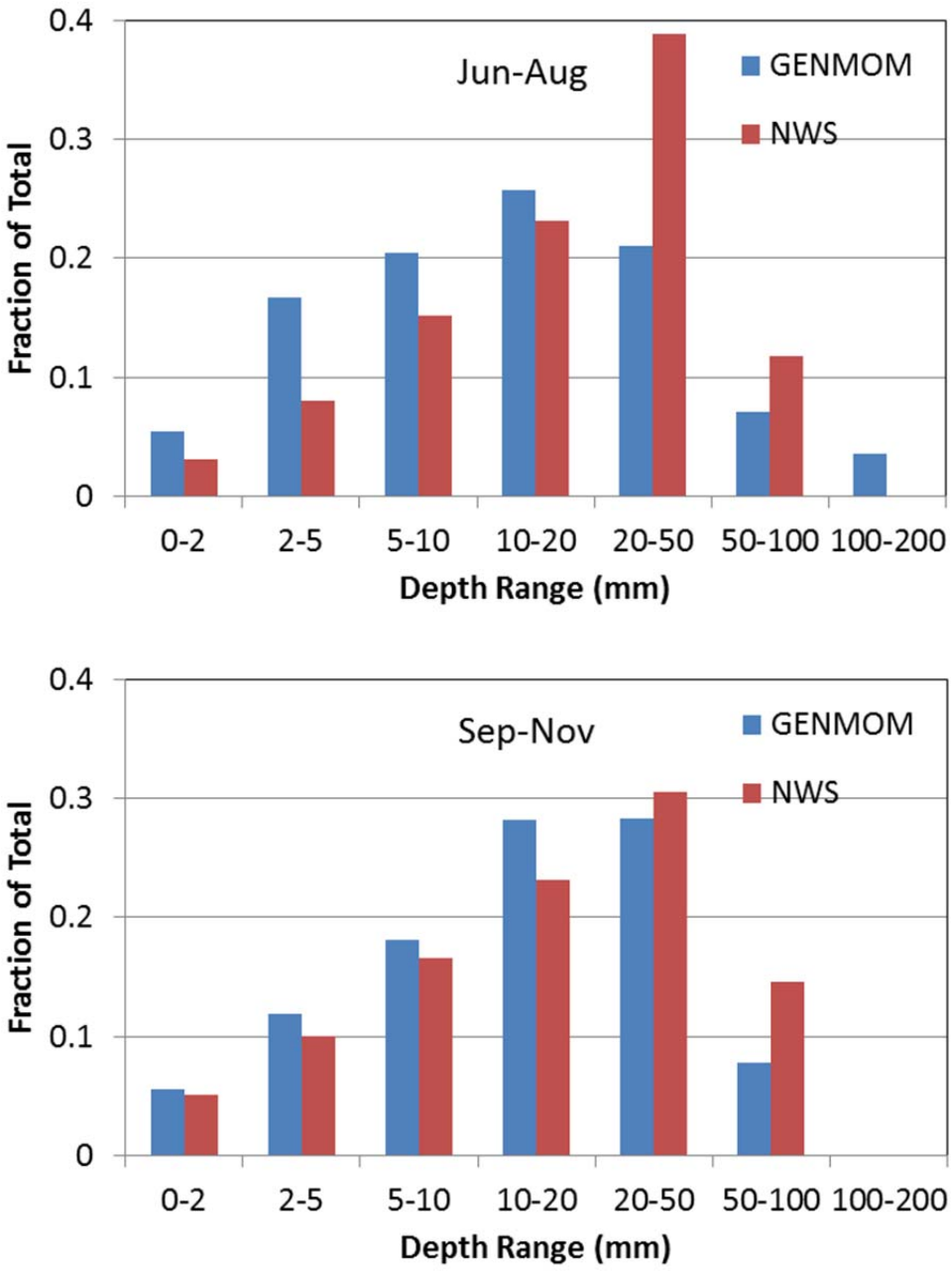

Figure 3.12. Seasonal distribution of seasonal precipitation fraction in ranges from 0-2 mm to 100-200 mm, for NWS observations at DLH and downscaled GENMOM output for the same location, 1980-1999, June-August (upper panel) and September-November (lower panel).

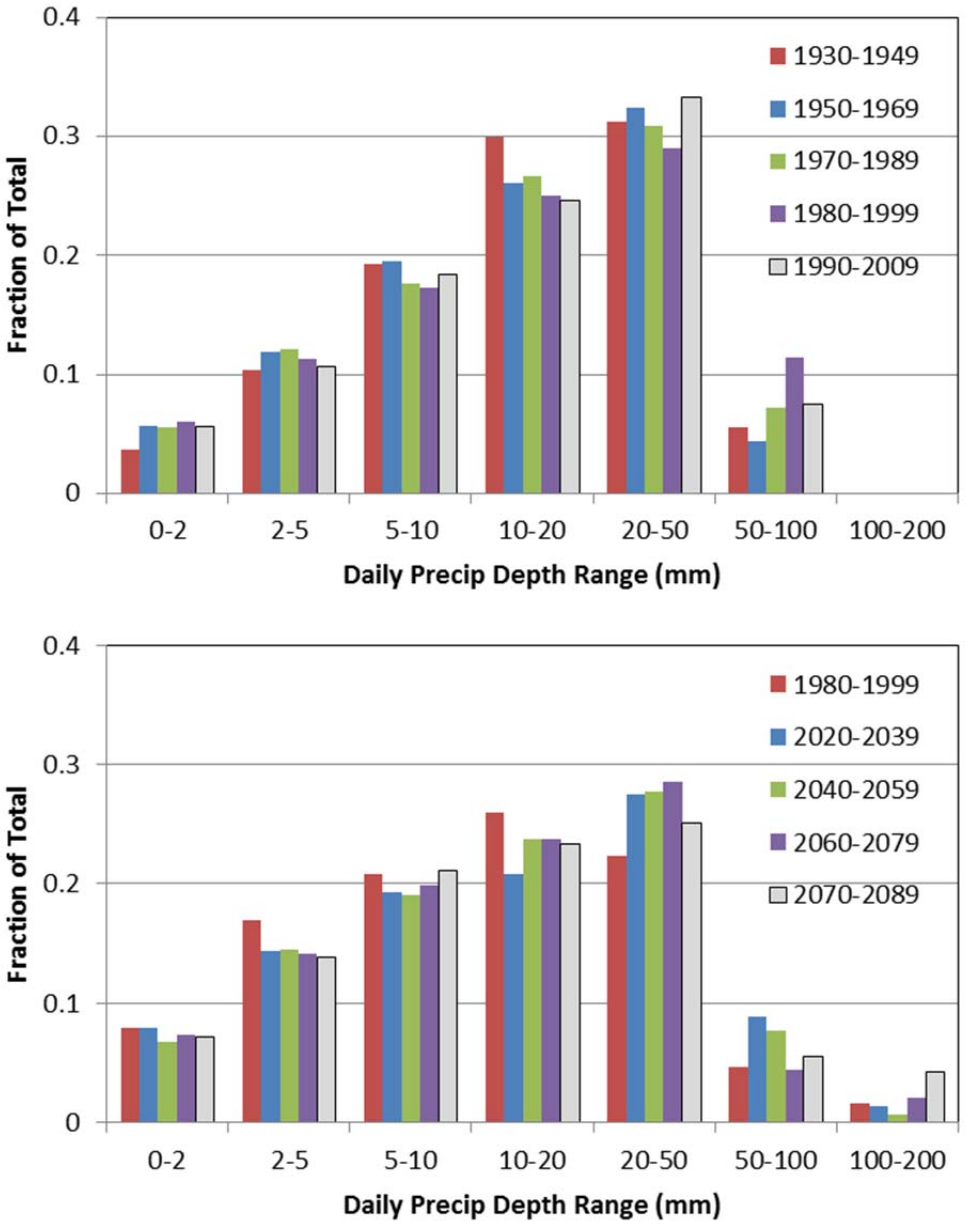

Figure 3.13. Distribution of total annual precipitation fraction in ranges from 0-2 mm to 100-200 mm, for historical NWS data (upper panel) and downscaled GENMOM projections (lower panel) for Duluth, MN.

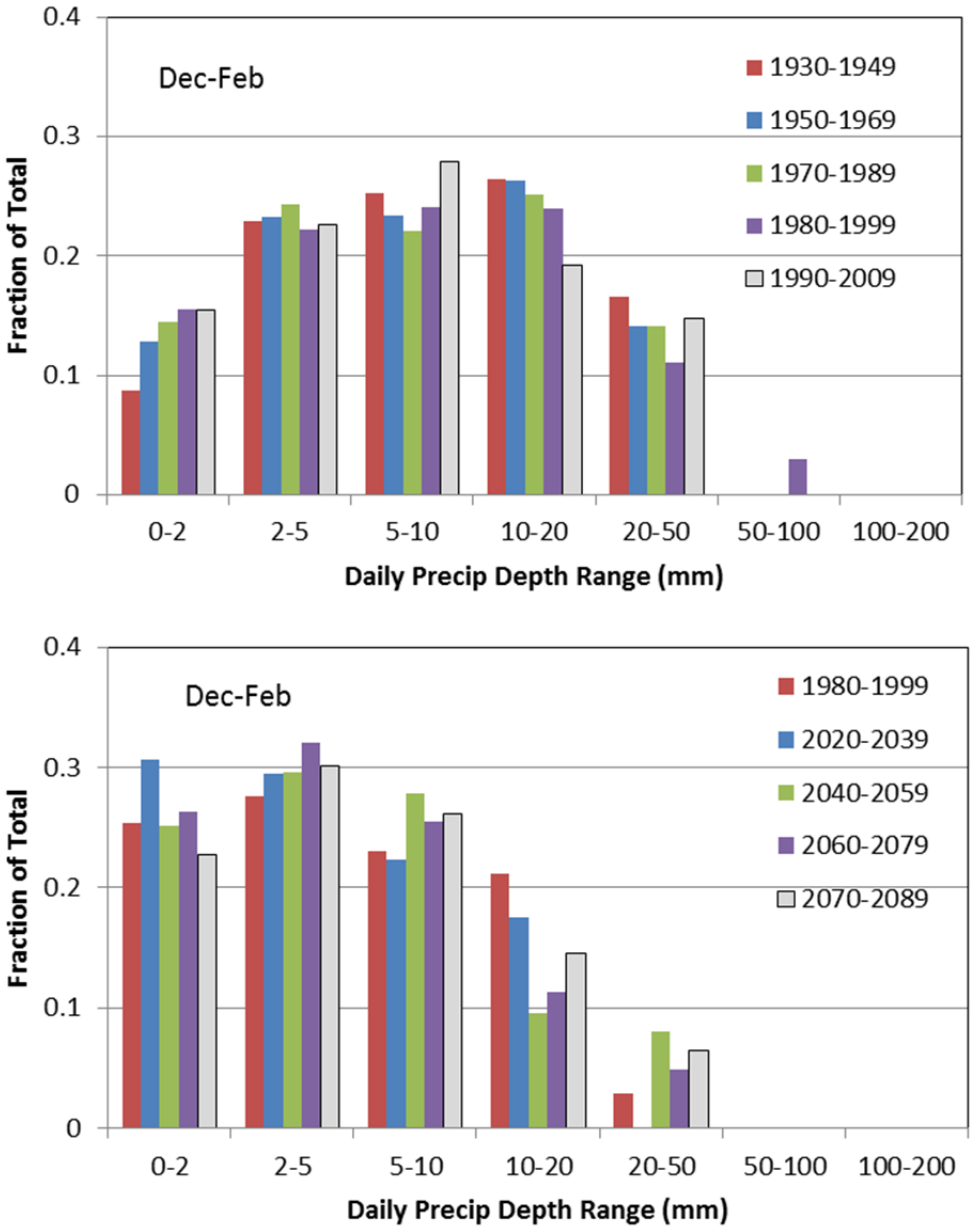

Figure 3.14. Distribution of seasonal precipitation fraction in ranges from 0-2 mm to 100-200 mm, for December – February, for historical NWS data (upper panel) and downscaled GENMOM projections (lower panel) for Duluth, MN.

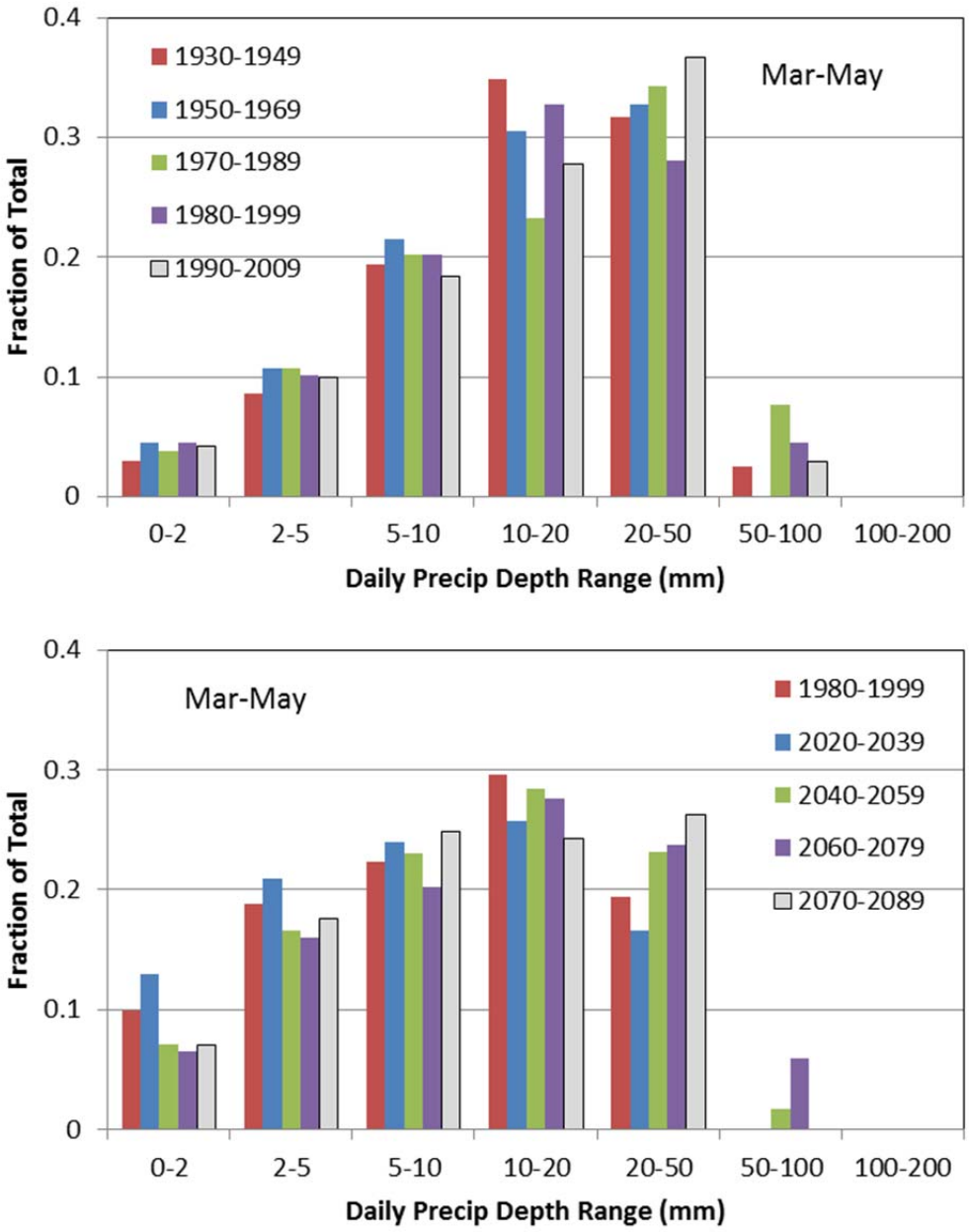

Figure 3.15. Distribution of seasonal precipitation fraction in ranges from 0-2 mm to 100-200 mm, for March - May, for historical NWS data (upper panel) and downscaled GENMOM projections (lower panel) for Duluth, MN.

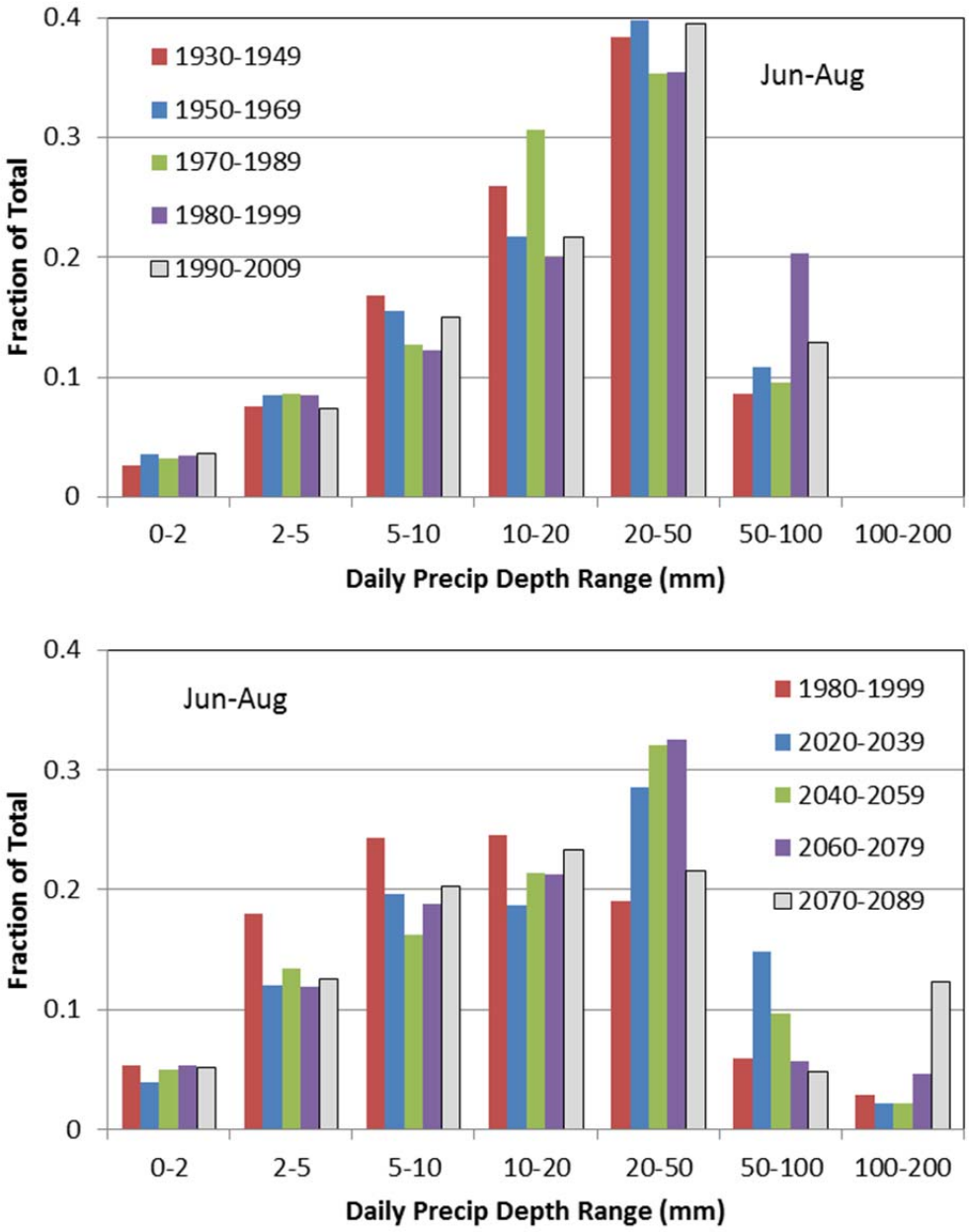

Figure 3.16. Distribution of seasonal precipitation fraction in ranges from 0-2 mm to 100-200 mm, for June - August, for historical NWS data (upper panel) and downscaled GENMOM projections (lower panel) for Duluth, MN.

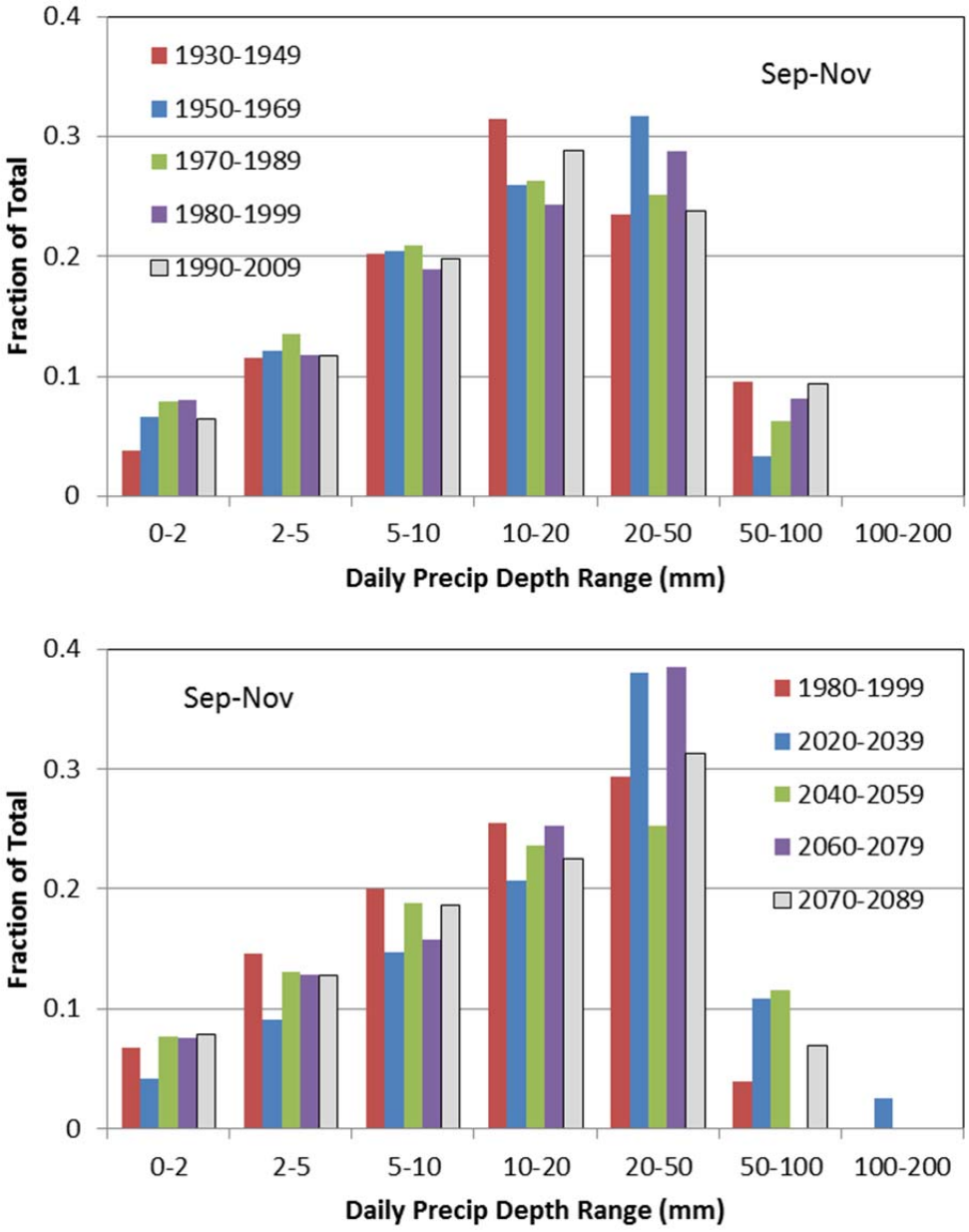

Figure 3.17. Distribution of seasonal precipitation fraction in ranges from 0-2 mm to 100-200 mm, for September - November, for historical NWS data (upper panel) and downscaled GENMOM projections (lower panel) for Duluth, MN.

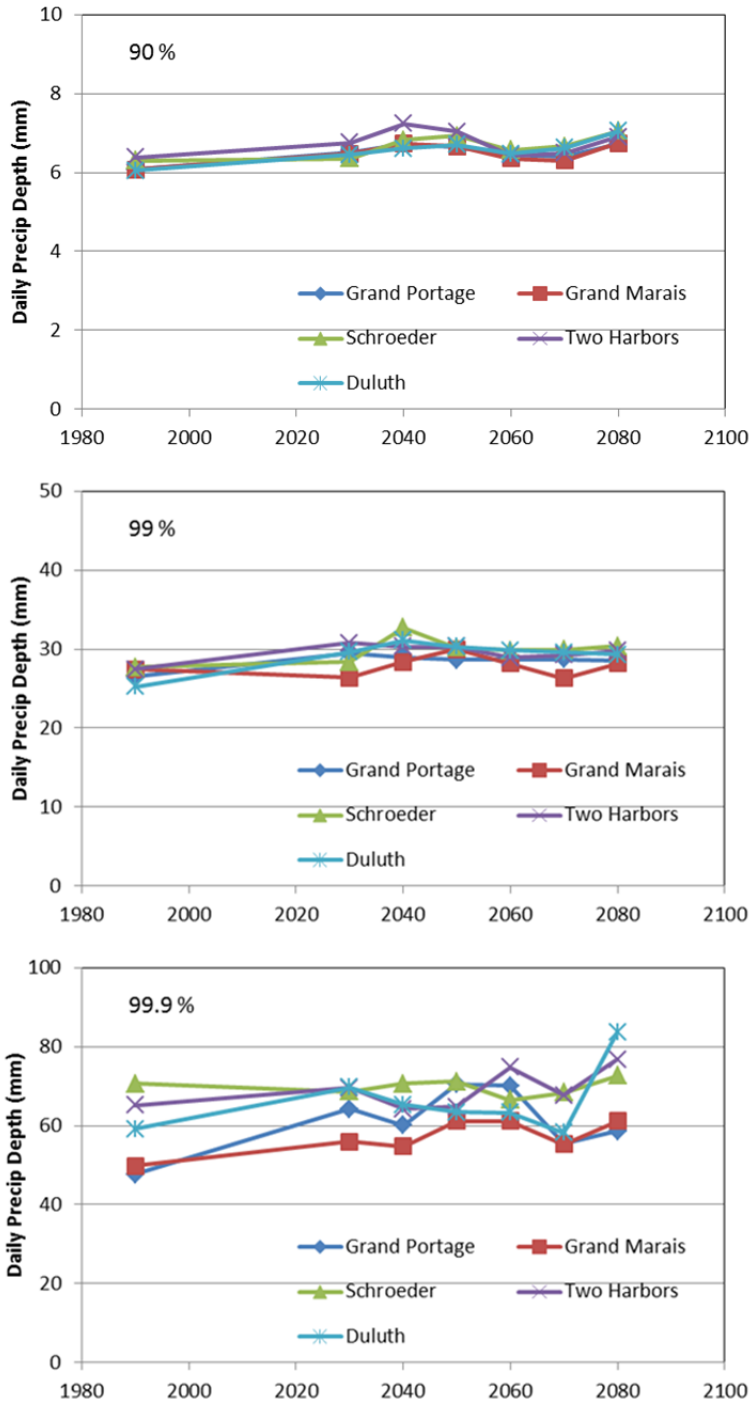

Figure 3.18. Ninetieth, 99th, and 99.9th percentile daily precipitation depth for historical NWS and projected GENMOM precipitation data for five north shore sites.

References

Hostetler, S.W., Alder, J.R. and Allan, A.M., 2011, Dynamically downscaled climate simulations over North America: Methods, evaluation and supporting documentation for users: U.S. Geological Survey Open-File Report 2011-1238, 64 p. (link)

IPCC, 2007. "Climate Change 2007 - Synthesis Report." The Fourth Assessment Report of the Intergovernmental Panel on Climate Change (IPCC), 2007, Cambridge University Press, Cambridge, United Kingdom and New York, NY, USA.

Nash, J. E. and J. V. Sutcliffe, 1970. River flow forecasting through conceptual models part I — A discussion of principles, Journal of Hydrology, 10(3), 282–290.

4. Empirical Models for North Shore Streamflow

To provide present and future streamflow estimates for north shore streams, an analysis was undertaken to relate streamflow observations to precipitation, air temperature, surficial geology, and land cover characteristics. For purposes of characterizing trout habitat, emphasis was placed on prediction of summer low flows and spring high flows. This strategy is similar to previous work in the Great Lakes basin to develop empirical models for ecologically-significant stream flows (Seelbach et al 2011). The Seelback study related August low flow, April high flow, and annual median flow to catchment area, precipitation, slope, surficial geology, and land use. The present study is localized to the north shore region, with the expectation that the unique hydrogeology of the region requires unique empirical models.

Other relevant background work includes the work by Detenbach et al. (2005) to relate stream flow characteristics and hydrologic storage to basin characteristics for Lake Superior tributary streams. Mature forest fraction and wetland fraction were found to be key parameters in determining hydrologic storage, low flow, and high flow characteristics. Neff et al. (2005) developed relationships between surficial geology and baseflow index for streams in the Great Lakes basin. Coarse-textured sediments associated with the highest baseflow index, and fine-textured and organic sediments associated with the lowest baseflow index. Another model was developed to add the effects of surface storage (lakes, wetlands) for regions where it contributes significant baseflow.

4.1 Spatial data

In addition to the stream gage, precipitation, and air temperature data summarized in Section 2, GIS spatial data sets compiled for this study included the 2001 NLCD land cover data set, the National Wetlands Inventory data set, the USGS quaternary geology layer, the STATSGO soil data, a lithology data layer assembled by the USGS Rocky Mountain Geographic Science Center, and a detailed forest plant community layer derived from White and Host (2000).

Based on the Minnesota DNR list of designated trout streams and the Minnesota DNR trout stream data layer, a set of 153 trout streams was assembled for Minnesota's Lake Superior north shore region. The set includes rivers that drain directly to Lake Superior, such as the Knife river, tributaries of these rivers, and tributaries of other rivers that are not trout streams (e.g. tributaries of the Pigeon River). A list of the 153 streams and a map of the extent of the drainage area of these streams is given in Appendix 4.1. The land cover and surface geology parameters were attributed to the cumulative (network) catchments of the 153 designated north shore trout streams which were delineated using ArcHydro. To evaluate how representative the 8 gaged catchments are of the 153 designated trout stream catchments, histograms of 9 parameters were generated for the 8 catchment and 153 catchment sets (Figure 4.1). Quat28 and Quat32 are specific quaternary geology types found to be significant in the regression analysis given in Sections II and III, and NWI wetland fraction is based on the total wetland area given by the National Wetlands Inventory. In general, the 8 catchments and 153 catchments have similar

parameter distribution, except for catchment area – the catchment area distribution of the 8 catchment set does not include smaller catchments (< 10 km^2) present in the 153 catchment set. The 8 catchment set also does not capture the wide variation in wetland fraction present in the 153 catchment set.

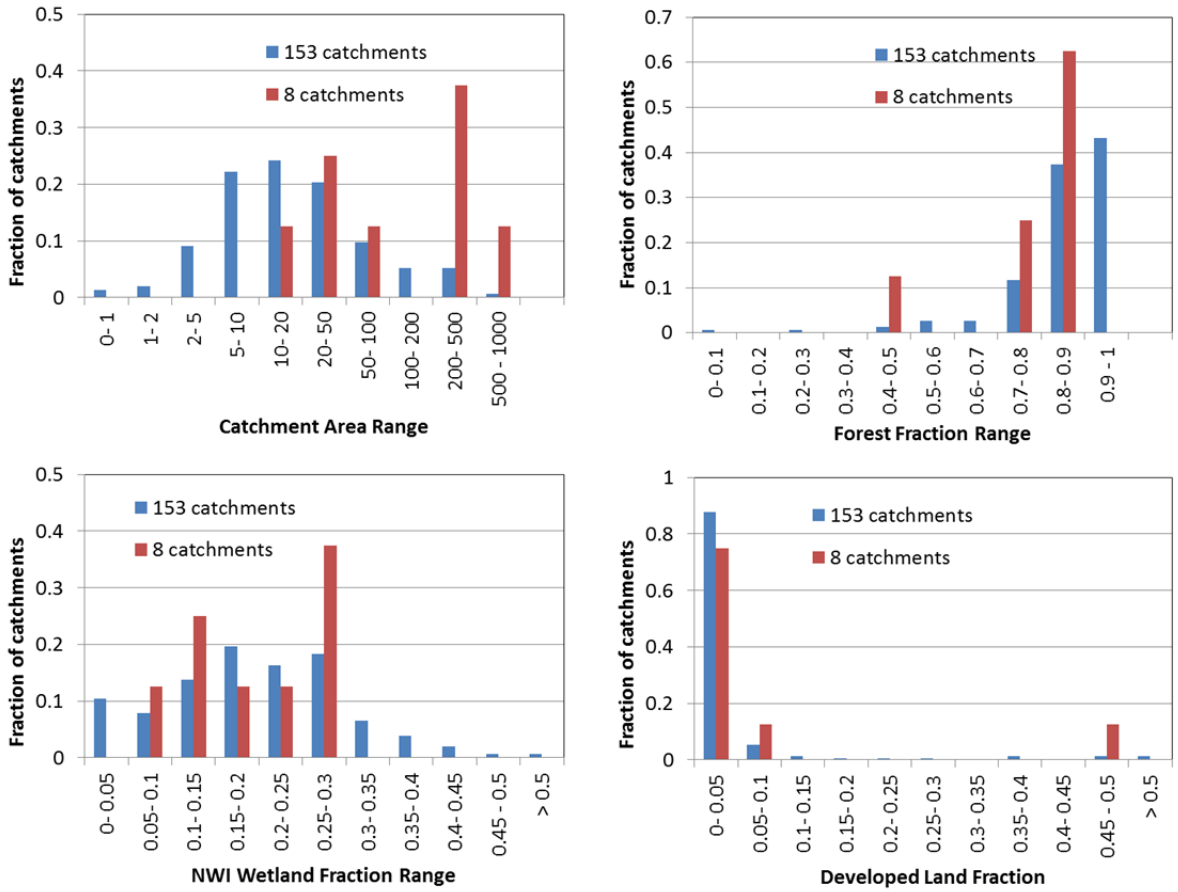

Figure 4.1. Distribution of various catchment land cover properties for the 153-catchment set and the 8 catchment subset with stream gages.

4.2 Regression equations for long-term average flows

August Q10 and April Q90 were calculated for eight north shore streams with available daily flow observations – the Knife Airport site was not used because it has only a 3-year record. For purposes of relating streamflow statistics to contemporary land cover, the analysis was restricted to the 30-year period 1981-2010. Full year flow statistics, such as annual mean (Q50) were not analyzed, because most flow records did not include winter data.

Using stepwise multiple linear regression to maximize adjusted r^2 and minimize the AIC score, the best August Q10 model was found to be:

$$\log(Q10) = c0 + c1*\log(Area) + c2*\log(NWI\_Wet) + c3*\log(Quat32) \qquad (4.1)$$

where area is the cumulative catchment area (m^2), NWI_Wet is the fraction of wetland area (including open water) in the cumulative catchment from the National Wetlands Inventory, and Quat32 is the fraction of quaternary geology type 'Superior Lobe--Mill Lacs-Highland Moraine'. No significant correlations were found between Quat32 and the STATSGO soil properties, e.g. sand fraction or permeability. Examination of more detailed, localized surficial geology maps for the region from the Minnesota Geological Survey does suggest, however, that the Quat32 type has a relatively high sand fraction compared to the geology types immediately adjacent to the Lake Superior shoreline. Note that precipitation depth was not a significant predictor of Q10, probably because there is minimal variation of precipitation between the stations. Eliminating the Quat32 variable from Eq. 4.1 reduces the adjusted r^2 from 0.96 to 0.80, and changes the significance level of the other variables from 0.05 to 0.1.

Similarly good results were obtained using the form of Eq. 4.1a, where Q10/Area, or flow yield, is the dependent variable:

$$\log(Q10/Area) = c0 + c2*\log(NWI\_Wet) + c3*\log(Quat32) \qquad (4.1a)$$

Applying Eq. 4.1 to all eight stations gives the coefficients in Table 3.1, with the adjusted r^2 = 0.958. The model worked slightly better using the NWI wetland fraction (adj. r^2 = 0.958, AIC=12.3) compared to the NLCD wetland fraction (adj. r^2 = 0.951, AIC=13.7).

The robustness of the model was evaluated using bootstrapping methods. Eq. 4.1 was applied to 56 combinations of 5 station subsets, with the results summarized in Table 3.4.

The best April Q90 model was found to be:

$$\log(Q90) = c0 + c1* \log(Area) + c2* \log(Quat28) \qquad (4.2)$$

where Quat28 is the fraction of quaternary geology type 'Superior Lobe - Nickerson Moraine'. Quat28 is highly correlated to sand fraction (r^2=0.89), but gives slightly better results compared to sand in the Q90 regression. As with Q10, precipitation was not found to be a significant predictor of Q90, probably because multi-year average precipitation does not vary greatly over the region. Table 5 summarizes the results of a bootstrapping analysis, by applying Eq. 4.2 to 56 combinations of 5 station subsets.

Table 4.1. Model fit results in program R for August Q10 for Eq. 4.1 applied to 8 north shore stream gages

	Estimate	*Std. Error*	t value	Pr(>|t|)
(Intercept)	Pr(>|t|)	3.84	-3.6	0.023
log(Area)	0.675	0.17	3.9	0.018
log(NWI_Wet)	1.615	0.48	3.3	0.029
log(Quat32)	-0.712	0.16	-4.4	0.012

Residual standard error: 0.395 on 4 degrees of freedom
Multiple R-squared: 0.976, Adjusted R-squared: 0.959

F-statistic: 55.02 on 3 and 4 DF, p-value: 0.0010

Table 4.2. Variation of Q10 model coefficients (Eq. 1) for 56 combinations of 5 station subsets.

	Intercept	Log(Area)	log(NWI_Wet)	log(Quat32)	Adj r^2
Max	50.3	1.32	8.97	-0.18	1.0
Min	-27.8	-2.24	0.40	-6.71	0.72
St Dev	10.0	0.46	1.17	0.86	0.057
Mean	-12.3	0.61	1.81	-0.89	0.94
Median	-13.1	0.64	1.60	-0.75	0.95

Table 4.3. Model fit results in program R for April Q90 for Eq. 4.2 applied to 8 north shore stream gages.

Parameter	Estimate	Std. Error	t value	Pr(>|t|
(Intercept)	-17.6	1.2	-15.0	<0.001
log(Area)	1.10	0.067	16.3	<0.001
log(Quat28)	0.23	0.052	4.48	<0.001

Residual standard error: 0.18 on 5 degrees of freedom
Multiple R-squared: 0.985, Adjusted R-squared: 0.980
F-statistic: 168.4 on 2 and 5 DF, p-value: 2.59e-05

Table 4.4. Variation of Q90 model coefficients (Eq. 2) for 56 combinations of 5 station subsets.

	Intercept	Log(Area)	log(Quat28)	Adj r^2
Max	-6.16	1.35	0.59	1.00
Min	-21.3	0.38	-0.53	0.92
St Dev	2.17	0.13	0.14	0.013
Mean	-17.8	1.11	0.24	0.98
Median	-17.7	1.11	0.23	0.98

4.3. Models for annual high and low flows

The models for mean annual flow statistics given in Section 4.2 relate Q10 and Q90 to catchment characteristics, but do not relate flows to precipitation or air temperature, and are therefore of limited use for projecting future streamflow regimes. To develop relationships between streamflow and precipitation, the flow and precipitation data were broken down into individual years, to introduce the inter-annual variability of precipitation into the empirical flow models. Since Q10 and Q90 are typically calculated based on multiple years of flow data, the highest weekly average streamflow in April (Q7high) and the lowest weekly averaged streamflow in August (Q7low) were used as the dependent flow variables in this analysis.

There were a total of 85 observations of August low flow (Q7low) for the 8 stream gages from 1981 to 2010. Q7low was found to depend on the same variables as Q10, but Q7low additionally depends on the total July/August precipitation (P78) and the May through August average air temperature (T58), as summarized in Eq. 4.3 and Table 4.6.

$$\log(Q7low) \sim \log(Area) + \log(P78) + \log(Quat32) + \log(NWI\_Wet) + \log(T58) \quad (4.3)$$

Using a linear or log transformed air temperature term gave similarly good results. Figure 4.2 plots the fitted vs. observed values of August low flow. Although the adjusted $r^2 = 0.81$, it is apparent the lowest values of August low flow are not predicted as well compared to the higher values. Omitting the Quat32 term from Eq. 4.3 reduces the predictive power of the model only slightly (adjusted $r^2 = 0.79$), and eliminates a variable that does not have obvious physical significance for streamflow:

$$\log(Q7low) \sim \log(Area) + \log(P78) + \log(NWI\_Wet) + \log(T58) \quad (4.3a)$$

There were a total of 69 observations of Q7high (highest April weekly average flow) available from the 8 north shore stream gages. Using all observations, Q7high was found to depend on catchment area (Area), total April precipitation (P4), average March/April air temperature (T58), with the adjusted r^2=0.86 (Eq. 4.3, Table 4.8). No additional catchment variables improved the fit. Adding in February and/or March precipitation totals to April precipitation did not improve

the fit. Using the same coefficients in a linear mixed model, with a random stream term, gave insignificant random terms (order of 1e-13).

$$\log(Q7high) \sim \log(Area) + \log(P4) + T34 \quad (4.4)$$

For the Q7high fit, using a linear temperature term (T34) worked significantly better than log transformed temperature. Table 4.9 summarizes the results of a bootstrapping analysis, by applying Eq. 4.4 to 100 random combinations of 40 station-year subsets from the full 69 station-year set. Overall, the precipitation coefficient shows the greatest variability in the bootstrapping analysis (mean =0.395, stan. dev. = 0.127). Figure 4.3 plots the fitted vs. observed values of April high flow. As with the August low flows, there is more scatter in the fit relationship for lower flow values.

Overall, good relationships were found between stream flows, precipitation, air temperature, and land cover characteristics for the north shore region. The available streamflow observations were limited to eight sites, and skewed towards larger catchment areas. The empirical relationships developed in this study agree with previous work in that surficial geology and wetland fraction are important determinants of hydrologic storage and stream high and low flow exceedances. Urban and agricultural land uses were not found to be significant predictors of streamflow characteristics. Empirical relationships developed using multi-year flow statistics did not include air temperature and precipitation, because these climate parameters do not vary significantly over the study region. Therefore, creating empirical streamflow relationships to precipitation and air temperature needed to consider inter-annual climate variability.

Table 4.5. Model fit results in program R for August low flow (Q7low) for Eq. 3.3 applied to 85 north shore stream gage-years.

	Estimate	Std. Error	t value	Pr(>|t|)
(Intercept)	-8.54	3.8	-2.2	0.027
log(Area)	0.737	0.10	7.1	<0.001
log(Pann2)	0.884	0.20	4.4	<0.001
log(NWI_Wet)	1.536	0.28	5.6	<0.001
log(Quat32)	-0.303	0.10	-2.9	0.0047
log(Tann)	-2.807	1.04	-2.7	0.0085

Residual standard error: 0.70 on 79 degrees of freedom
Multiple R-squared: 0.82, Adjusted R-squared: 0.81
F-statistic: 73.2 on 5 and 79 DF, p-value: < 0.0001

Table 4.6. Model fit results in program R for August low flow (Q7low) for Eq. 3.3a applied to 85 north shore stream gage-years.

	Estimate	Std. Error	t value	Pr(>|t|
(Intercept)	-8.871	4.0	-2.2	0.028
log(Area)	0.791	0.11	7.4	<0.001
log(Pann2)	0.784	0.21	3.8	<0.001
log(NWI_Wet)	1.473	0.29	5.1	<0.001
log(TANN)	-2.888	1.1	-2.7	0.0096

Residual standard error: 0.73 on 80 degrees of freedom
Multiple R-squared: 0.80, Adjusted R-squared: 0.79
F-statistic: 81.76 on 4 and 80 DF, p-value: < 0.0001

Table 4.7. Variation of Q7low model coefficients (Eq. 3) for 100 random selections of 40 station subsets from the 85 observations.

	Intercept	Log(Area)	log(P78)	log(Quat32)	log(NWI_Wet)	T78	Adj r^2
Max	-1.61	1.14	1.87	-0.034	2.36	-0.010	0.92
Min	-22.0	0.301	0.079	-0.491	0.683	-0.362	0.73
StDev	3.69	0.151	0.363	0.082	0.341	0.060	0.046
Mean	-13.5	0.751	0.887	-0.295	1.453	-0.202	0.82
Median	-13.6	0.761	0.845	-0.299	1.419	-0.204	0.83

Table 4.8. Model fit results in program R for April high flow (Q7high) for Eq. 4 applied to 69 north shore stream gage years.

	Estimate	Std. Error	t value	Pr(>|t|)
(Intercept)	-17.3	1.0	-16.9	< 0.001
log(Area)	0.988	0.053	18.5	<0.001
log(P4)	0.397	0.099	4.0	<0.001
T34	-0.133	0.022	-6.1	<0.001

Residual standard error: 0.45 on 65 degrees of freedom
Multiple R-squared: 0.86, Adjusted R-squared: 0.86
F-statistic: 136.4 on 3 and 65 DF, p-value: < 0.0001

Table 4.9. Variation of Q7high model coefficients (Eq. 4) for 100 random selections of 40 station subsets from the 69 observations.

	Intercept	Log(Area)	log(P4)	T34	Adj r^2
Max	-14.9	1.14	0.769	-0.047	0.92
Min	-20.4	0.854	0.115	-0.185	0.79
StdDev	1.089	0.056	0.127	0.021	0.025
Mean	-17.1	0.978	0.395	-0.135	0.86
Median	-16.9	0.972	0.391	-0.137	0.86

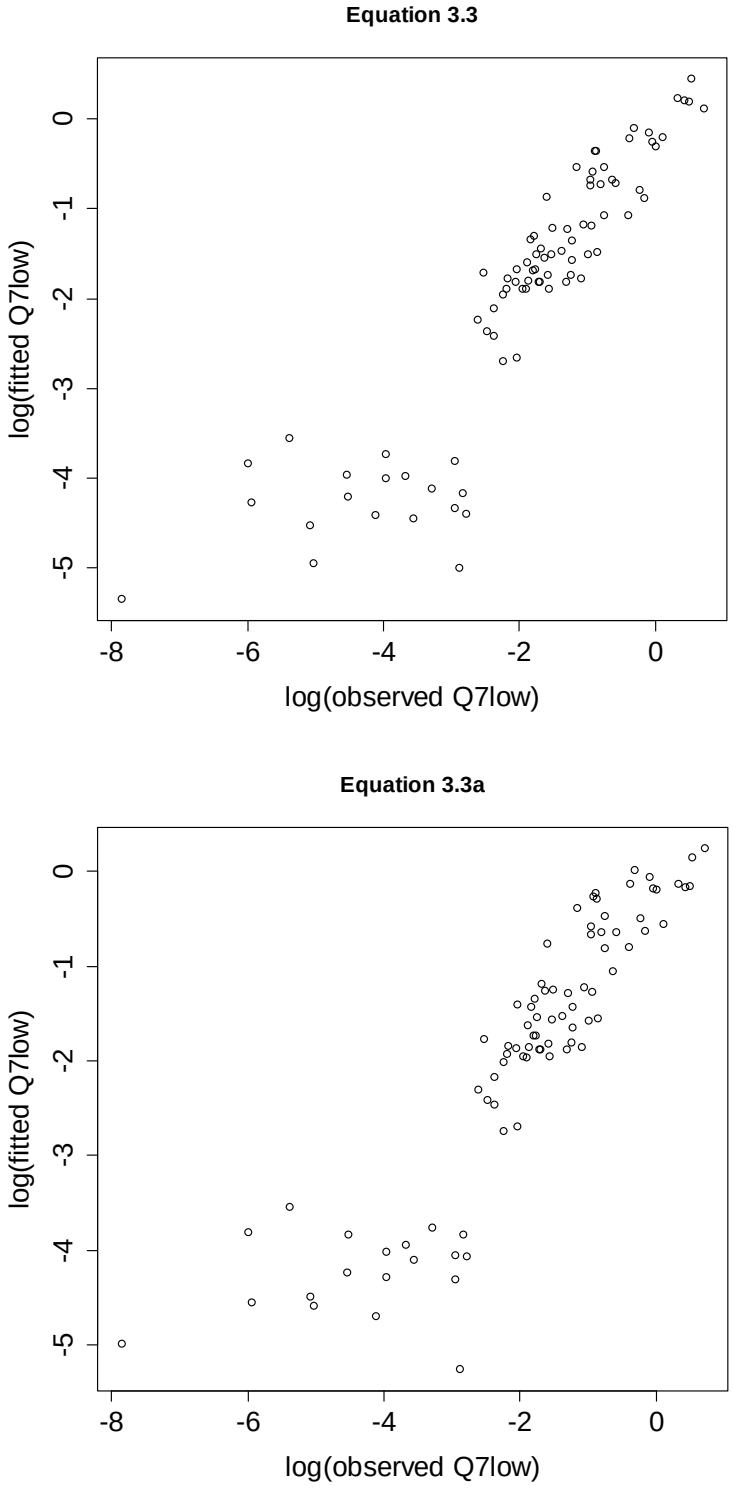

Figure 4.2. Fitted vs. observed August low flow (Q7low) for Eq. 4.3 (upper panel) and Eq. 4.3a (lower panel) applied to 89 observations at 8 north shore streams.

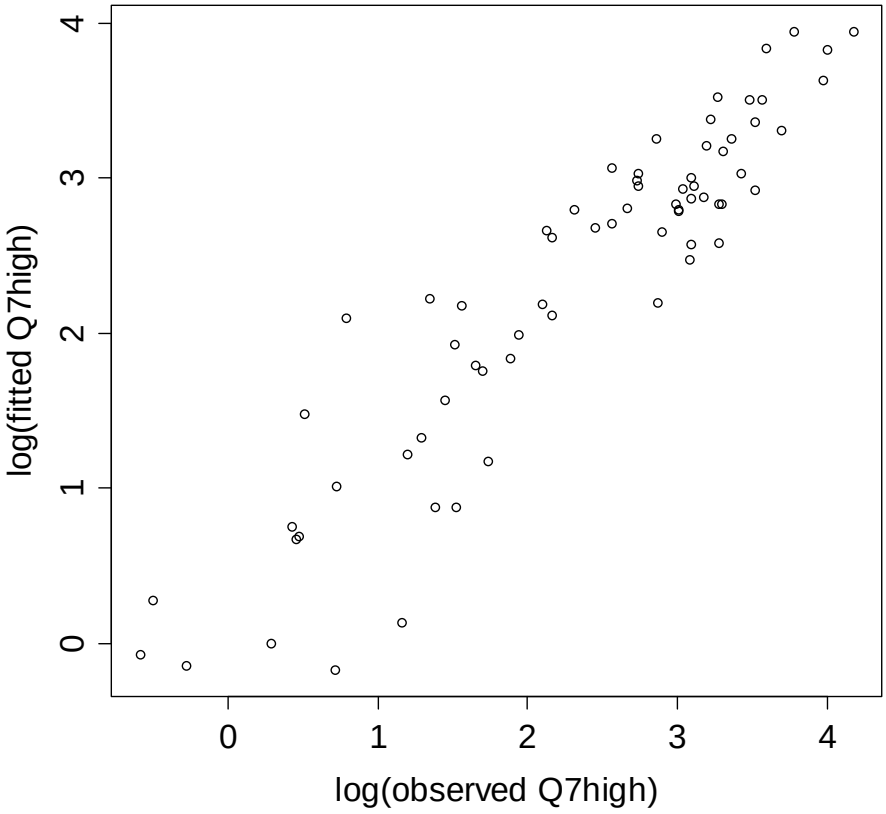

Figure 4.3. Fitted vs. observed April high flow (Q7high) for Eq. 4 applied to 89 observations at 8 north shore streams.

References

Detenbeck, N.E., Brady, V.J., Taylor, D.L., Snarski, V.M., Batterman, S.L., 2005. Relationship of stream flow regime in the western Lake Superior basin to watershed type characteristics. Journal of Hydrology 309, 258–276.

Neff, D.A., Day, S.M., Piggott, A.R., Fuller, L.M., 2005. Base Flow in the Great Lakes Basin, Scientific Investigations Report 2005-5217, US Geological Survey, Washington, D.C.

Seelbach, P.W., Hinz, L.C., Wiley, M.J., Cooper, A.R., 2011. Use of Multiple Linear Regression to Estimate Flow Regimes for All Rivers Across Illinois, Michigan, and Wisconsin. Michigan Department of Natural Resources, Fisheries Division Report 2095, Lansing, MI, 31 pp.

White, M. A. and G. E. Host. 2000. Mapping range of natural variation ecosystems classes for the northern Superior uplands: draft map and analytical methods. Natural Resources Research Institute Technical Report NRRI/TR-2000/39. 13 p.

5. Deterministic Water Budget Models for North Shore Trout Streams

The following is a summary of work in progress at SAFL on a deterministic hydrologic model to predict streamflows in trout streams on the north shore of Lake Superior. The model will be operated in conjunction with a model to predict stream temperatures. Model results are expected to be useful to project trout habitat in north shore streams under projected climate scenarios and for water management decisions.

5.1 Hydrologic (water budget) model development

The hydrologic model was developed using the structure of MINRUN96, previously developed by Mohseni and Stefan (1998) with emphasis on water budget components and climate parameter connections. MINRUN96 is a lumped parameter water budget model that estimates stream flow on a monthly time scale. MINRUN96 is attractive because it uses a modular approach to the water budget, estimates streamflow year round (has a snow melt routine) and was developed using the Baptism River in Northeast Minnesota as an example. It uses a water budget approach to estimate four components of streamflow: (1) baseflow, (2) interflow, (3) direct runoff, and (4) snowmelt. A flow chart for MINRUN96 is given in Figure 5.1.

The model input requires specification of physical characteristics of the watershed including watershed area, stream length, overland slope, percent forest cover, soil properties (porosity, field capacity, wilting point, hydraulic conductivity). Some physical properties are used as calibration parameters including root zone depth, critical solar radiation for onset of snowmelt, shading factor. Climate variables that are necessary as model input include air temperature and dew point, solar radiation, percent cloud cover, precipitation, and wind speed. Two climate properties are used as calibration parameters: number of rain days in each month and number of rain days that produce runoff.

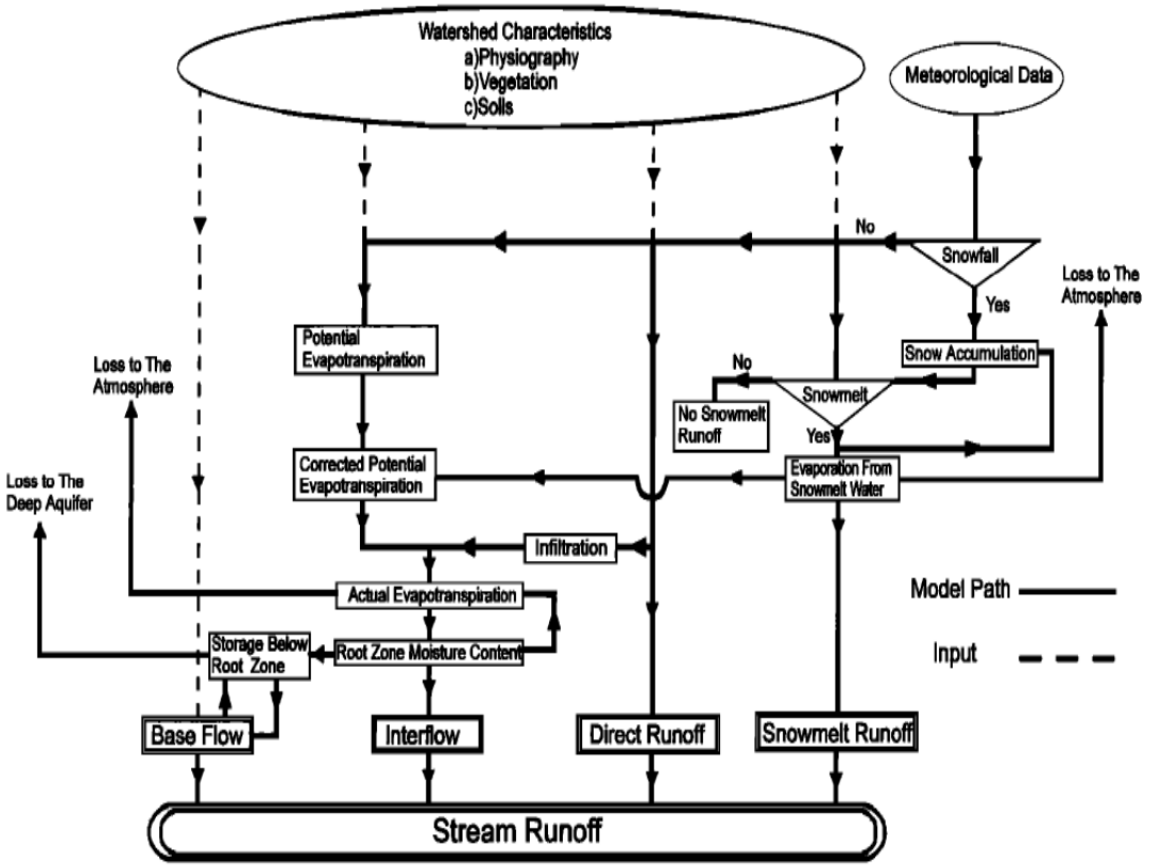

Figure 5.1. Flow chart for the MINRUN96 stream flow model (from Mohseni and Stefan 1998).

The model estimates streamflow as the sum of four components: direct runoff, snowmelt, interflow, and baseflow. Direct runoff is estimated by using a runoff coefficient depended on soil moisture, precipitation intensity, and a calibrated monthly probability that rainfall will generate runoff. An energy (heat) balance used to estimate snowmelt runoff from the snow stored in the watershed. Interflow estimation uses the water budget and an interflow coefficient along with an effective drainage area. Baseflow is dependent on the water stored below the root zone and soil properties and is lagged by one month to account for travel time through the ground. Evapotranspiration is estimated using the Penman-Moneith method (Allen, 1992).

Timescale of the hydrologic stream flow model

The MINRUN96 stream flow model uses a monthly timescale to estimate the water budget and streamflow components. This timescale is ideal for a water budget approach, since the timescale of the runoff processes for most components of the water budget and streamflow are less than a month. A monthly timescale may, however, be to coarse a timescale for modeling stream temperature since the variability in stream temperature, especially at low flows will be lost. Mean monthly stream water temperatures can give an idea of seasonal variations, but fish habitat, (survival, growth, reproduction, etc.) depends on weekly or daily water temperatures.

To investigate the timescale of actual north shore stream responses, statistical methods correlograms of stream flows were created. A correlogram is a plot of the correlation statistic p against a time lag. Separate correlograms were created for mean weekly streamflow, for stormflow, and for baseflow. With a time lag in weeks, the correlogram shows the dependence of stream flow on the flows in previous weeks, i.e., it is a measure of the memory of the system, and can be used to see over what time periods stream runoff responds to previous events. First, correlograms of mean weekly stream flows were created for eight streams include the Pigeon, Baptism, and Knife rivers. (Figure 5.2). Then daily streamflows were separated into the stormflow and baseflow components using a digital filter described in Nathan and McMahon (1990). Correlograms of storm flows and base flows were created with this information (Figures 5.3 and 5.4).

Mean weekly streamflows in the Baptism River and the Knife rivers show a memory up to 5 weeks (Figure 5.2), the Pigeon River shows a dependence up until 7 weeks. The longer dependence in the Pigeon River is most likely due to the larger size of watershed. The dependence of stormflows on previous weeks vanishes more rapidly than that of mean weekly streamflow (Figure 5.3). Baseflow shows an extended dependence on previous streamflows, ranging from 5 weeks to 8 weeks (Figure 5.4). All three correlograms give the expected results: stormflow occurs at a relatively fast timescale (1 to 3 weeks) and baseflow is dependent on events that occur over a much longer time (5 to 8 weeks).

These timescales suggest that 1) for unmodified version of MINRUN96, a monthly timescale model would be appropriate, and 2) to run the model at a weekly time step, a simple routing algorithm is needed to give appropriate delays between precipitation events and streamflow peaks at the outlet of the watershed.

For the purposes of this study, a set of calibrated, fixed delays were added to the MINRUN96 model, such that the total stream discharge at the outlet of a watershed is composed of surface runoff from weekly precipitation up to 5 weeks prior:

$$Q_i = \sum_{j=0}^{n} c_j \cdot q(i-j)\, Q_i = \sum_{j=0}^{n} c_j \cdot q(i-j) \qquad (5.1)$$

where Q_i is the total surface runoff discharge at the watershed outlet for the current time, q is the calculated surface runoff due to precipitation at time step (i-j), and c_j are the calibrated weighting coefficients.

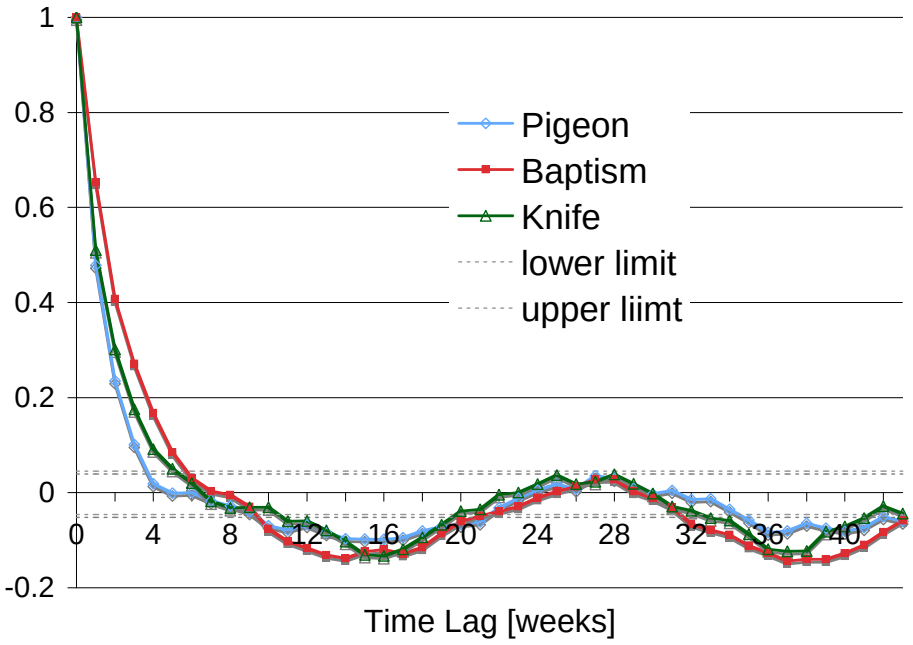

Figure 5.2. Correlograms for weekly streamflows in three north shore trout streams.

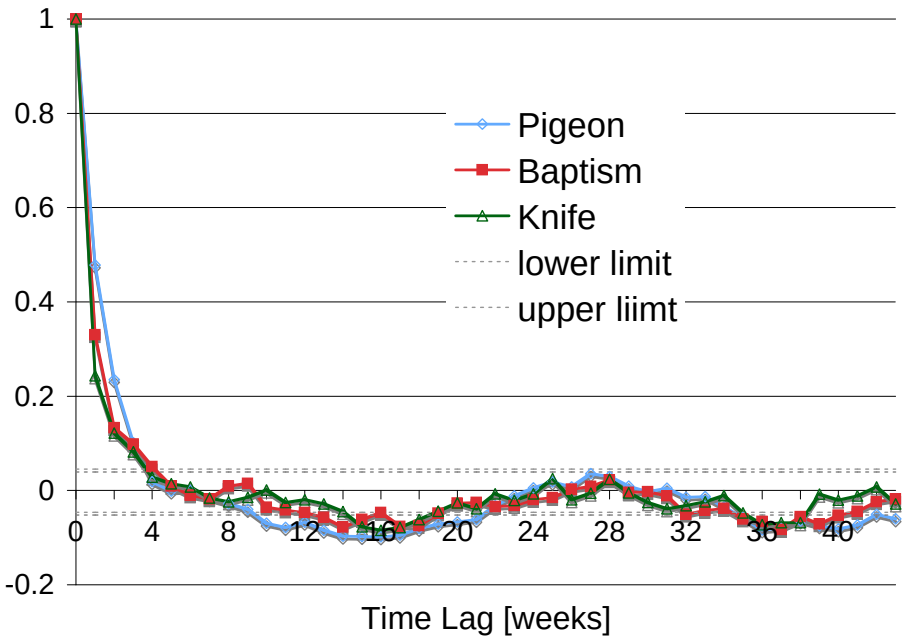

Figure 5.3. Correlograms for weekly stormflows in three north shore trout streams.

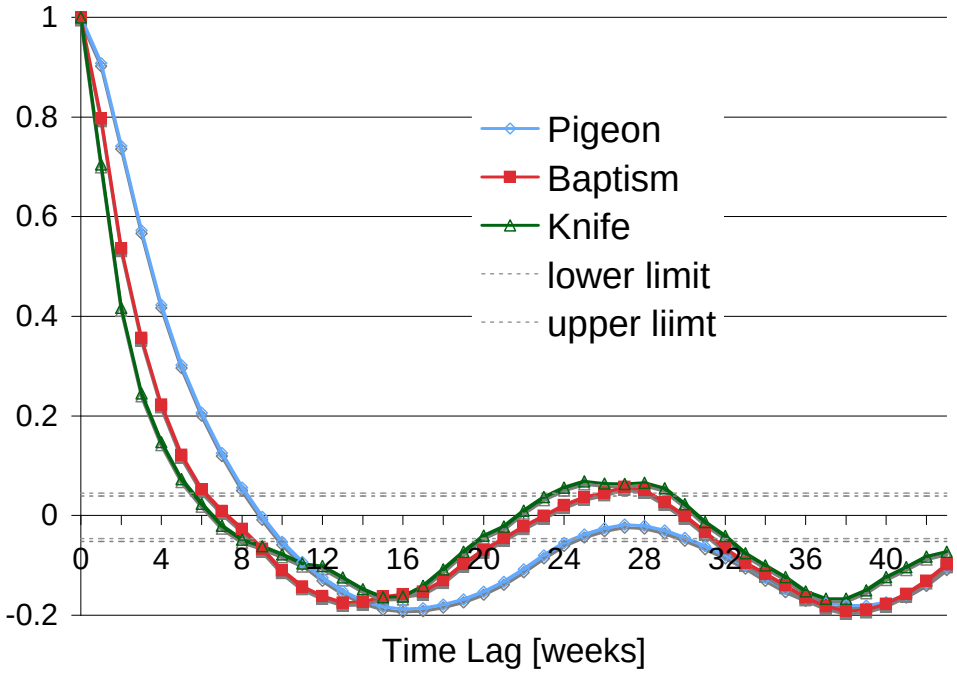

Figure 5.4. Correlograms for weekly baseflows in three north shore trout streams.

Surface water storage

Water storage in the watershed is a most important hydrologic process especially for low flow maintenance in trout streams. Water storage in watersheds of the north shore trout streams can be expected to be in wetlands, bogs, forests and only to a minor degree in the subsoil. This is very different from the large, shallow aquifer that feeds the Vermillion River, and from the Karst systems that feed trout streams in the driftless area.

The MINRUN96 model does not have a surface water storage component; it has two soil storage components (root zone and below root zone) that release water as interflow and baseflow. A surface storage component was added to make the model more robust and applicable to streams with significant water storage in lakes, ponds, and wetlands. The surface storage component may act much like the soil storage routines, have both evapotranspiration and a head-driven flow routine. Two model parameters are used to assign a fixed fraction of the watershed to be surface storage, and to route a fixed fraction of surface runoff to surface storage. For example, 10% of the watershed can be defined as surface storage, with 20% of the watershed contributing surface runoff to surface storage. The release of water from surface storage depth (q_{out}) and the current depth of surface storage (d_i), and are calculated for each time step based on Equations 5.2 and 5.3:

$$q_{out} = f_1 \cdot A \cdot (d_{i-1})^k \quad q_{out} = f_1 \cdot A \cdot (d_{i-1})^k \tag{5.2}$$

$$d_i = d_{i-1} + \frac{f_2 \cdot (q_i - q_{out}) \cdot \Delta t}{f_1 \cdot A} \quad d_i = d_{i-1} + \frac{f_2 \cdot (q_i - q_{out}) \cdot \Delta t}{f_1 \cdot A} \tag{5.3}$$

where f_1 is the fraction of the total watershed area (A) assigned to surface storage, f_2 is watershed fraction contributing runoff to surface storage, and q_i is the total surface runoff for the current time step.

5.2 Hydrologic model calibration

The hydrologic model was calibrated for 3 north shore trout streams with year-round flow records: Amity Creek, the Baptism River, and the Knife River (Figure 5.5). The characteristics of the three case study stream systems are summarized in Table 5.1. The precipitation station used as model input for each stream is also given in Table 5.1. Other climate data needed for model input (air temperature, humidity wind speed) were taken from DLH. Solar radiation observations are generally unavailable for the region, so that simulated solar radiation values obtained from the National Solar Radiation Data Base (http://rredc.nrel.gov/solar/old_data/nsrdb/).

Many of the model parameters were set based on spatial data for the region, e.g. watershed area, percent forest cover (National Land Cover Database 2001) and soil characteristics (STATSGO). The seasonal crop coefficients for the Penman-Monteith evapotranspiration (ET) model were adjusted to obtain a seasonal water balance, but were set the same for all three watersheds. In

general, there is a lack of information on ET rates and coefficients for forests in the region, in particular, for the seasonal variation of ET for deciduous versus evergreen forests.

Once an approximate water balance was achieved, several additional parameters were adjusted to improve the R^2 of the relationship between simulated and observed weekly stream discharge, the Nash-Sutcliffe metric (Nash and Sutcliffe, 1970), and general agreement of the simulated and observed flow duration curves. The surface storage coefficients were the main parameters that were varied between the three watersheds: f1, f2 and k in Equations 5.3 and 5.4. The calibrated surface storage fraction (f1) is strongly related to the actual watershed wetland fraction taken from the National Wetlands Inventory (Figure 5.8).

Partial records of simulated and observed runoff time series are given in Figure 5.6 for the 3 sites. Note that the Amity Creek gage had had no winter available. The corresponding flow exceedance plots are given in Figure 5.7. Overall, the success of the hydrologic model calibration process for each site was strongly related to how well stream flow observations were correlated to precipitation data (Section 2.5), with the Knife River model giving the best R^2 and Nash-Sutcliffe coefficient (Table 5.2) and the best correlation of observed monthly precipitation and streamflow (R^2=0.59, Figure 2.11b). Although the hydrologic model for Amity Creek had relatively low predictive ability (R^2=0.2), it nonetheless provides a case study for a watershed with low hydrologic storage.

Table 5.1. Summary of the three case study watersheds for the north shore stream study.

Name	Amity Creek	Baptism River	Knife River
Watershed Area (sq. km)	43	355	225
Mean Slope (%)	4.71	5.27	4.72
Forest Cover (%)	80	88	87
Wetland Cover (%)	1.2	30	16
Developed Cover (%)	2.0	0.17	0.15
Flow Record Start Year	2002	1928	1974
Flow Record, No. Complete Years	6	63	36
Precipitation Station	Duluth Int. Airport	Isabella	Two Harbors

Table 5.2. Summary of the model accuracy achieved for the three watersheds.

	Amity Creek	Baptism River	Knife River
R^2	0.20	0.35	0.50
Nash-Sutcliffe	-0.20	0.34	0.47

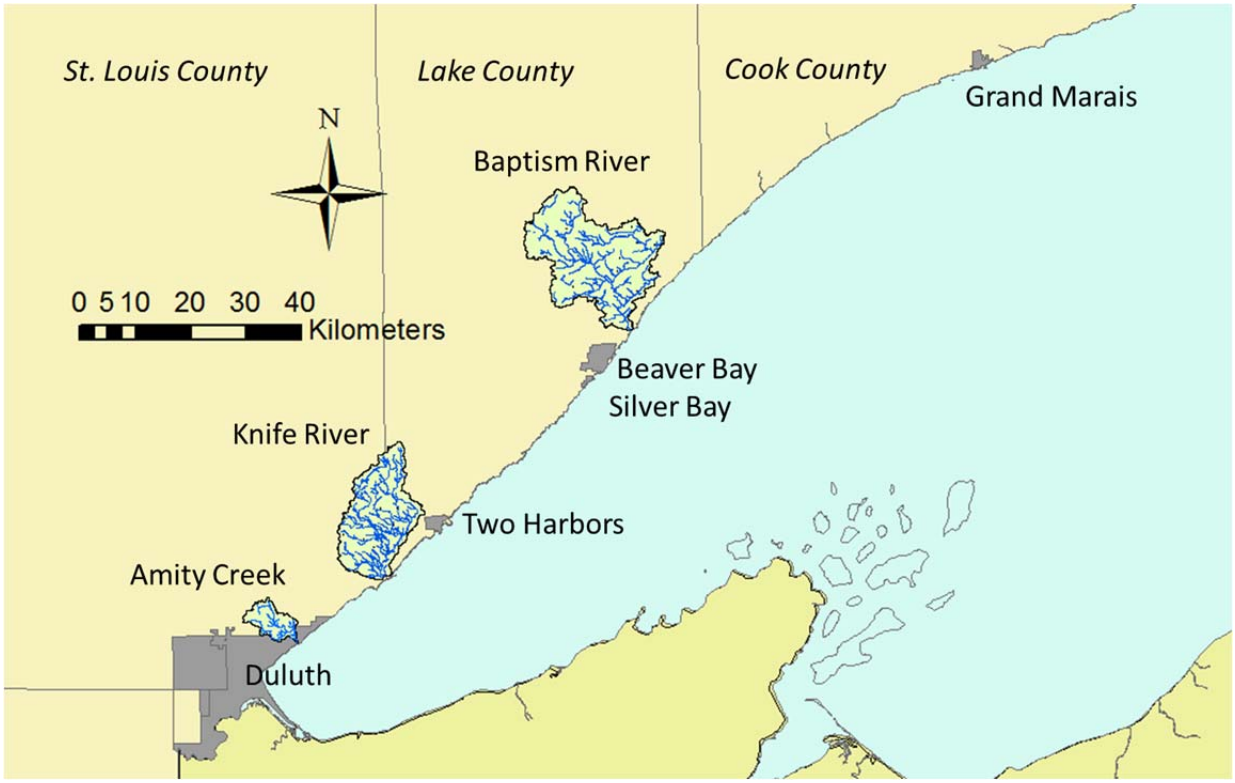

Figure 5.5. Location of the three case study streams along the Lake Superior north shore in St. Louis and Lake counties, Minnesota.

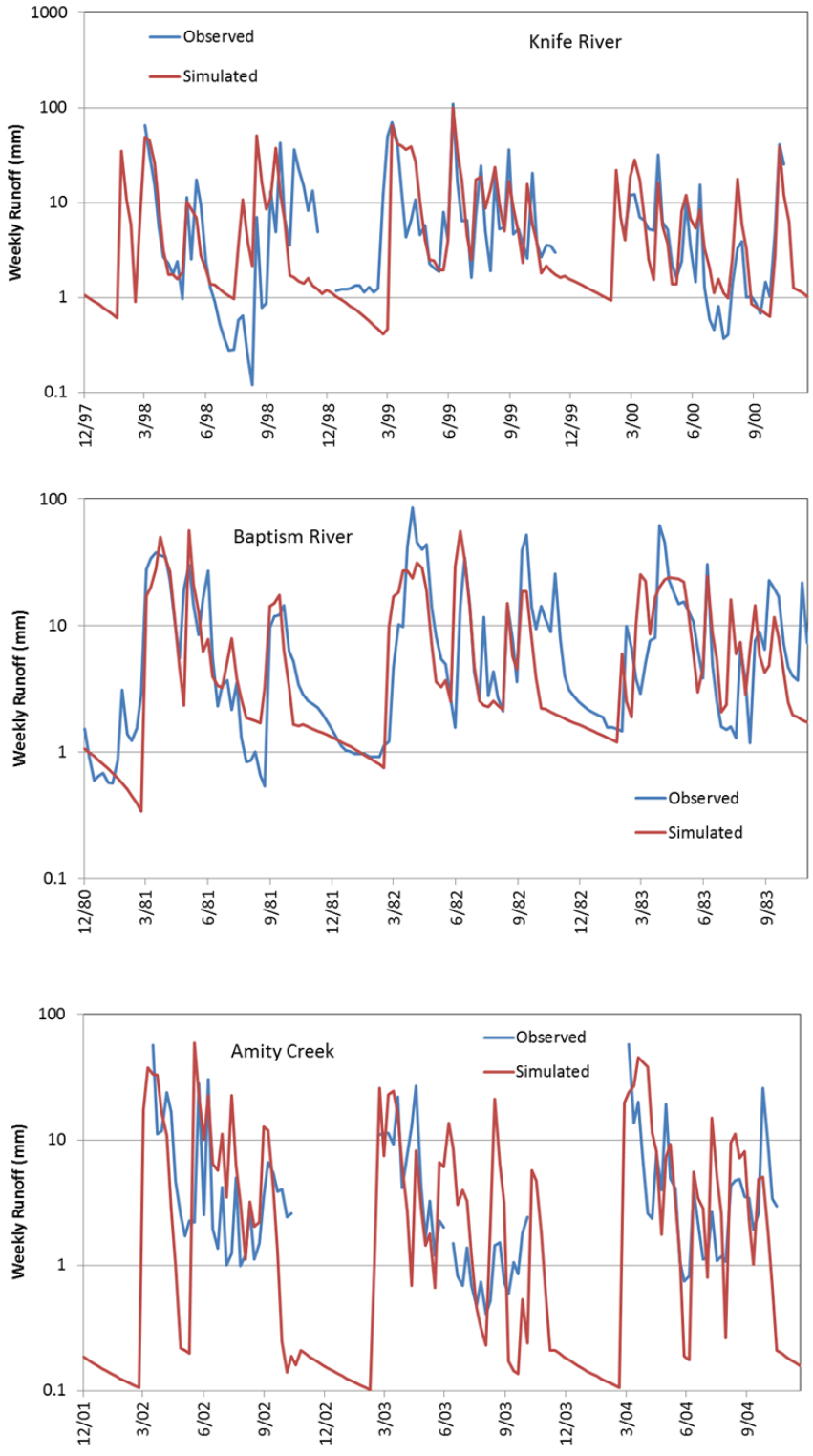

Figure 5.6. Observed and simulated runoff time series for the Knife River, the Baptism River, and Amity Creek.

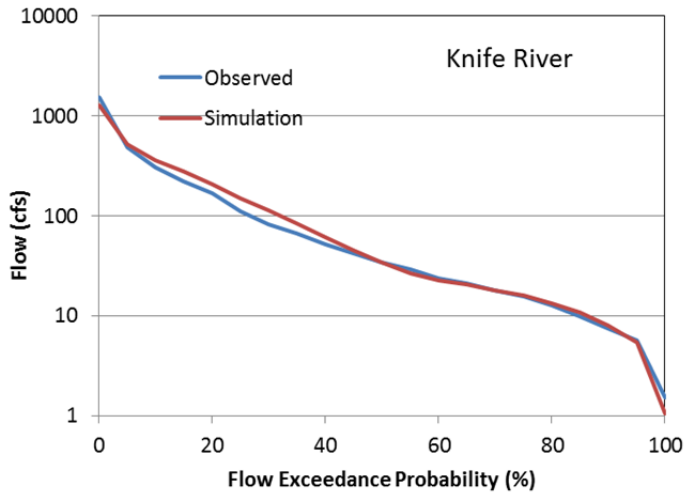

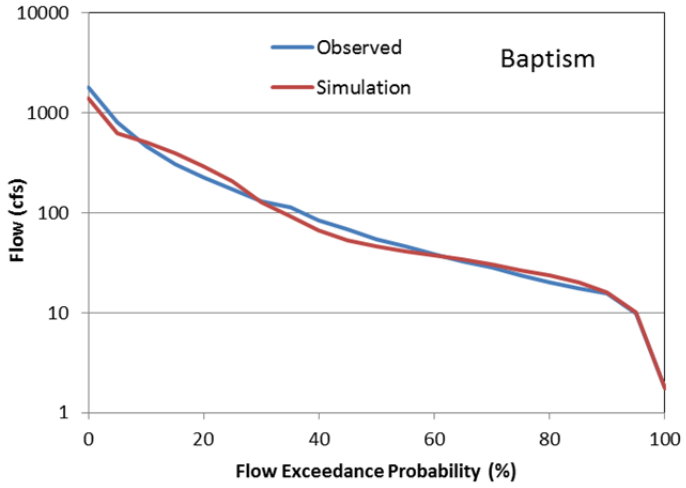

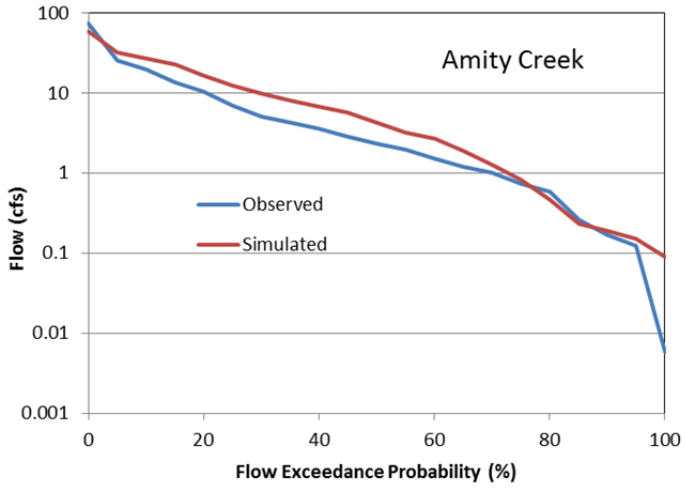

Figure 5.7. Observed and simulated flow exceedance curves for the Knife River, the Baptism River, and Amity Creek.

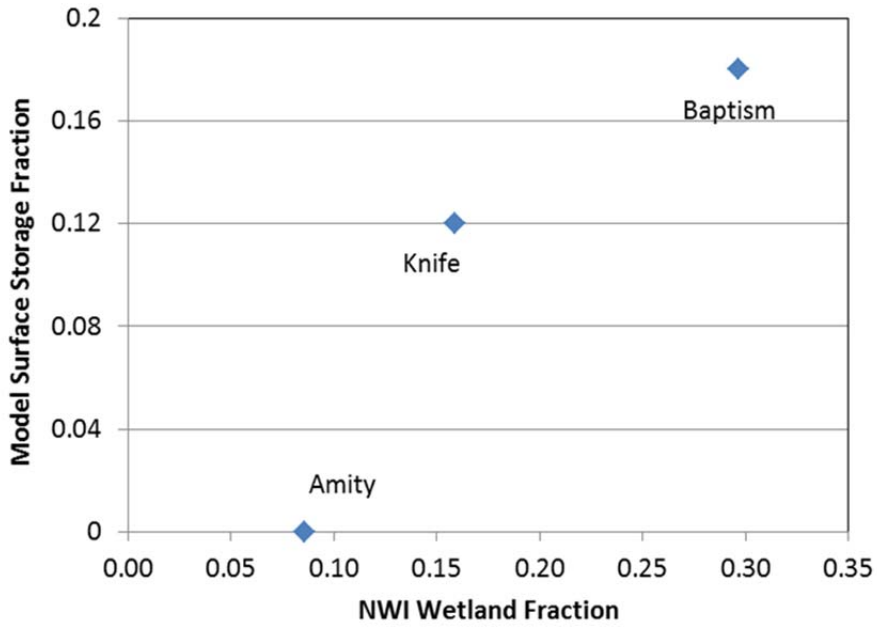

Figure 5.8. Calibrated surface storage fraction vs. actual wetland fraction (National Wetlands Inventory) for the Knife River, the Baptism River, and Amity Creek.

5.3 Sensitivity analysis of the hydrologic model

The calibrated hydrologic budget model for the Knife River was used as a basis for a climate sensitivity analysis. This analysis gives insight on the sensitivity of hydrology to changes in climate that are not dependent on GCM predictions.

The change in streamflow statistics was evaluated for uniform increments in air temperature, dew point, precipitation, and wind speed. The baseline climate was the historical Duluth (airport), 1980-99. For air temperature and dew point temperature, the increment was applied as an additive increase (+1 °C), while precipitation and wind speed were multiplied by a factor of 1.1. The sensitivity to air temperature was evaluated by itself, and then the sensitivity to an increase in both air temperature and dew point temperature was evaluated. The sensitivity to dew point temperature was not evaluated separately, since increasing dew point temperature while keeping air temperature fixed leads to nonsensical humidity values (RH > 100%).

The sensitivity of stream flow to the various climate increments was evaluated as seasonal changes in the streamflow percentiles, e.g. the seasonal median (50%), low flow (10%), and high flows (90%), as summarized in Table 5.3. 20-year average monthly water budget components are given in Figures 5.10 and 5.11 for the baseline climate conditions and for a 1 °C increase in air temperature.

The change in streamflow due to an increase in air temperature are due to 1) increased ET and 2) shifts in precipitation from snow to rain (the water budget model assumes precipitation to be

snow or rain based on the ambient air temperature). The annual mean streamflow decreases 1.9% for the 1 °C increase in air temperature, due to increased evapotranspiration. Winter streamflow generally increases with increasing air temperature, as more precipitation falls as rain. The lower snowpack leads to lower spring streamflow. As ET becomes significant in summer, increasing air temperature leads to decreased stream flow, with the mean and median streamflow decreasing by 5.8 and 6.7% for the 1 °C increase in air temperature. As ET becomes less significant in the autumn, streamflow increases as more precipitation falls as rain. Low flows (10%) behave somewhat differently over the seasons compared to median and high flows. For example, higher ET during summer decreases stored water in the soil, and leads to lower autumn baseflow, while more precipitation as rain in autumn and winter leads to higher winter baseflow.

Increasing air temperature (TA) and dew point temperature (TD) together gives somewhat different results compared to increasing air temperature alone (Table 5.3, 5.4). Increasing humidity along with air temperature tends to reduce evapotranspiration rates, as the gradient in humidity from plants, open water, and soil to the atmosphere is lower. For the case of increasing TA and TD together, mean summer streamflow and summer baseflow decrease less (1% and 7.9%, respectively) compared to the case of increasing TA alone (2% and 13.7%, respectively). In spring, increasing TD along with TA gives further reductions in streamflow via increases in net radiation that tend to shift snowmelt towards late winter.

Increasing precipitation by 10% (a multiplicative factor of 1.1) gives the expected result of increased streamflow, with the predicted percent increase in streamflow generally exceeding the 10% increase in precipitation. Since only about 45% of precipitation is translated into streamflow, with the rest lost to ET, a 10% increase in precipitation increases the available water (precip-ET) by more than 10%. Increasing wind speed by 10% (a multiplicative factor of 1.1) gave measurable decreases in low flows, due to increased evapotranspiration and evaporation from open water.

The sensitivity of the peak spring snowmelt and the spring peak streamflow to increases in air temperature were also evaluated separately, as summarized in Table 5.5. The peak spring snowmelt and streamflow see only moderate changes in magnitude and timing with a 1 °C increase in air temperature, with the simulated streamflow peak decreasing by about 2% and the peak timing shifting earlier in the year by 1 day.

Table 5.3. Mean, 10, 50, and 90 percentile streamflow, in cms, for baseline Duluth climate and for incremented climate, based on the calibrated Knife River water budget model.

		Streamflow (cms)				
Season	Percentile	Baseline	+ Ta	+ Ta, Td	+ Precip	+ Wind
Full	10	0.104	0.124	0.118	0.155	0.095
Full	50	0.539	0.541	0.529	0.611	0.526
Full	90	7.54	7.042	6.92	8.72	7.33
Full	Mean	2.22	2.18	2.15	2.64	2.21
Winter	10	0.057	0.053	0.054	0.096	0.050
Winter	50	0.214	0.232	0.230	0.268	0.213
Winter	90	0.487	0.493	0.488	0.547	0.486
Winter	Mean	0.458	0.474	0.445	0.514	0.455
Spring	10	0.051	0.077	0.074	0.073	0.048
Spring	50	1.49	1.39	1.335	1.82	1.493
Spring	90	11.6	11.5	11.09	12.2	11.6
Spring	Mean	3.99	3.76	3.68	4.51	3.97
Summer	10	0.350	0.302	0.323	0.379	0.348
Summer	50	0.851	0.816	0.813	0.994	0.833
Summer	90	6.82	6.12	6.12	8.37	6.15
Summer	Mean	2.29	2.24	2.27	2.80	2.28
Autumn	10	0.255	0.215	0.228	0.304	0.227
Autumn	50	0.549	0.575	0.557	0.632	0.536
Autumn	90	4.43	4.71	4.70	5.40	4.54
Autumn	Mean	1.78	1.90	1.89	2.16	1.77

Table 5.4. Percent change in mean, 10, 50, and 90 percentile streamflow for incremented climate parameters, based on the calibrated Knife River water budget model.

		% Change			
Season	Percentile	+1 Ta	+ Ta, Td	+ Precip	+ Wind
Full	10	18.5	13.6	49.0	-8.47
Full	50	0.42	-1.80	13.4	-2.31
Full	90	-6.56	-8.12	15.7	-2.71
Full	Mean	-1.87	-3.07	18.8	-0.54
Winter	10	-7.28	-6.77	68.1	-13.0
Winter	50	8.49	7.74	25.6	-0.28
Winter	90	1.32	0.33	12.5	-0.16
Winter	Mean	3.44	-2.92	12.2	-0.73
Spring	10	50.4	44.7	43.1	-5.75
Spring	50	-6.71	-10.6	21.8	-0.08
Spring	90	-0.42	-4.02	5.71	0.00
Spring	Mean	-5.79	-7.87	13.2	-0.49
Summer	10	-13.8	-7.90	8.20	-0.59
Summer	50	-4.06	-4.47	16.9	-2.10
Summer	90	-10.2	-10.3	22.6	-9.87
Summer	Mean	-2.12	-1.02	22.1	-0.44
Autumn	10	-15.6	-10.5	19.3	-10.9
Autumn	50	4.77	1.42	15.1	-2.24
Autumn	90	6.35	6.12	21.9	2.38
Autumn	Mean	6.65	6.26	21.5	-0.53

Table 5.5. Sensitivity of 20-year average spring snowmelt and streamflow peak to a 1 °C uniform increase in air temperature, based on the calibrated Knife River water budget model.

	Nominal Climate		Ta + 1 °C	
	Snowmelt	Streamflow	Snowmelt	Streamflow
Peak rate (cms)	10.5	12.8	9.7	12.5
Stan dev (cms)	2.7	4.2	2.9	3.6
Median date (day-month)	14-Apr	15-Apr	13-Apr	14-Apr
Stan dev (days)	11.1	14.5	8.8	13.0

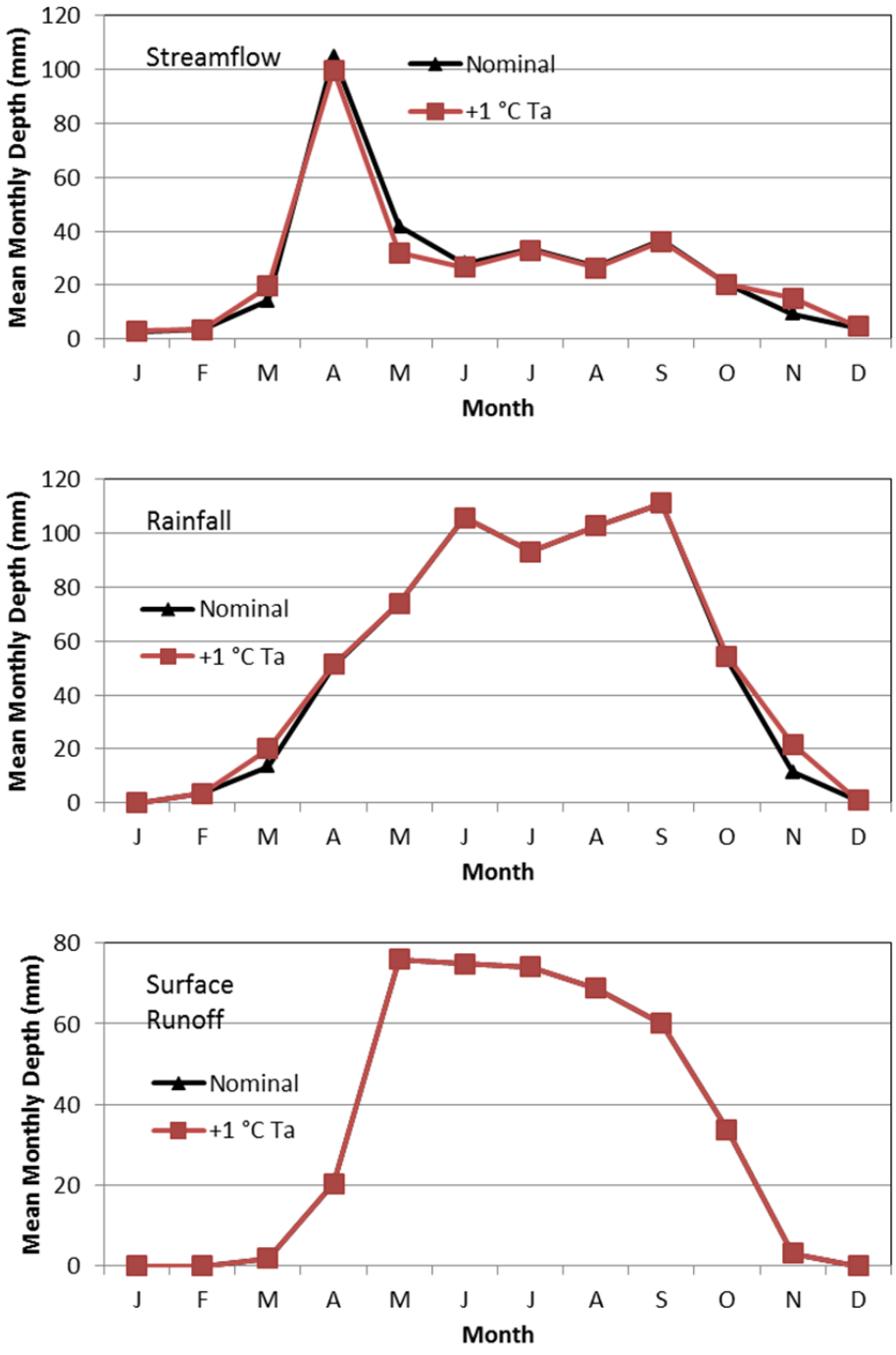

Figure 5.9. Simulated average monthly streamflow, rainfall, and surface runoff for the Knife River, for 1980-99 Duluth climate and for nominal conditions with a 1 °C uniform increase in air temperature.

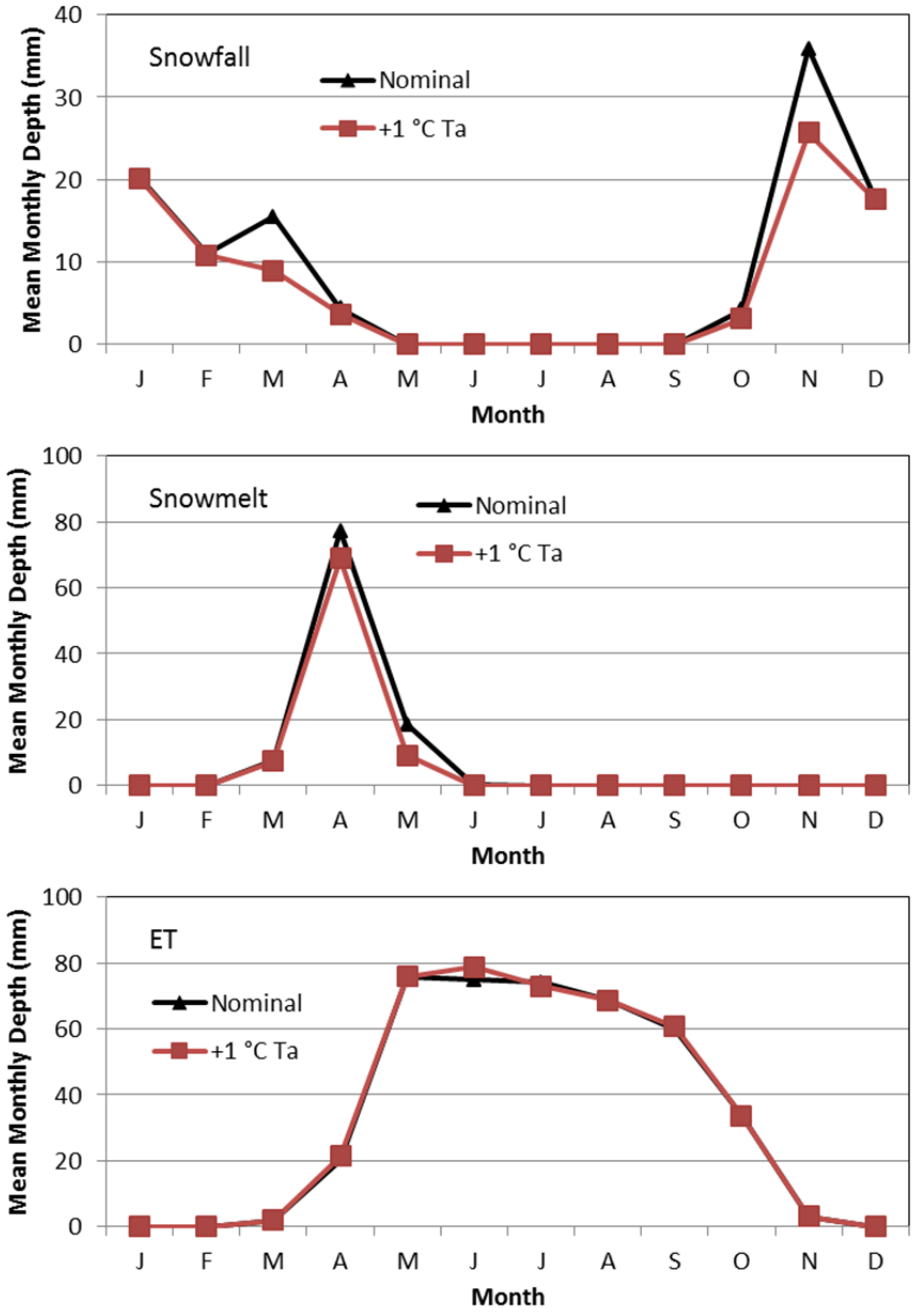

Figure 5.10. Simulated average snowfall, snowmelt, and ET for the Knife River, for 1980-99 Duluth climate and for nominal conditions with a 1 °C uniform increase in air temperature

References

Mohseni, O., Stefan, H.G., 1998. A monthly streamflow model. Water Resources Research 34, 1287–1298.

6. Hydrologic Response of North Shore Streams to Climate Change

The downscaled RegCM3 climate projections described in Section 5 were used as input to both the deterministic hydrologic models described in Section 4 and the empirical streamflow models described in Section 3. The analysis summarizes in this section focuses on results obtained using the downscaled GENMOM GCM climate projections (A2 scenario), but results for the GFDL and ECHAM5 model are also included. Results are given first for the monthly climate increments, followed by results using daily time series of future climate.

6.1 Response to projected monthly climate increments (deterministic hydrologic models)

The analysis given here emphasizes the Knife River hydrologic model, because it is the intermediate case in surface storage capacity and because this model was the most accurate of the three cases studies. The calibrated hydrologic model for the Knife River was run for baseline Duluth climate (1980-1999) and for Duluth climate with the monthly GCM increments applied for the periods 2020-39, 2040-59, 2060-79, and 2070-89, as summarized in Section 5.

The projected hydrologic response of the Knife River to future climate is summarized in Figures 6.1 to 6.7. The response of the full season flow duration curves to the GCM climate increments is given in Figure 6.1, and broken down by season in Figures 6.2 to 6.5. Overall, increased flow rates (cfs) are projected in winter (Figure 6.2) and autumn (Figure 6.5) for all three GCMs. Spring median and high flows are projected to be fairly stable, but low flows are projected to increase (Figure 6.3), probably due to changes in the distribution between rainfall and snow. Summer flows are also projected increase slightly (Figure 6.4). The projected trends in annual median flows, spring high flows, and summer low flows for the Knife River are illustrated more explicitly in Figures 6.6 and 6.7. From the 1980-99 period to the 2070-89 period, the median annual flow is projected to increase from 19.2 cfs to 22.2 cfs based on the GENMOM increments and to 24.3 cfs based on the ECHAM5 increments (Figure 6.6). August low flows (90% and 99% exceedance) are projected to be relatively stable, although the ECHAM5 model projects a modest increase in August 90% exceedance flows (Figure 6.6). April high flows (1% and 10% exceedance) are projected to vary ±15% over the four time periods, and generally do not undergo systematic trends (Figure 6.7). The end of the century flows, however, are predicted to be somewhat lower than the 1980-1999 period.

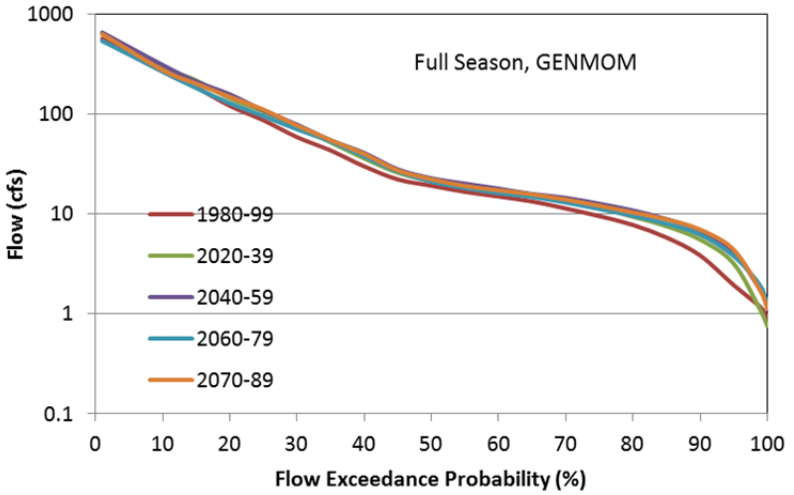

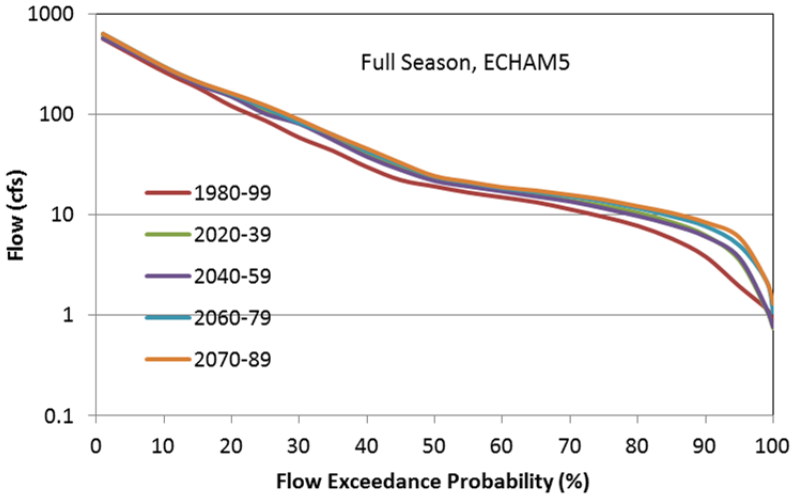

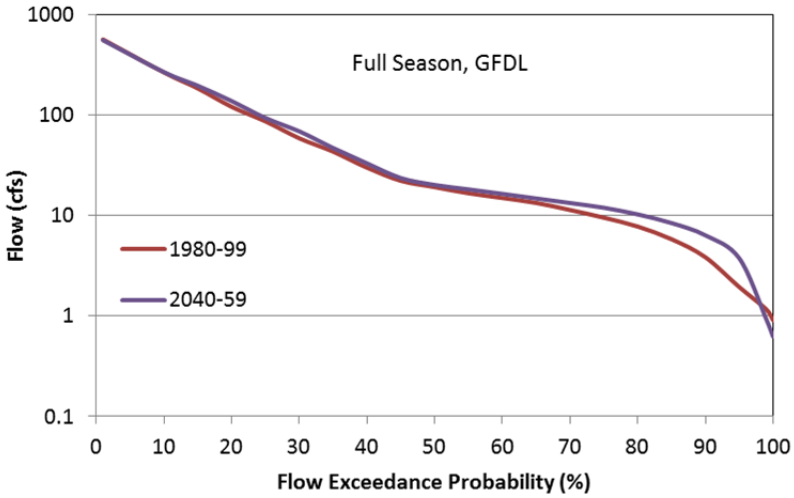

Figure 6.1. Simulated response of the full season flow-duration curves for the Knife River to GENMOM, ECHAM5, and GFDL climate increments for the periods 2020-39, 2040-59, 2060-79, and 2070-89.

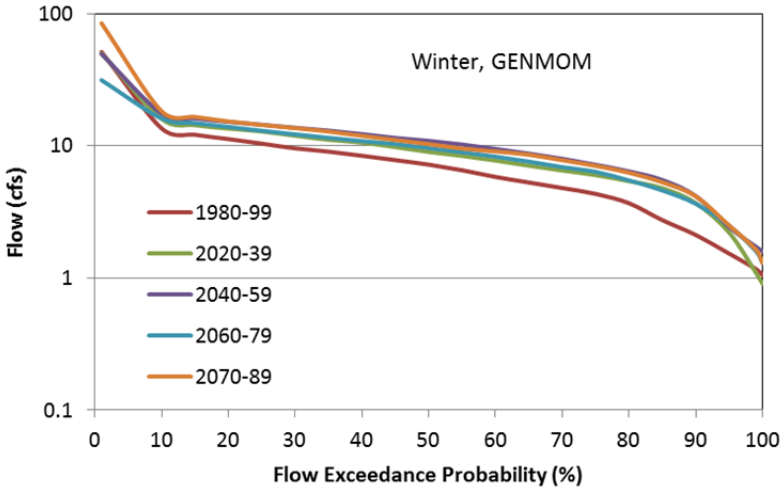

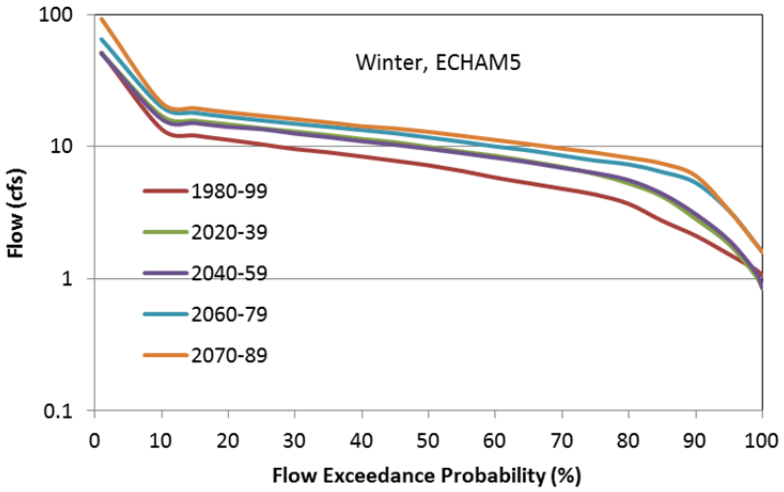

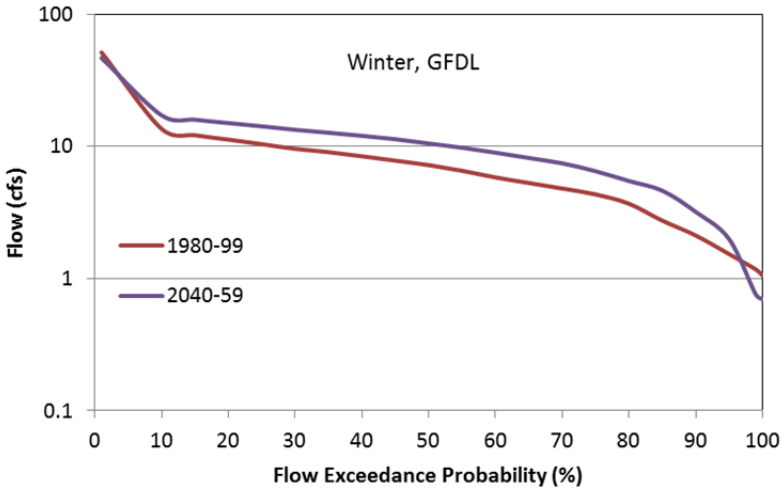

Figure 6.2. Simulated response of the winter (Dec-Feb) flow-duration curves for the Knife River to GENMOM, ECHAM5, and GFDL climate increments for the periods 2020-39, 2040-59, 2060-79, and 2070-89.

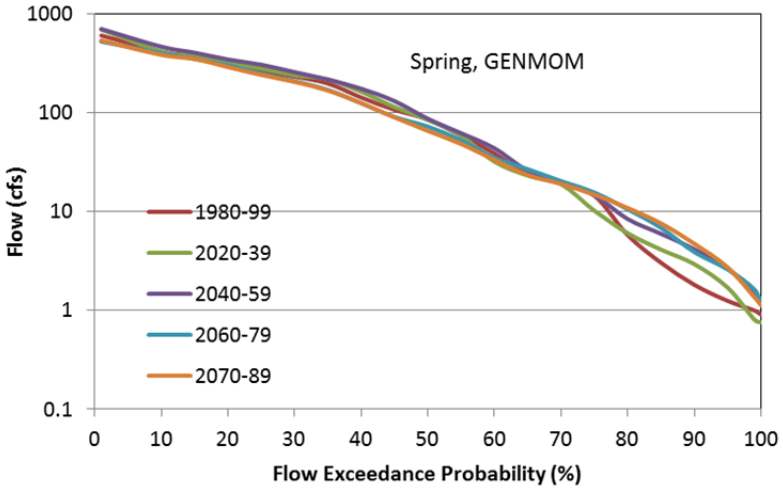

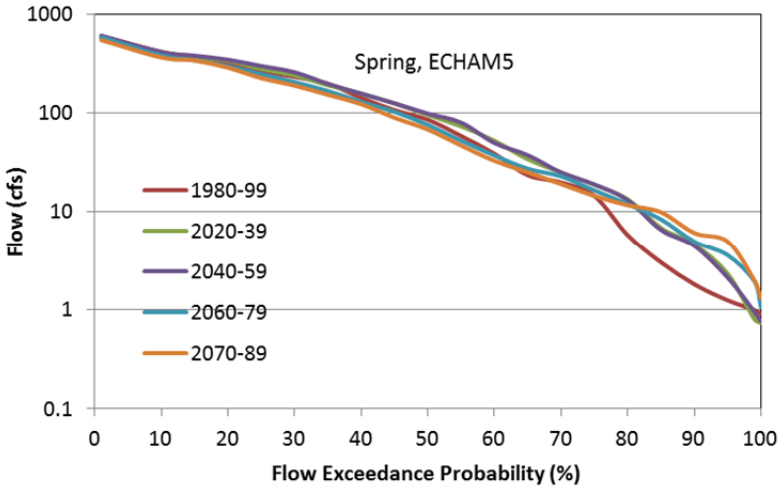

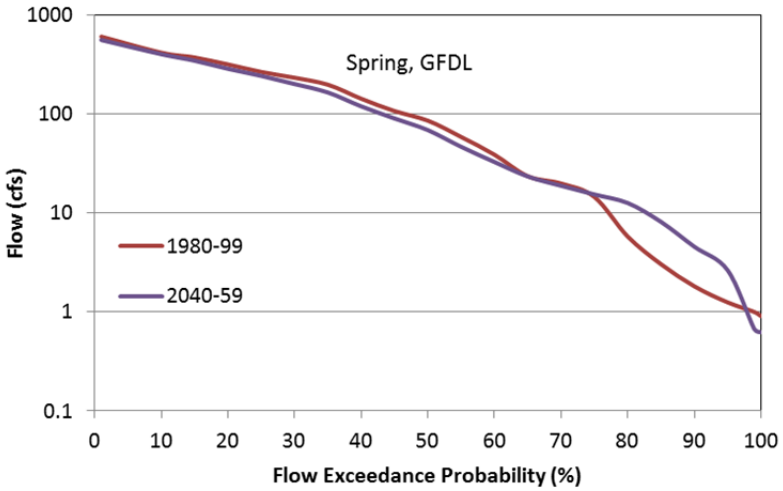

Figure 6.3. Simulated response of the spring (Mar-May) flow-duration curves for the Knife River to GENMOM, ECHAM5, and GFDL climate increments for the periods 2020-39, 2040-59, 2060-79, and 2070-89.

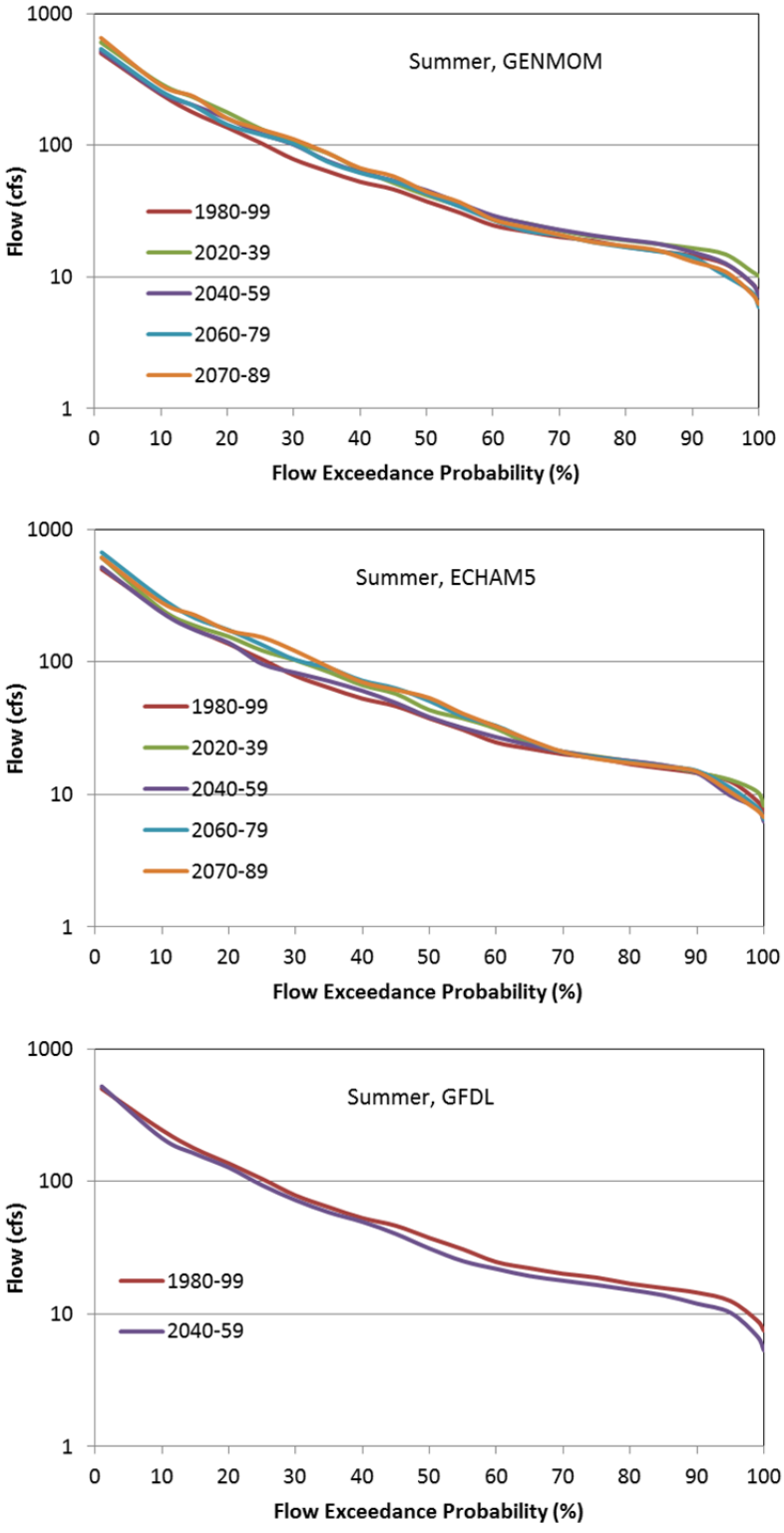

Figure 6.4. Simulated response of the summer (Jun-Aug) flow-duration curves for the Knife River to GENMOM, ECHAM5, and GFDL climate increments for the periods 2020-39, 2040-59, 2060-79, and 2070-89.

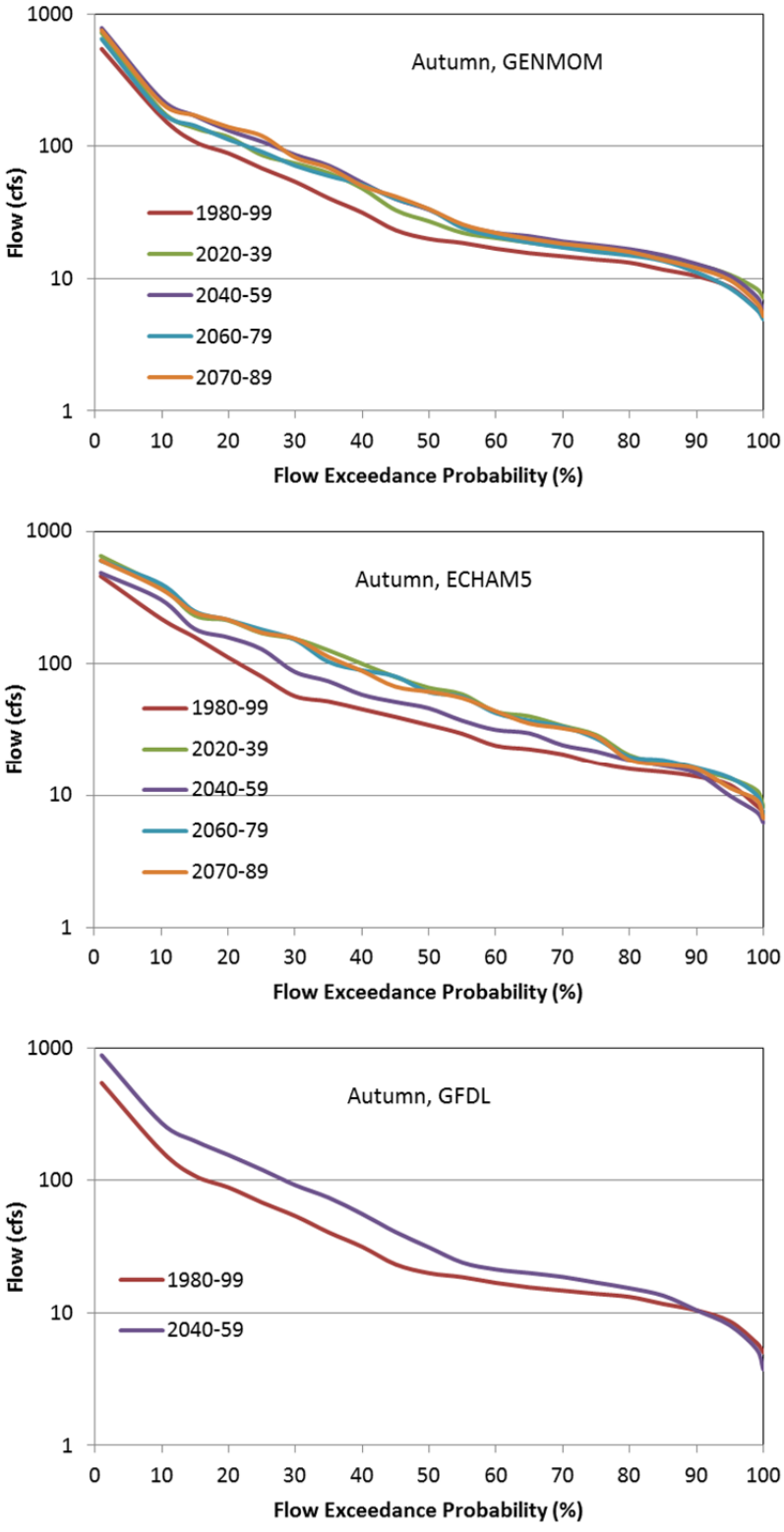

Figure 6.5. Simulated response of the autumn (Sep-Nov) flow-duration curves for the Knife River to GENMOM, ECHAM5, and GFDL climate increments for the periods 2020-39, 2040-59, 2060-79, and 2070-89.

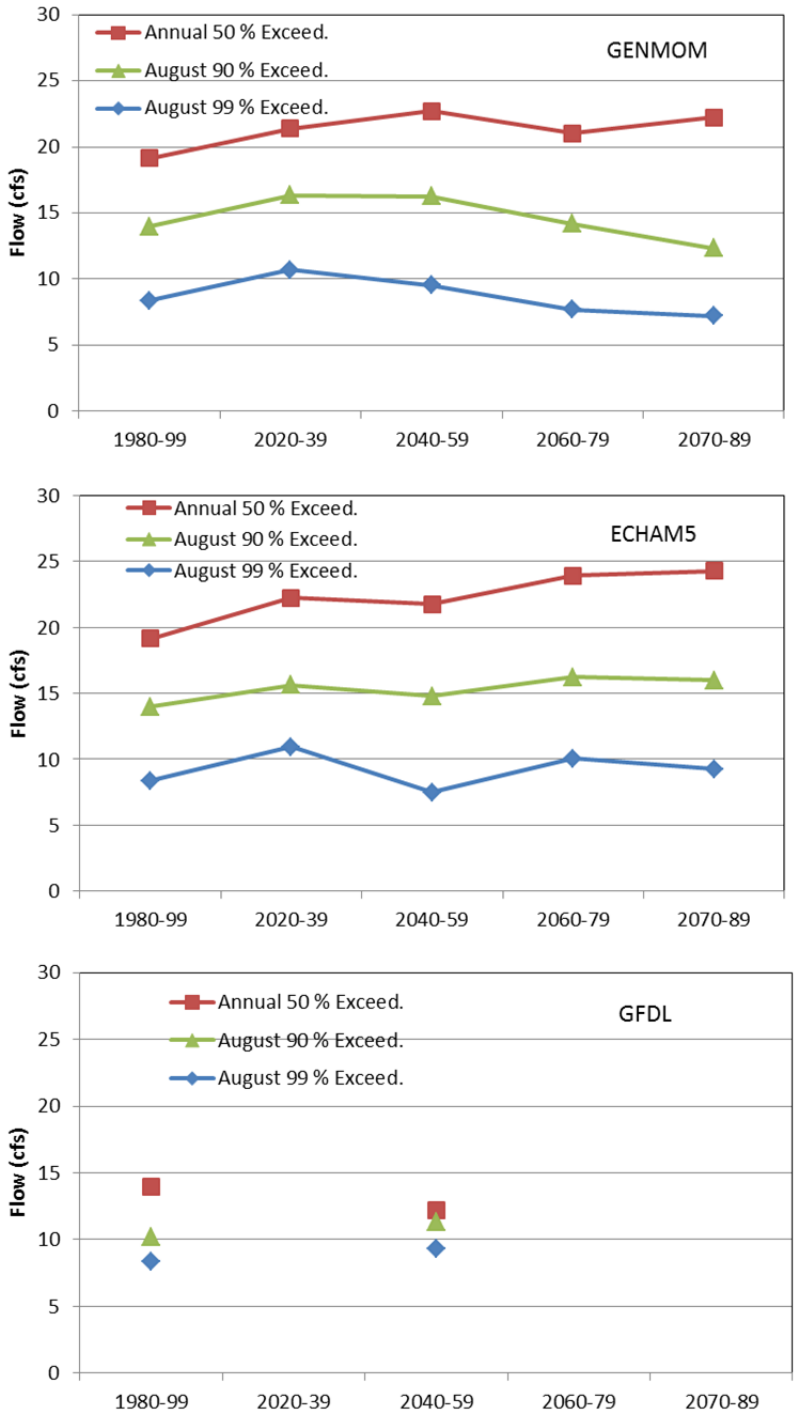

Figure 6.6. Simulated response of the Knife River annual median flow (50% exceedance) and August low flows (90% and 99% exceedance) to GENMOM, ECHAM5, and GFDL climate increments for the periods 2020-39, 2040-59, 2060-79, and 2070-89.

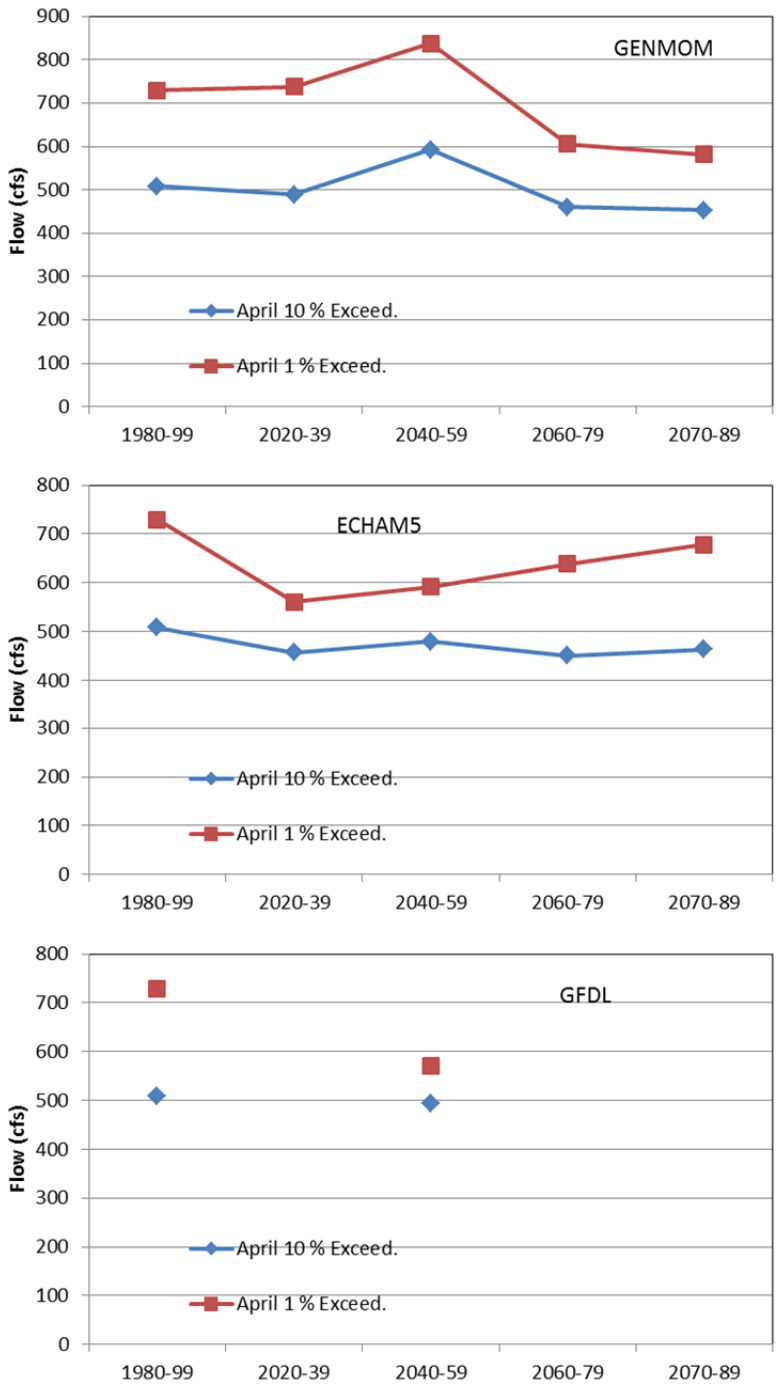

Figure 6.7. Simulated response of the Knife River April high flows (1% and10% exceedance) to GENMOM, ECHAM5, and GFDL climate increments for the periods 2020-39, 2040-59, 2060-79, and 2070-89.

6.2 Hydrologic response to projected daily climate (GENMOM)

The hydrologic simulations summarized in Section 6.1 are based on projected changes in climate in terms of 20-year average, monthly increments. In this section, hydrologic simulation results are given using the GENMOM daily climate time series, which introduces the possibility of more dynamic changes in flow at both inter-annual and weekly time scales. Results are given for the Knife River, the Baptism River and Amity Creek.

Time series of simulated annual mean and annual median flows are given in Figure 6.8, 6.9, and 6.10 for the Knife River, the Baptism River, and Amity Creek, respectively. Annual mean flows for all three sites increase modestly to 2040, and then decrease slightly towards 2090. Median flows. Median annual flows have a more consistent increasing trend over the simulation period, and trend testing using the Mann-Kendall procedure show statistically significant trends for all three sites. Box plots of the annual flow data for the Knife River suggest that inter-annual flow variability may increase in the future, particularly for the 2060-2079 period (Figure 6.11).

The projected annual flow duration curves based on the daily GENMOM climate are given in Figure 6.12. The flow duration curves for the Knife River can be compared to the previously given results based on monthly climate increments (Figure 6.1), which appear to be quite similar. For the summer time period (Figure 6.13), the simulated flow-duration curves change the most for the stream with the least surface storage (Amity) and respond the least for the stream with the most surface storage (Baptism).

The projected trends in annual median flows, August low flows, and April high flows are illustrated more explicitly in Figures 6.14 and 6.15. Again, Amity Creek responds more strongly to climate changes, in particular, with a stronger upward trend in the annual median flow. The results given in Figure 6.14 for the Knife River (using daily GENMOM data) can be compared to the previous results using monthly increments (Figure 6.6) – the flow trends obtained using the two methods are fairly similar, except that the results obtained for the daily GENMOM climate give a more distinct upward trend in the August 10% exceedance. April high flows (Figure 6.15) respond very similarly for the three streams, but have an weak downward trend over the century. In comparison, April high flow projections made using the GENMOM monthly increments showed upward trend or neutral trends (Figure 6.7). Only a weak trend in the timing of spring peak flow was found for the projected flow in the Knife River (Figure 2.16).

The relative contribution of snowfall and rainfall to the overall hydrologic budget can be expected to change as air temperatures systematically increase. For the GENMOM data set, the fraction of annual snowfall to total annual precipitation was found to decrease from 0.14 in 1980-99 to 0.11 in 2070-89 (Table 6.1). Based on the Knife River model, the corresponding fraction of annual snowmelt to annual streamflow decreased from 0.32 to 0.25 (Table 6.1).

Table 6.1. Relative fraction of annual snowfall to annual precipitation and relative fraction of snowmelt to streamflow based on the GENMOM daily climate projections and the Knife River hydrologic model.

Period	Snow/Precip	Snowmelt/Streamflow
1980-99	0.14	0.32
2020-39	0.12	0.27
2040-59	0.14	0.29
2060-79	0.10	0.22
2070-89	0.11	0.25

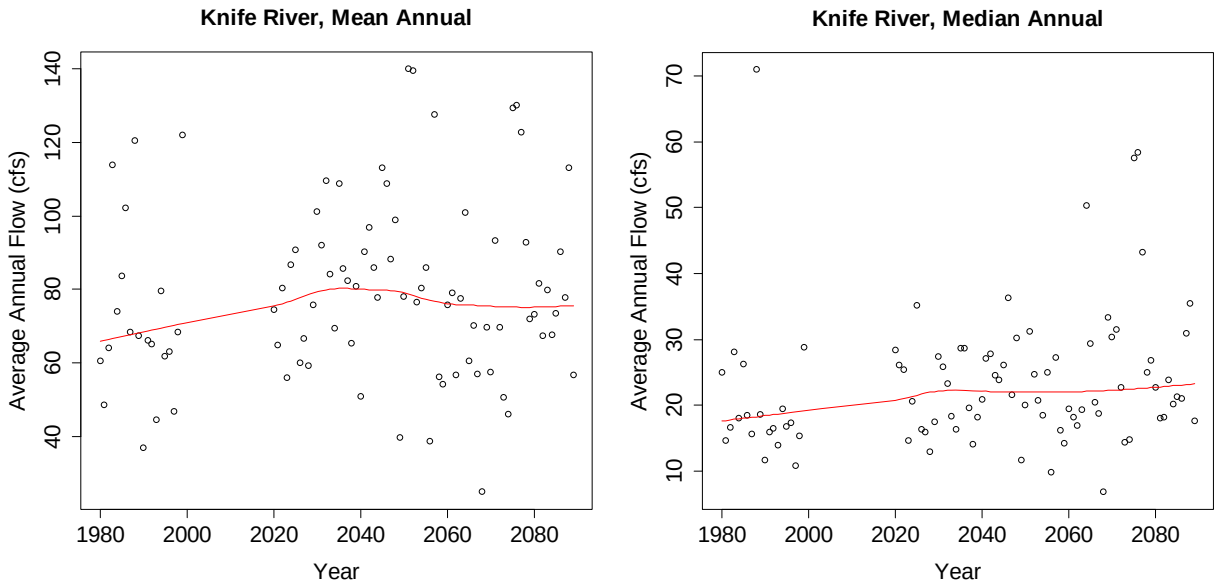

Figure 6.8. Projected mean annual flow and median annual flow in the Knife River based on GENMOM daily climate projections. A LOWESS trend line is also shown for each series.

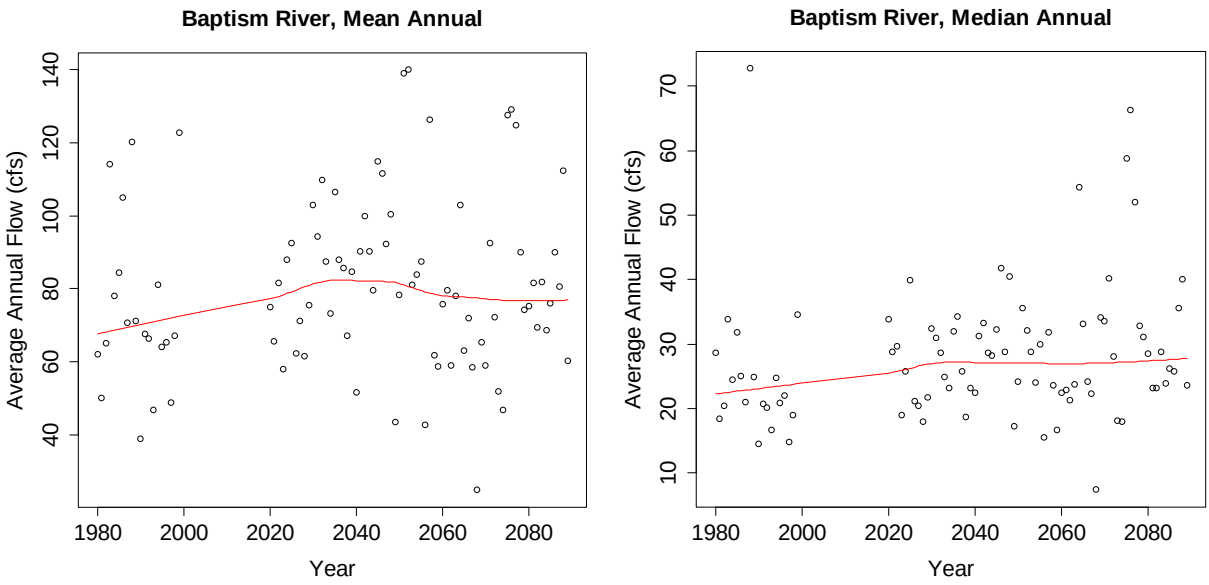

Figure 6.9. Projected mean annual flow and median annual flow in the Baptism River based on GENMOM daily climate projections. A LOWESS trend line is also shown for each series.

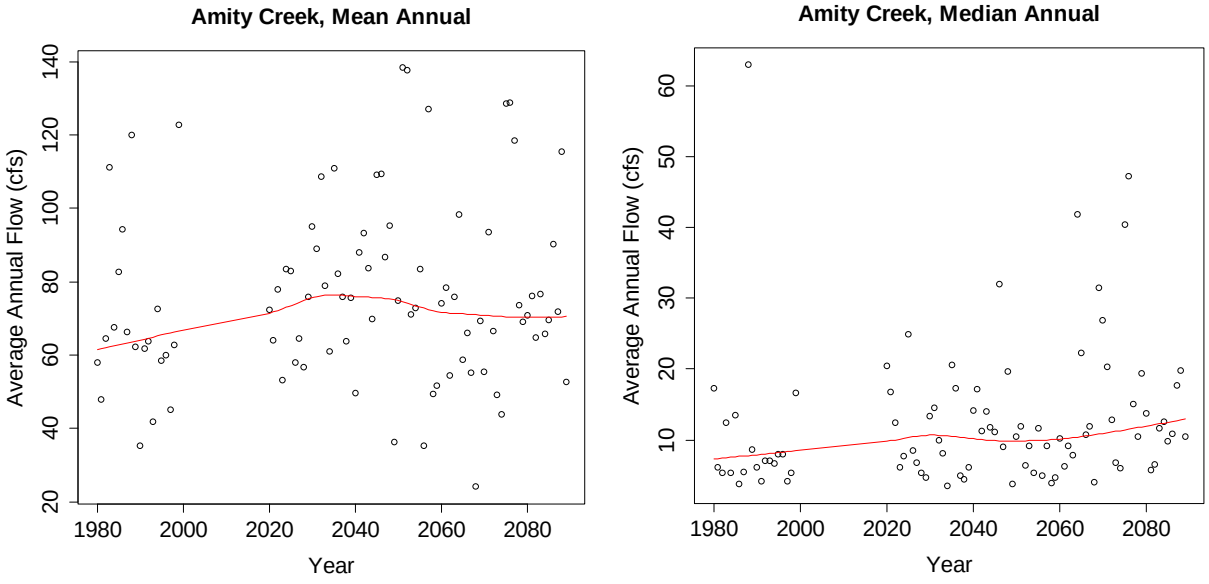

Figure 6.10. Projected mean annual flow and median annual flow in Amity Creek based on GENMOM daily climate projections. A LOWESS trend line is also shown for each series.

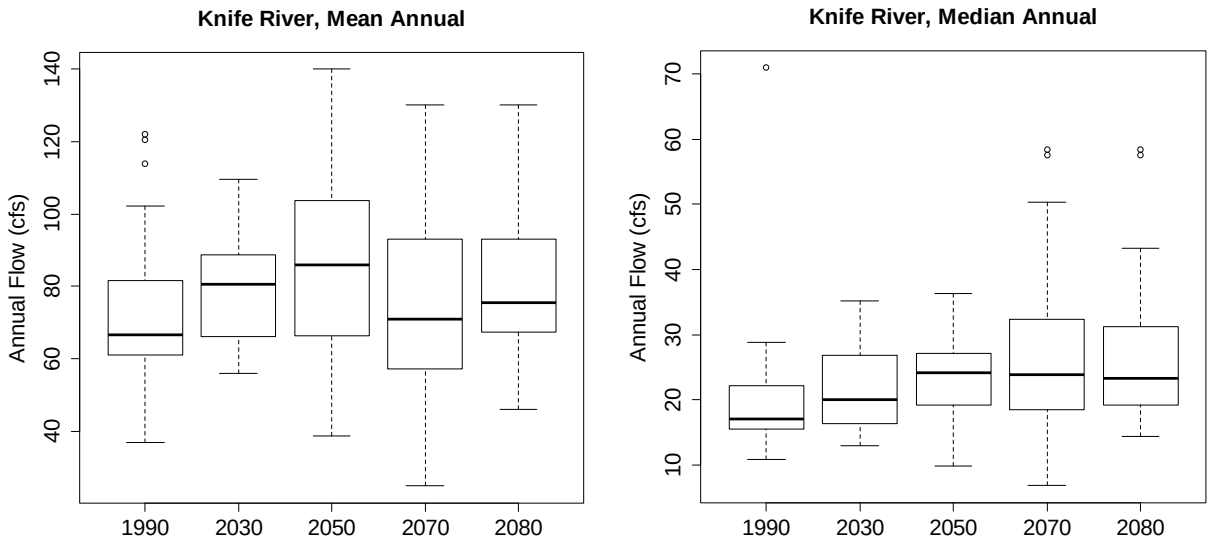

Figure 6.11. Box plots of projected mean annual flow and median annual flow in the Knife River based on GENMOM daily climate projections. The box plots summarize the annual flow data in 20-year blocks, 1980-99, 2020-29, 2040-59, 2060-769, and 2070-89.

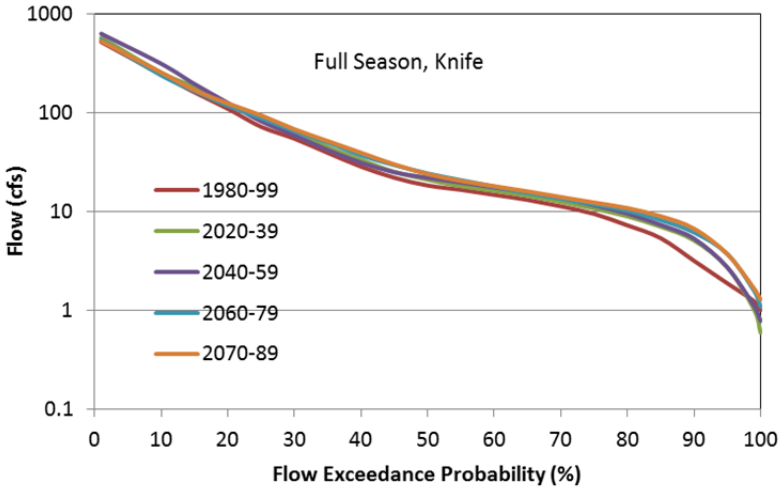

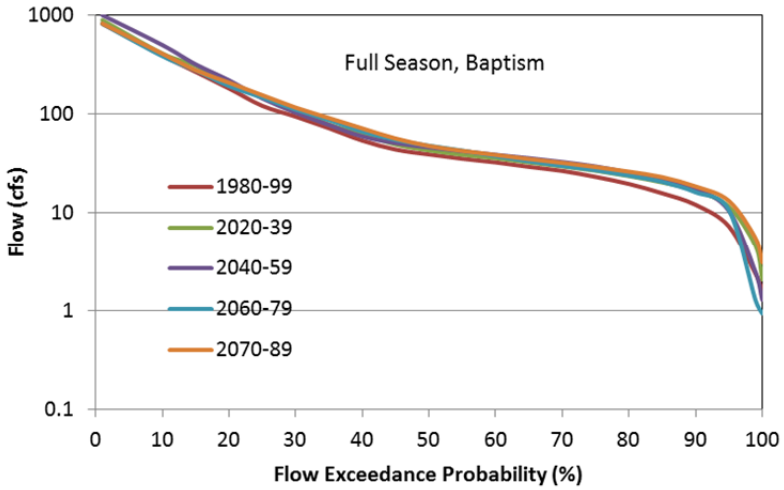

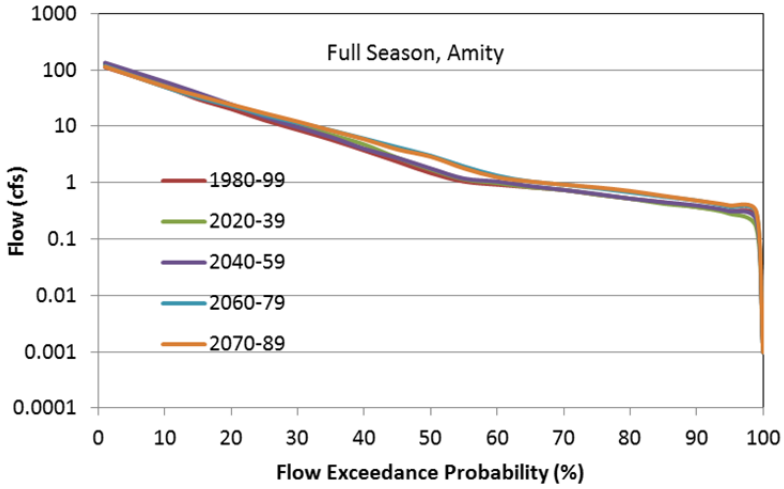

Figure 6.12. Simulated response of the full season flow-duration curves for the Knife River, the Baptism River, and Amity Creek to GENMOM daily climate, summarized for the periods 2020-39, 2040-59, 2060-79, and 2070-89.

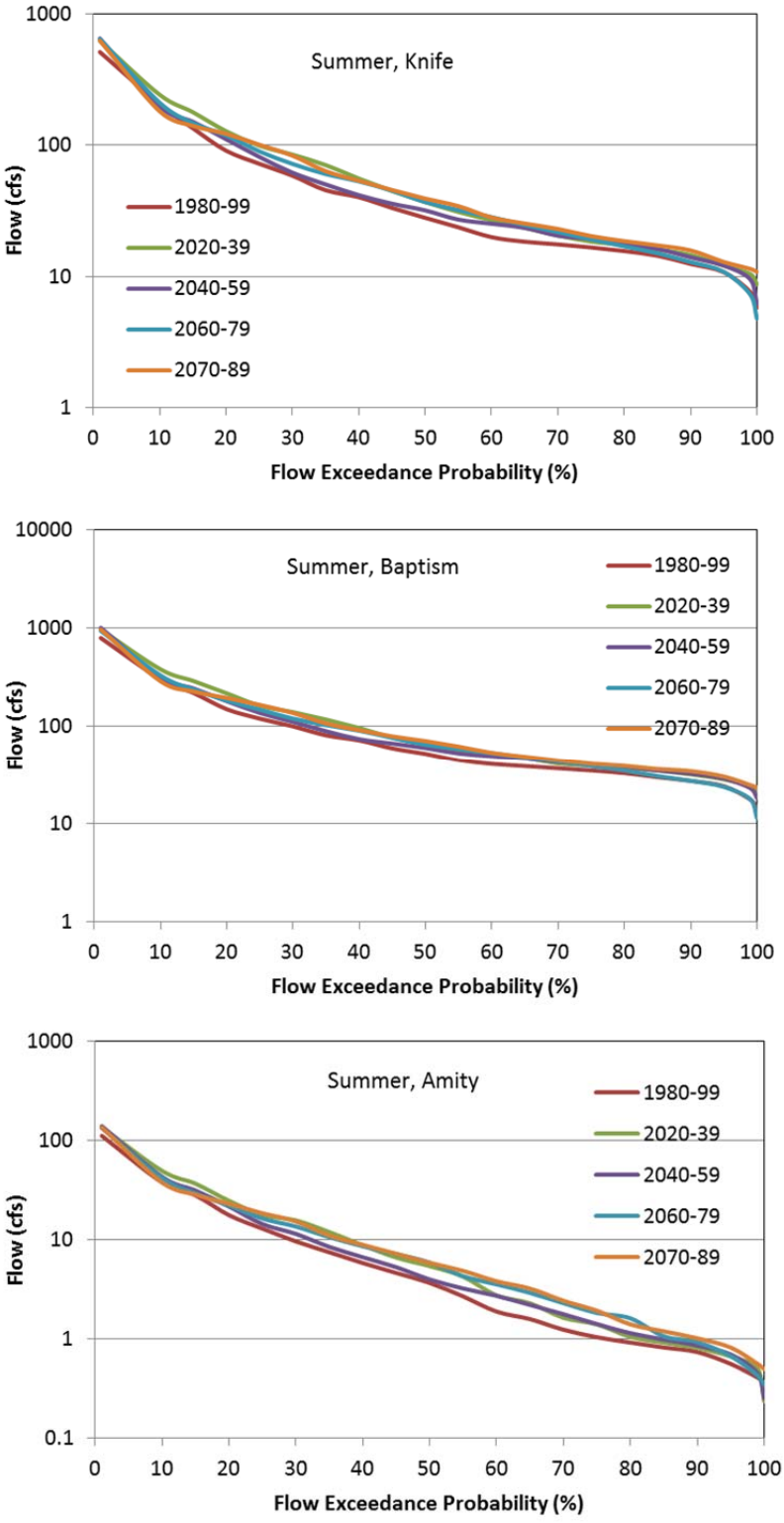

Figure 6.13. Simulated response of the summer (Jun-Aug) flow-duration curves for the Knife River, the Baptism River, and Amity Creek to GENMOM daily climate, summarized for the periods 2020-39, 2040-59, 2060-79, and 2070-89.

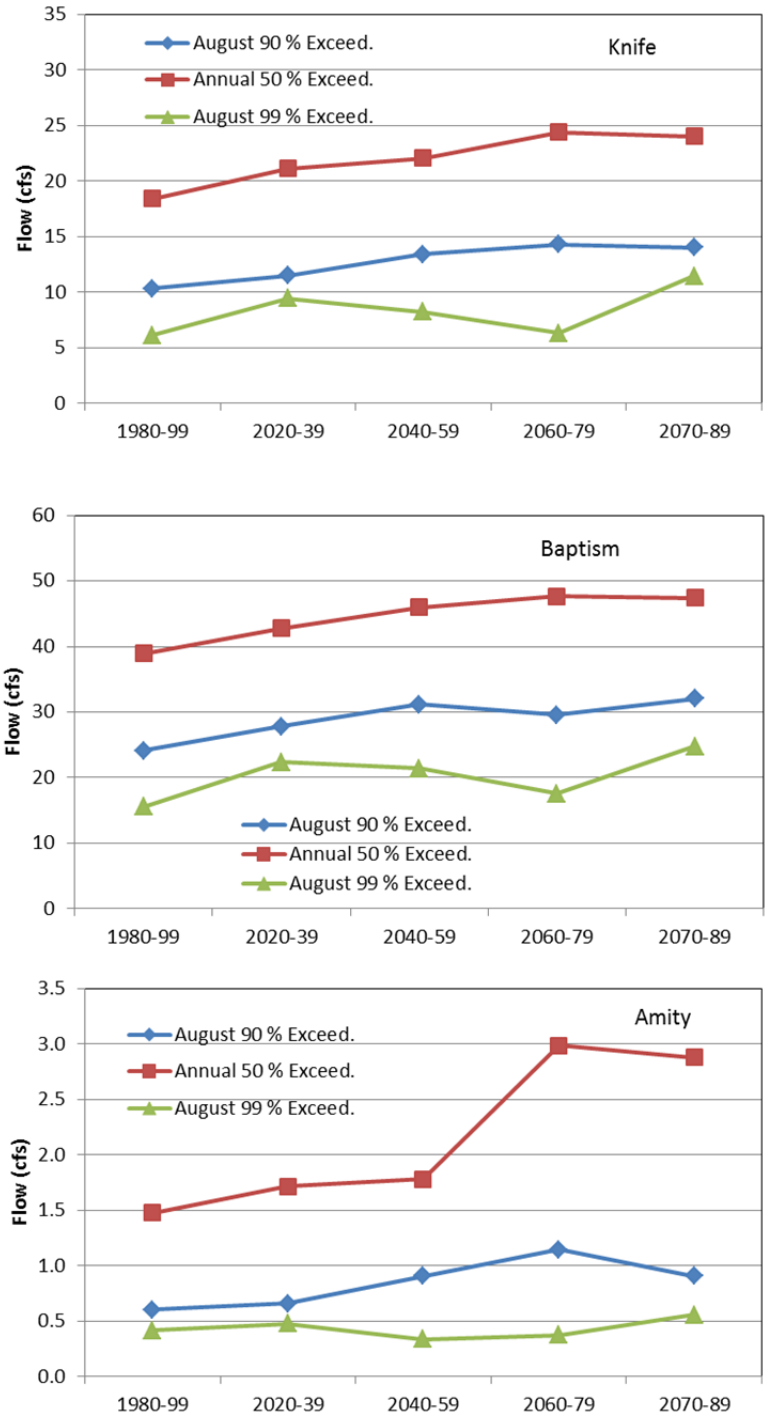

Figure 6.14. Simulated response of the annual median flow (50% exceedance) and August low flows (90% and 99% exceedance) for the Knife River, the Baptism River, and Amity Creek, using the daily GENMOM climate and summarized for the periods 2020-39, 2040-59, 2060-79, and 2070-89.

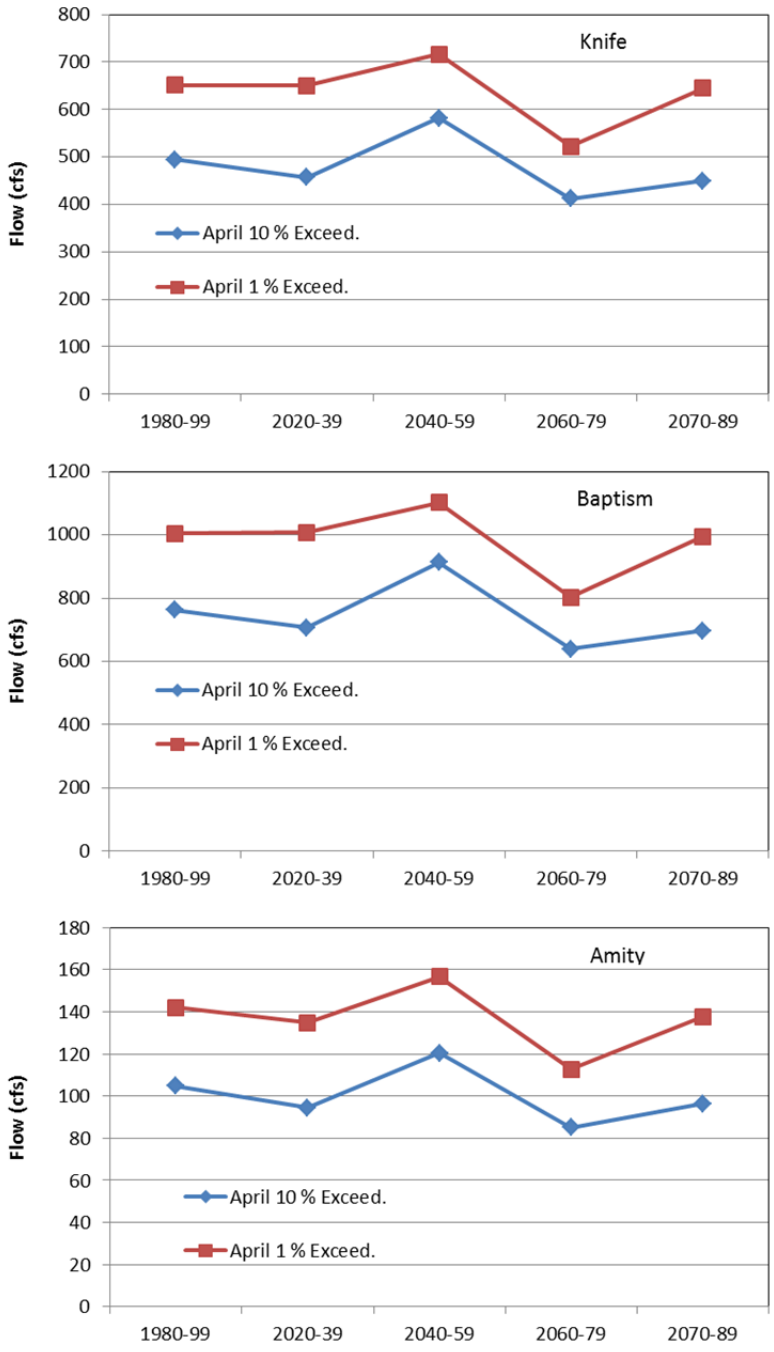

Figure 6.15. Simulated response of the April high flows (1% and 10% exceedance) for the Knife River, the Baptism River, and Amity Creek, using the daily GENMOM climate and summarized for the periods 2020-39, 2040-59, 2060-79, and 2070-89.

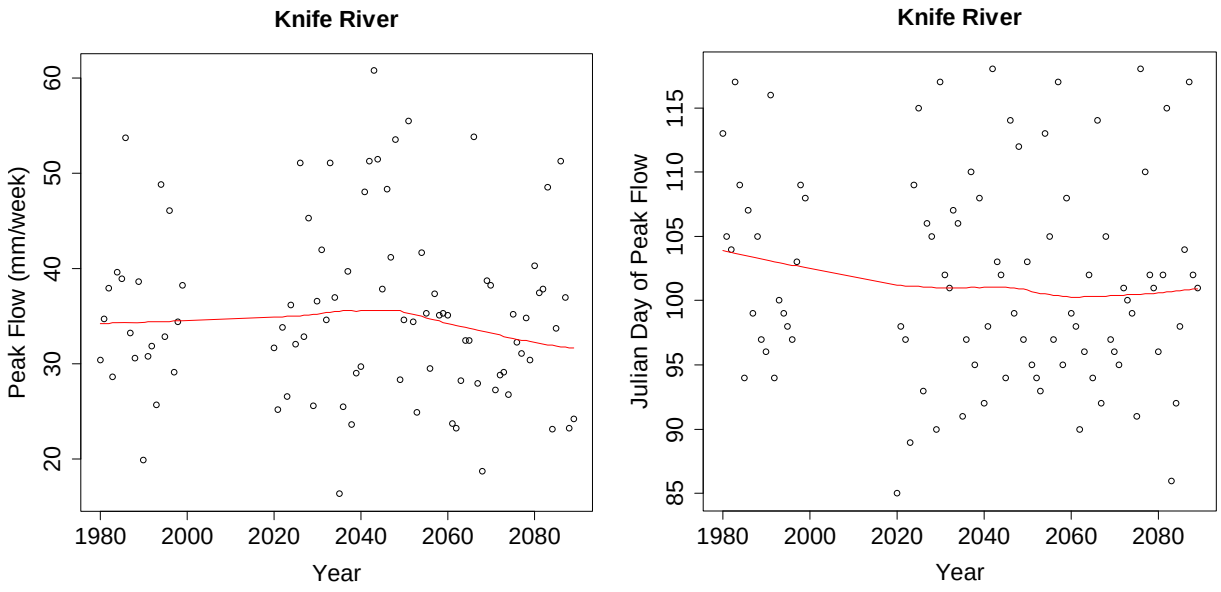

Figure 6.16. Simulated spring peak flow magnitude and timing for the Knife River, using the daily GENMOM climate.

6.3 Projected hydrologic response based on empirical models

The regression Equations given in Section 3 for the August 7-day low flow and the April 7-day high flow can be used in conjunction with the GCM climate projections to project future low and high flows. In this section, results are given based on the GENMOM climate projections, for eight north shore streams. The monthly time series of air temperature and precipitation depth was generated for each regression equation: Eq. 3.3a for low flow, Eq. 3.4 for high flow. Although these results could be expanded to a wider selection of north shore trout streams, the relatively simple nature of the regression equations makes the projected flow response quite consistent between streams.

Figure 6.17 gives the projected response of the 7-day low flow and the April 7-day high flow to the GENMOM climate projections, for eight north shore streams. The low and high flows for the different streams have identical trends, and vary only in magnitude, mainly based on the watershed area. The 20-year mean, April 7-day high flows projected by the regression model are essentially flat out to 2090. The August 7-day low flow has an overall decreasing trend over the century, with a 14% decrease in flow from 1980-99 to 2070-89. This decreasing trend is in contrast to the August low flow results based on the deterministic hydrologic models, which predicted modest increasing trends in low flow. The decreasing trend in the regression-based low flows is due to a relatively high sensitivity to air temperature compared to the deterministic model. For a 1 °C increase in air temperature, the regression equation predicts a 16% decrease in August low flow, while the deterministic model predicts only a 4% decrease.

Figure 6.18 gives the 20-year mean and standard deviation of the low and high flow, for the Knife River. Like the 20-year mean values, the standard deviation (year-to-year variability) of the low and high flows do not vary greatly over the climate simulation period.

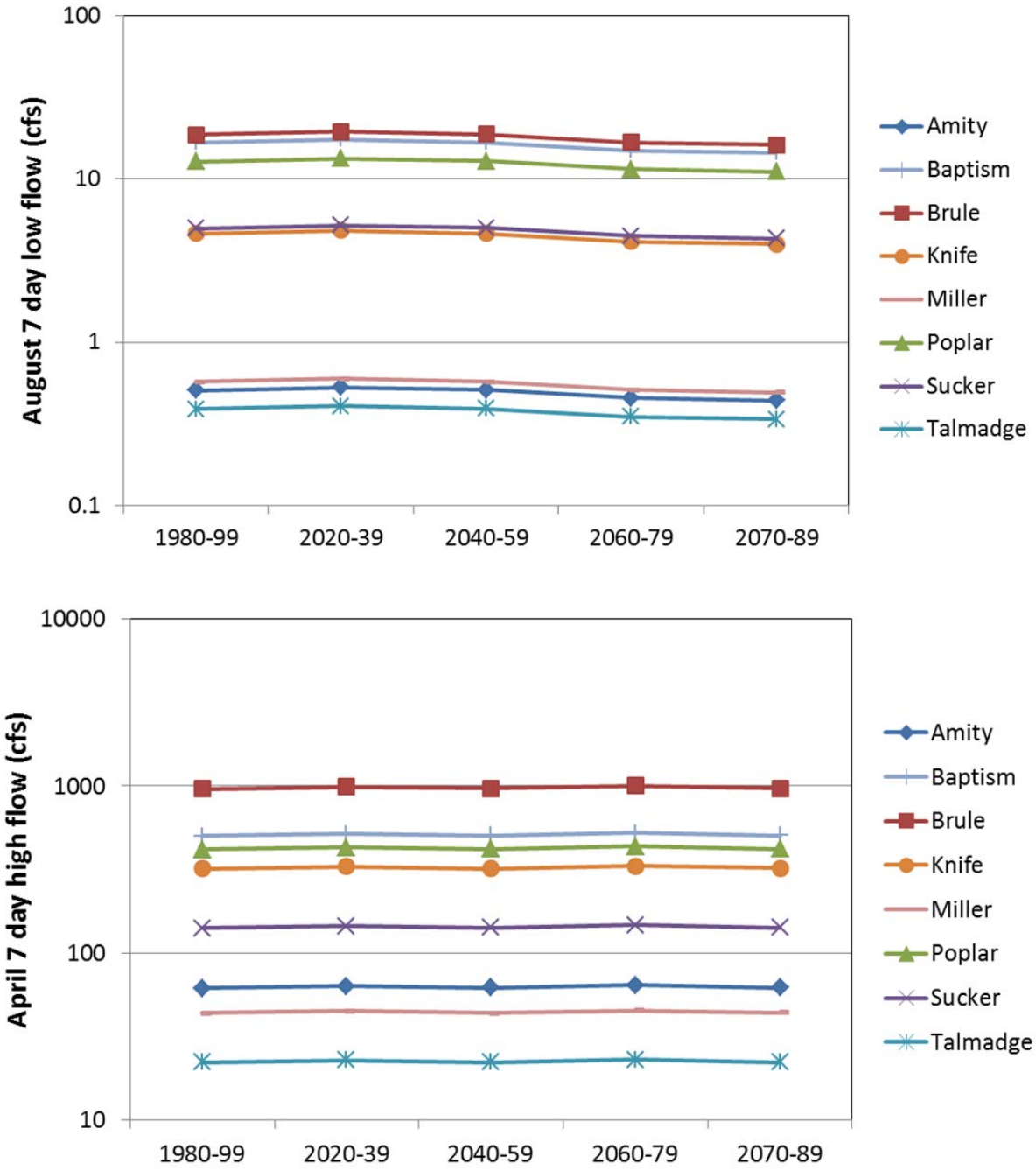

Figure 6.17. Projected 20-year mean of August 7 day low flows and April 7 day high flows based on regression models (Section 3) and the GENMOM monthly climate projections.

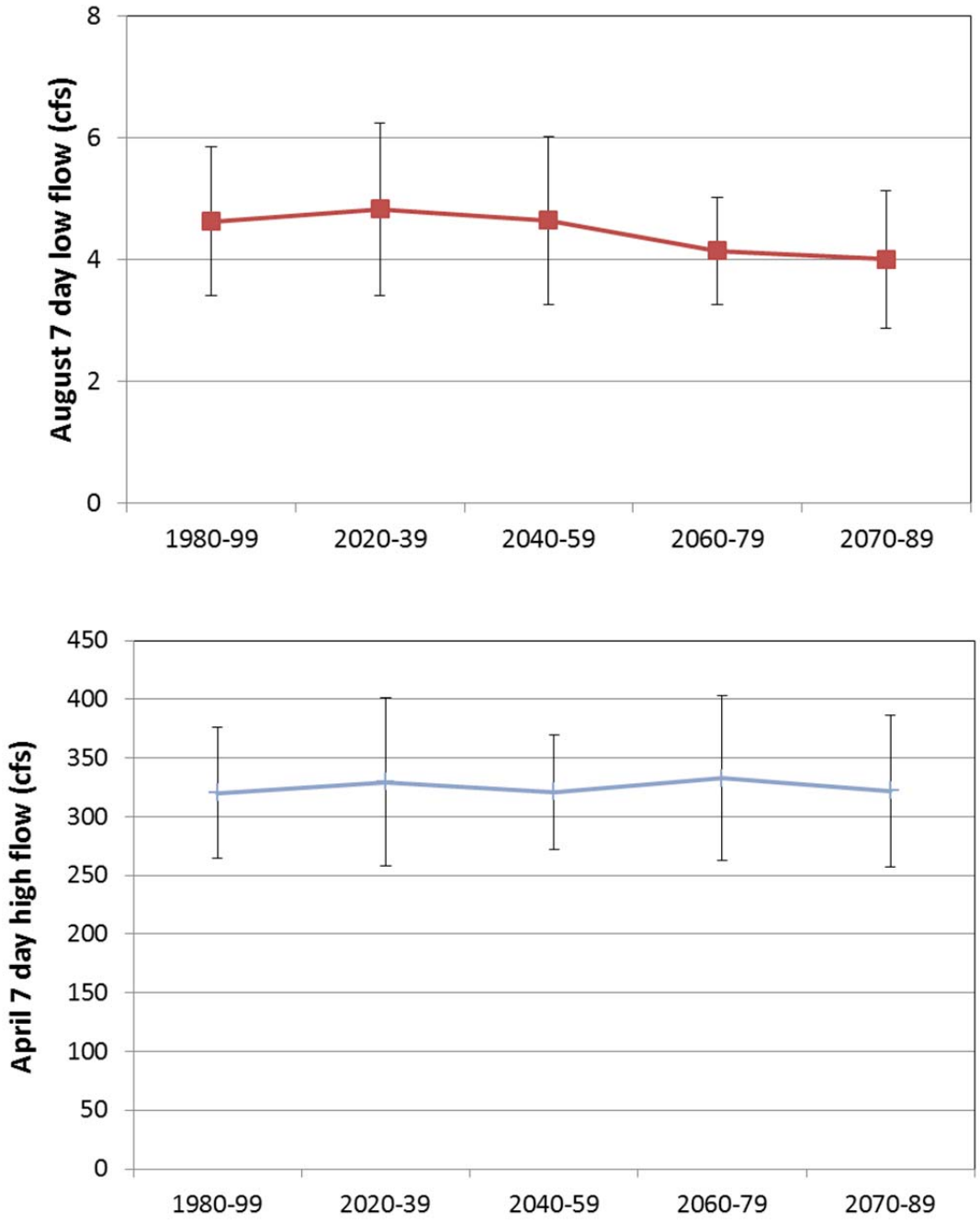

Figure 6.18. Projected 20-year mean and standard deviation of the August 7 day low flow and April 7 day high flow for the Knife River, based on regression models (Section 3) and the GENMOM monthly climate projections.

7. Deterministic Stream Temperature Modeling of North Shore Trout Streams

7.1. Stream temperature model development

The stream temperature model used for this study (Herb and Stefan, 2011) was developed under a previous, LCCMR funded project, "Impacts on Minnesota's aquatic resources from climate change". The model has some similarities to the USGS SNTEMP model, which was used for the Miller Creek TMDL study (Herb et al.and Stefan, 2009). While the SNTEMP model is designed to model a network of channels, the stream temperature model used in this study models stream temperature at the outlet of a catchment, based on spatially averaged properties of the catchment. It was, therefore, well suited to use in conjunction with the lumped-parameter water budget model used for hydrologic analyses in this study.

Like the SNTEMP model, the stream temperature model used in this study is based on the concept equilibrium temperature, the temperature that surface water tends toward as it approaches thermal equilibrium with the atmosphere. Typically, equilibrium temperature considers only atmospheric heat transfer (Edinger et al., 1974), however, the formulations for determining equilibrium temperature can be modified to include heat inputs due to groundwater and sediment conduction (Herb and Stefan 2011). The basic equations to be solved for this modified equilibrium temperature are:

$$T_e^* = \frac{\left(h_s + h_{li} - 306 + (K - 4.48)T_d^{'}\right) + K_s^* T_g}{K + K_s^* + 0.05T_d^{'} - 0.025T_e^*} \tag{7.1}$$

$$K_s^* = \frac{k_{sed}}{\delta} + \frac{W_p}{B}\frac{\rho C_p q_g}{B} \quad K_s^* = \frac{k_{sed}}{\delta} + \frac{W_p}{B}\frac{\rho C_p q_g}{B} \tag{7.2}$$

$$K = 4.5 + 0.05T_e^* + (0.47 + \beta) f(W) \tag{7.3}$$

$$T_d^{'} = T_d + \frac{0.47\left(T_a - T_d\right)}{\beta + 0.47} \quad T_d^{'} = T_d + \frac{0.47\left(T_a - T_d\right)}{\beta + 0.47} \tag{7.4}$$

where T_e* is the modified equilibrium temperature, h_s is solar radiation input, h_{li} is incoming long wave radiation input, K is the bulk heat transfer coefficient for atmospheric heat transfer, K_s* is a heat transfer coefficient for the sediment/water interface, T_g is the groundwater and sediment temperature, and T_a is air temperature, T_d is dew point temperature, β is the slope of the vapor pressure – temperature curve, and f(W) is a wind speed function. K_s* depends on the sediment thermal conductivity (k_{sed}), a characteristic length scale for conduction (δ), the wetted

perimeter (W_p) and width (B) of the stream cross section, the product of density and specific heat of water (ρC_p), and groundwater input rate per unit length, q_g (m^2/s).

Equations 7.1 – 7.4 were implemented in a Excel spreadsheet. Note that T_e* appears on both sides of Equation 7.1 and in Equation 7.3, so that an iterative solution is required. Incoming solar radiation is adjusted based on albedo, cloud cover and riparian shading.

In addition to the stream temperature model, a previously developed model for wetland temperature was also used in this study. The purpose of the wetland temperature model was to provide estimated historical and future source water temperatures for input to the stream temperature model. The model was developed as part of the MPCA-funded work at SAFL in support of the Vermillion River heat loading study (Herb et al. 2007), and is a 1-D model for the vertical temperature profile of standing water over saturated soil, with emergent vegetation covering the surface.

7.2. Stream temperature model application and calibration

The stream temperature model was calibrated for three sites (case studies): Amity Creek, the Knife River, and the Baptism River (Figure 7.1). The general characteristics of the three study sites and the available temperature records for points near the watershed outlet are summarized in Table 7.1.

The wetland temperature model was calibrated using one season of temperature observations of standing water in an upland wetland in the Miller Creek watershed. The density of the emergent plant cover was the main parameter that was adjusted for the calibration. Flow from wetland areas to the stream channel were assumed to be primarily subsurface, therefore, the water/soil temperature at a depth of 30 cm below the surface was used as the source temperature for the stream temperature model.

In addition to estimating a wetland source temperature, an estimate of the overall rate of inflow of the wetland source water was needed. For the historical wetland inflow rates needed for model calibration, baseflow separation was used to distinguish the surface runoff and baseflow components of daily stream discharge observations. A simple digital filter in an Excel spreadsheet was used for baseflow separation (Arnold and Allen 1999), as exemplified in Figure 7.2. The extracted baseflow was then attributed entirely to the wetland sources for the three study watersheds (Knife, Baptism, Amity); however, in some cases this baseflow could also be attributed to lake sources.

Obtaining suitable climate data for stream temperature can be a challenge. In particular, solar radiation observation data are both crucial to the stream temperature model and relatively difficult to obtain. For this study, simulated solar radiation values for Duluth were obtained from the National Solar Radiation Data Base (http://rredc.nrel.gov/solar/old_data/nsrdb/). These estimated solar radiation values are based on modeled clear sky solar radiation, observed cloud cover, and other factors such as humidity. Air temperature, humidity, and wind speed values are

also needed for the stream temperature model; however, the climate station used for these data was not as crucial as the precipitation data used for the hydrology model. Daily stream temperature observations in the Baptism River were found to be well correlated (R^2 = 0.80 – 0.82) to NWS air temperature data from Duluth and Two Harbors. For the Knife River, water temperatures were better correlated to air temperature data from Duluth (R^2=0.73) compared to Two Harbors (0.68). As a result, air temperature, humidity, and wind speed values from DLH were used for all three study streams.

One season (May – November) of stream temperature observations was used to calibrate the temperature model for each of the three study sites. The main model parameter used for calibration was the shading coefficient – a parameter that varies from 0 to 1, where 0 represents no riparian shading (full sun) and 1 represents complete shading (no solar radiation input). The stream temperature models were calibrated using 1) a monthly varying shading coefficient and 2) a constant shading coefficient. The resulting shading coefficients for the three sites are given in Figure 7.4. The calibrated (seasonally) constant shading coefficients vary from 0.52 for Amity Creek to 0.57 for the Baptism River. The calibrated monthly shading values have a similar seasonal variation for the three streams, with the expected increase towards mid-summer as riparian foliage maximizes in leaf coverage. The October/November Baptism River coefficients do not follow the general trend; rather, there is a sharp increase at the end of the season compared to the other two sites. This could be due to 1) the combination of topographical shading and a lower sun angle or 2) inaccuracies in some other model input, such as groundwater inflows. Overall, the seasonally constant shading coefficients perform almost as well as the monthly values, as summarized in Table 7.2.

For the Knife River, the model calibrated using 2005 flow and climate data was also run for 2004 and 2006 using the same calibration. The 2004 and 2006 data were run to verify that the model calibration established in 2005 was robust over multiple years.The model gave lower values of RMSE (root-mean-square error) for 2004 and 2006, with all RMSE values below 1.0 °C (Table 7.2).

Table 7.1. Summary of the three case study watersheds for the north shore stream study. Source for land use data is 2001 NLCD.

Name	Amity Creek	Baptism River	Knife River
Watershed area (sq. km)	43	355	225
Mean slope (%)	4.71	5.27	4.72
Forest cover (%)	80	88	87
Wetland cover (%)	1.2	30	16
Developed cover (%)	2.0	0.17	0.15

Table 7.2. Summary of root-mean-square error (RMSE) for constant and monthly shading coefficients.

Name	RMSE (°C)	
	Constant Shading	Variable Shading
Amity Creek (2006)*	0.94	0.78
Baptism River (1981)*	1.03	0.91
Knife River (2004)	0.73	0.75
Knife River (2005)*	1.08	0.95
Knife River (2006)	0.72	0.89

*Calibration year

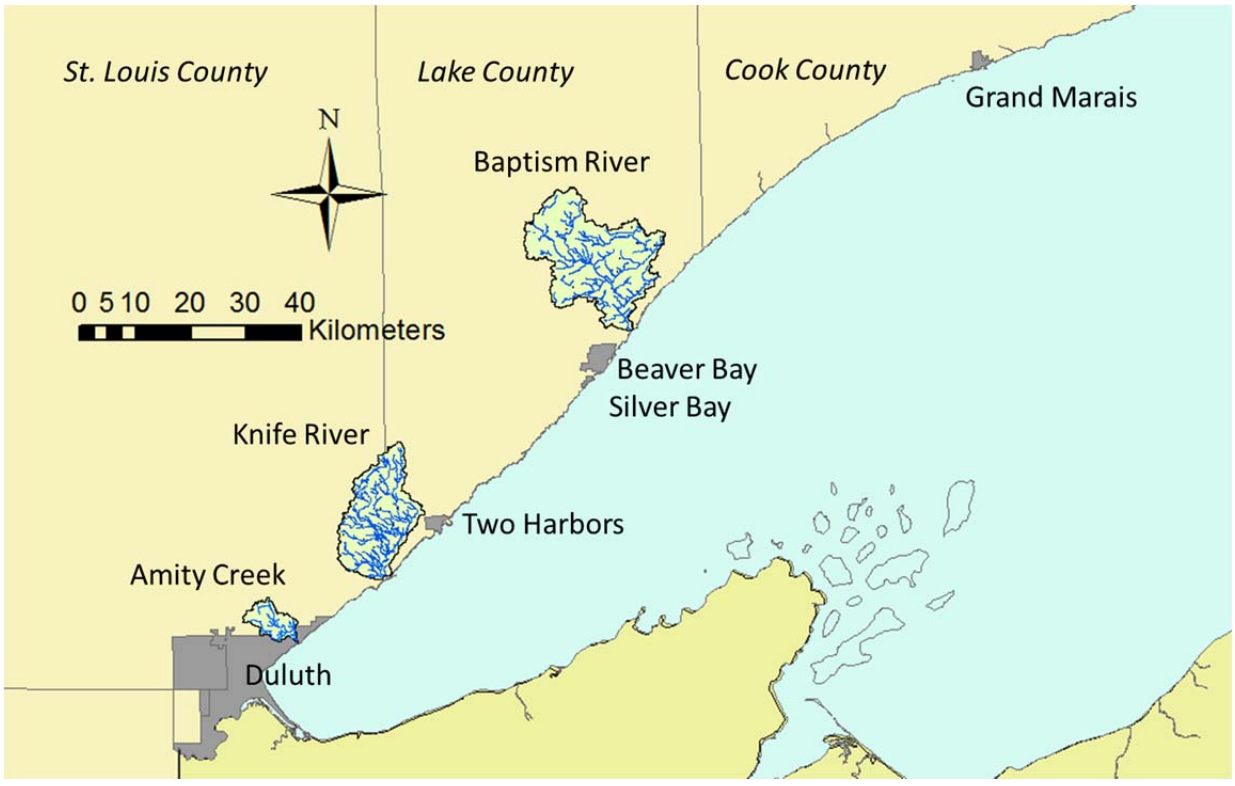

Figure 7.1. Location of the three case study streams along the Lake Superior north shore in St. Louis and Lake counties, Minnesota.

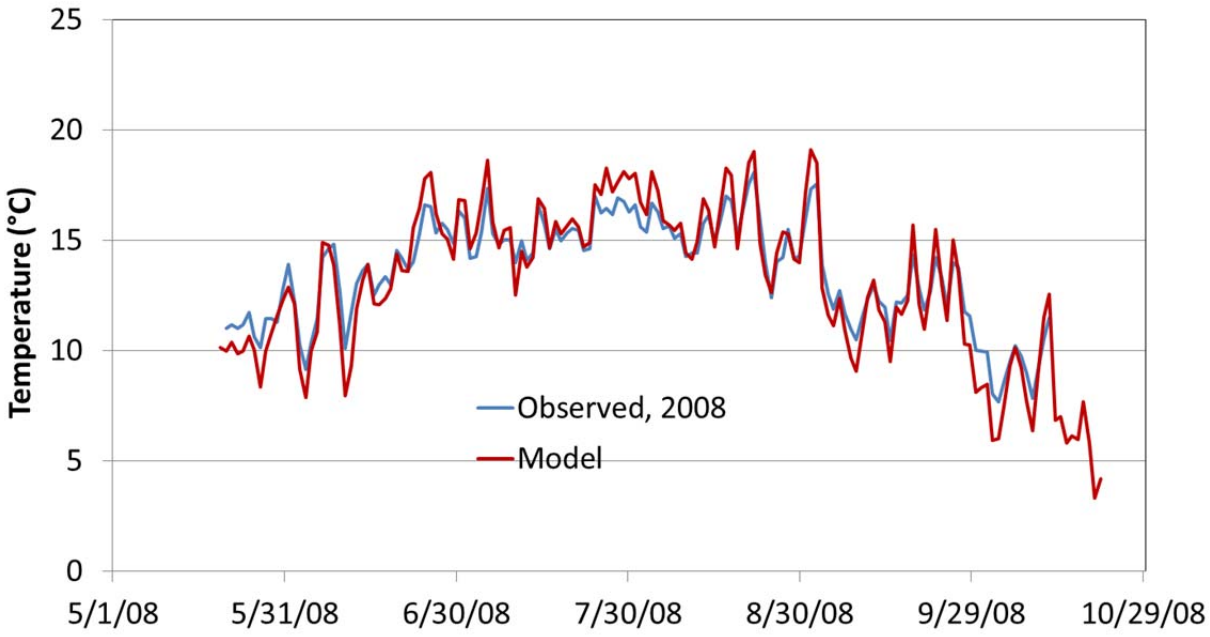

Figure 7.2. Observed and simulated Miller Creek wetland temperatures for 2008.

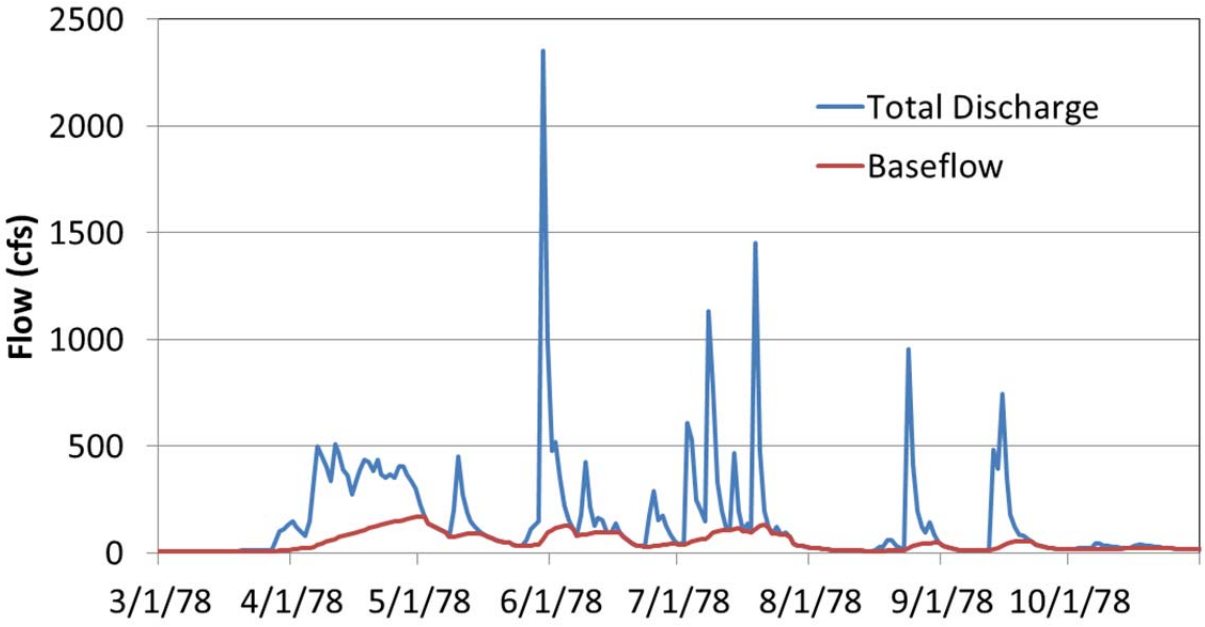

Figure 7.3. Observed discharge and the extracted baseflow for the Knife River in 1978.

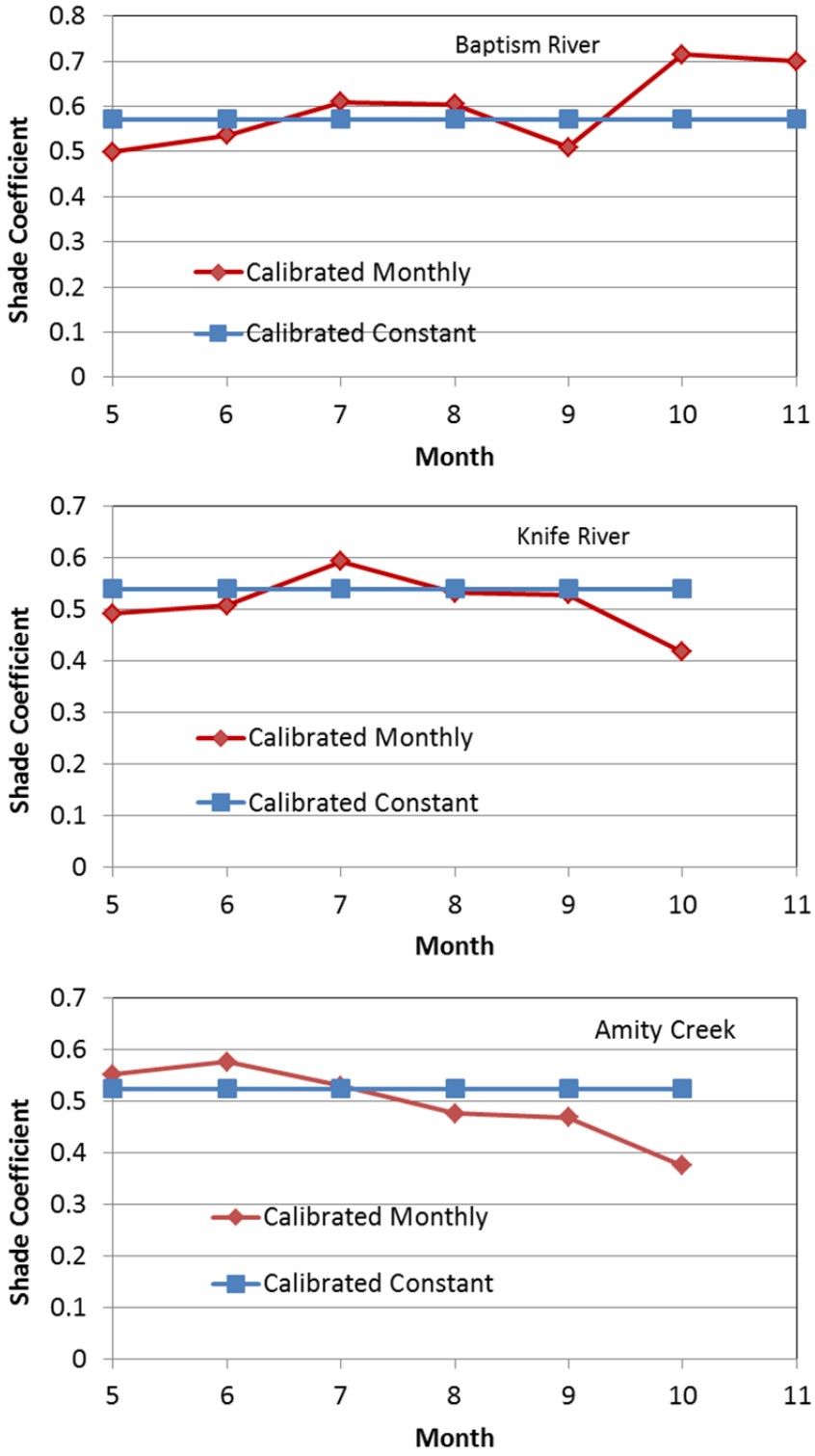

Figure 7.4. Calibrated shading coefficients (varying monthly or seasonally constant) for the Knife River, the Baptism River, and Amity Creek. The shading coefficient determines the fraction of incoming solar radiation blocked by the riparian canopy.

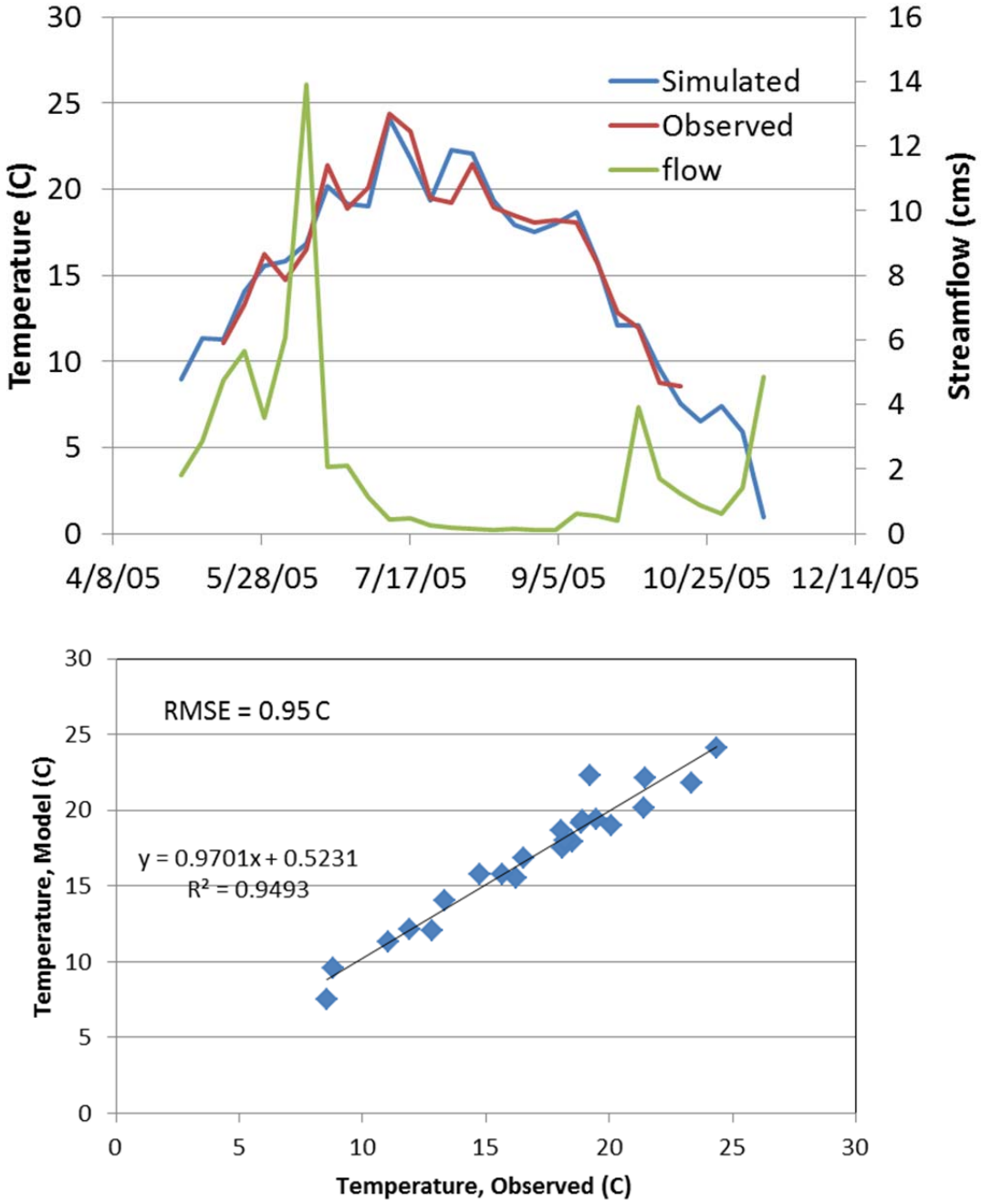

Figure 7.5. Comparisons of simulated and observed weekly average-stream temperature for the Knife River in 2005, using calibrated monthly shading coefficients (Figure 7.4).

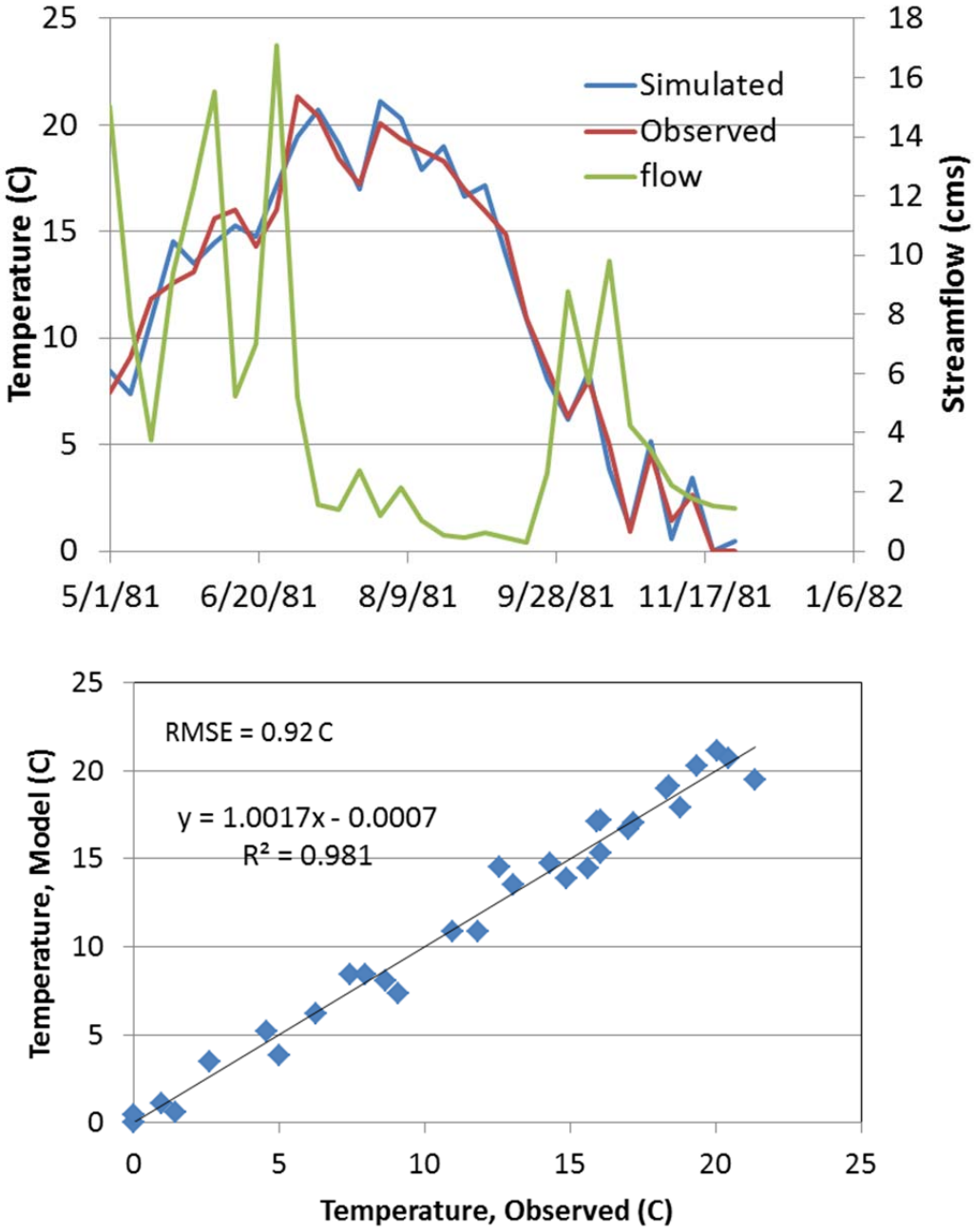

Figure 7.6. Comparisons of simulated and observed weekly average-stream temperature for the Baptism River in 1981, using calibrated monthly shading coefficients (Figure 7.4).

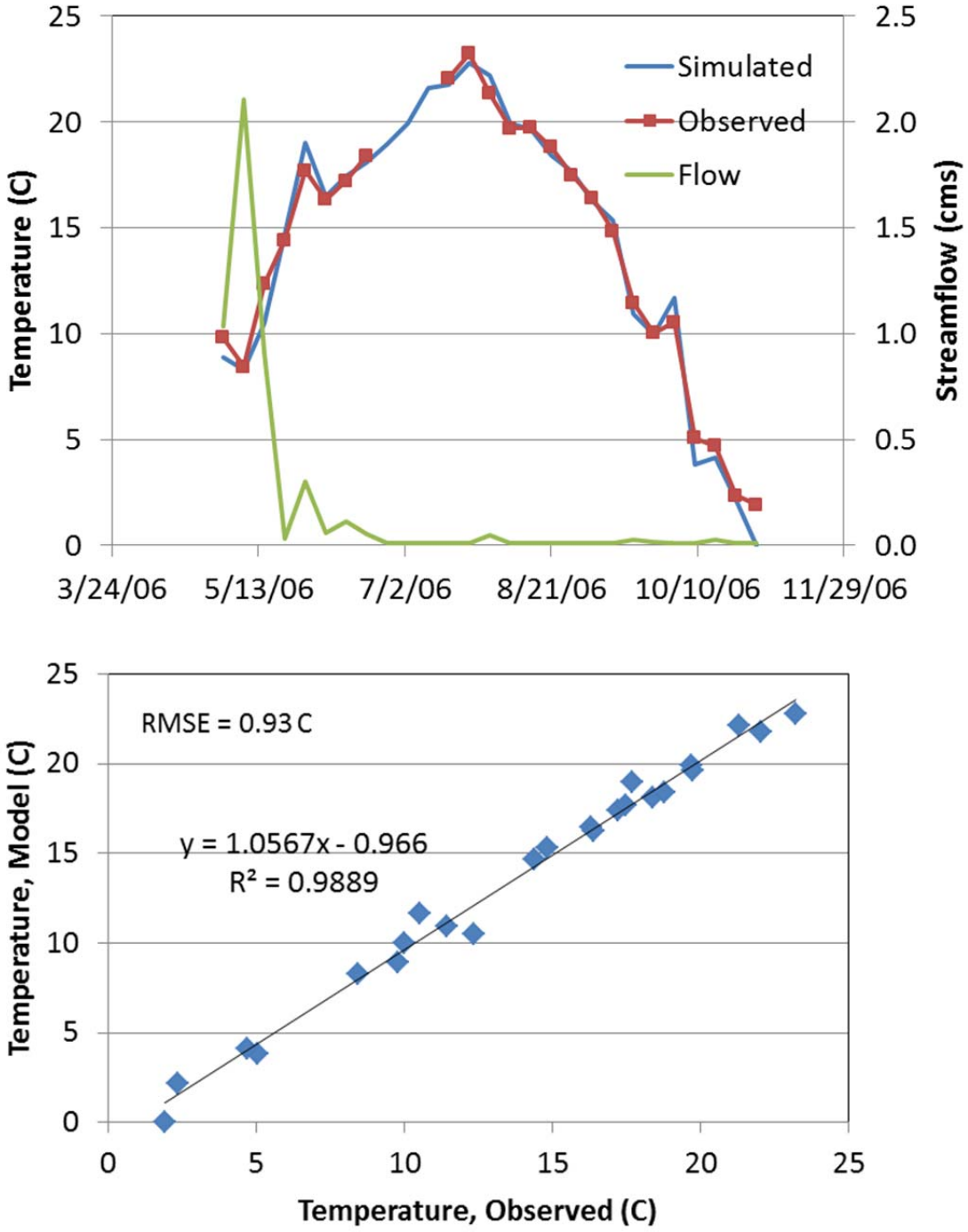

Figure 7.7. Comparisons of simulated and observed weekly average-stream temperature for Amity Creek in 2006, using calibrated monthly shading coefficients (Figure 7.4).

7.3. Stream temperature model sensitivity analysis

The calibrated Knife River stream temperature model was set for 20 years of simulations, May through October, using Duluth climate data from 1980 – 1999. Streamflow and baseflow inputs were taken from the hydrologic model output for the same period; wetland temperatures were also simulated. The model was then run for the following cases, where one parameter was changes, keeping the rest at nominal values. All parameter changes were applied uniformly over the simulation period.

Case 0= Nominal conditions
Case 1= 1 °C increase in air temperature
Case 2= 1 °C increase in baseflow source temperature
Case 3= 10% increase in streamflow
Case 4= 10% increase in groundwater inflow rate
Case 5 = 10% reduction in shading

For each case, the 20-year average monthly stream temperatures was recorded, as well as the difference in monthly temperature from the nominal case (Case 0). The results are summarized in Table 7.3 and 7.4. Stream temperature was relatively sensitive to increases in air temperature (Case 1), with a 0.44 to 0.56 °C increase in stream temperature for a 1.0 °C increase in air temperature. Stream temperature was less sensitive to changes in baseflow source temperature (Case 2), with a 0.2 °C increase in stream temperature for a 1.0 °C increase in source temperature. The relatively low sensitivity to source temperature can be attributed to relatively low rates of groundwater inputs. Stream temperature increased very slightly (0.01 – 0.02 °C) for 10% increase in streamflow (Case 3), which can be attributed to a small increase in stream width. A 10% increase in the baseflow input rate led to variable changes in stream temperature, with the biggest change (-0.13 °C) in May, when there is a relatively large fractions of baseflow input to the stream. A 10% reduction in riparian shading produced a substantial increase in stream temperature, with a maximum 0.82 °C increase in July.

Table 7.3. Twenty-year mean monthly stream temperature for nominal conditions (Cases 0) and five modified cases 1 – 5, as described in the text.

Monthly Mean Stream Temperature (°C)						
Month	Case 0	Case 1	Case 2	Case 3	Case 4	Case 5
5	14.2	14.6	14.4	14.2	14.0	14.8
6	20.7	21.2	20.9	20.7	20.6	21.4
7	21.7	22.2	21.9	21.8	21.7	22.6
8	20.0	20.5	20.2	20.0	19.9	20.7
9	14.3	14.8	14.5	14.3	14.3	14.8
10	7.81	8.37	7.98	7.81	7.83	8.11

Table 7.4. Difference in 20-year mean monthly stream temperature from nominal conditions (Case 0) for Cases 1 – 5.

Mean Temperature Difference (°C)					
Month	Case 1	Case 2	Case 3	Case 4	Case 5
5	0.44	0.28	0.02	-0.13	0.60
6	0.47	0.16	0.02	-0.10	0.70
7	0.47	0.17	0.02	-0.08	0.82
8	0.48	0.18	0.01	-0.06	0.72
9	0.51	0.19	0.00	-0.02	0.52
10	0.56	0.17	0.00	0.02	0.30
Average	0.49	0.19	0.01	-0.06	0.61

7.4. Deterministic Stream Temperature Model Summary

Previously developed, equilibrium-temperature based stream temperature models have been successfully applied to Amity Creek, the Knife River, and the Baptism River, with root-mean-square errors of about 1 °C for weekly-average temperature predictions. For seasonally constant riparian shading, the calibrated riparian shading coefficient was in the range of 0.5 to 0.6 for all three study sites. For the case of a seasonally variable, calibrated shading coefficient, moderate differences were evident between sites that may not correspond to expected seasonal changes in the tree canopy. The model was found to be relatively sensitive to change in air temperature and riparian shading, insensitive to specified flow conditions and moderately sensitive to baseflow temperature.

References

Edinger, J.E., D.K. Brady and J.C. Geyer (1974), Heat exchange and transport in the environment. Report No. 14, Electric Power Research Institute, Cooling Water Discharge Research Project (RP-49), Palo Alto, CA.

Herb, W.R. and H.G. Stefan, 2009. Stream temperature modeling of Miller Creek, Duluth, Minnesota, St. Anthony Falls Laboratory Report 535, 78 pp.

Herb, W.R. and H.G. Stefan, 2011. Equilibrium temperature models for coldwater streams, Water Resources Research, 47: W06519.

8. Regional (Empirical) Models for Stream Temperature

8.1 Data Acquisition

From 1989 to 2009, hourly stream water temperature was monitored by MN DNR and EPA in streams along Lake Superior's north shore region (Figure 8.1). As most sites were surveyed from 1996 to 2009 (Figure 9.2), this study was limited to 427 survey sites during these 14 years, representing the majority of available temperature survey data. Water temperature monitoring was not continuous from one year to another; consequently most sites were monitored for only one to three years. Trout are sensitive to high temperature (Raleigh 1982), and water temperature in July tended to approach thermal limit to trout; therefore July mean and July maximum temperature were chosen as the temperature model response variables (Picard et al. 2003, Wehrly et al.2006). For sites measured for one year only, the July mean or July maximum temperature was determined by averaging or maximizing the hourly temperature values. For sites measured for multiple years, the mean or maximum July temperature were computed for each survey year; July mean and maximum across survey years were then averaged.

July monthly average water temperature generally ranged from 14 to 23^{o}C with average of 18^{o}C, whereas monthly maximum temperature could be as high as more than 30^{o}C (Figure 8.3). Monthly variation of water temperature tended to be around 11^{o}C.

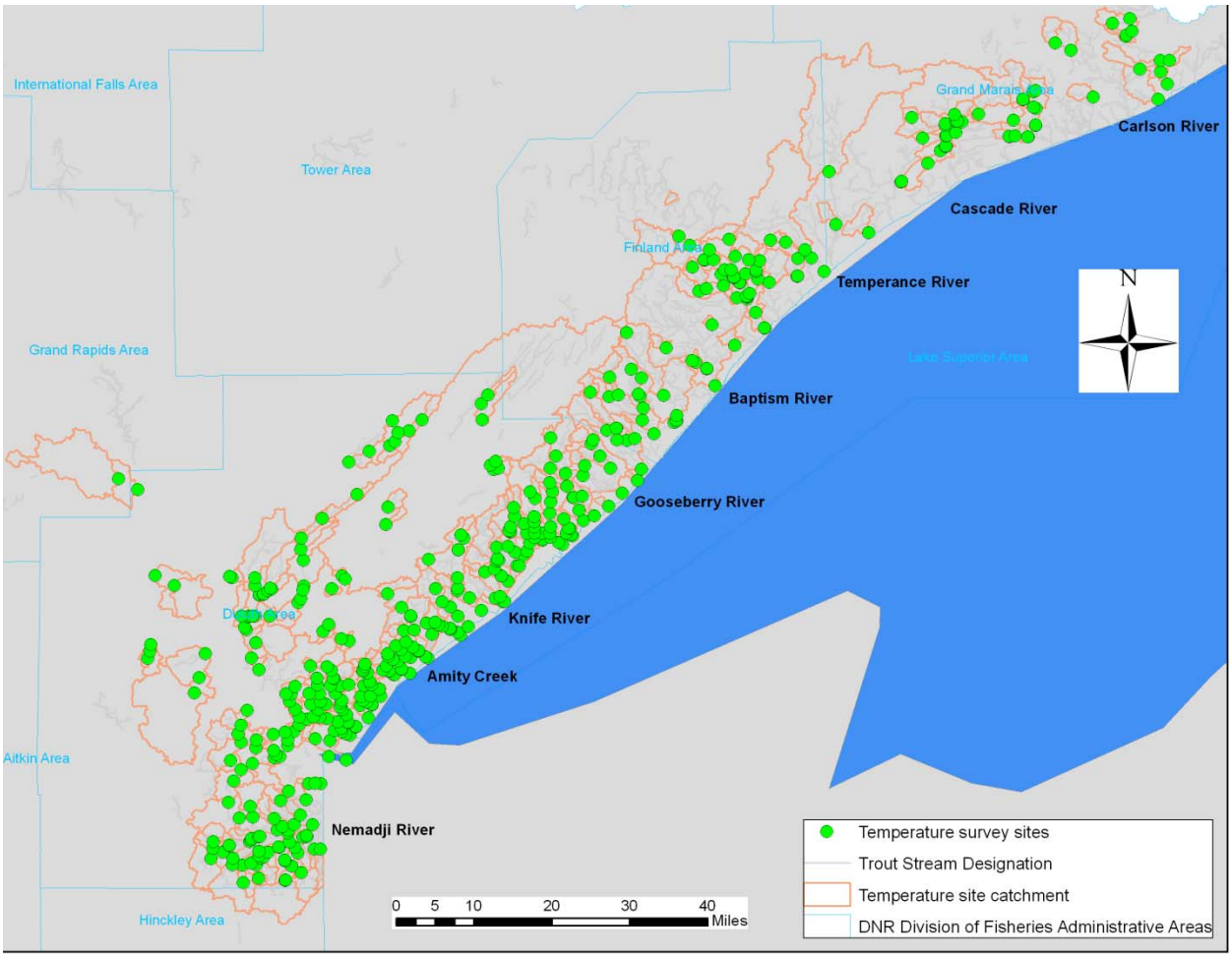

Figure 8.1. Map of stream water temperature survey sites, and studied catchments in north shore region of Lake Superior.

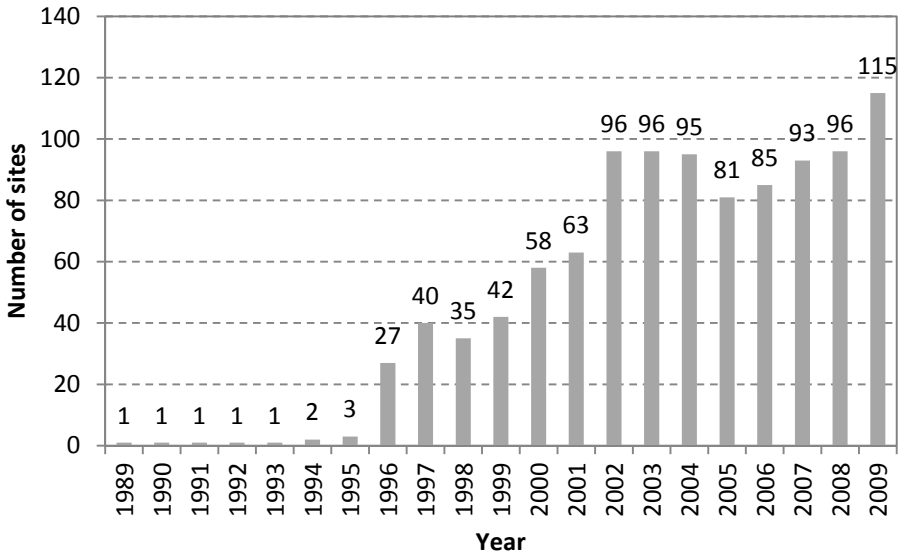

Figure 8.2. Number of stream water survey sites from 1989 to 2009.

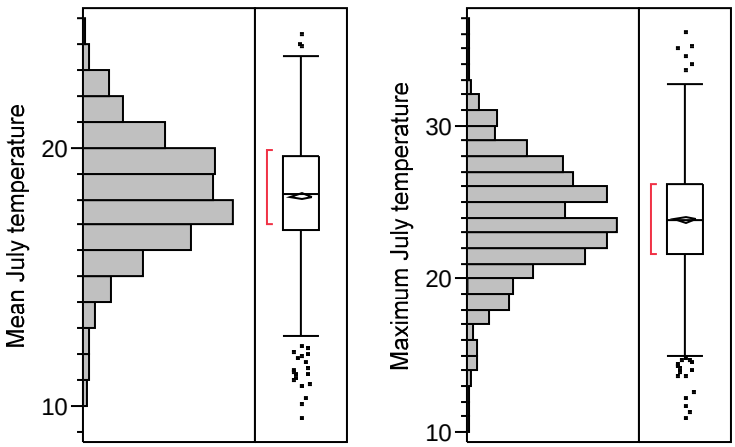

Figure 8.3. Distribution of mean and maximum July monthly water temperature using data from 1996 to 2009. Unit as degree Celsius.

To predict stream water temperature, variables related to climate change and land characteristics were collected from a variety of sources. Potential predictors included air temperature, watershed area, land cover, forest type, Quaternary geology class, lithology type, soil properties, wetland cover, percentage of impervious cover area, slope, latitude and distance to shoreline (Table 8.1; Appendices 8.1 – 8.5).

Unique watershed was delineated in ArcMap 10.1 for each of 427 survey sites based on 10×10 m DEM file (Figure 8.1). Landscape features associated with each watershed were characterized with existing maps from 1996 to 2006 using USGS NAWQA toolbox (Table 8.1). Percent of land cover types were determined from NLCD 2001 map for entire watershed, and 50 m, 100 m and 150 m stream buffer areas. The same calculations were applied to obtain percent of forest type, quaternary geology and lithology for each watershed. As there were too many zero values, only geology or lithology types present in more than 10% number of study catchments were used as candidate landscape predictors. Soil properties for each soil type were composited for top 150 m soil from STATSGO because most soil layer reached bedrock at that depth. After that, the composited soil properties were computed for each watershed based on the percent of a soil type.

To avoid strong skewness of landscape data, data transformation was applied to predictors as: (1) no transformation to slope variables and latitude; (2) log10 transformation to watershed area, depth to bedrock, permeability rate and distance to shoreline; and (3) arcsin square root transformation to predictor variables represented as proportional values.

The selection of water temperature model predictors was performed in JMP 9 using stepwise regression by following criteria: (1) largest model R-square; (2) entire model fit p-value less than 0.05; (3) p-value for each selected predictor less than 0.05; (4) each predictor variable is not leveraged by extreme values; (5) variance inflation factor (VIF) less than 2 to avoid collinearity among predictors; and (6) normal distribution of residuals.

In the empirical models for north shore stream temperature, response variables were 1) July monthly mean temperature and 2) July monthly maximum temperature. . The range of hourly July temperatures also was calculated; since no significant models were identified for this variable, therefore, it will not be discussed further. Around 90% of the 427 sites were chosen to develop the regression model while the remaining 10% of data were used to validate the model. To ensure that validation sites were uniformly distributed from north to south across the study area, all sites were classified into 10 groups (around 40 sites for each) based on latitude. Four sites were then randomly selected from each of ten groups to be used as validation sites.

Table 8.1. Potential landscape predictor variables used in developing empirical stream water temperature model.

Group	Variables	Source	Unit
Air temperature	July maximum air temperature, July minimum air temperature, July mean air temperature	Calculated from observation	degrees C
Area	Entire catchment, 50m stream buffer, 100m stream buffer, 150m stream buffer	GIS spatial analysis	ha
Land cover - Entire catchment, 50m stream buffer, 100m stream buffer, 150m stream buffer	Open water Developed: open space, low intensity, medium intensity, high intensity Forest: deciduous forest, evergreen forest, mixed forest Barren land Shrub/Scrub Grassland/Herbaceous Pasture/Hay Cultivated crops Woodland wetland Emergent Herbaceous	NLCD	percent
Forest type	Aspen birch, Aspen birch spruce fir Jack pine Lowland conifer, Lowland hardwood Mixed lowland hardwood conifer Northern hardwood, Northern hardwood conifer Red white pine Sphagnum spp. Spruce fir	Wolter and White (2002)	percent
Quaternary geology	28_Superior lobe Nickerson Moraine 32_Superior lobe Mille Lacs-Highland Moraine 33_Superior lobe Mille Lacs-Highland Moraine 36_Superior lobe 37_Superior lobe Glacial Lake Sediment 43_Rainy lobe St. Croix Moraine	USGS	percent
Soil properties	Permeability rate, soil texture fraction (sand, silt, clay), soil depth to bed rock, hydrologic group soil fraction	NRCS STATSGO	cm hr^{-1} for permeability rate, cm for soil depth, percent for others
Lithology	10_Glacial Till, Loamy 14_Glacial Outwash and Glacial Lake Sediment, Coarse-Textured 9_Glacial Till, Clayey	USGS	percent
Slope	Min slope, Max slope, Average slope Range of slope	GIS spatial analysis	degree
Impervious	Impervious area	GIS spatial analysis	percent
Wetland	Wetland area	NWI	percent
Compound topographic index	Min, max, mean, range and standard deviation		
Latitude	Latitude	GIS	meter
Distance	Distance to shoreline	GIS calculation	meter

8.2 Stream water temperature models

Two types of multiple regression models were developed for July mean and July maximum temperature: best model and generalized model. A generalized model contains the same group of predictors for both July mean and July maximum temperature to facilitate comparison between models. The model fit output (Appendices 8.6, 8.7) indicated that selected models were statistically reasonable, as all criteria such as VIF, residues distribution, leverage plot, significance of each predictors, and p value for entire model, were completely satisfied.

8.2.1 Model to predict average July mean temperature (T_{mean})

Using the potential independent variables in Table 8.1 and maximizing the model adjusted R^2, the best model, (which was also the generalized model) for average July mean temperature was found to be:

$$T_{mean} = -33.35 + 0.67T_{ave\_air} + 1.51\log(Wshed\_Area) + 2.05sqrt[\arcsin(\%WoodyWetlands\_150m)] - 1.33\log(Permeability) + 6.52 \times 10^{-6}Latitude \quad (8.1)$$

$$n = 369,\ R^2=0.40,\ R^2_{adj}=0.39,\ p<0.01$$

Stream water temperature was positively affected by air temperature, basin area, woody wetlands area in the riparian zone and latitude, but negatively correlated to soil permeability. The model predicts that an increase of air temperature by 1^{o}C would raise water temperature by 0.67^{o}C.

To check the effects of each predictor in model prediction of water temperature, sum of squares (SS) for each parameter was summarized in Table 8.2. SS represents the difference between the complete model and a reduced model. The complete model is one with all predictors included (five predictors in this model) while reduced model is the model that leaves out one of the predictor variables. If all predictor variables are orthogonal, the sum of SS should equal to the model SS, and the ratio of each predictor's SS to model SS should be the proportion of variance explained by each variable. However, VIF values (Appendix 8.6) indicated that the five selected predictors were slightly correlated with one another other. A VIF =1 will be expected if orthogonal. In this case, the absolute values of SS for each variable and ratio of predictor's SS to sum of SS were compared to each other to estimate the relative contribution of each parameter to model predictor.

The variable with larger SS values tended to explain more variance in the model. SS values of air temperature and basin area were almost five times those of the other three variables. The combined ratio of these two predictors to the sum was 80%, roughly accounting for 80% of model variance in other words. The remaining 20% of model variance was explained by the combination of soil permeability, percent of woody wetlands in the riparian zone and latitude.

Table 8.2. Effects of selected independent variables to average July mean water temperature model.

Predictor variables	Sum of squares	F Ratio	Prob > F	SS/sum
T_{ave_air}	254.0	100.4	<.0001	0.422
Wshed area	231.6	91.53	<.0001	0.384
Soil permeability	52.78	20.86	<.0001	0.088
Latitude	22.59	8.92	0.003	0.037
%Woody wetlands_150m	41.47	16.39	<.0001	0.069
sum	602.5			1

8.2.2 Model predicting average July maximum temperature (T_{max})

The best model (Equation 8.2) and the generalized model (Equation 8.3) for average July maximum temperature were developed as:

$$T_{max} = -79.13 + 1.04T_{\min\_air} + 2.22\log(Wshed\_Area) + 3.1sqrt[arcsin(\%WoodyWetlands\_150m)] - 1.21\log(Permeability) + 1.58 \times 10^{-5}Latitude \quad (8.2)$$

N = 369, R^2=0.35, R^2_{adj}=0.34, p<0.01

$$T_{max} = -86.63 + 0.96T_{\text{ave}\_air} + 2.25\log(Wshed\_Area) + 2.21sqrt[arcsin(\%WoodyWetlands\_150m)] - 2.41\log(Permeability) + 1.65 \times 10^{-5}Latitude \quad (8.3)$$

N = 369, R^2=0.33, R^2_{adj}=0.32, p<0.01

Where, T_{min_air} is the July minimum air temperature.

Both models had same correlation patterns as the model for average July mean temperature, including a negative correlation with permeability and positive correlation for all other predictors. The model predicted by minimum air temperature (Equation 8.2) explains about 2% more variance in maximum water temperature than the generalized model. When the predictor changed from average air temperature to minimum air temperature, the proportion of model variance explained by air temperature was increased from 0.37 to 0.43 (Table 8.3).

Table 8.3. Effects of selected independent variables to average July maximum temperature model.

Predictor variables	Sum of Squares	F Ratio	Prob > F	SS/sum
Best model (Equation 8.2)				
Tmin_air	591.2	85.58	<.0001	0.433
Area	504.0	72.96	<.0001	0.369
Permeability	42.26	6.12	0.0138	0.031
Latitude	136.6	19.78	<.0001	0.100
PCT_Woody Wetlands_150m	92.67	13.41	0.0003	0.068
	1367.0			1
Generalized model (Equation 8.3)				
Tave_air	520.7	73.32	<.0001	0.370
Area	521.9	73.48	<.0001	0.370
Permeability	173.5	24.43	<.0001	0.123
Latitude	144.4	20.34	<.0001	0.103
%Woody Wetlands_150m	48.51	6.83	0.0093	0.034
sum	1409.0			1

It should be noted that an increase of mean air temperature by 1° C, results in elevation of the maximum water temperature by 0.96^{o}C. In contrast, average water temperature is raised by only 0.67^{o}C. This suggests that an increase in air temperature would lead to larger variation in water temperature.

8.3 Water temperature model validation

Previously developed best and generalized models were validated by comparing predicted water temperature and observed values in select validation sites (Figure 8.4). The model fit between predicted and observed data were generally good for both mean and maximum water temperature. Only one low temperature site was significantly over-estimated by the model.

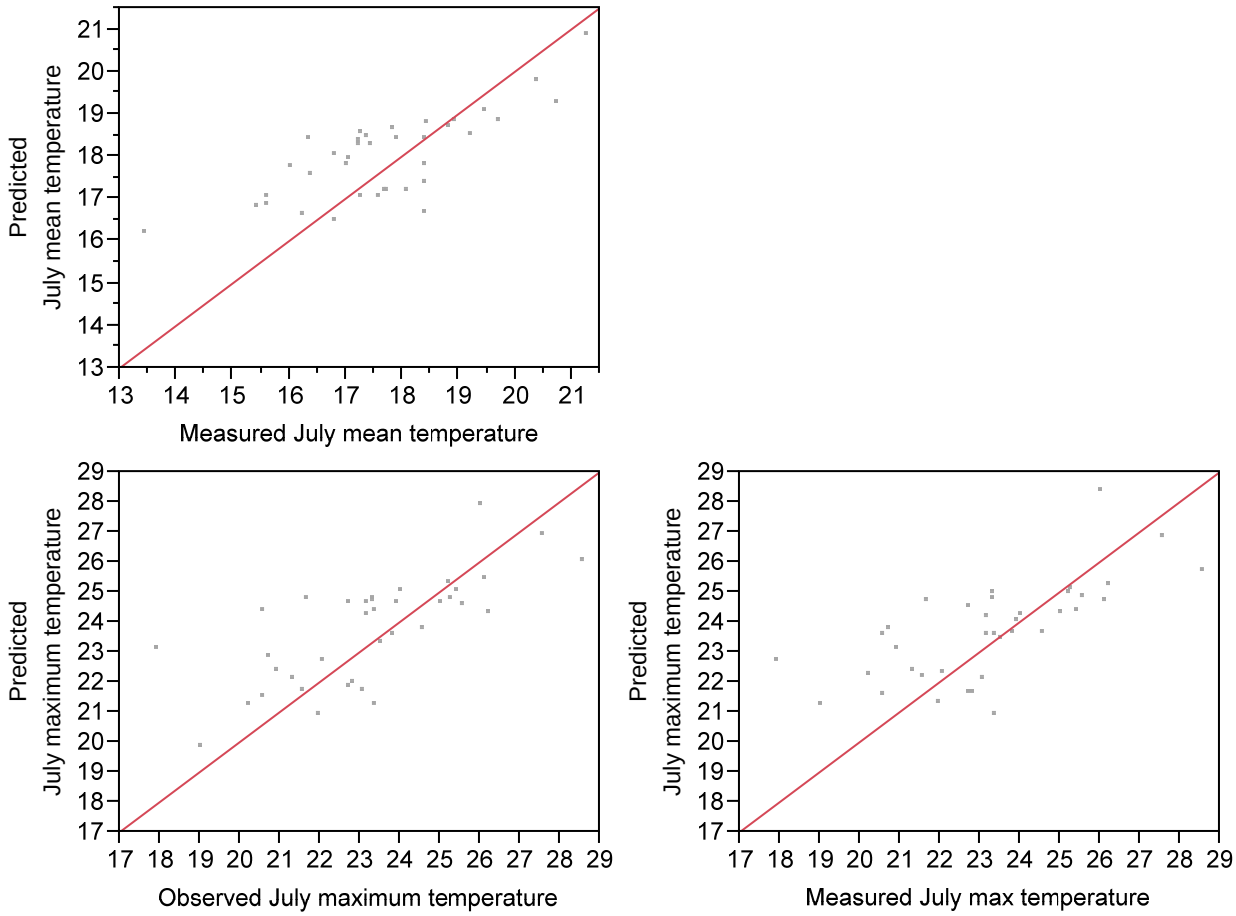

Figure 8.4. Comparison of model predicted and observed water temperature for average July mean temperature (top), and average July maximum temperature (bottom left for best model, bottom right for generalized model) in 37 validation sites.

8.4 Discussion

Air temperature and land characteristics including watershed area, soil property, land cover and latitude, demonstrated significant impacts to stream water temperature. The multiple regression model for stream water temperature accounted for around 40% variation of July mean temperature, and around 33-35% variation of July maximum temperature. Other model unexplained data variation might be attributed to survey variation caused by field operation or instruments, or by local factors such as local shading by bankside or riparian vegetation, or local groundwater inputs. As land cover and air temperature variation were relative small across this small study area, these measurement errors became significant contributors to model prediction.

Air temperature significantly influenced water temperature, with a predicted increase of 0.69^{o}C in the July monthly mean temperature and 0.96^{o}C July in the monthly maximum temperature per every Celsius degree increase of air temperature. The magnitude of the July mean water

temperature falls in the range of two projected values reported for Lower Michigan (0.46^{o}C and 0.92^{o}C, respectively; Eaton and Scheller 1996, Wehrly et al. 2006).

Except for air temperature, drainage area was the most important parameter predicting water temperature. Drainage area is commonly found to be a predictor of stream water temperature (e.g., Wehrly et al. 2006). The typical positive relationship between catchment area and stream water temperature could be explained by heat exchange duration and solar radiation input. Stream drained from larger catchment have longer water residence time, with greater exposure to the atmosphere and great potential for heat exchange (Jonson 2003). Moreover, stream size becomes larger when flowing to downstream, consequently to generate great surface area to enhance solar radiation at downstream (Gaffield et al. 2005).

Poorly drained soil, indicated by low permeability rate, reduced the infiltration ratio but increased the ratio of overland flow. Surface flow tended to be less buffered than groundwater. As a result, water temperature in surface flow was warmer than groundwater in summer but colder in winter. Because this study focused on summer, high permeability was expected to generate low water temperature. The negative coefficient for permeability in water temperature model was consistent with this expectation.

In 150 m buffer area around streams, woody wetland is the dominant wetland types in the study area, averaging 35% of total area. Two other wetland types, open water and emergent herbaceous wetland, comprise 2% and 6.5% of total area, respectively. Compared to forest area, woody wetlands provide less shading and more open space to water for direct solar radiation to accumulate heat energy (Wehrly et al. 2006). Although woody wetland provides some shade, summer water temperature in wetland still are expected to be higher than groundwater, due to heat exchange and solar radiation. Heat exchange between air and water plus additional solar radiation in these wetlands can raise water temperature in wetlands. Thus, the recharge of water from wetlands to stream can increase stream temperature, and result in higher stream temperatures.

Latitude was expected to contribute negative effect to water temperature. Interestingly a positive relationship was found here. Catchments in the northern portion of the study area tend to be larger in area than those in the southern and middle portion of the study area, thus this relationship is likely to partially explain this result.

References

Eaton, J.G. and Scheller, R.M. (1996). Effects of climate warming on fish thermal habitat in streams of the United States. Limnology and Oceanography 41: 1109-1115.

Gaffield, S.J., Potter, K.W. and Wang, L. (2005). Predicting the summer temperature of small streams in southwestern Wisconsin. Journal of the American Water Resources Association: 25-36.

Johnson, S.L. (2003). Stream temperature: scaling of observations and issues for modeling. Hydrological Processes 17: 497-499.

Picard, C.R., Bozek, M.A. and Momot, W.T. (2003). Effectiveness of using summer thermal indices to classify and protect book trout streams in northern Ontario. North American Journal of Fisheries Management 23: 206-215.

Wehrly, K.E., Wiley, M.J. and Seelbach, P.W. (2006). Influence of landscape features on summer water temperatures in Lower Michigan streams. American Fisheries Society Symposium 48: 113-127.

Wolter, P.T. and White, M.A. (2002). Recent forest cover type transitions and landscape structural changes in northeast Minnesota, USA. Landscape Ecology 17: 133-155.

9. Response of Stream Temperature to Climate Change

The calibrated Knife River, Baptism River, and Amity Creek stream temperature models were used to evaluate the response of stream temperature to projected climate change. As with the sensitivity analysis given in Section 3, models were set for 20 years of simulations, May through October, using Duluth (DLH) climate data from 1980 – 1999. Monthly climate increments were then applied to the baseline climate, and the changes in monthly stream temperature were summarized.

There are several pathways for climate change to influence stream temperature which were considered in this study (Figure 9.1). In addition to applying the incremented climate directly to the stream temperature model, corresponding streamflow and baseflow inputs were calculated by applying the incremented climate to the hydrologic models (Section 5), and baseflow temperature inputs were calculated using the wetland temperature model (Section 7).

9.1 Available climate projections

Several GCM projections were available for this study, summarized here but discussed in more detail in Section 3 and Appendix 3.1. Dynamically downscaled GCM output (15 km grid spacing) made by Oregon State University for the USGS National Fish Habitat Assessment Project, were available for three GCMs: GENMOM, GFDL, ECHAM5. All of the GCM data described in this report were regionally downscaled using the RegCM3 model using the A2 emissions scenario (Hostetler et al. 2011).

The available downscaled GCM data were used to calculate monthly increments to historical climate for 2020-2039, 2040-2059, 2060-2079, 2070-2089. These data were used to calculate weekly-averaged climate, and input directly in the hydrologic, wetland temperature, and stream temperature models. Changes in air temperature, humidity, precipitation, wind speed, and solar radiation data were considered.

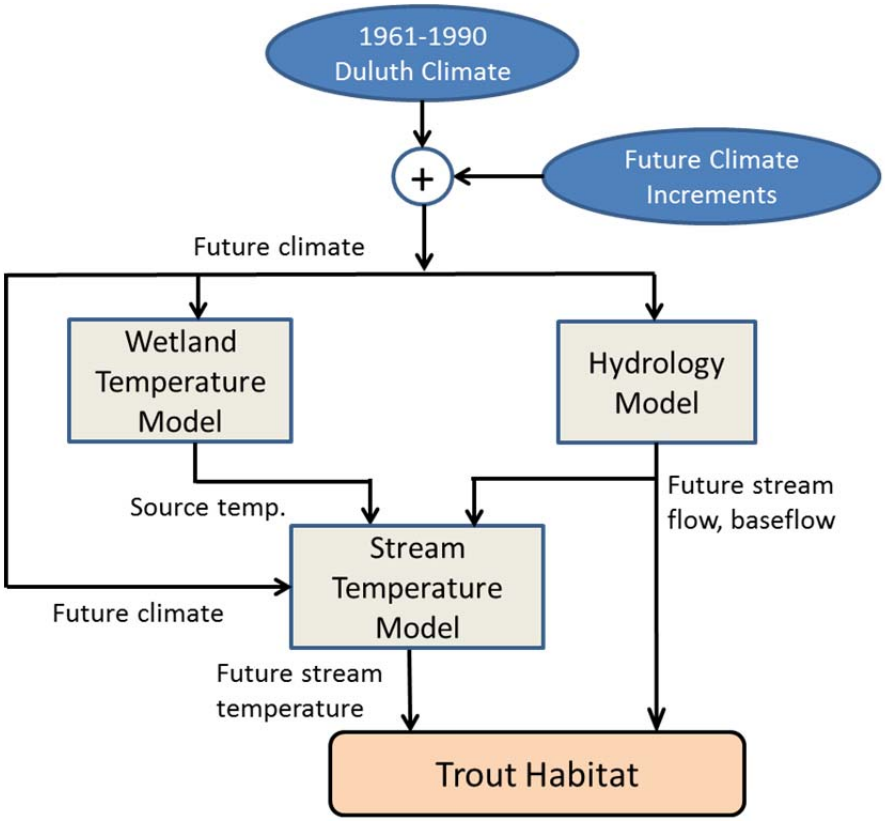

Figure 9.1 Schematic diagram summarizing the procedures used to analyze the response of stream temperature to climate change.

9.2 Response of Wetland (baseflow) Temperatures to Monthly Climate Increments

The wetland temperature model was run for nominal Duluth climate (1980-1999) and for the incremented climate. Table 9.1 summarizes the response of simulated wetland temperatures to projected climate changes for the GENMOM, ECHAM5, and GFDL climate increments. The wetland model is not set up for year-round simulations; therefore, temperature simulations were initiated April 1of each year, with identical initial conditions for all cases. As a result, the projected increases in temperature may be underestimated, because higher soil temperatures are not carried through to the next year.

Table 9.1. Projected change in average wetland temperature (May-October) for the GENMOM, ECHAM5, and GFDL increments.

	Change in temperature (°C)			
	2020-39	2040-59	2060-79	2070-89
GENMOM	0.52	0.67	1.30	1.30
ECHAM5	0.62	1.27	2.08	2.50
GFDL		1.67		

9.2 Response of Knife River water temperatures to monthly climate increments

The calibrated stream temperature model for the Knife River was run for nominal Duluth climate (1980-1999) and for the incremented climate, along with corresponding simulated stream flows (Section 6) and wetland temperatures (Section 9.1) generated using the same climate projections. Table 9.2 summarizes the response of mean monthly stream temperature in the Knife River to the GENMOM, ECHAM5, and GFDL climate increments, while Table 9.3 gives the change in mean monthly temperature from the 1980-99 period to the future periods. Table 9.3 also gives the corresponding GCM air temperature increments, for reference. Figures 9.2, 9.3, and 9.4 plot the 20-year average weekly temperatures and monthly temperature increases for the GENMOM, ECHAM5, and GFDL climate projections, respectively.

Overall, months with the largest air temperature increments also have the largest stream temperature increments. The GENMOM climate increments result in relatively moderate, uniform increases in stream temperature from May to October, ranging from 1.37 to 1.91 °C by the 2070-89 time period. The ECHAM5 climate increments give larger stream temperature increases in all months, but particularly in May and October, with a 3.6 and 3.1 °C increase, respectively, by 2070-89. The ECHAM5 projections continue on an upward slope from 2060-79 to 2070-89, while the GENMOM projections level out or decrease slightly between these last two increments. The GFDL climate increments, while limited, project relatively large increases in mid-summer stream temperature for the 2040-59 increment, with a 2.4 °C increase in August stream temperature, matching the 2070-89 ECHAM5 increases in mid-summer stream temperature.

Table 9.2. Projected monthly average stream temperature for the Knife River based on the GENMOM, ECHAM5, and GFDL monthly climate increments.

Monthly average stream temperature, GENMOM (°C)

	1980-99	2020-39	2040-59	2060-79	2070-89
May	11.8	11.8	12.1	12.9	13.1
Jun	17.7	18.2	18.4	19.2	19.3
Jul	19.4	20.2	20.6	20.9	20.8
Aug	18.8	19.0	19.2	20.0	20.2
Sept	13.6	14.3	14.2	15.0	14.9
Oct	7.7	8.6	8.4	9.7	9.6

Monthly average stream temperature, ECHAM5 (°C)

	1980-99	2020-39	2040-59	2060-79	2070-89
May	11.8	13.2	13.2	14.8	15.3
Jun	17.7	18.4	19.5	19.7	20.1
Jul	19.4	19.9	20.7	21.4	21.7
Aug	18.8	18.7	20.1	20.7	21.1
Sept	13.6	13.7	14.4	15.5	15.8
Oct	7.7	9.0	9.0	10.0	10.8

Monthly average stream temperature, GFDL (°C)

	1980-99	2020-39	2040-59	2060-79	2070-89
May	11.8		13.3		
Jun	17.7		19.6		
Jul	19.4		21.4		
Aug	18.8		21.1		
Sept	13.6		15.5		
Oct	7.7		9.2		

Table 9.3. Projected change in monthly average stream temperature for the Knife River based on the GENMOM, ECHAM5, and GFDL monthly climate increments.

	Monthly air temperature difference, GENMOM (°C)				Monthly stream temperature difference, GENMOM (°C)			
	2020-39	2040-59	2060-79	2070-89	2020-39	2040-59	2060-79	2070-89
May	-0.04	0.59	1.28	1.72	0.03	0.35	1.18	1.37
Jun	0.70	0.84	1.63	1.79	0.50	0.69	1.43	1.56
Jul	1.18	1.42	1.89	1.80	0.79	1.15	1.54	1.40
Aug	0.28	0.58	1.75	2.20	0.27	0.47	1.29	1.47
Sept	0.66	0.75	1.62	1.41	0.65	0.63	1.38	1.31
Oct	1.05	0.77	2.46	2.27	0.89	0.66	2.01	1.91

	Monthly air temperature difference, ECHAM5 (°C)				Monthly stream temperature difference, ECHAM5 (°C)			
	2020-39	2040-59	2060-79	2070-89	2020-39	2040-59	2060-79	2070-89
May	2.01	2.16	3.88	4.26	1.39	1.44	3.08	3.55
Jun	0.78	1.84	2.12	2.64	0.71	1.80	2.01	2.42
Jul	0.53	1.45	2.22	2.61	0.46	1.29	1.95	2.28
Aug	0.06	1.69	2.37	2.86	-0.09	1.35	1.93	2.40
Sept	0.25	1.08	2.31	2.69	0.04	0.83	1.87	2.22
Oct	1.42	1.38	2.68	3.56	1.21	1.22	2.28	3.06

	Monthly air temperature difference, GFDL (°C)				Monthly stream temperature difference, GFDL (°C)			
	2020-39	2040-59	2060-79	2070-89	2020-39	2040-59	2060-79	2070-89
May		1.88				1.53		
Jun		2.23				1.90		
Jul		2.14				2.02		
Aug		2.65				2.36		
Sept		2.17				1.86		
Oct		1.59				1.50		

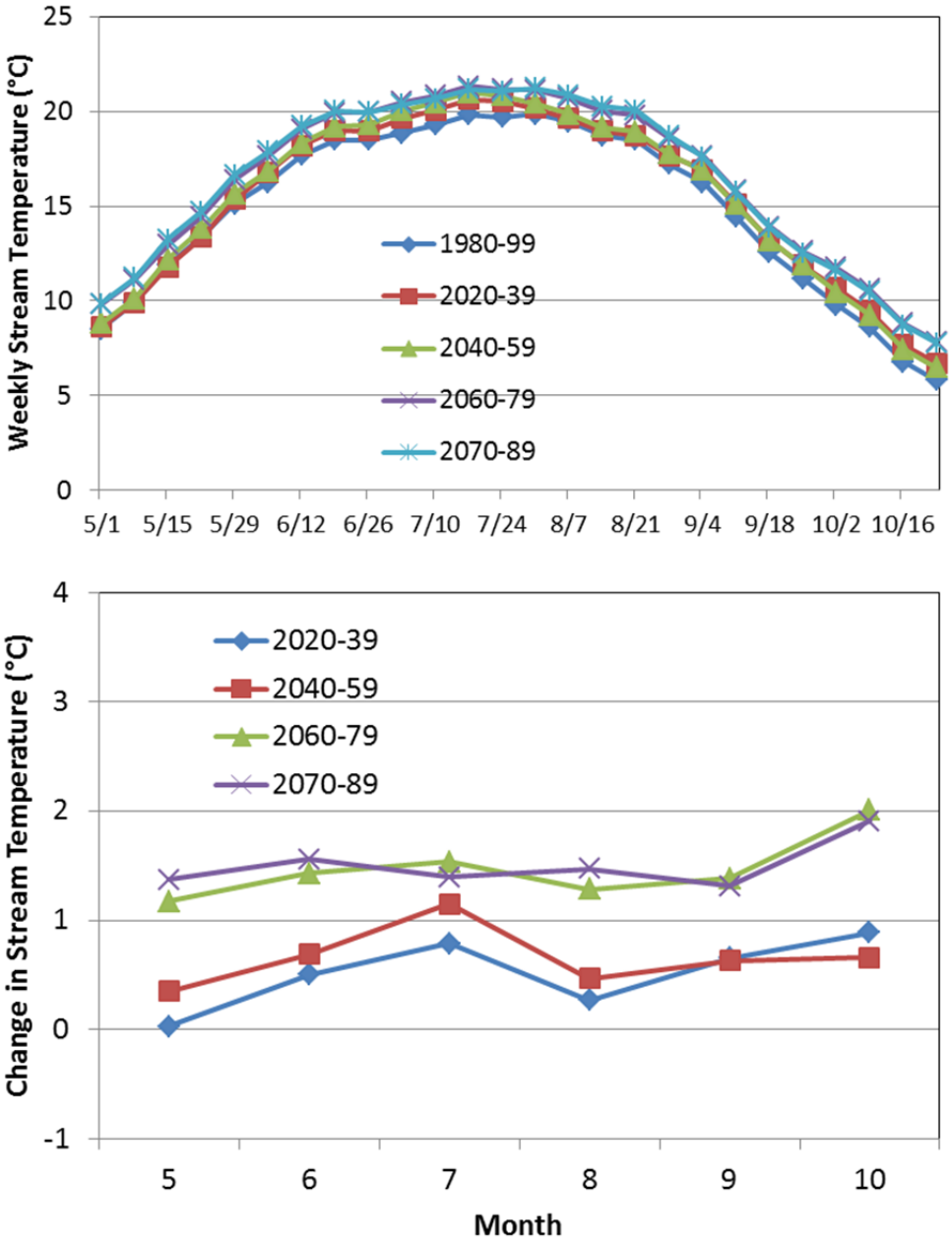

Figure 9.2. Projected 20-year average weekly stream temperatures and 20-year average change in weekly stream temperature for the Knife River during the time periods 1980-99, 2020-39, 2040-59, 2060-79, and 2070-89, based on GENMOM climate increments.

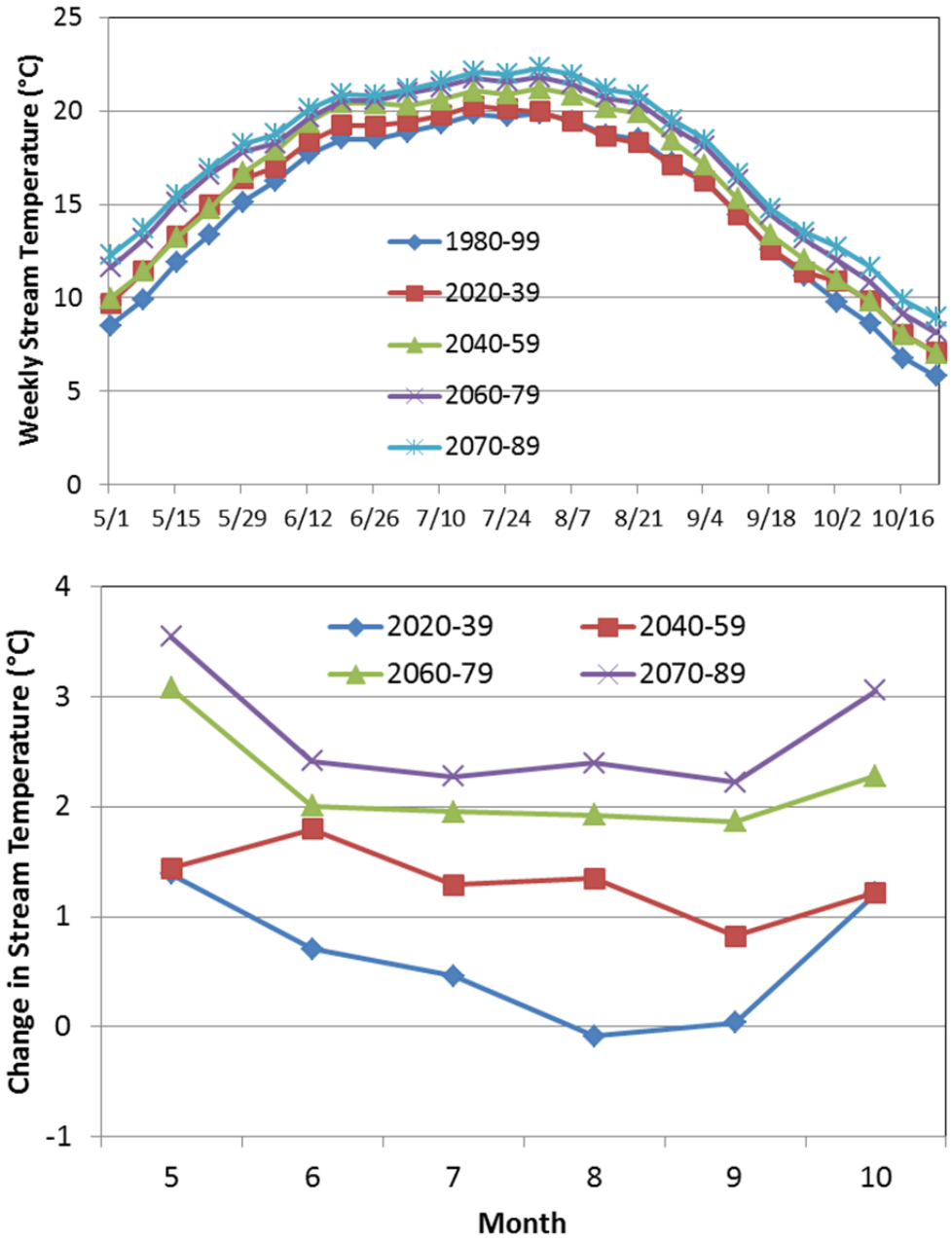

Figure 9.3. Projected 20-year average weekly stream temperatures and 20-year average change in weekly stream temperature for the Knife River during the time periods 1980-99, 2020-39, 2040-59, 2060-79, and 2070-89, based on ECHAM5 climate increments.

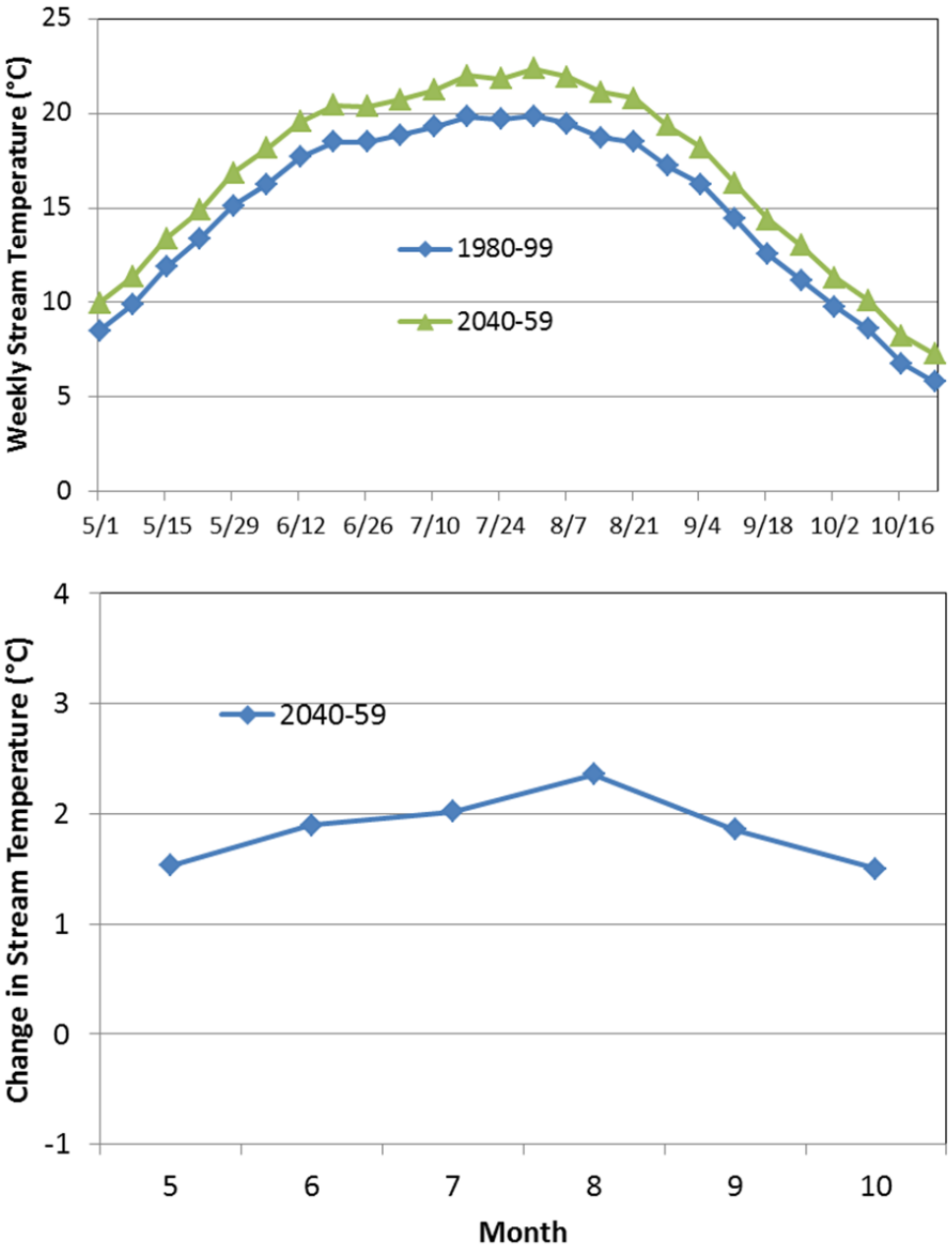

Figure 9.4. Projected 20-year average weekly stream temperatures and 20-year average change in weekly stream temperature for the Knife River during the time periods 1980-99 and 2040-59, based on GFDL climate increments.

9.4 Response of Knife River, Baptism River, and Amity Creek Water Temperatures to the GENMOM Daily Climate Projections

For the previous analysis using monthly increments, the short term (week to week) and inter-annual temperature fluctuations were established by the historical climate data set. The downscaled GCM climate time series available for this study removes this constraint, so that the GCM model can introduce more dynamic changes in future climate. The downscaled, daily time step GENMOM climate projections for 1980-99 and 2020-89 were used to generate a weekly time series of climate for the historical and future periods. These weekly climate data were then used as input to the stream temperature models for the Knife River, the Baptism River, and Amity Creek, along with corresponding stream flow and wetland temperature data generated using the GENMOM climate data.

Since the monthly climate increments used in the previous section are based on the same data, the stream temperature simulation results using the weekly time series and the monthly increments should be quite similar when compared as, e.g., 20-year averages. Indeed, the projected 20-year average, seasonal stream temperatures for Knife River obtained using the weekly climate time series (Figure 9.5) are very similar to the results obtained using the monthly climate increments (Figure 9.2). The same GENMOM weekly climate time series input to the Baptism River and Amity Creek stream temperature models gives slightly different results, due to differences in shading and baseflow input (Figures 9.6, 9.7). Interestingly, Amity Creek, with the lowest baseflow (wetland) inputs, maintains the lowest summer temperatures (Figure 9.7). Note that this is consistent with the observed stream temperature – air temperature slopes given in Section 2.6. This is likely due to a combination of two mechanism: 1) the temperature of the Knife River and the Baptism River is subject to the compounding effects of increased atmospheric heat transfer directly to the stream and increases in baseflow temperature, whereas Amity Creek, with very little baseflow input from wetlands, is subject only to atmospheric heat transfer, and 2) Amity Creek has a smaller watershed than the Knife and Baptism, and therefore has a shorter water residence time, so that atmospheric heat transfer has less time to heat the stream water.

The projected stream temperatures in the Knife River, Baptism River, and Amity Creek are summarized in Tables 9.4 to 9.6, respectively for the 50^{th}, 90^{th} and 100^{th} percentiles of the distribution. Results show that the 20 °C exceedances will occur rarely towards the end of the century in the 50^{th} percentile during July, but will be common throughout the summer in the 90^{th} and 100^{th} percentiles. Examples of the raw stream temperature model output using the weekly climate series are given in Figure 9.8, which plots the projected July weekly stream temperatures. The LOWESS trends lines included with the time series show a similar pattern for the Knife and Baptism Rivers, with an increasing trend in stream temperature to 2089, but with a lower slope after 2040-2050. The same data are given in Figure 9.9 as box plots. The projected temperatures for the Knife River, the Baptism River, and Amity Creek have similar future trends,

with temperatures peaking in the 2060-79 period (Figure 9.9). August stream temperatures, however, continue increasing through the 2070-89 period (Figure 9.10).

The projected July and August stream temperature extreme values are examined in more detail in Figure 9.11. For each 20-year block (1980-99, 2020-39, 2040-59, 2060-79, 2070-89), the 20-year average July and August maximums (Ave-Max), and the highest July and August maximum (Max-Max) are plotted. The average Ave-Max July and August temperatures show increases similar to those of the monthly means (Figures 9.5-9.7), with increases of up to 2 °C. The Max-Max stream temperatures show greater increases to 2089, up to 4 °C for the Knife River (Figure 9.11). For the Knife River and Amity Creek, the July Max-Max temperature peaks earlier in the century (2040-59) compared to the Ave-Max temperature (2060-79).

Changes in stream temperature can also be described in terms of temperature thresholds. For trout, a weekly-averaged stream temperature of 20 °C is often used as a threshold (e.g., Raleigh 1982) for suitable habitat. To examine temperature thresholds, the stream temperature model outputs were used to calculate the number of weeks per year that stream temperature is projected to exceed 20 °C. For stream temperature projections based on the GENMOM weekly climate series (Figure 9.12, upper panel), the average number of weeks per year with stream temperature exceeding 20 °C increases significantly, from 3 weeks per year in 1980-99 to about 8 weeks per year in 2070-89 in the Knife and Baptism rivers, and from less than 1 week per year to over 2 weeks per year in Amity creek. The results are similar for projected stream temperatures based monthly climate increments (Figure 9.12, lower panel), with the ECHAM5-based results showing slightly more weeks per year above 20 °C by 2070-89, and the limited GFDL-based results show the greatest increases for the 2040-59 period.

Table 9.4. Summary of stream temperature projections for the Knife River based on weekly GENMOM time series for the 50th, 90th and 100th percentiles of the distribution. Shaded areas represent temperatures that are believed to exceed the tolerances for brook trout.

Month	Percentile	1980-99	2020-39	2040-59	2060-79	2070-89
May	50	11.62	12.02	12.24	13.09	13.31
Jun	50	17.86	18.11	18.69	19.10	19.45
Jul	50	19.65	20.44	20.75	21.21	20.94
Aug	50	18.85	19.34	19.81	20.28	20.62
Sep	50	14.24	14.69	14.66	15.52	15.44
Oct	50	7.93	9.22	8.68	10.37	10.26
May	90	15.21	15.77	16.18	16.14	16.43
Jun	90	19.45	20.75	20.72	21.28	21.23
Jul	90	21.13	22.21	22.38	22.85	22.41
Aug	90	20.93	21.40	21.28	22.11	22.58
Sep	90	16.50	17.24	17.51	17.81	17.72
Oct	90	11.15	12.14	11.71	13.34	13.36
May	100	16.11	18.39	17.55	19.74	19.62
Jun	100	21.16	22.86	22.88	22.84	23.31
Jul	100	21.89	24.19	26.12	25.28	24.98
Aug	100	22.10	23.33	23.12	24.99	26.02
Sep	100	18.05	19.17	19.73	20.02	19.87
Oct	100	13.98	13.98	14.36	14.68	15.83

Table 9.5. Summary of stream temperature projections for the Baptism River based on weekly GENMOM time series for the 50th, 90th and 100th percentiles of the distribution. Shaded areas represent temperatures that are believed to exceed the tolerances for brook trout.

Month	Percentile	1980-99	2020-39	2040-59	2060-79	2070-89
May	50	12.42	12.68	13.24	13.75	13.95
Jun	50	17.41	18.60	18.62	19.28	19.17
Jul	50	19.66	20.94	20.58	21.29	21.16
Aug	50	18.59	19.07	19.56	19.97	20.34
Sep	50	13.86	14.74	14.63	15.44	15.69
Oct	50	6.69	7.57	7.34	8.77	8.61
May	90	16.44	16.34	16.57	17.32	16.88
Jun	90	19.77	20.67	20.81	21.14	21.12
Jul	90	21.31	22.23	22.71	22.89	22.88
Aug	90	20.45	21.41	21.16	22.12	22.80
Sep	90	16.82	17.18	17.74	17.99	17.77
Oct	90	9.58	10.55	10.19	11.75	11.84
May	100	18.27	19.20	17.87	20.38	19.83
Jun	100	21.01	22.88	22.44	22.73	22.78
Jul	100	22.51	24.39	25.22	25.08	25.92
Aug	100	22.29	22.99	23.02	24.50	26.43
Sep	100	18.53	19.67	19.18	19.95	20.29
Oct	100	11.62	11.76	11.82	12.97	14.89

Table 9.6. Summary of stream temperature projections for Amity Creek based on weekly GENMOM time series for the 50th, 90th and 100th percentiles of the distribution. Shaded areas represent temperatures that are believed to exceed the tolerances for brook trout.

Month	Percentile	1980-99	2020-39	2040-59	2060-79	2070-89
May	50	9.09	9.29	9.58	10.64	11.08
Jun	50	14.66	14.91	15.59	16.06	16.23
Jul	50	17.80	18.86	19.11	19.24	18.94
Aug	50	17.84	18.46	18.58	18.94	19.29
Sep	50	13.51	14.32	14.41	15.05	15.00
Oct	50	8.01	9.12	8.54	9.98	9.89
May	90	12.63	12.68	13.57	13.97	14.08
Jun	90	16.47	17.15	17.63	17.82	17.70
Jul	90	19.60	20.57	21.13	21.17	20.39
Aug	90	19.67	20.08	20.21	20.73	21.84
Sep	90	15.78	16.34	17.11	17.16	17.25
Oct	90	10.72	11.36	11.47	12.81	12.65
May	100	13.67	15.49	15.59	16.74	16.58
Jun	100	17.92	18.82	18.57	19.62	20.01
Jul	100	20.26	21.92	23.04	22.43	21.67
Aug	100	20.89	22.98	21.91	23.82	23.29
Sep	100	17.13	18.66	18.92	19.32	19.39
Oct	100	13.78	13.36	14.15	13.72	13.93

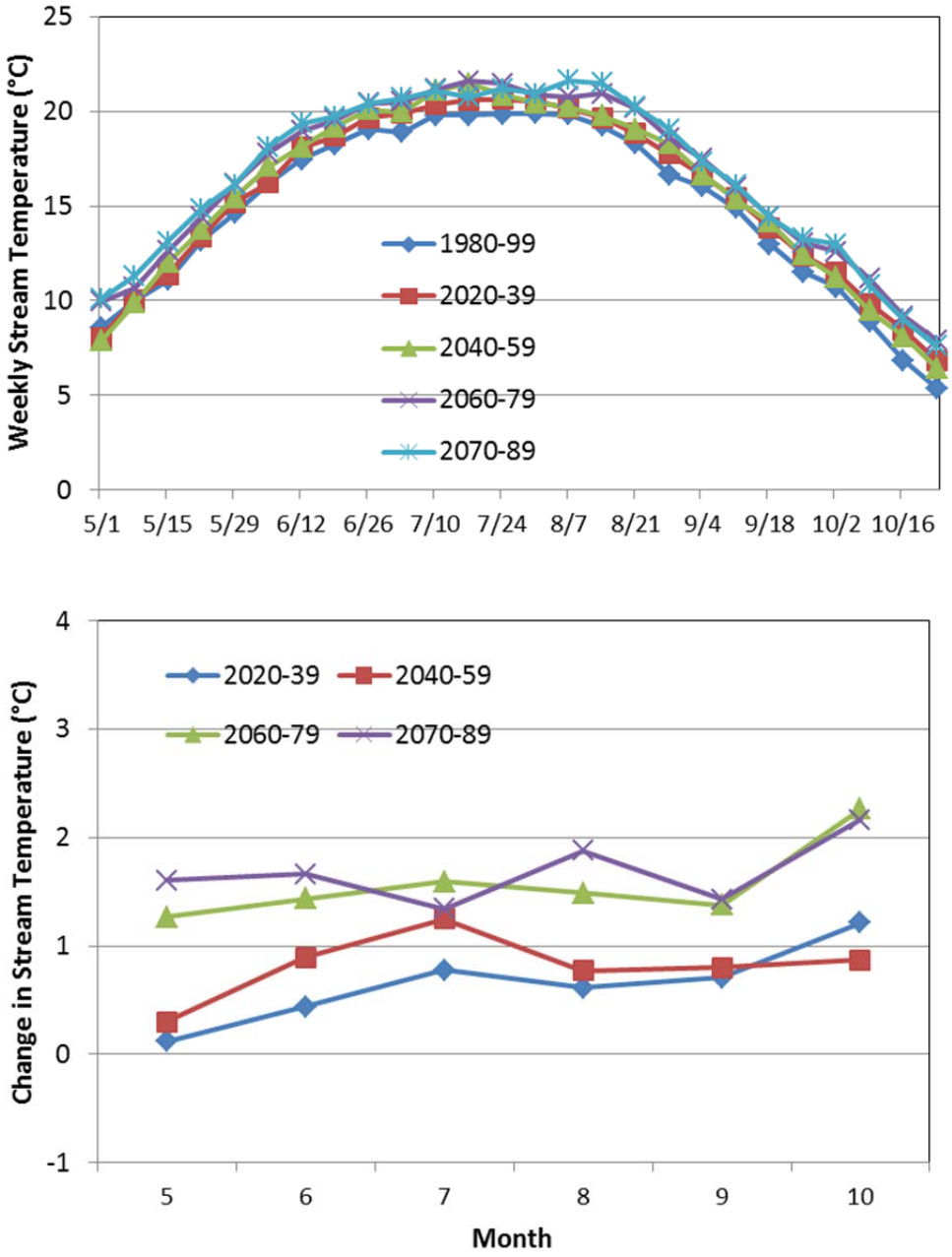

Figure 9.5. Projected 20-year average weekly stream temperatures and 20-year average change in weekly stream temperature for the Knife River during the time periods 1980-99, 2020-39, 2040-59, 2060-79, and 2070-89, based on daily GENMOM climate time series.

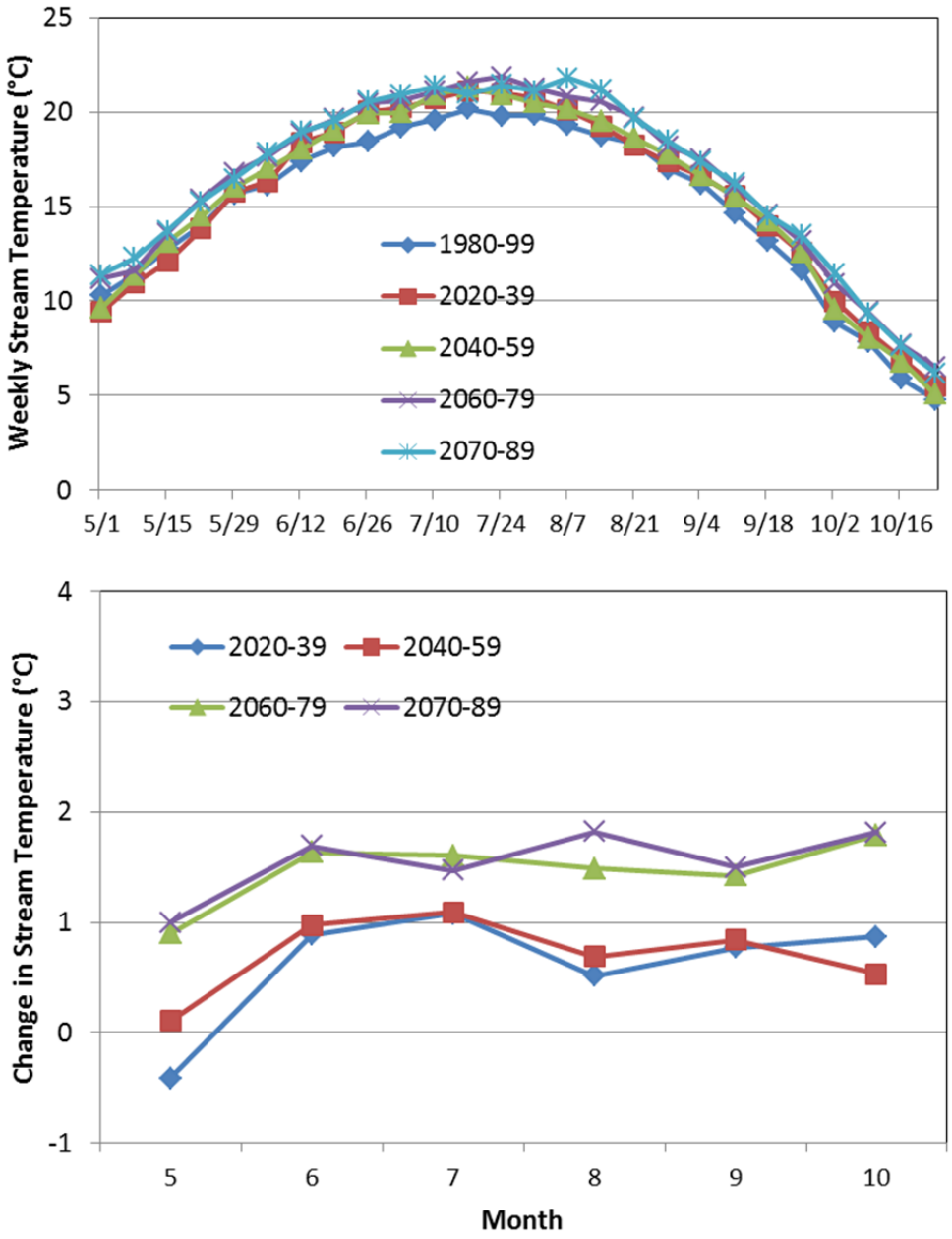

Figure 9.6. Projected 20-year average weekly stream temperatures and 20-year average change in weekly stream temperature for the Baptism River during the time periods 1980-99, 2020-39, 2040-59, 2060-79, and 2070-89, based on daily GENMOM climate time series.

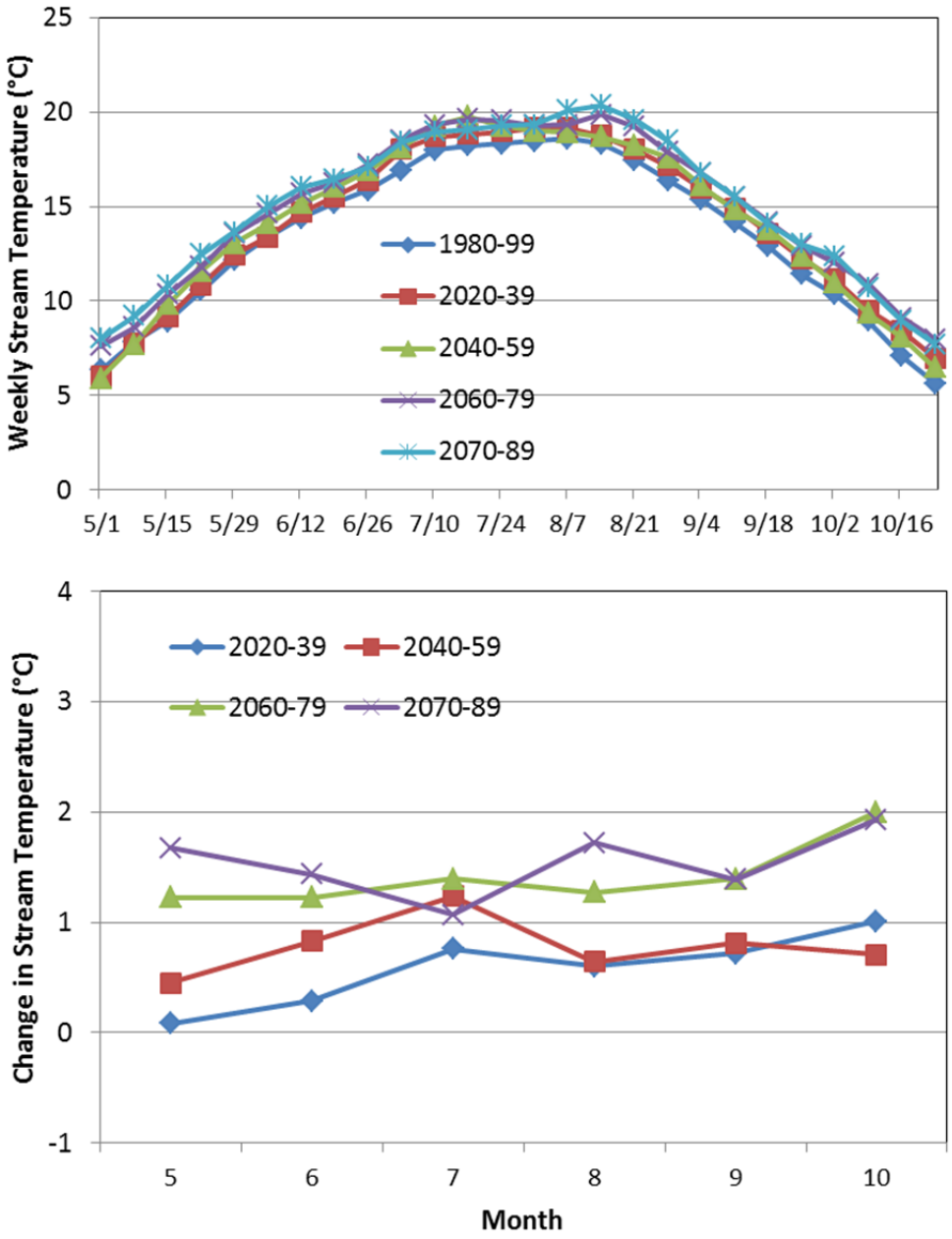

Figure 9.7. Projected 20-year average weekly stream temperatures and 20-year average change in weekly stream temperature for Amity Creek during the time periods 1980-99, 2020-39, 2040-59, 2060-79, and 2070-89, based on daily GENMOM climate time series.

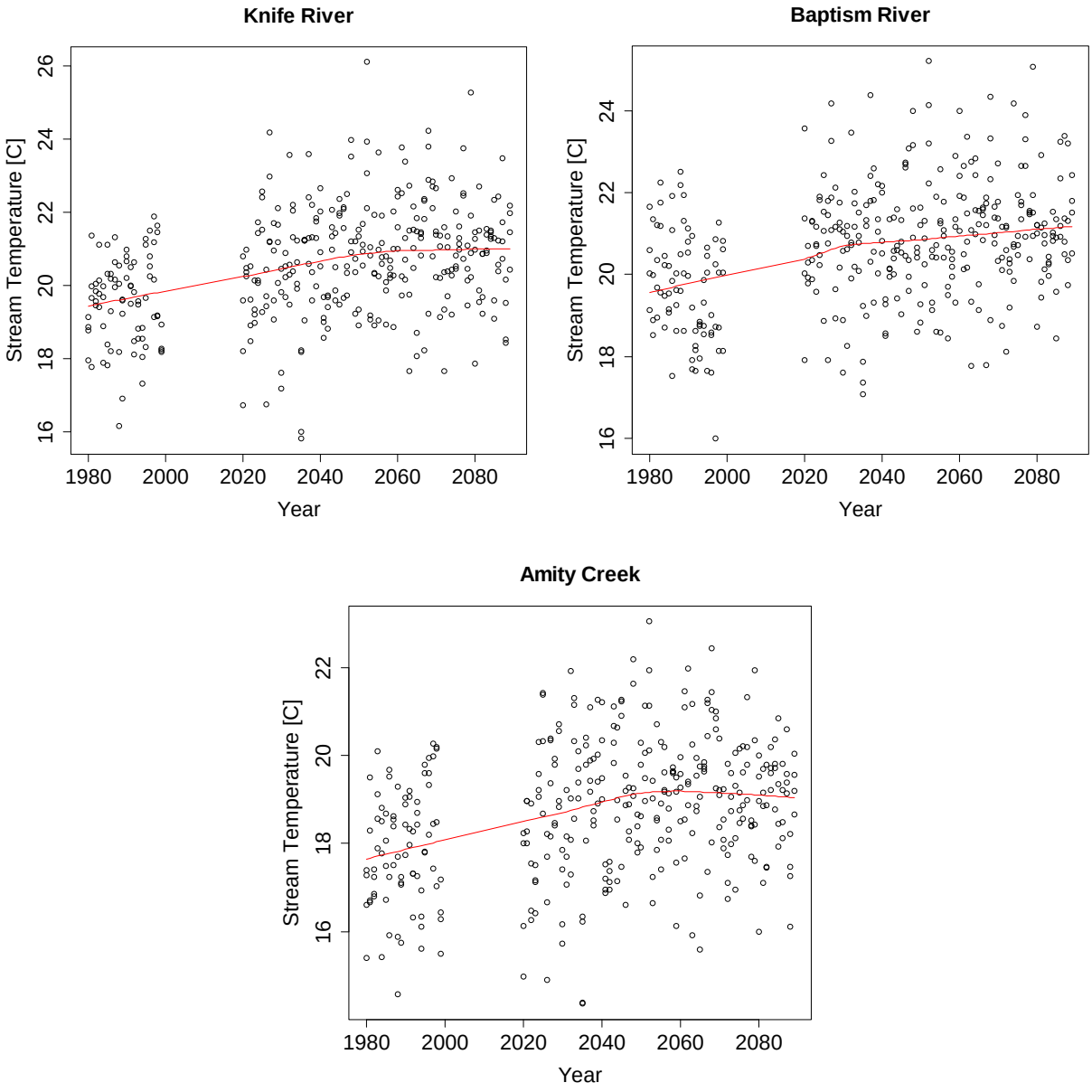

Figure 9.8. Projected July weekly stream temperatures for the Knife and Baptism rivers, and Amity Creek, based on daily GENMOM climate time series. A LOWESS trend line is included in each plot.

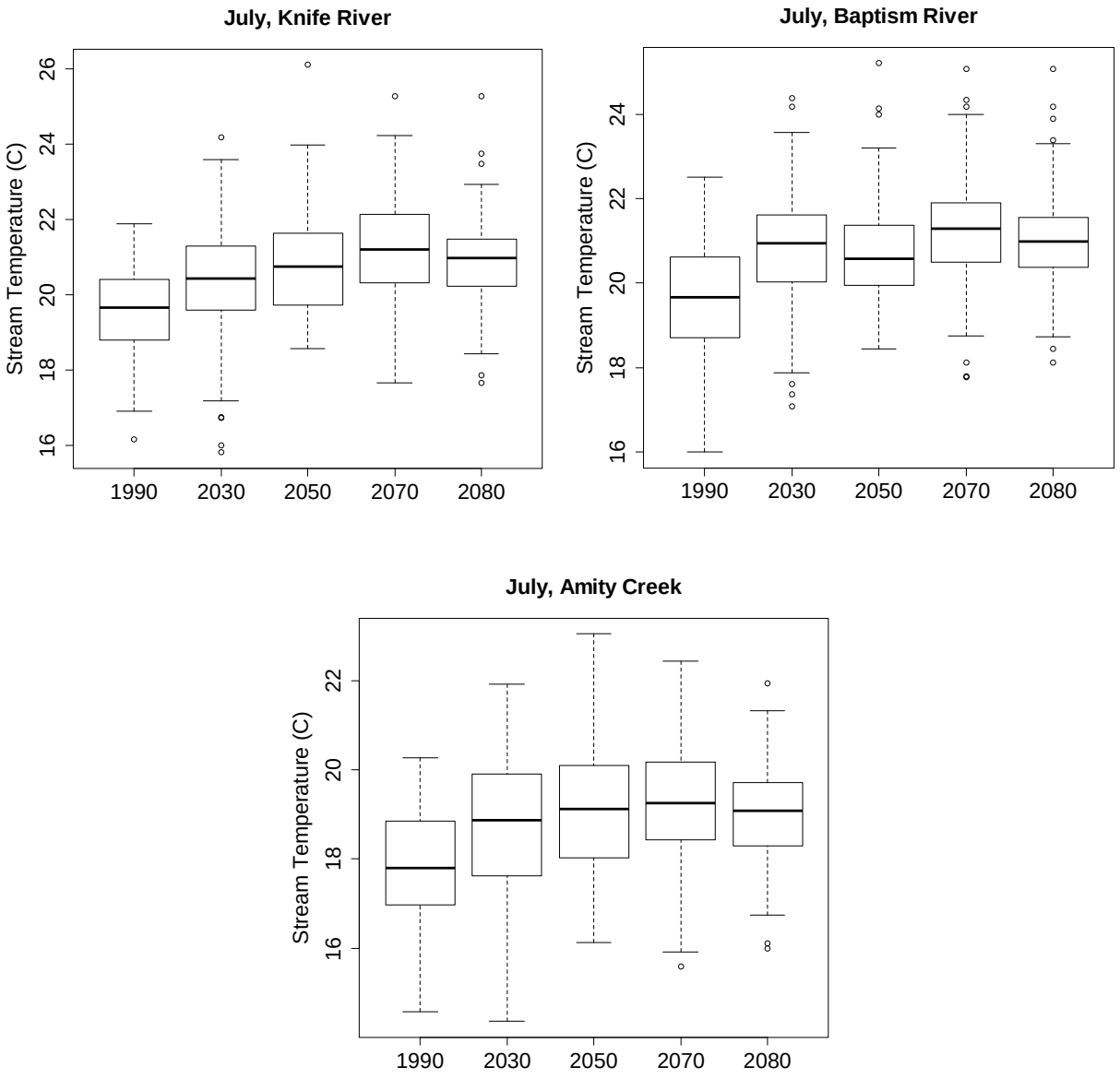

Figure 9.9. Projected July weekly stream temperatures for the Knife and Baptism rivers, and Amity Creek, based on daily GENMOM climate time series. The temperature data are summarized in 20-year blocks, with the center year given on the x-axis.

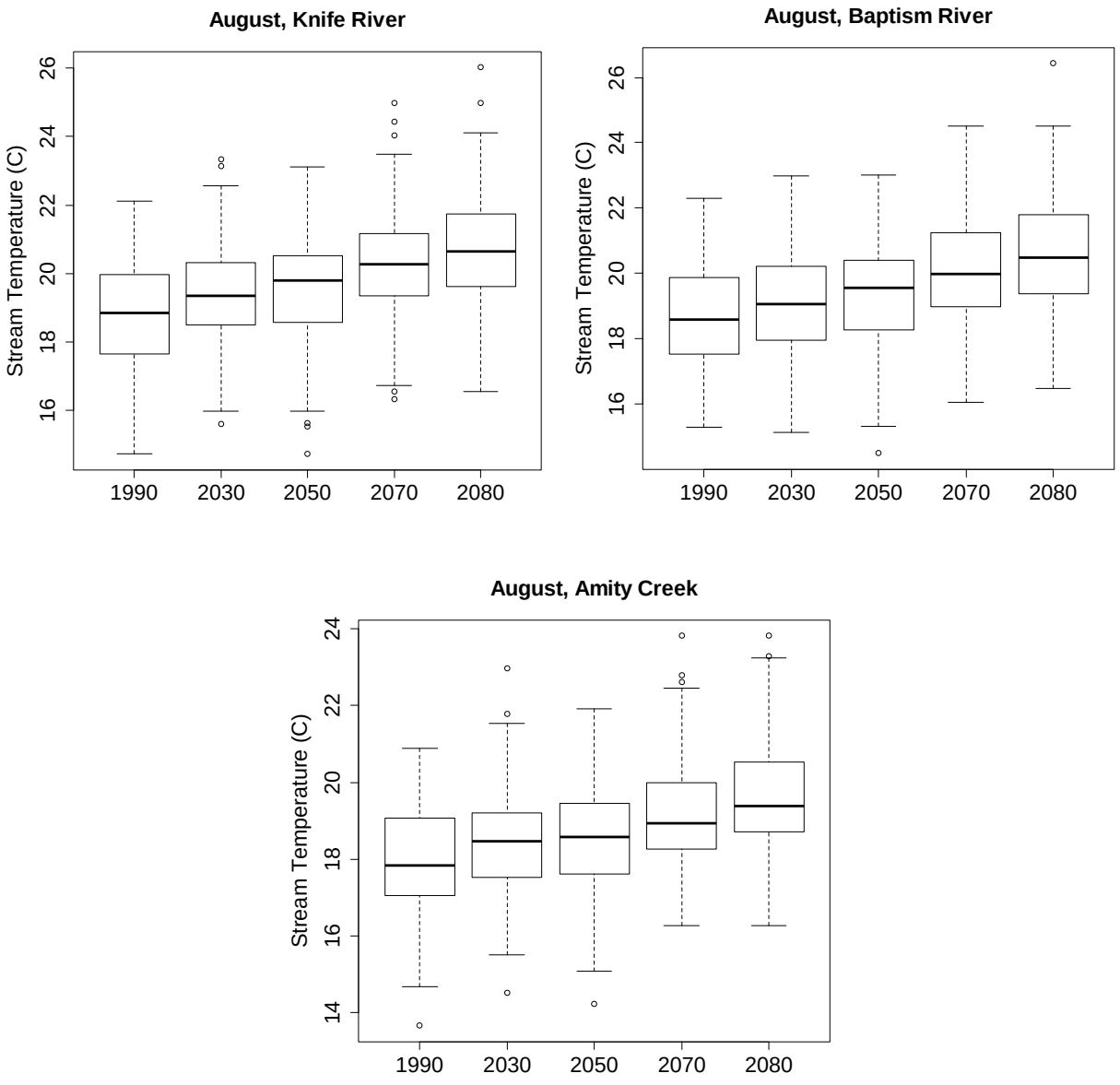

Figure 9.10. Projected August weekly stream temperatures for the Knife and Baptism rivers, and Amity Creek, based on daily GENMOM climate time series. The temperature data are summarized in 20-year blocks, with the center year given on the x-axis.

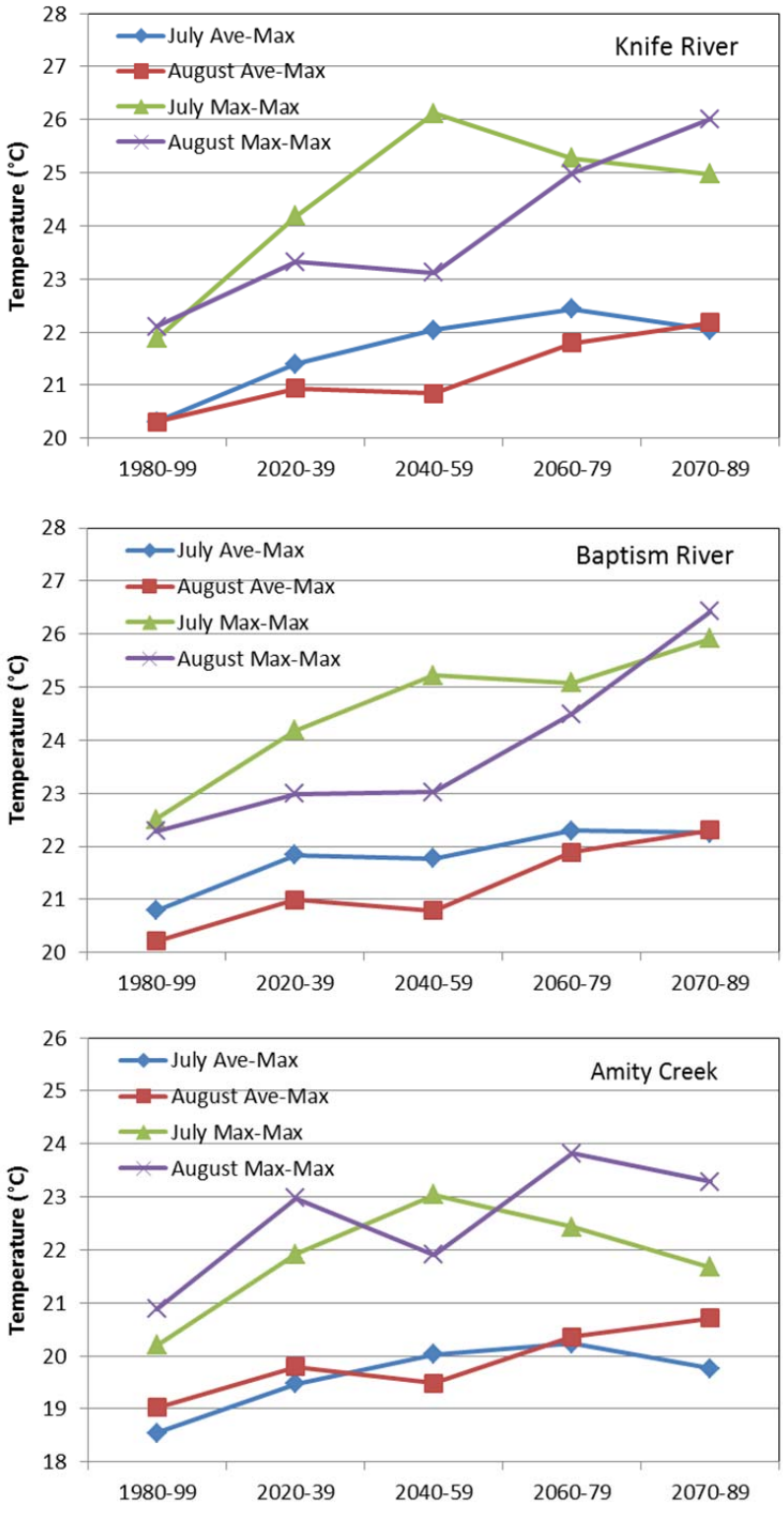

Figure 9.11. Projected July and August maximum weekly stream temperature in Amity Creek, Knife, and Baptism rivers, summarized for 20-year blocks (1980-99, 2020-39, 2040-59, 2060-79, and 2070-89), based on daily GENMOM climate time series.

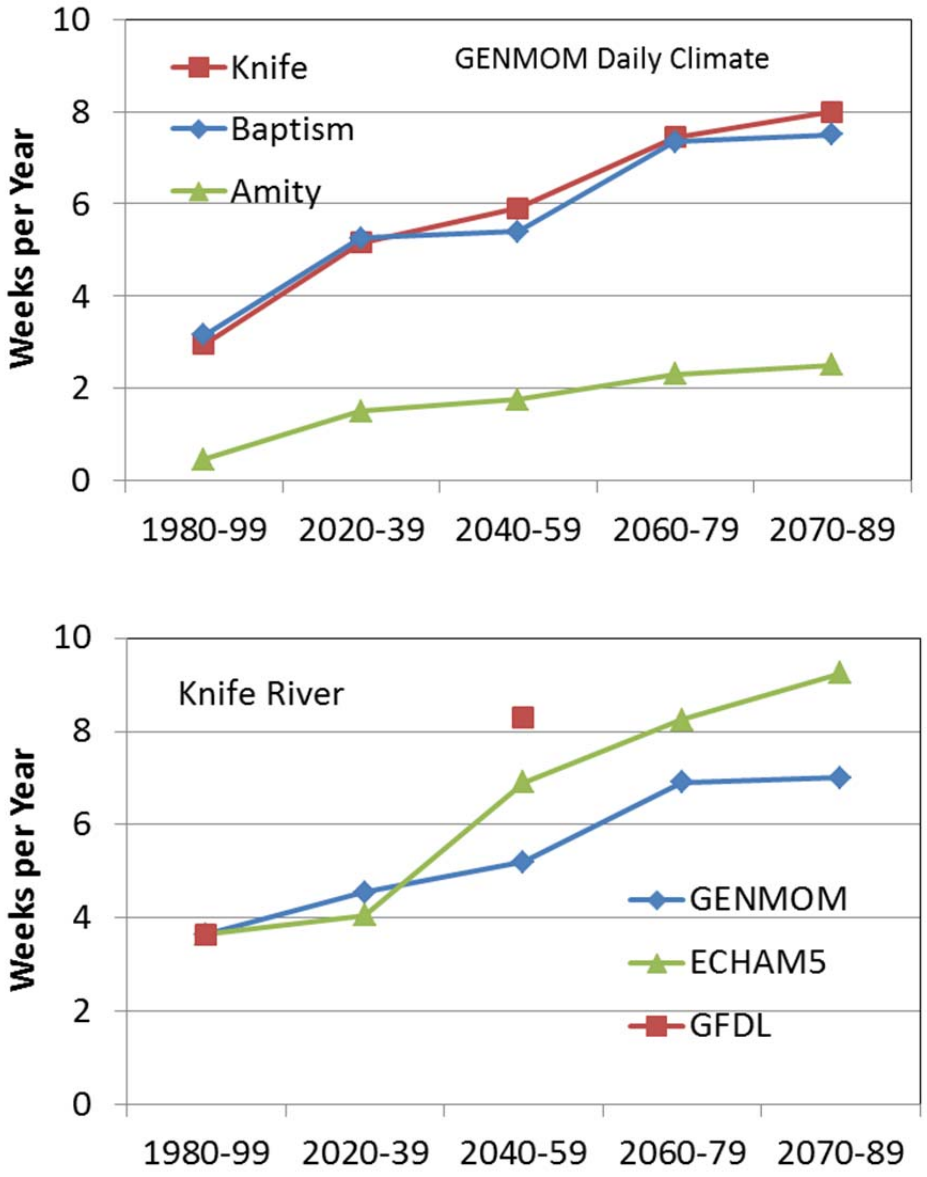

Figure 9.12. Projected number of weeks per year with mean stream temperature above 20 °C. The upper panel gives results for Amity Creek, the Knife River, and the Baptism River in response to the daily GENMOM climate data, while the lower panel gives results for the Knife River in response to the GENMOM, ECHAM5, and GFDL monthly climate increments.

9.5 Regional response of July stream temperatures to the GENMOM daily climate projections

Empirical models of stream temperature in Section 8 indicated that water temperature was determined by air temperature and landscape characteristics, including watershed area, woody wetland proportion in 150 m stream buffer area, soil permeability and latitude (Equation 8.1). The variables that contributed most to the model variance were watershed area and air temperature. Watershed area and site latitude should not change over time. In addition, we assumed no significant change for wetland proportion and soil permeability from present to 2089. Therefore, air temperature became the only variable to determine the change of water temperature over the projection period. Using the empirical models, current landscape data and estimated future air temperature by the GENMOM daily climate projections, we predicted the responses of July mean water temperature for every ten years from 2020 to 2089 for five studied HUCs (Figures 9.13 and 9.14).

Averagely July water temperature was expected to increase by 0.7^{o}C from 2020 to 2069, after that drop around 0.1^{o}C to 2089. The increase magnitude was particularly large from present to 2020-2029, especially in HUC 4010102 area, the coastal area of middle north shore region.

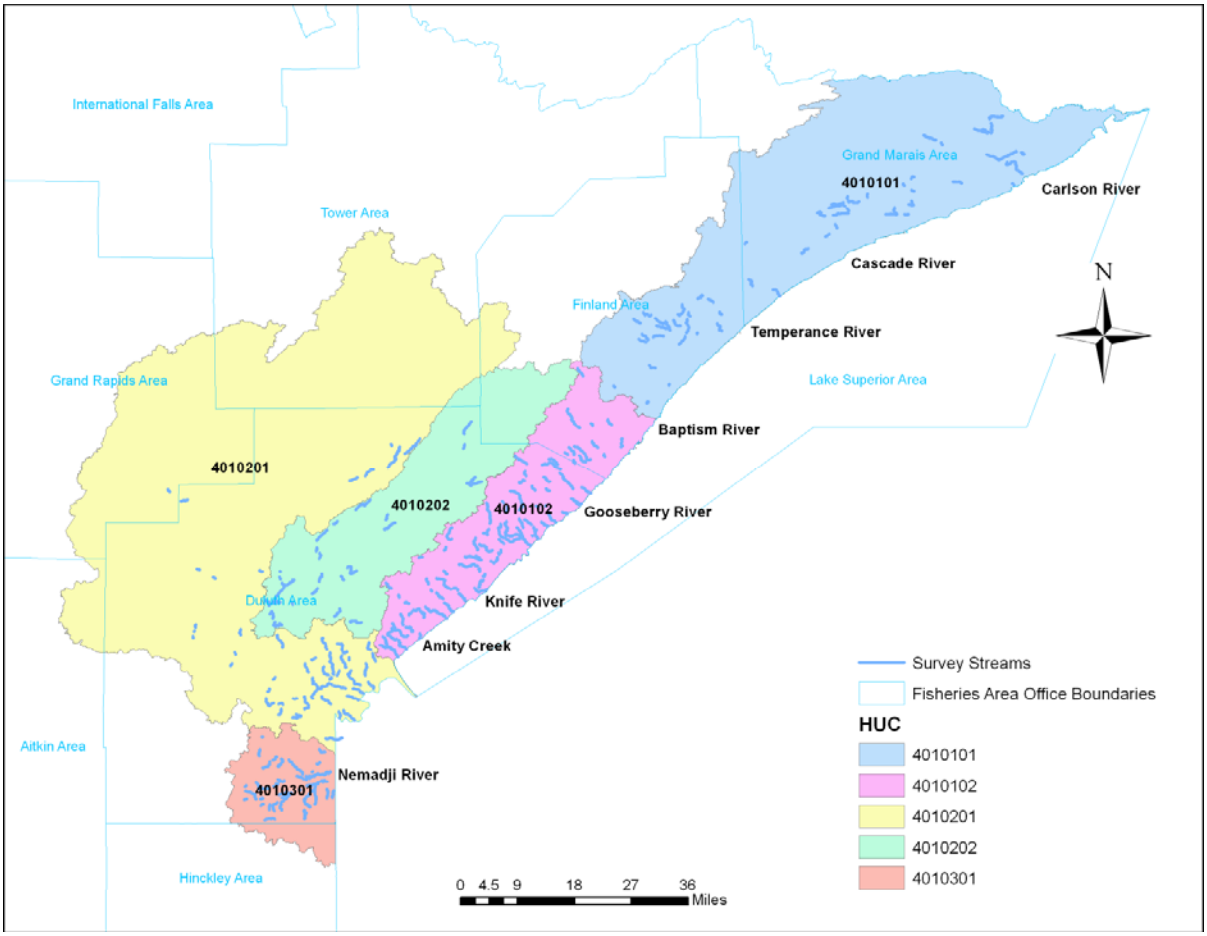

Figure 9.13. HUC map of Lake Superior North Shore region.

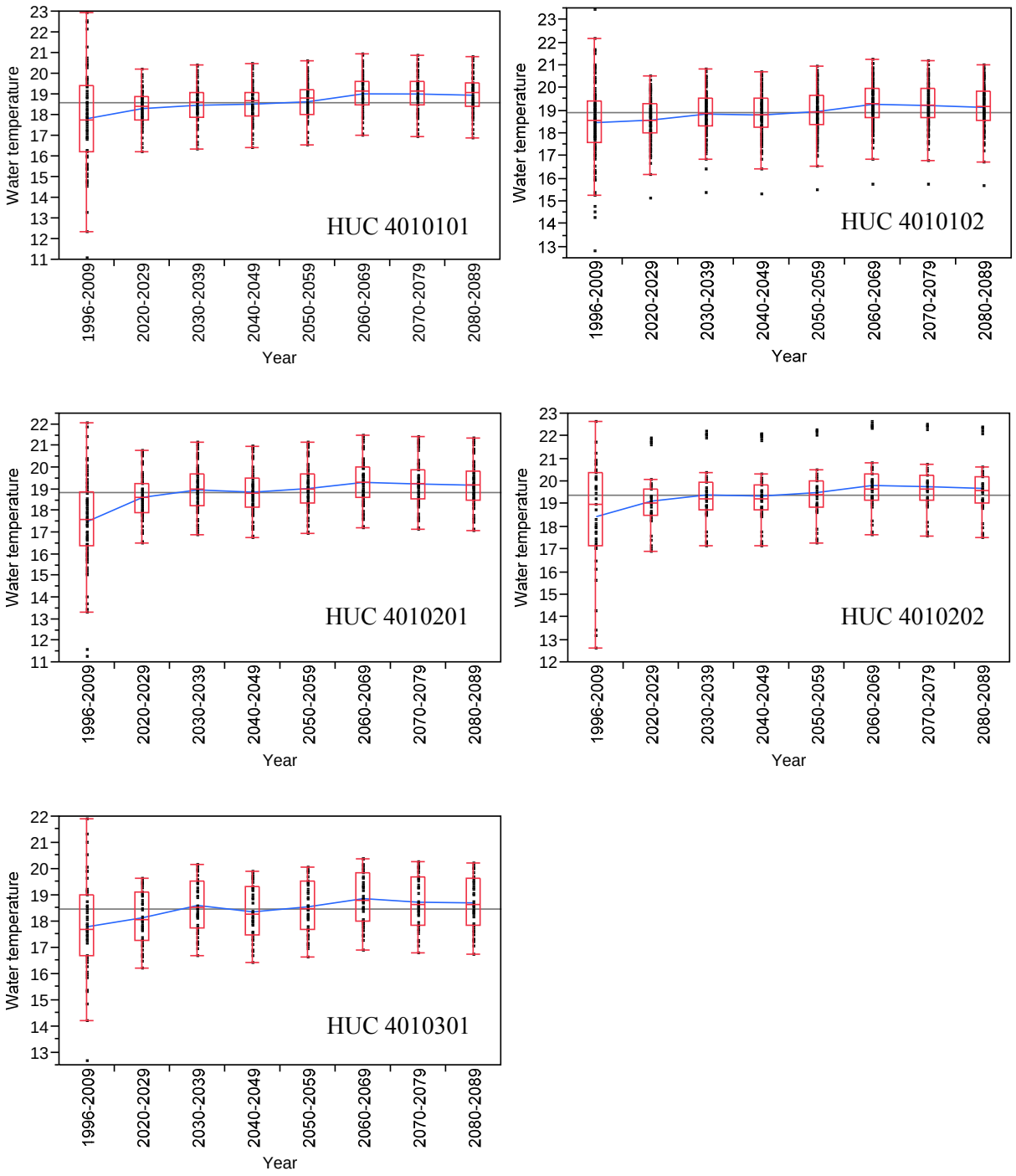

Figure 9.14. Measured July mean water temperature (^{o}C) from 1996 to 2009 and predicted 10-year averaged July mean water temperature in five HUC areas. Horizontal line represents the grand mean for overall time period. Blue line exhibits the change of mean.

9.6 Summary of Stream Temperature Response to Climate Change

The deterministic stream temperature models used in this study allowed projections of future stream temperatures to be made based on changes in atmospheric heat transfer, changes in wetland source temperatures, and changes in streamflow driven by climate change. Stream temperature analyses based on the GENMOM climate data give the result of fairly uniform seasonal increases in stream temperature ranging from 1.3 to 1.9 °C. Stream temperature analyses based on the ECHAM5 climate data projected somewhat greater increases, ranging from 2.2 to 3.5°C, with the largest increases in the spring and autumn. Application of the GENMOM climate data to the deterministic stream temperature models produced fairly similar stream temperature changes for the three study sites (Knife, Baptism, Amity). Interestingly, the stream with the least hydrologic storage (Amity Creek) and baseflow input had slightly lower projected temperature increases, likely because 1) it avoids the additive effects of increased atmospheric heat transfer and increased temperature of baseflow inputs from wetlands, and 2) has a smaller watershed and lower residence time.

The regional (empirical) study found stream water temperature in the north shore region to be positively affected by air temperature, catchment size, percentage of woody wetlands around a stream and latitude of site, but negatively affected by soil permeability rate. Generally more than 30% of water temperature variance was explained by these five variables. Air temperature and basin size accounted for more than 75% of model variance, while other three parameters determined the remaining 25% or less variation of model. Increases in monthly average air temperature can elevate average stream water temperature by 0.69^{o}C and maximum water temperature by 0.96^{o}C per each degree increase. This relationship implied that climate change can alter stream water temperature, particularly the peak temperature. These temperature sensitivities are consistent with those found with the deterministic models, which averaged about 0.8 ^{o}C stream temperature increase per degree air temperature.

In response to climate change projected by the GENMOM GCM, the regional stream temperature model projects July mean water temperature to rapidly increase by approximately 0.5^{o}C from 1990s to 2020s, and then gradually increase another 0.7^{o}C from 2020s to 2060s, after that drop around 0.1^{o}C to 2089. The increase magnitude was particularly large in the coastal area of middle north shore region. Again, these increases are slightly lower than, but consistent with, the results of the deterministic model study.

References

Arnold, J. G., and P. M. Allen, 1999. Automated methods for estimating baseflow and ground water recharge from streamflow records, J. Am. Water Resour. Assoc., 35: 411–424.

Edinger, J.E., D.K. Brady and J.C. Geyer, 1974. Heat exchange and transport in the environment. Report No. 14, Electric Power Research Institute, Cooling Water Discharge Research Project (RP-49), Palo Alto, CA.

Herb, W.R., Janke, B., Mohseni O., and H.G. Stefan, 2007. Estimation of runoff temperatures and heat export from different land and water surfaces, St. Anthony Falls Laboratory Report 488, 34 pp.

Herb, W.R. and H.G. Stefan, 2011. Equilibrium temperature models for coldwater streams, Water Resources Research, 47: W06519.

Hostetler, S.W., Alder, J.R. and Allan, A.M., 2011, Dynamically downscaled climate simulations over North America: Methods, evaluation and supporting documentation for users: U.S. Geological Survey Open-File Report 2011-1238, 64 p. http://pubs.usgs.gov/of/2011/1238/pdf/ofr20111238.pdf, accesses Jan 2013

Raleigh, R.F. 1982. Habitat suitability index models: brook trout. U.S.D.I. Fish and Wildlife Service. FWS/OBS-82/10.24.

10. Brook Trout Presence/Absence Model

10.1 Data sources

Surveys of brook trout in north shore region were conducted by Minnesota Pollution Control Agency (MPCA), U.S. EPA, and Natural Resources Research Institute (NRRI) at 371 sites located in 201 stream segments during the periods from 1997 to 1999, and from 2008 to 2011 (Figure 10.1). Most fish sites were monitored one time; 26 sites were sampled once from 1997 to 1999 and another time from 2008 to 2011. Brook trout were either consistently present or absent at same site across that 10 year interval. With this result, we are relatively confident that the one-time survey results can be used to represent trout presence or absence during the time period of 1996 to 2009.

In the surveyed 371 trout sites, 117 sites had brook trout present while the remaining 254 sites did not have brook trout (Figure 10.1). Brook trout were found in tributaries of Lake Superior and were absent from tributaries at the outer edges of the Lake Superior basin. There are 153 designated trout streams managed by the MN DNR (Fig 10.1).

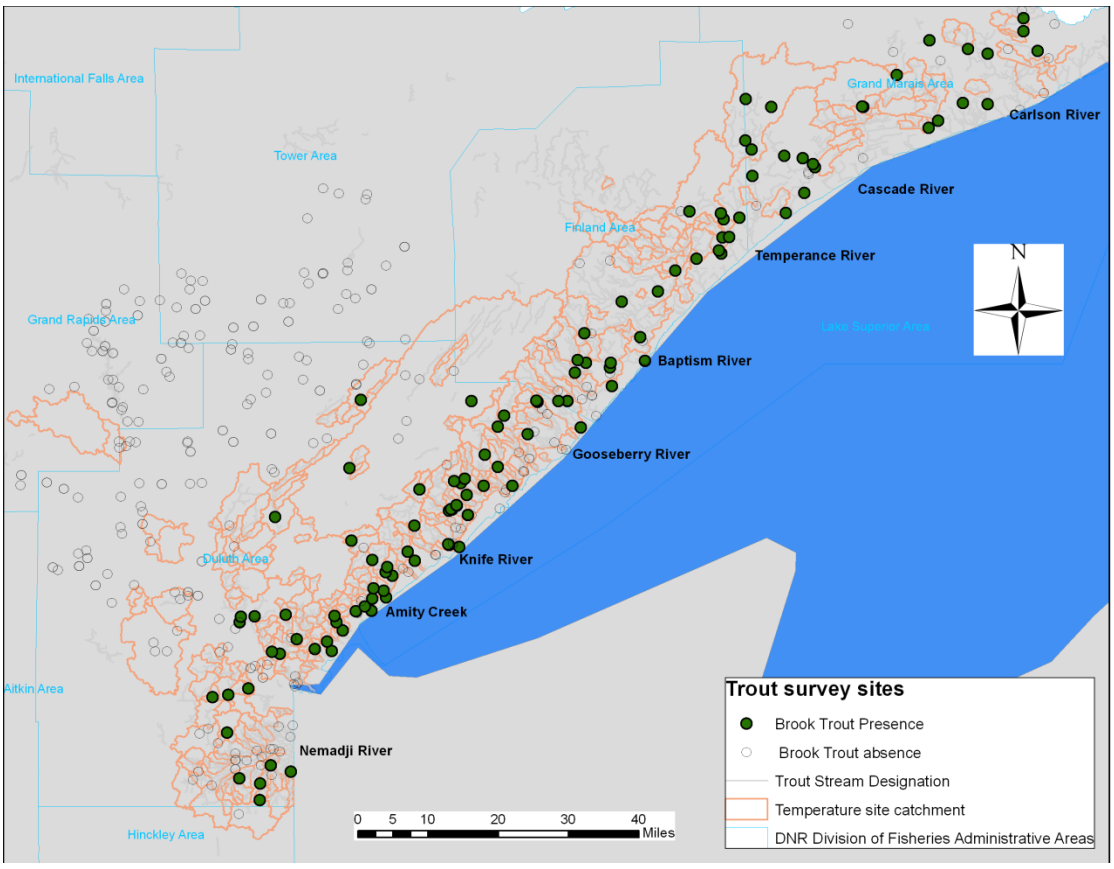

Figure 10.1. Map of brook trout survey sites in the North Shore region.

Trout survey and water temperature survey were generally performed by different agencies. As a result, the survey sites were not always located at same place. In order to match data sets, a

temperature site and a trout site was defined as collocated if the distance between them was less than 1 km with no tributary between sample sites. A total of 79 pairs of temperature sites and trout sites were found to be co-located with one another.

Brook trout presence or absence at 79 collocated sites was modeled in JMP 9 by generalized linear model using logit link and binomial distribution function (Equation 10.1).

$$log\frac{p}{1-p} = b_0 + b_1x_1 + b_2x_2 \qquad (10.1)$$

Where p represents the probability of trout presence, 1-p is the absence probability, b_0, b_1 and b_2 are model coefficients, x_1 and x_2 are predictors. Eq. 10.1 is a simple example of logistic model using two predictors. The number of model predictors could be more than two.

At model development, presence was set as 1 while absence was defined as 0 in data table. July mean temperature, 10th percentile August low flow and other possible predictors from Table 8.1 were selected as the model independent variables. Potential models were evaluated based on the following criteria: (1) model p-value below 0.05, (2) p-value for each parameter less than 0.1, (3) model predictors are not significantly correlated to each other, and (4) largest correct classification rate. The proportion of correctly classified sites was computed as the number of sites correctly predicted divided by the total number of sites. In addition, a Kappa test was performed to examine the real proportion of correct classification after removing the effect of chance classification (Titus et al. 1984). (Larger Kappa values are better.)

10.2 Brook trout presences/absence model

10.2.1 Selection of temperature variable

To determine if July mean or July maximum temperature should be used in predicting brook trout presence or absence, an ANOVA of these two temperature variables were performed in JMP 9 (Figure 10.2). July mean temperature was significantly lower in brook trout presence sites than in trout absence sites. The difference for July maximum temperature was not as distinct as July mean temperature; therefore, July mean temperature was chosen as the best predictor for trout presence or absence.

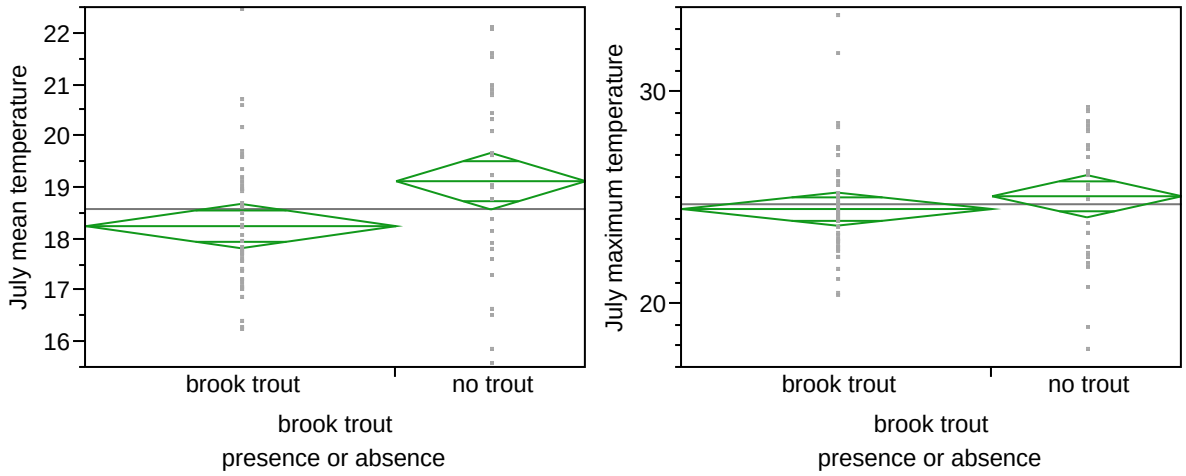

Figure 10.2. Comparison of July mean temperature and July maximum temperature between brook trout presence sites and trout absence sites.

Because maximum temperature is viewed as an important predictor of brook trout presence / absence, we used both July mean and July maximum temperatures as the sole predictor in logistic regression models for trout presence and absence (Appendices 10.1 and 10.2). However, no valid model was obtained for July maximum temperature (p = 0.34). In contrast, valid models with July mean temperature were successfully developed with the best model shown below (p= 0.015) as Equation 10.2.

$$log\,\frac{p}{1-p} = 7.48 - 0.37T_{mean} \qquad (10.2)$$

Where p is the probability of trout presence, T_{mean} represents the July mean temperature. This model was used to estimate the probability of brook trout presence at different July mean water temperatures (Table 10.1).

Table 10.1. Predicted brook trout presence probability using July mean temperature as sole predictor based on Equation 10.2.

Probability of trout presence	Corresponding July mean temperature, ^{o}C
0.68	18
0.62	18.68*
0.59	19
0.50	20*
0.41	21
0.32	22
0.25	23
0.18	24
0.13	25
0.023	30

*The cut-off water temperature for trout risk levels.

Cut-off thresholds for trout presence were set at a probability equaling 0.62 and 0.5; the former represents the prevalence proportion based on the ratio of trout presence sites to total survey sites, and the latter is a commonly used threshold. Based on these thresholds, the logistic models predicted that trout would be present if July mean temperature is below 18.68^{o}C, but would be considered as at risk between 18.68^{o}C and 20^{o}C, and assumed to be absent above 20^{o}C (Table 10.2). The comparison of mean water temperature in trout presence and absence sites in Figure 10.2 suggests that the cut-off temperature of 18.68^{o}C is very close to the 95% upper limit of average July mean temperature in trout presence site, also to the 95% of the lower limit in trout absence site. These results suggested that the selection of 18.68^{o}C as a threshold temperature might be reasonable for this region.

Thermal limits for salmonids are species- and region-specific (Magnuson et al. 1979). Water temperature of 20^{o}C was often determined as the thresholds for brook trout (Jonsson and Jonsson 2009). Brook trout presence probability was reduced to 50% or less when water temperature was above 20^{o}C. This was the 85th percentile of July mean temperature in our 427 study sites. This value was comparable to a study in low Michigan and Wisconsin streams, where thermal tolerance limits for trout was found to be 21^{o}C at the exposure duration 21-63 days (Wehrly and Wang 2007).

10.2.2 Final logistic model

We hypothesize that trout presence or absence are linked to water temperature, stream flow and other possible landscape characteristics (see Arismendi et al. 2012). In this study we have used T_{mean} and Q10 as estimates of relevant temperature and flow characteristics. In addition, all predictors in Table 8.1 were added one by one to test if the model with T_{mean}, Q10 and additional predictor resulted in valid models. Table 10.2 summarizes all possible models and the proportion of correct classification. The model predicted by T_{mean} results in a very high correct classification of trout presence sites, but poorly classifies trout absence sites, with a correct classification rate of only 40%.

The model with predictors of T_{mean}, Q10 and %Deciduous_Forest_150m generally had the largest correct classification rates for presence, absence and overall sites. Therefore, this model was selected to predict trout presence and absence in the north stream study area (Equation 10.3; see Appendix 10.3 for details).

$$log\frac{p}{1-p} = 15.19 - 0.63T_{mean} + 0.37Q_{10} - 5.28\ \%Deciduous\_Forest\_150m \quad (10.3)$$

Where, T_{mean} is the July mean water temperature, Q10 is the 10th percentile August flow, and %Deciduous_Forest_150m represents the proportion of deciduous forest cover in a150m stream buffer area.

Table 10.2. Comparison of correct classification rates and kappa statistics of logistic regression models to predict brook trout presence and absence in 79 north shore streams of Lake Superior region.

		Cut-off =0.5					Cut-off=0.62				
Predictors in model	Model p-value	Presence (%)(n=49)	Absence (%) (n=30)	Overall (%) (n=79)	Kappa	p-value for Kappa test	Presence (%) (n=49)	Absence (%) (n=30)	Overall (%) (n=79)	Kappa	p-value for Kappa test
T_{mean}	0.0149	45 (91.8)	12 (40)	57 (72.15)	0.45	5.5×10^{-5}	33 (67.35)	18 (60)	51 (64.56)	0.45	5.5×10^{-8}
T_{mean}+Q10	0.0134	42 (85.71)	12 (30)	54 (68.35)	0.28	0.03	33 (67.35)	17 (56.67)	50 (63.29)	0.43	4.9×10^{-7}
T_{mean}+Latitude	0.0029	44 (89.8)	13 (43.33)	57 (72.15)	0.36	0.005	33 (67.35)	22 (73.33)	55 (69.62)	0.39	0.0007
T_{mean}+Q10+ PCT_woody_wetland_150m	0.0075	42 (85.71)	15 (50)	57 (72.15)	0.38	0.003	35 (71.43)	21 (70)	56 (70.89)	0.4	0.0005
T_{mean}+Q10+ PCT_Jack_Pine_100m	0.0057	44 (89.8)	13 (43.33)	57 (72.15)	0.36	0.005	34 (69.39)	19 (60.33)	53 (67.19)	0.32	0.006
T_{mean}+Q10+ PCT_Deciduous_forest_150m	0.0023	40 (81.63)	16 (63.33)	56 (70.89)	0.36	0.003	35 (71.43)	22 (73.33)	57 (72.15)	0.44	0.0001
T_{mean}+Q10+HSBG+ PCT_Deciduous_forest_150m*	0.0005	42 (85.71)	16 (53.33)	58 (73.42)	0.41	0.001	35 (71.43)	21 (70)	56 (70.89)	0.41	0.0004

*HSGB is hydrological soil group B, which is characterized by moderate run-off potential.

The coefficients in Equation 10.3 indicate that the probability of brook trout presence is negatively correlated with both water temperature and deciduous forest coverage in the riparian zone, and is positively associated with Q_{10}. These relationships suggest that brook trout are positively associated with higher baseflows and negatively associated with higher water temperatures and riparian zones with deciduous cover. The declining presence of trout was more strongly attributable to water temperature than to change of flow regime in our model predictions. At face value the negative correlation between trout presence and deciduous cover in the riparian zone seems counter-intuitive; however, this result reflects a number of co-occurring factors related to landform, latitude, and soil permeability. Deciduous cover is concentrated in the southern-most portion of the study area, in the vicinity of the St. Louis River estuary. These catchments are associated with landforms with higher proportions of sands and clay sediments and tend to have lower elevational gradients compared to streams in other parts of the study area. Streams further north in the study area tend to have a larger gradient of elevations, are dominated by coniferous cover, and have soils that at the extremes are either bedrock-dominated (resulting in flashy flows), or are highly to moderately pervious.

The coincidence of low base flows and high temperatures is viewed as “double trouble” for coldwater biota (Arismendi et al. 2012). Earlier spring flows and lower amounts of summer precipitation (or extended periods during the summer without precipitation) can lead to conditions in which high stream temperatures coincide with low flow. Extended periods of high stream temperatures are known to be particularly stressful to salmonids (Wehrly and Wang

2007). Our model predictions suggest that the southern extent of the study area is already vulnerable to conditions that put brook trout at risk; future projections suggest that the streams in the middle portion of the study area are at risk of losing brook trout, while those in the far north are projected to support brook trout populations until the latter part of the century. Adaptation strategies that increase stream shading with coniferous cover and enhance base flows by maintaining low levels of impervious surface cover could improve the potential for maintaining brook trout populations in the future.

References

Arismendi, I., M. Safeeq, S. L. Johnson, J.B. Dunham, R. Haggerty. 2012. Increasing synchrony of high temperatures and low flow in western North American streams: double trouble for coldwater biota? Hydrobiologia DOI 10.1007/s10750-012-1327-2.

Jonsson, B. and Jonsson, N. (2009). A review of the likely effects of climate change on anadromous Atlantic salmon Salmo salar and brown trout Salmo trutta, with particular reference to water temperature and flow. Journal of Fish Biology 75: 2381-2447.

Titus, K., Mosher, J.A. and Williams, B.K. (1984). Chance-corrected classification for use in discriminant analysis: Ecological application. The American Midland Naturalist 111(1): 1-7.

Wehrly, K.E. and Wang, L. (2007). Field-based estimates of thermal tolerance limits for trout: Incorporating exposure time and temperature fluctuation. Transactions of the American Fisheries Society 136: 365-374.

11. Response of North Shore Brook Trout Habitat to Climate Change

Logistic model developed by current water temperature and flow data was applied into future scenarios, in which model output was used to assess the stream risk of brook trout. Trout presence probability model was dependent on three predictors, average July mean temperature, August low flow (Q10) and proportion of deciduous forest in 150 m stream buffer area (Equation 10.3). Stream water temperature was estimated by multiple regression models using GENMOM daily climate projection (see Chapter 9.5 for details). Percent of deciduous forest in 150 m stream buffer area was assumed to remain constant from 1996 to 2089. Current August low flow in temperature sites was predicted by multiple regression equation (Equation 4.1). However, none of model predictors (area, wetland proportion and geology variable) can reflect flow change by future climate. In this case, we assumed the temporal change of stream flow in this region had same change rate as three hydrology stations (Baptism, Knife, and Amity). Therefore, the future 10-year average flows predicted by GENMOM for these three stations were compared with the average flow of 1980-1999 to obtain the change rate (Figure 11.1). After that, these ratios were applied to 427 temperature survey sites to estimate 10-year average Q10 from 2020 to 2079.

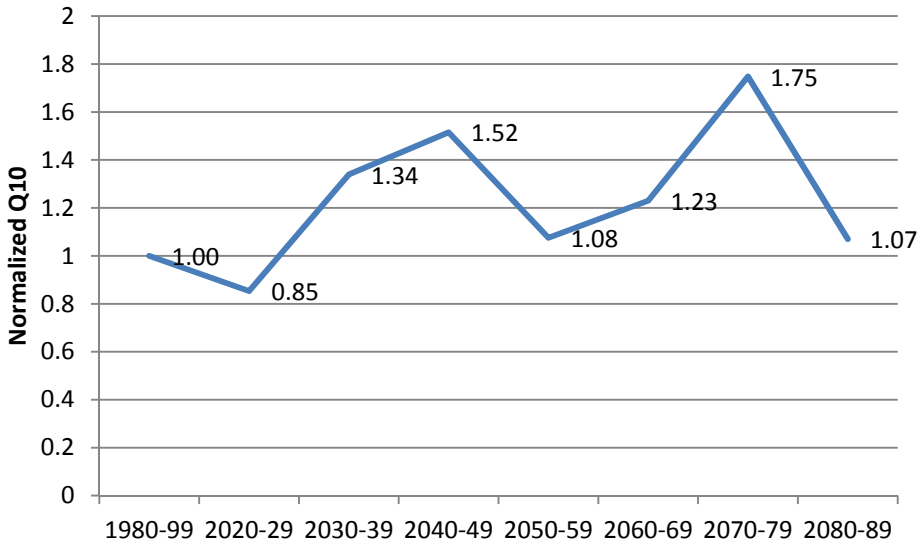

Figure 11.1. Normalized Q10 of three study sites in hydrology model (Baptism, Knife and Amity). Average Q10 from 1980 to 99 was used as the base to estimate the flow change ratios.

Logistic model gave the results of probability or suitability. This result description is not as practical as species presence or absence data. Very often a probability equaling 0.5 was set as the cut-off value to determine presence or absence (Manel et al. 2001, Bailey et al. 2002). However, this fixed cut-off value method is very arbitrary, and would produce large error in predicting rare share for unbalanced data (Cramer 1999). Liu et al. (2005) compared 12 methods in determining the cut-off value, and finally recommended prevalence method to generate thresholds of occurrence. In prevalence method, the cut-off value was set to the share of trout presence in total trout data (Cramer 1999, Cramer 2003). In current dataset, 79 trout sites have trout data, but trout was present for 49 sites and absent for remaining 30 sites. Obviously the share of trout presence site was 0.62, a cut-off value as suggested. We estimated that water temperature would be 20^{o}C at cut-off value 0.5 (see Chapter 10.2 for details). Twenty degrees Celsius was often used the thermal thresholds for brook trout, therefore both cut-off probability values of 0.5 and 0.62 were used to classify three types of sites, predicted trout absence with probability below 0.5, at risk sites if probability between 0.5 and 0.62, and predicted trout presence for probability above 0.62.

These site predictions were applied into stream segment. If one stream segment has only one survey site located, the model prediction result for this site was used to represent trout presence/absence for this segment. If multiple sites are located in one segment, the average of trout presence probability was used to describe this segment. Generally the length of each stream segment was less than 1 km. Through this way, 329 stream segments were picked in the north shore region.

The changes of stream risk over time were present in maps at 10-year interval for each HUC area (Figures 11.2-11.6, see Figure 9.13 for overall HUC map). Overall, streams in north shore region had increasing risk for trout survival over time, particular the low shore area where most streams were predicted to be trout absence. The major change of risk level occurred in middle shore area, where streams were changed from trout presence dominated in 2000s to be half presence and half absence in 2080s. Streams in upper shore area were least impacted by climate change, at least in current study period from 1996 to 2089.

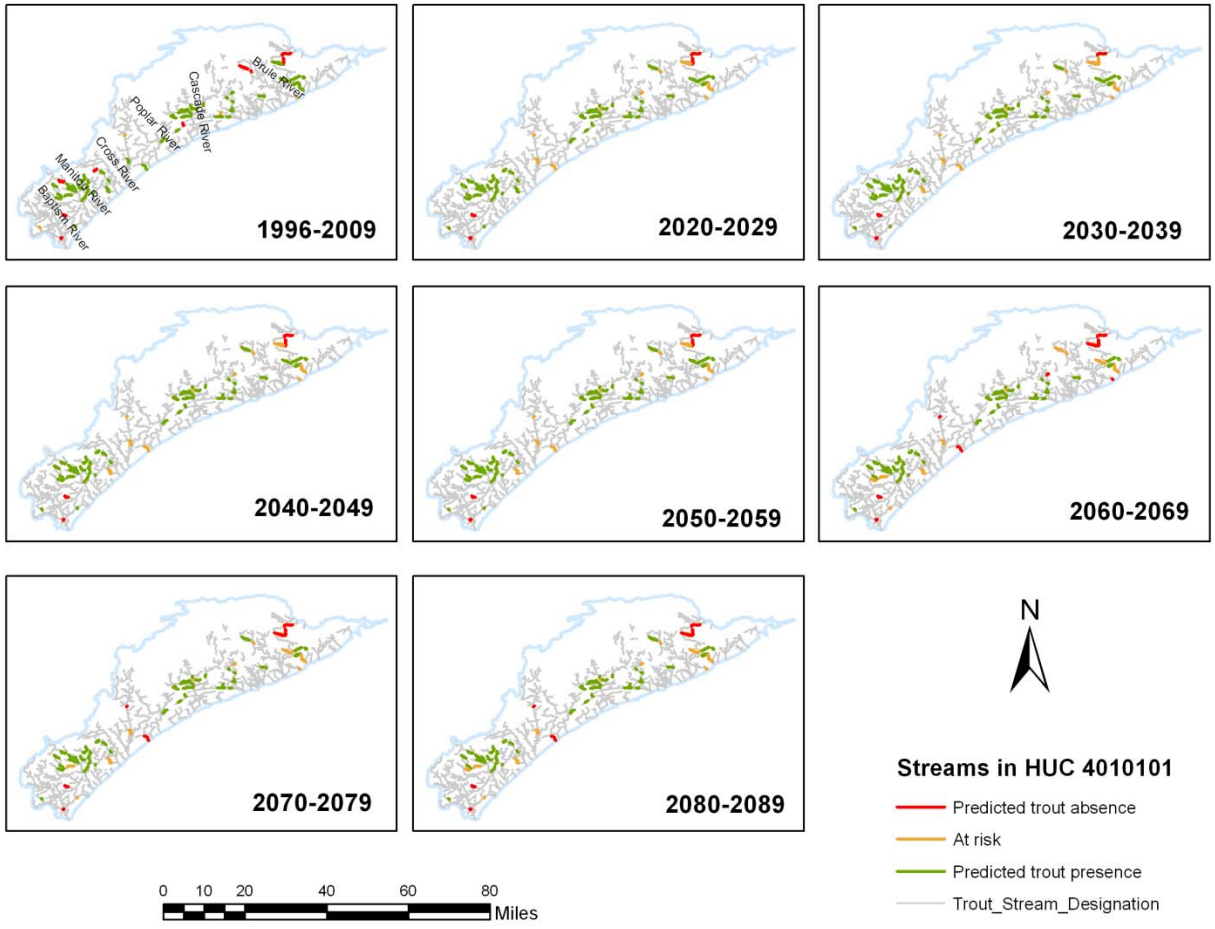

Figure 11.2. Stream map of predicted 10-year average brook trout risk in HUC 4010101.

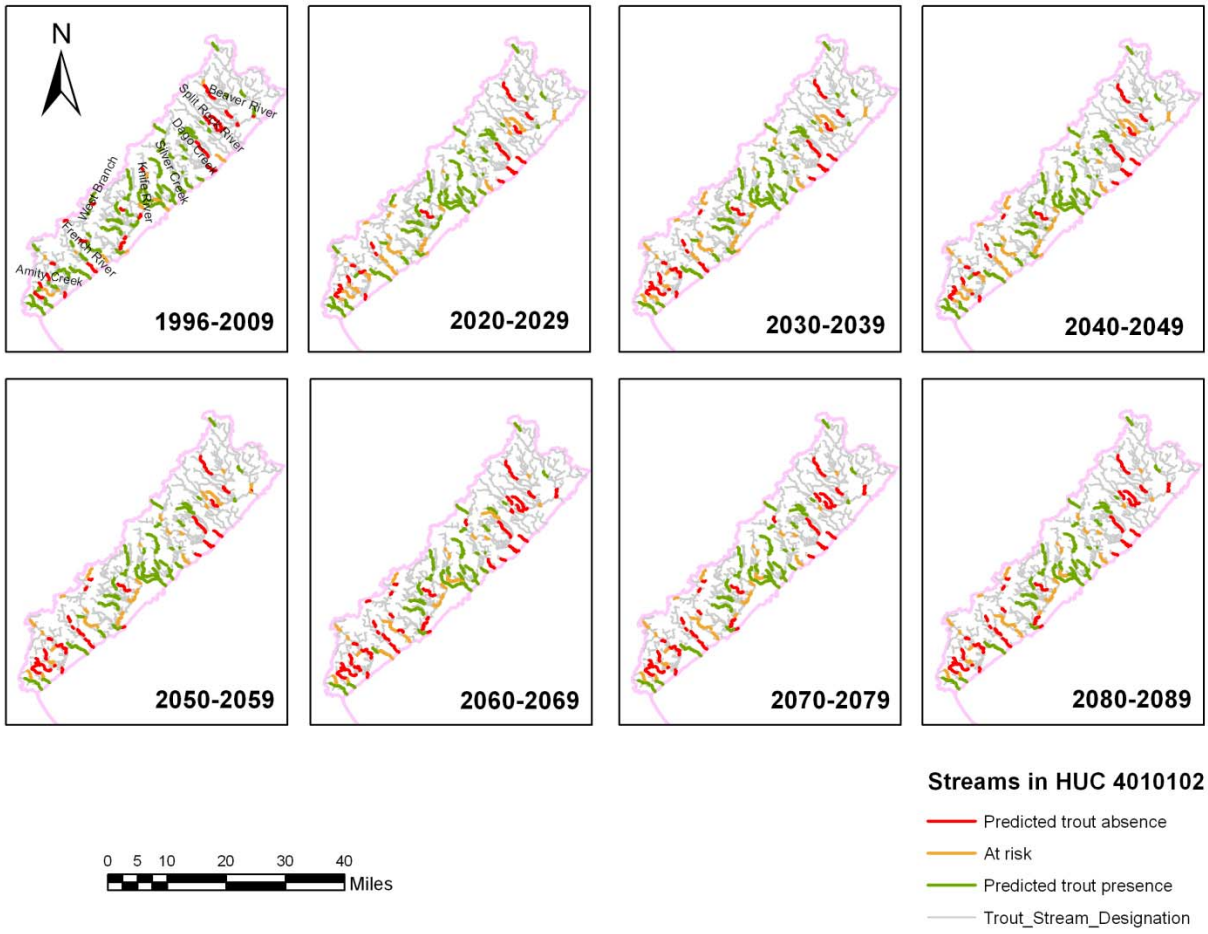

Figure 11.3. Stream map of predicted 10-year average brook trout risk in HUC 4010102.

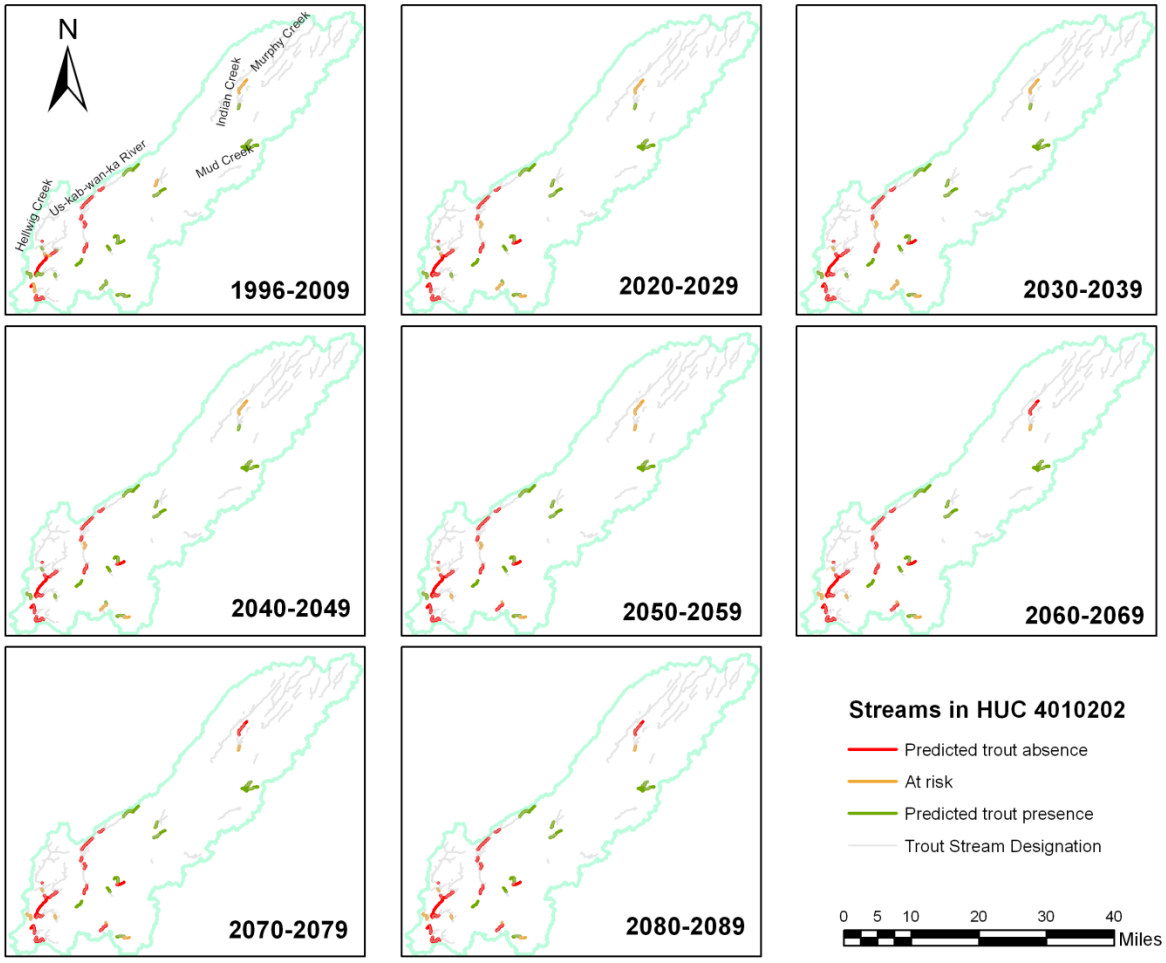

Figure 11.4. Stream map of predicted 10-year average brook trout risk in HUC 4010202.

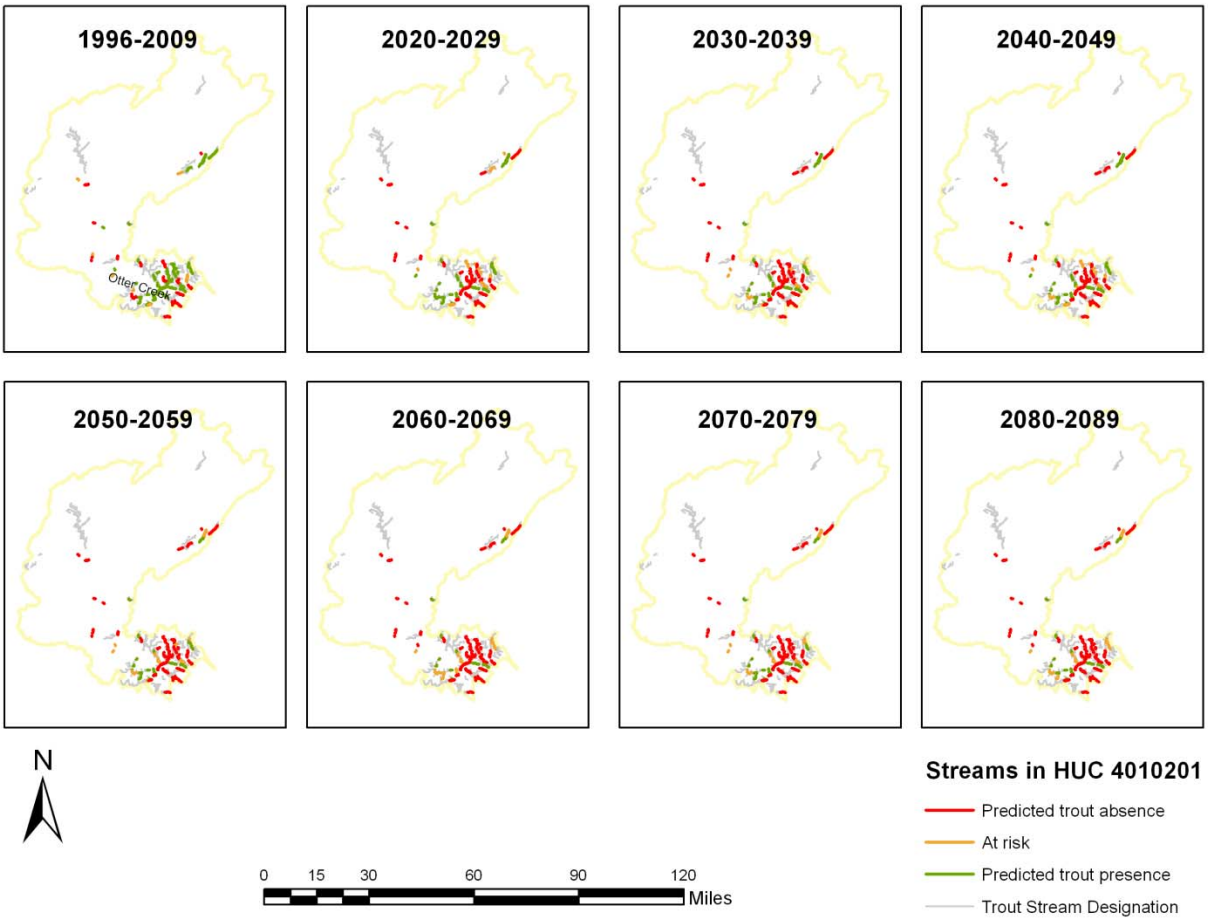

Figure 11.5. Stream map of predicted 10-year average brook trout risk in HUC 4010201.

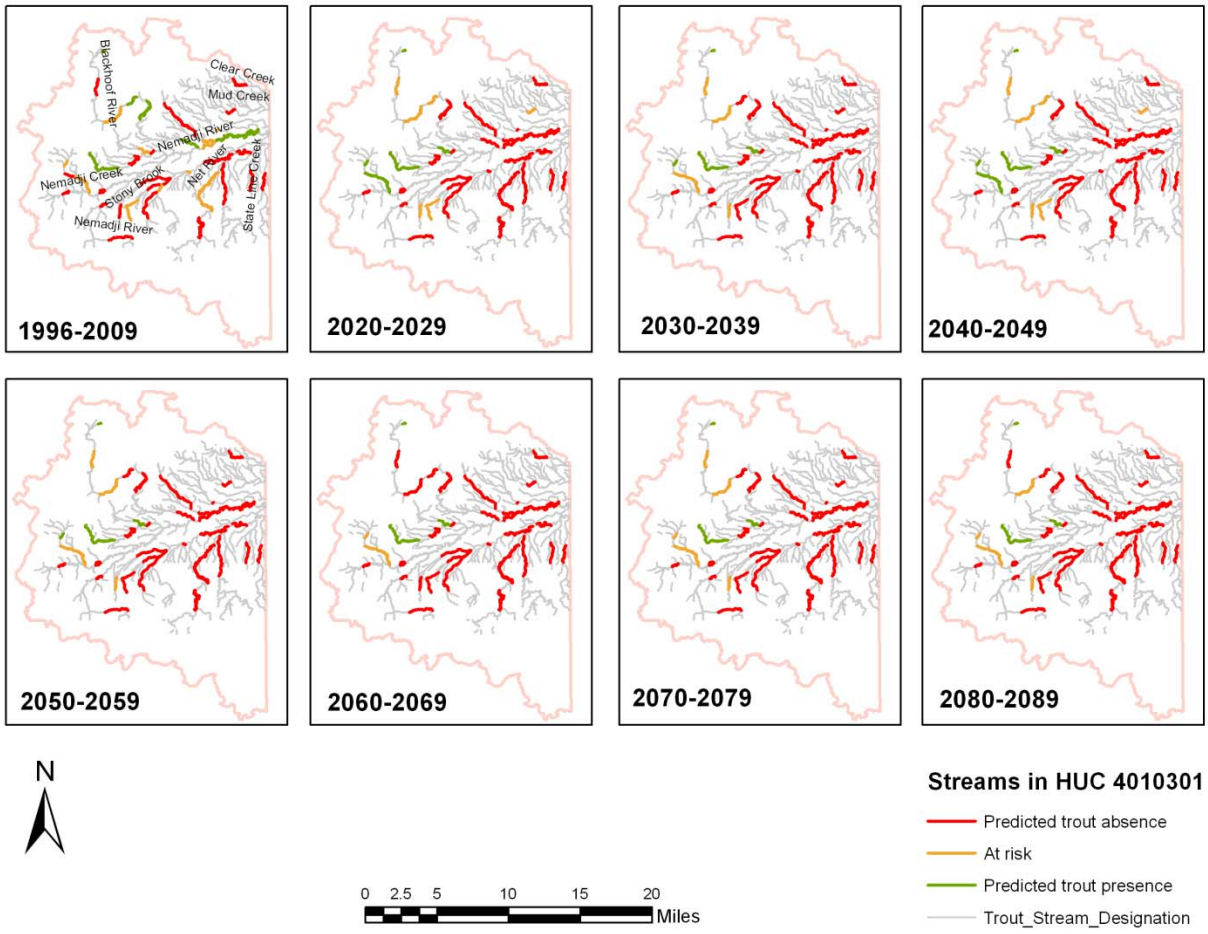

Figure 11.6. Stream map of predicted 10-year average brook trout risk in HUC 4010301.

References

Bailey, S.A., Haines-Young, R.H. and Watkins, C. (2002). Species presence in fragmented landscapes: modeling of species requirements at the national level. Biological Conservation 108: 307-316.

Cramer, J.S. (1999). Predictive performance of the binary logit model in unbalanced samples. Journal of the Royal Statistical Society 48(1): 85-94.

Cramer, J.S. (2003). Logit models: from economics and other fields. Cambridge University Press, pp. 66-67.

Liu, C., Berry, P.M., Dawson, T.P. and Pearson, R.G. (2005). Selecting threshods of occurrence in the prediction of species distributions. Ecography 28: 385-393.

Manel, S., Williams, H.C. and Ormerod, S.J. (2001). Evaluating presence-absence models in ecology: the need to account for prevalence. Journal of Applied Ecology 38: 921-931.

12. Summary and Conclusions

12.1 North shore climate and hydrology

The hydrology of north shore streams is mainly driven by air temperature and precipitation trends and patterns. Historical air temperatures in the region have a significant upward trend, particularly since 1980. GCM outputs project a continued increasing trend in air temperature, with an increase in mean annual air temperature of 2 to 3 °C by 2089. Precipitation trends are less clear. The historical precipitation data shows an increasing trend for total annual precipitation at Duluth and Two Harbors between 1900 and 2010, whereas Grand Marais and Grand Portage do not have a clear trend. Based on an analysis of daily precipitation totals, there is some indication of an increasing trend in the number of days in summer with high precipitation (10-20 cm). The daily GCM output projects further increases in these larger summer precipitation events; however, these results are based on the analysis of only one GCM output (GENMOM). Both the GENMOM and the ECHAM5 GCMs project overall increases in precipitation of about 15%, but differ with respect to the seasonal distribution of the precipitation changes.

While an increasing trend in precipitation leads to increasing streamflow, the increasing trend in air temperature tends to reduce streamflow (by increasing evapotranspiration). Plots of the available streamflow records for north shore streams suggest there may be a decreasing trend in mean annual flow and summer low flow, but the trends are not statistically significant. Future projections of streamflow based on the GCM output were also mixed. The deterministic water budget models project increases in mean annual streamflow and summer low flow. Using the same GCM data, the regional regression models for summer low flow project a decrease in low flow, due to a relatively high sensitivity to air temperature. A significant and relatively certain impact of climate change on the regional hydrology will be a shift in precipitation from snowfall to rainfall. Based on the GENMOM climate projections, the relative contribution of snowmelt to the hydrologic budget is predicted to decrease by 20%. Interestingly, the deterministic hydrologic projections did not show a marked trend in the timing of the spring peak flow.

12.2 North shore stream temperature

The deterministic stream temperature models used in this study allowed projections of future stream temperatures to be made based on changes in atmospheric heat transfer, changes in wetland source temperatures, and changes in streamflow driven by climate change. Stream temperature analyses based on the GENMOM climate data give the result of fairly uniform seasonal increases in stream temperature ranging from 1.3 to 1.9 °C. Stream temperature analyses based on the ECHAM5 climate data projected somewhat greater increases, ranging from 2.2 to 3.5°C, with the largest increases in the spring and autumn. Application of the GENMOM climate data to the deterministic stream temperature models produced fairly similar stream temperature changes for the three study sites (Knife, Baptism, Amity). Interestingly, the

stream with the least hydrologic storage (Amity Creek) and baseflow input had slightly lower projected temperature increases, likely because 1) it avoids the additive effects of increased atmospheric heat transfer and increased temperature of baseflow inputs from wetlands, and 2) has a smaller watershed and lower residence time.

The regional (empirical) study found stream water temperature in the north shore region to be positively affected by air temperature, catchment size, percentage of woody wetlands around a stream and latitude of site, but negatively affected by soil permeability rate. Generally more than 30% of water temperature variance was explained by these five variables. Air temperature and basin size accounted for more than 75% of model variance, while other three parameters determined the remaining 25% or less variation of model. Increases in monthly average air temperature can elevate average stream water temperature by 0.69^{o}C and maximum water temperature by 0.96^{o}C per each degree increase. This relationship implied that climate change can alter stream water temperature, particularly the peak temperature. These temperature sensitivities are consistent with those found with the deterministic models, which averaged about 0.8 ^{o}C stream temperature increase per degree air temperature.

In response to climate change projected by the GENMOM GCM, the regional stream temperature model projects July mean water temperature to rapidly increase by approximately 0.5^{o}C from 1990s to 2020s, and then gradually increase another 0.7^{o}C from 2020s to 2060s, after that drop around 0.1^{o}C to 2089. The increase magnitude was particularly large in the coastal area of middle north shore region. Again, these increases are slightly lower than, but consistent with, the results of the deterministic model study.

12.3 Brook trout habitat projections

Brook trout in north shore streams were highly affected by water temperature and low flow. Water temperature had the strongest effect in reducing trout presence when July mean temperature increased. If water temperature was above 18.68^{o}C, brook trout were predicted to be at risk, and be expiated from streams if temperature was over 20^{o}C. Stream flow imposed negative effect on trout presence though not as strong as water temperature. Overall these data predict that brook trout may be extirpated from lower shore area, have increasing risk in middle shore region, and remain present in upper shore streams from present to 2089.

12.4 Future Work

This work would benefit greatly from a number of modifications to the GCM's, the spatial data used in the development of both the deterministic and empirical models, and implementation of a more detailed, spatially explicit, hydrologic model. First, the use of an ensemble of downscaled GCM projections, rather than reliance on the individual model results presented herein would provide more robust predictions for the study region and would encompass a larger range of model outcomes. Next, the results of these modeling efforts could be regionalized more easily through the use of the National Hydrologic Dataset Plus (v. 2) stream linework. The current work was based on streams from 1:24,000 scale maps, with watersheds delineated uniquely for

each sample point using ArcHydro. The use of NHD+ data, although less highly resolved than the 1:24,000 maps, would permit model predictions to be applied across the entire study region, and to allow incorporation of additional temperature and fish data to the empirical models as it becomes available. Further improvements could be gained from updated spatial data, including: digital soils data for Cook and Lake Counties (SURGO; work in progress), updated National Wetland Inventory (NWI) data (work ongoing), more detailed digital elevation maps (now available), and more detailed riparian vegetation cover maps. In addition, use of a spatially explicit hydrologic model (.e.g, Boreal SWAT) would likely improve base flow predictions, and would greatly improve our ability to predict high flow conditions. Finally, additional fish data, including cool and warm water assemblage data, along with descriptors of landscape structure (i.e., connectivity) would allow us to assess the areas where cold water species may be threatened by the presence or potential presence of coolwater competitors.

Acknowledgements

This study was conducted with support from the Minnesota Department of Natural Resources, St. Paul, Minnesota, with Don Pereira as the project officer. Deserae Hendrickson, Don Schreiner, and Mary Negus at the Minnesota DNR provided substantial input, feedback, and data for this project. Fish data also were provided by the Minnesota Pollution Control Agency. Downscaled climate projections were supplied by Steve Hostetler, USGS/Oregon State University. Additional flow and temperature data were provided by Debra Taylor at the US EPA, and Brian Black, Natural Resources Research Institute. Dr. Heinz Stefan and Tim Erickson (U of M, SAFL) contributed to the hydrologic and temperature model development. Gerry Sjerven, Jeremy Erickson and Dan Breneman (NRRI) developed the spatial data sets used in this study. Margy Bell (NRRI) provided administrative and editing support for this project.

Appendix 3.1. Listing of GCM Climate Increments

	Air Temperature Increment (°C)								
	GENMOM				GFDL	ECHAM5			
month	2020-2039	2040-2059	2060-2079	2070-2089	2040-2059	2020-2039	2040-2059	2060-2079	2070-2089
1	0.79	1.70	2.69	3.08	2.36	1.49	1.57	3.77	4.54
2	-0.22	0.40	1.90	2.23	2.45	0.11	-0.08	3.37	3.25
3	-0.30	-0.39	2.53	2.73	0.69	0.80	1.47	3.13	3.05
4	0.28	0.02	1.66	1.96	1.52	0.21	0.78	2.80	4.11
5	-0.04	0.59	1.28	1.72	1.88	2.01	2.16	3.88	4.26
6	0.70	0.84	1.63	1.79	2.23	0.78	1.84	2.12	2.64
7	1.18	1.42	1.89	1.80	2.14	0.53	1.45	2.22	2.61
8	0.28	0.58	1.75	2.20	2.65	0.06	1.69	2.37	2.86
9	0.66	0.75	1.62	1.41	2.17	0.25	1.08	2.31	2.69
10	1.05	0.77	2.46	2.27	1.59	1.42	1.38	2.68	3.56
11	0.29	1.90	2.62	3.09	1.80	0.74	1.24	2.77	2.78
12	1.57	0.51	2.33	3.34	2.39	0.47	1.99	2.78	3.30

	Precipitation Multiplier								
	GENMOM				GFDL	ECHAM5			
month	2020-2039	2040-2059	2060-2079	2070-2089	2040-2059	2020-2039	2040-2059	2060-2079	2070-2089
1	0.94	1.12	1.10	1.28	1.01	1.00	1.04	0.83	0.88
2	0.93	1.08	0.87	1.06	1.09	0.90	0.83	0.89	0.91
3	0.88	1.31	1.10	1.28	0.99	1.29	1.25	1.40	1.30
4	0.98	1.28	0.94	1.01	0.98	0.79	0.90	1.13	1.23
5	1.08	1.01	1.18	1.09	1.09	1.27	1.52	1.40	1.36
6	1.14	0.99	0.98	1.07	1.03	0.92	0.83	0.93	1.07
7	1.14	1.14	1.25	1.38	0.64	1.01	1.11	1.18	1.06
8	0.99	1.09	1.04	0.94	1.16	1.36	1.15	1.32	1.33
9	1.07	1.26	0.98	1.17	1.42	1.29	1.28	1.43	1.46
10	1.23	0.92	1.14	1.24	0.89	0.93	0.95	1.09	1.14
11	1.21	1.11	1.01	0.89	1.12	1.01	0.87	0.86	1.00
12	0.88	1.27	1.28	1.38	0.96	1.19	1.33	1.18	1.30

	Specific Humidity Multiplier								
	GENMOM				GFDL	ECHAM5			
month	2020-2039	2040-2059	2060-2079	2070-2089	2040-2059	2020-2039	2040-2059	2060-2079	2070-2089
1	1.07	1.17	1.23	1.30	1.19	1.12	1.12	1.31	1.38
2	0.99	1.05	1.16	1.20	1.19	0.99	0.99	1.26	1.26
3	0.98	0.99	1.20	1.22	1.03	1.03	1.09	1.25	1.23
4	1.00	1.01	1.08	1.14	1.11	0.99	1.05	1.22	1.34
5	1.00	1.05	1.09	1.13	1.17	1.13	1.16	1.28	1.31
6	1.06	1.06	1.07	1.12	1.17	1.05	1.09	1.14	1.17
7	1.05	1.07	1.11	1.13	1.14	1.04	1.09	1.15	1.17
8	1.07	1.08	1.09	1.14	1.16	1.02	1.13	1.17	1.19
9	1.07	1.09	1.09	1.12	1.18	1.04	1.09	1.18	1.22
10	1.08	1.05	1.14	1.16	1.11	1.10	1.09	1.19	1.27
11	1.04	1.16	1.21	1.27	1.14	1.07	1.10	1.23	1.23
12	1.10	1.05	1.19	1.29	1.17	1.06	1.17	1.23	1.29

	Solar Radiation Multiplier								
	GENMOM				GFDL	ECHAM5			
month	2020-2039	2040-2059	2060-2079	2070-2089	2040-2059	2020-2039	2040-2059	2060-2079	2070-2089
1	0.96	0.93	0.90	0.90	1.01	0.99	0.93	0.99	0.98
2	0.97	0.88	0.96	0.95	0.99	1.02	1.03	0.94	0.93
3	1.00	0.97	0.96	0.93	0.99	0.97	0.99	0.88	0.94
4	1.01	0.96	1.01	0.96	0.97	1.04	0.99	0.95	0.98
5	1.00	1.00	0.99	0.97	0.93	1.05	1.00	1.05	1.03
6	1.02	1.01	1.06	1.03	0.99	1.00	1.11	1.03	1.04
7	1.05	1.03	1.03	1.02	1.00	0.98	0.99	1.01	1.01
8	0.93	0.93	0.98	0.97	1.02	0.93	0.97	0.99	1.00
9	1.01	0.96	1.05	1.01	0.96	0.91	0.91	0.95	0.92
10	1.03	1.03	1.08	1.03	1.07	1.13	1.06	1.05	1.10
11	1.03	1.06	1.00	1.01	1.08	0.93	0.99	1.00	0.96
12	1.01	0.98	0.94	0.92	1.07	0.97	0.98	0.97	0.96

	Wind Speed Multiplier								
	GENMOM				GFDL	ECHAM5			
month	2020-2039	2040-2059	2060-2079	2070-2089	2040-2059	2020-2039	2040-2059	2060-2079	2070-2089
1	0.91	1.14	0.88	0.79	0.87	0.75	0.78	1.06	0.97
2	1.10	0.87	1.20	0.81	1.00	0.98	1.17	0.93	0.85
3	0.97	1.57	0.69	0.44	1.37	1.19	0.91	0.91	0.99
4	1.00	1.36	1.14	1.58	0.65	2.84	1.52	1.84	1.30
5	1.09	0.98	1.40	1.31	0.96	0.83	1.14	0.83	0.92
6	1.05	0.92	1.20	1.13	0.65	0.79	2.95	2.07	2.61
7	1.09	1.13	1.51	1.49	0.76	1.19	1.09	1.08	1.12
8	0.67	0.78	0.94	1.04	0.90	1.09	1.12	1.15	1.33
9	1.09	0.96	1.27	1.19	0.93	0.82	0.97	0.91	0.96
10	0.95	1.00	0.99	0.92	1.20	1.31	1.29	1.13	1.27
11	1.02	1.05	1.05	1.01	1.09	1.02	1.11	1.11	1.14
12	1.29	0.93	1.09	1.04	0.93	1.13	0.81	0.81	0.88

Appendix 4.1 North Shore Trout Stream Set

Map of accumulated catchments for the 153 Minnesota north shore trout streams

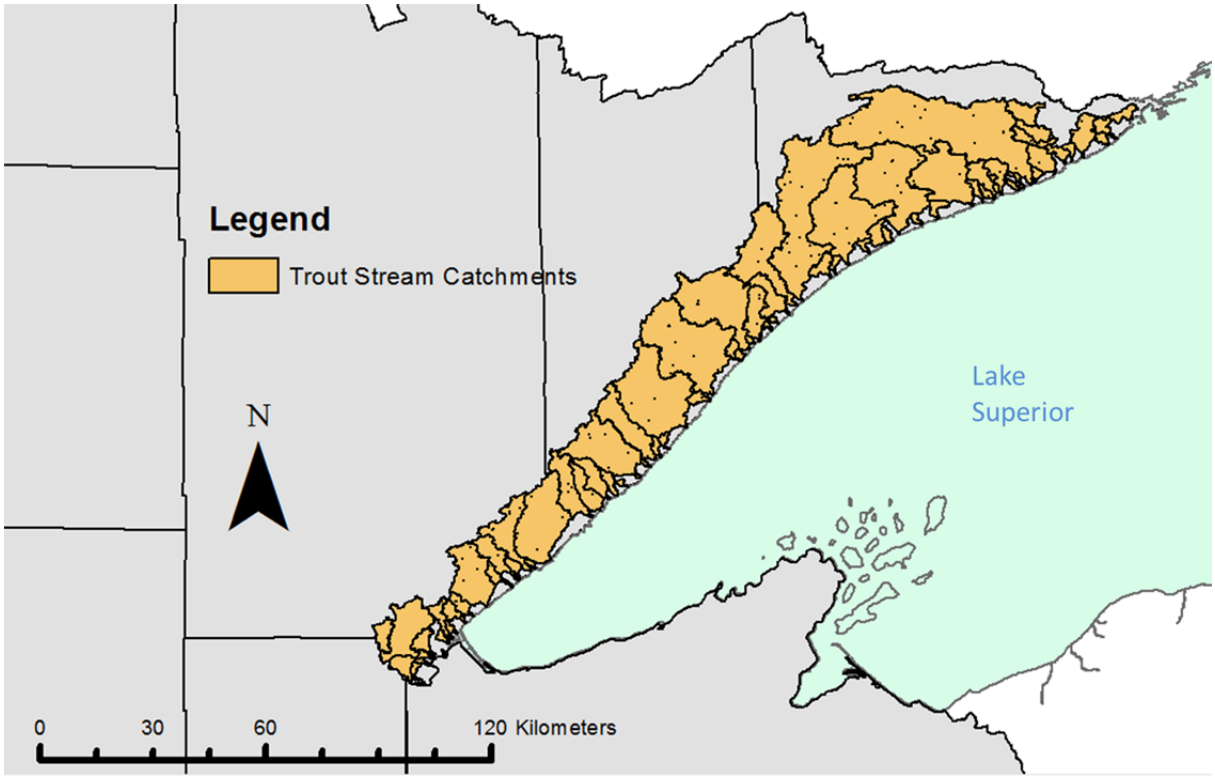

List of 153 Minnesota North shore trout streams, with accumulated catchment area

Stream Name	Catchment Area (km2)	Stream Name	Catchment Area (km2)
Amity Creek	42.5	Encampment River	44.7
Assinika Creek	47.7	Fall Creek	13.4
Bally Creek	10.8	Farquhar Creek	8.2
Balsam Creek	12.0	Fiddle Creek	12.8
Baptism River	355.9	Finland Creek	1.9
Baptism River, East	95.6	Flute Reed River	40.0
Barker Creek	23.4	Fox Farm Creek	4.6
Beaver River	316.2	Fredenberg Creek	5.7
Beaverdam Creek	13.5	French River	51.0
Big Sucker Creek	98.3	Fry Creek	4.7
Blesner Creek	5.9	Gauthier Creek	13.6
Blind Temperance Creek	11.6	Gooseberry River	192.8
Bluff Creek	167.2	Grand Portage River	18.7
Brule River	686.4	Greenwood River	70.2
Buckingham Creek	0.7	Hay Creek	30.2
Burnt Creek	20.1	Heartbreak Creek	44.6
Cabin Creek	36.4	Heffelfinger Ceek	11.4
Captain Jacobson Creek	14.4	Hockamin Creek	41.6
Caribou River	59.0	Hollow Rock Creek	17.4
Carlson Creek	15.2	Honeymoon Creek	6.7
Cascade River	287.3	Houghtailing Ceek	32.2
Cedar Creek	41.4	Indian Camp Creek	7.6
Chester Creek	17.9	Irish Creek	27.5
Chester Creek, East Branch	8.2	Jonvick Creek	7.3
Cliff Creek	7.4	Junco Creek	54.0
Coffee Creek	5.5	Kadunce Creek	29.5
Cross River	196.6	Keene Creek	0.9
Crow Creek	14.8	Kimball Creek	35.6
Crown Creek	74.3	Kingsbury Creek	24.2
Cutface Creek	5.3	Kit Creek	17.9
Dago Creek	22.8	Knife AP	36.7
Deer Yard Creek	21.6	Knife River	225.1
Devil Track River	188.2	Knowlton	5.6
Dragon Creek	5.3	Koski Creek	7.6
Durfee Creek	10.7	Leskinen Creek	6.9
East Colville Creek	4.8	Lester River	138.0
Egge Creek	6.0	Lindstrom Creek	11.4
Elbow Creek	52.4	Little Brule Creek	6.1

List of 153 trout streams (continued)

Stream Name	Catchment Area (km2)	Stream Name	Catchment Area (km2)
Little Devil Track River	22.0	Rock Cut Creek	6.8
Little Gooseberry River	25.7	Rollins Creek	7.6
Little Knife River	222.3	Sargent Creek	8.2
Little Manitou River	3.4	Sawbill Creek	89.5
Little Marais River	11.9	Sawmill Creek	23.1
Little Mississippi Creek	15.8	Schmidt Creek	12.8
Little Stewart River	13.3	Schoolhouse Creek	7.6
Little Stony Creek	15.6	Section 16 Creek	3.1
Little Sucker River	3.7	Shipwreck Creek	6.5
Lullaby Creek	4.3	Silver Creek	49.0
Manitou River	256.7	Sixmile Creek	24.2
Manitou River, South Branch	53.1	Split Rock River	113.5
Mark Creek	13.6	Stanley Creek	18.7
Martin Creek	3.4	Stewart Creek	3.9
Mc Carthy Creek	13.4	Stewart River	84.0
Merritt Creek	6.3	Stone Creek	5.6
Midway River	155.7	Stony Creek	8.8
Miller Creek	29.9	Stumble Creek	3.5
Mink Creek	13.4	Sugar Loaf Creek	3.7
Mission Creek	28.1	Sundling Creek	15.3
Mississippi Creek	49.3	Swamp River	24.4
Monker Creek	6.2	Swanson Creek	18.7
Moose Creek	128.0	Tait River	98.8
Mud Creek	13.7	Talmadge River	15.1
Myhr Creek	6.8	Temperance River	479.4
Nestor Creek	15.8	Thirtynine Creek, Big	57.5
Nicado Creek	11.6	Thirtynine Creek, Little	1.5
Ninemile Creek	89.3	Thompson Creek	7.7
Oliver Creek	10.2	Tikkanen Creek	5.4
Onion River	22.4	Timber Creek	9.1
Palisade Creek	14.4	Tischer Creek	18.9
Pancake Creek	11.7	Torgenson Creek	10.9
Pecore Creek	5.7	Tower Creek	1.8
Pike Lake Creek	3.0	Two Island River	51.8
Plouffs Creek	38.2	Unnamed Stream	3.0
Poplar River	295.1	Unnamed Stream	2.7
Portage Brook	39.2	Unnamed Stream	8.8
Red Rock Creek	8.4	Wanless Creek	9.6
Reservation River	46.8	Woods Creek	5.9

Appendix 8.1 Land cover map of NLCD 2001

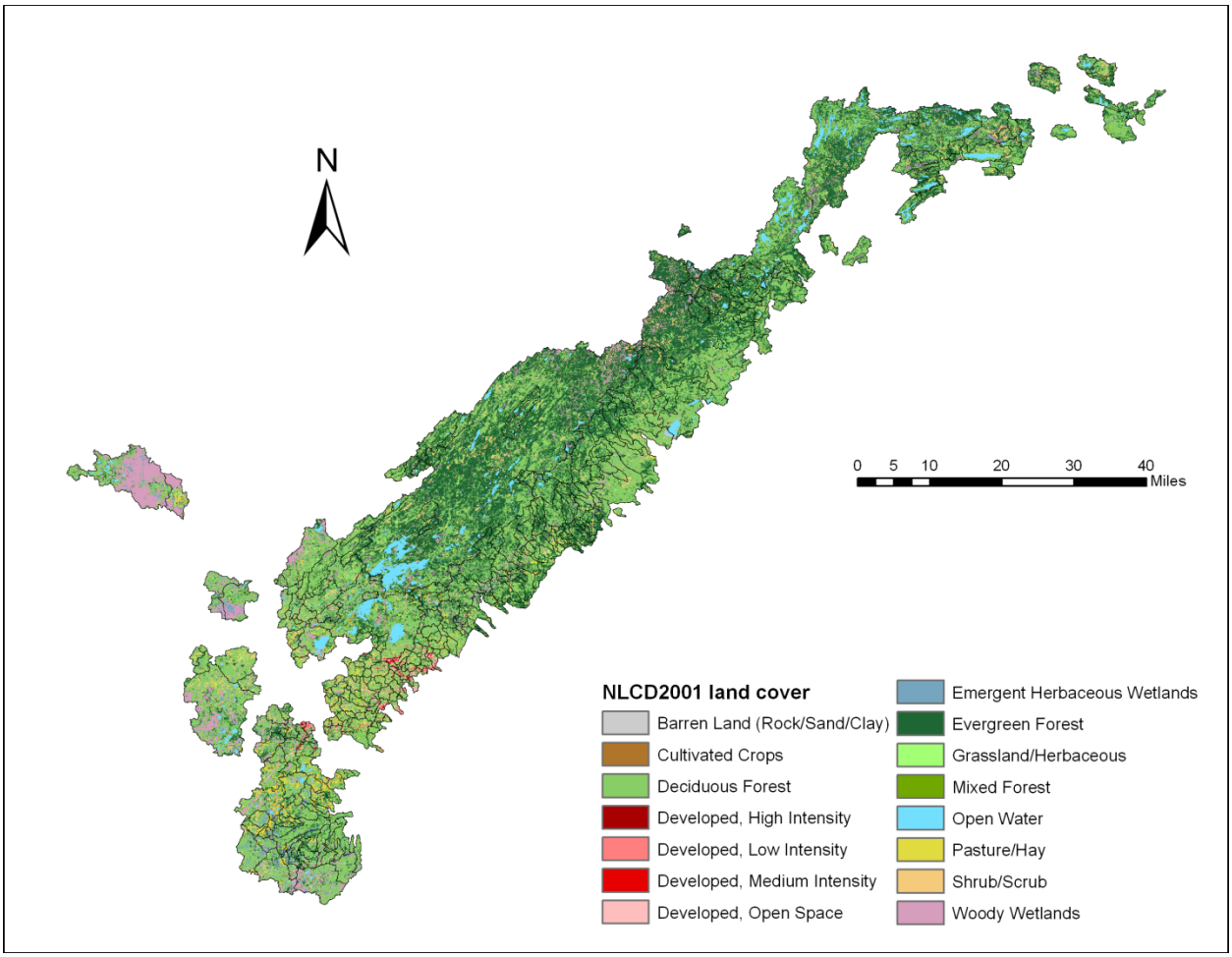

Appendix 8.2 Forest type map

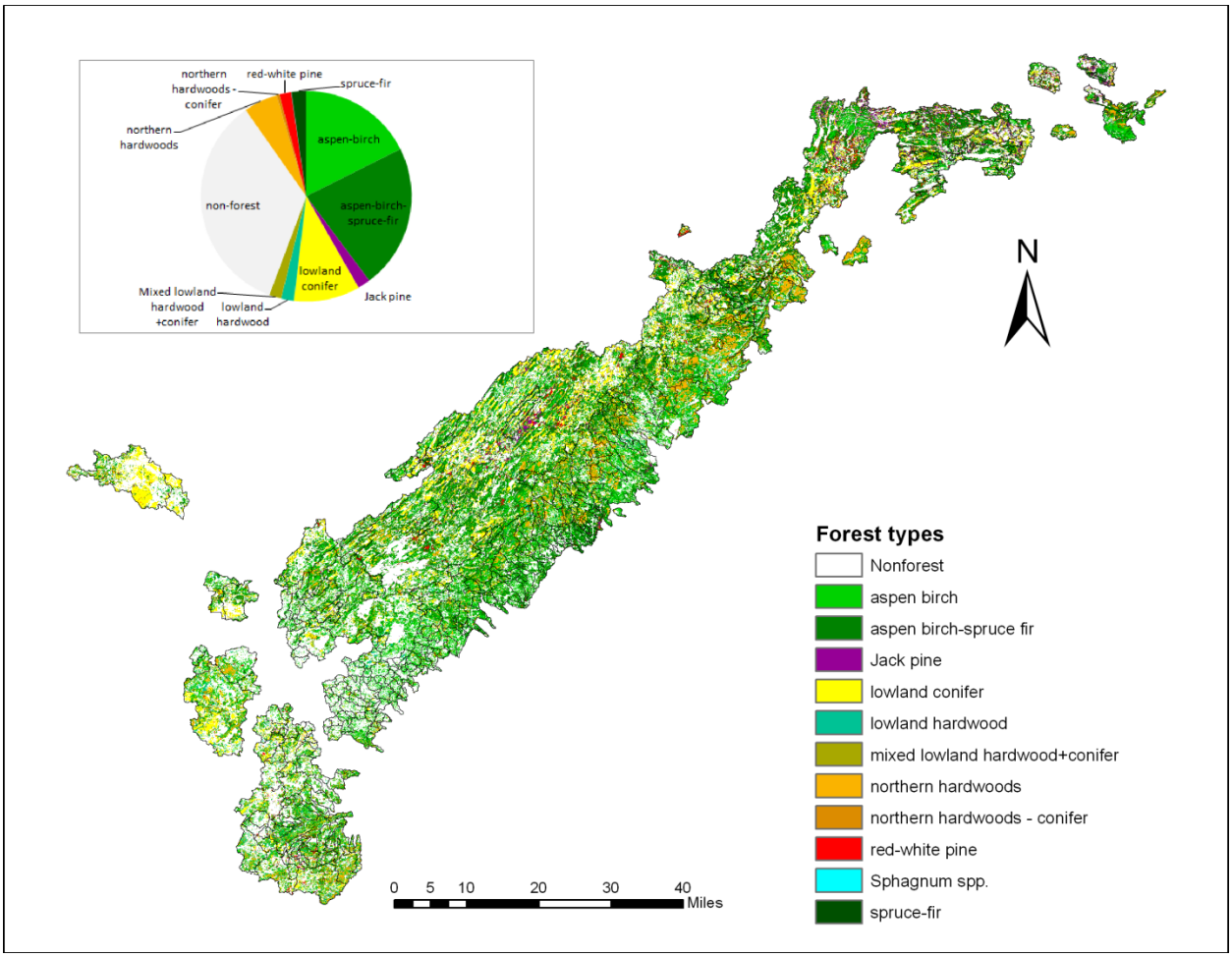

Appendix 8.3 Quaternary geology map

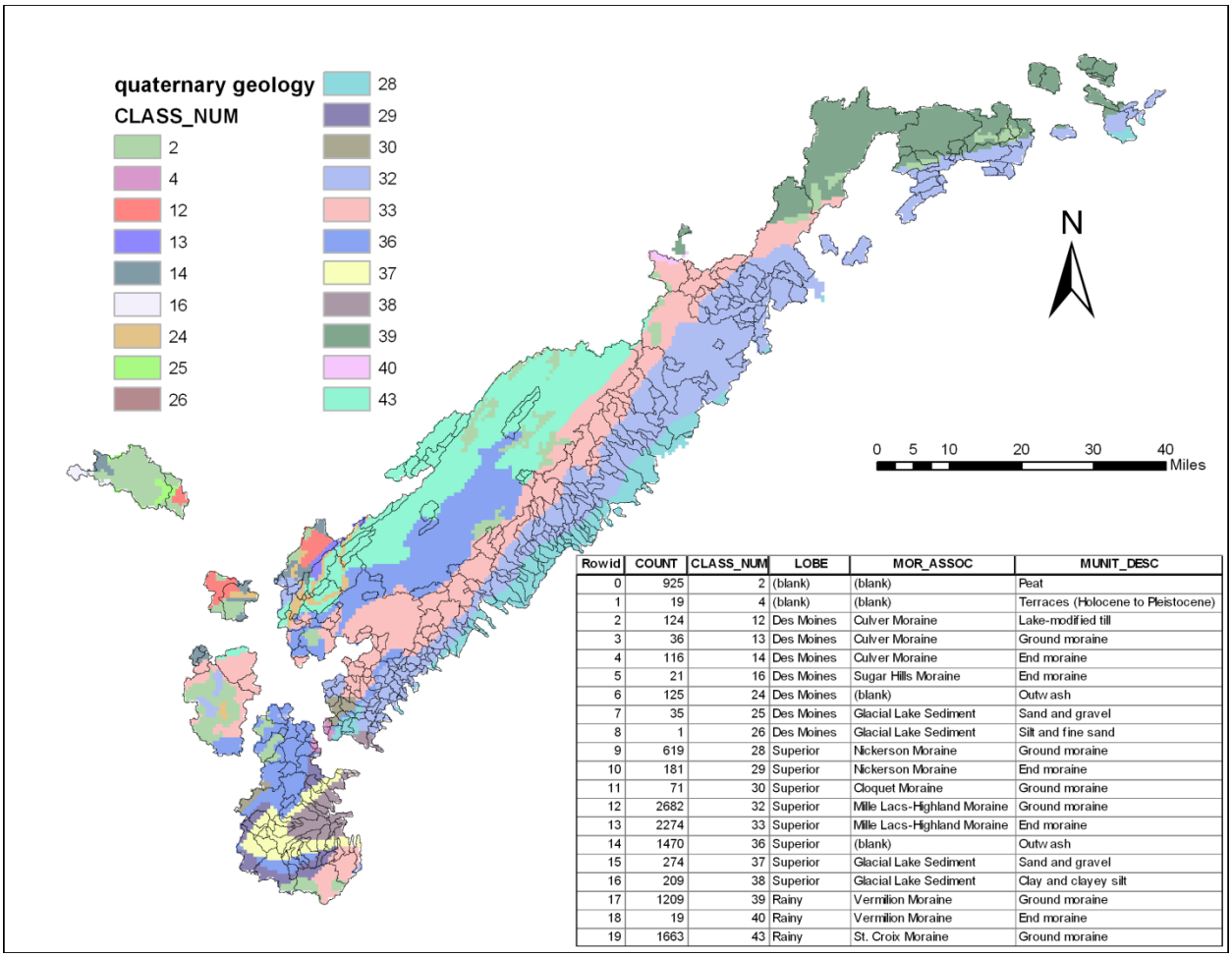

Rowid	COUNT	CLASS_NUM	LOBE	MOR_ASSOC	MUNIT_DESC
0	925	2	(blank)	(blank)	Peat
1	19	4	(blank)	(blank)	Terraces (Holocene to Pleistocene)
2	124	12	Des Moines	Culver Moraine	Lake-modified till
3	36	13	Des Moines	Culver Moraine	Ground moraine
4	116	14	Des Moines	Culver Moraine	End moraine
5	21	16	Des Moines	Sugar Hills Moraine	End moraine
6	125	24	Des Moines	(blank)	Outw ash
7	35	25	Des Moines	Glacial Lake Sediment	Sand and gravel
8	1	26	Des Moines	Glacial Lake Sediment	Silt and fine sand
9	619	28	Superior	Nickerson Moraine	Ground moraine
10	181	29	Superior	Nickerson Moraine	End moraine
11	71	30	Superior	Cloquet Moraine	Ground moraine
12	2682	32	Superior	Mille Lacs-Highland Moraine	Ground moraine
13	2274	33	Superior	Mille Lacs-Highland Moraine	End moraine
14	1470	36	Superior	(blank)	Outw ash
15	274	37	Superior	Glacial Lake Sediment	Sand and gravel
16	209	38	Superior	Glacial Lake Sediment	Clay and clayey silt
17	1209	39	Rainy	Vermilion Moraine	Ground moraine
18	19	40	Rainy	Vermilion Moraine	End moraine
19	1663	43	Rainy	St. Croix Moraine	Ground moraine

Appendix 8.4 Soil properties derived from STATSGO soil database

Appendix 8.4.1 STATSGO soil type map

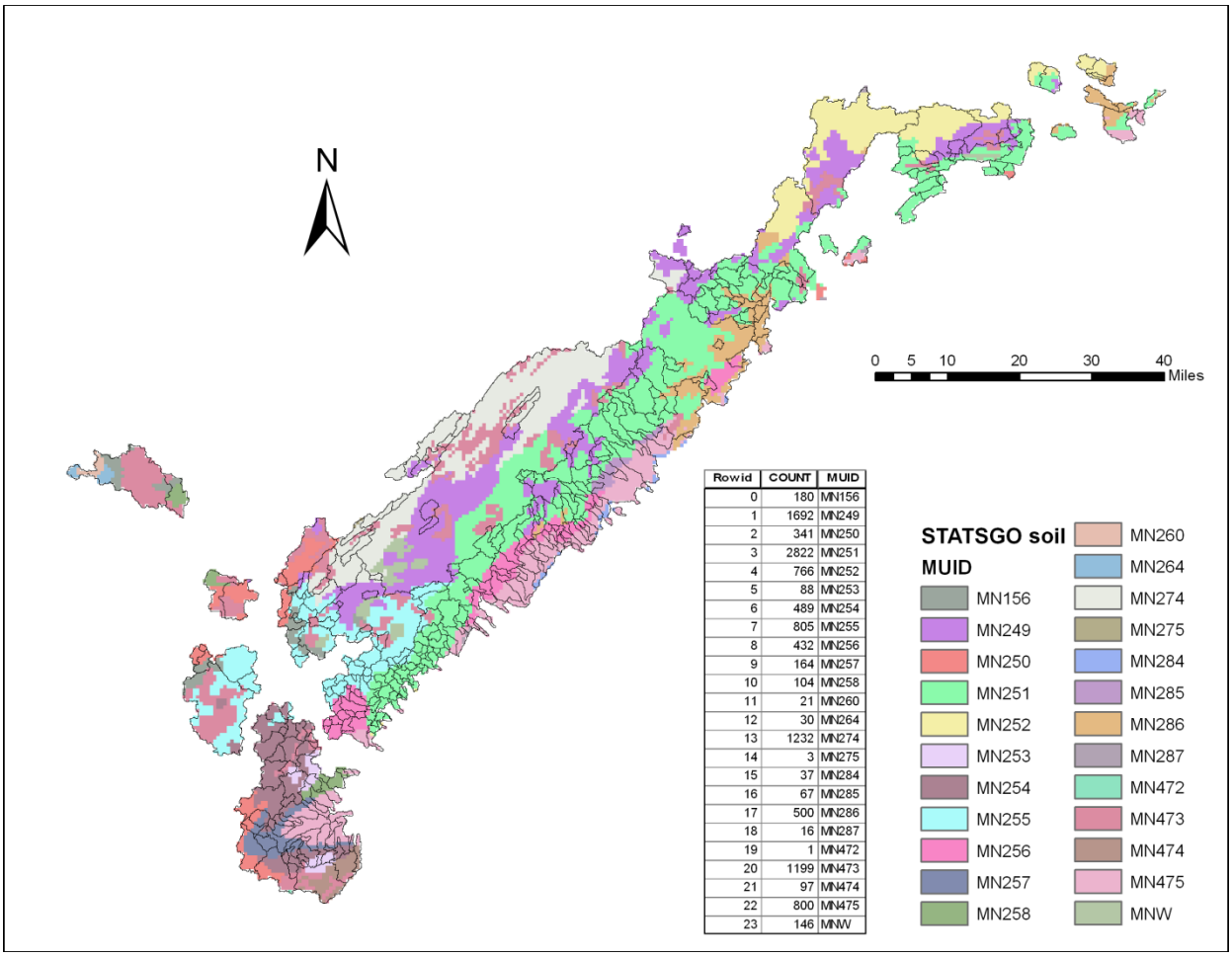

Rowid	COUNT	MUID
0	180	MN156
1	1692	MN249
2	341	MN250
3	2822	MN251
4	766	MN252
5	88	MN253
6	489	MN254
7	805	MN255
8	432	MN256
9	164	MN257
10	104	MN258
11	21	MN260
12	30	MN264
13	1232	MN274
14	3	MN275
15	37	MN284
16	67	MN285
17	500	MN286
18	16	MN287
19	1	MN472
20	1199	MN473
21	97	MN474
22	800	MN475
23	146	MNW

Appendix 8.4.2 Soil permeability rate and soil texture

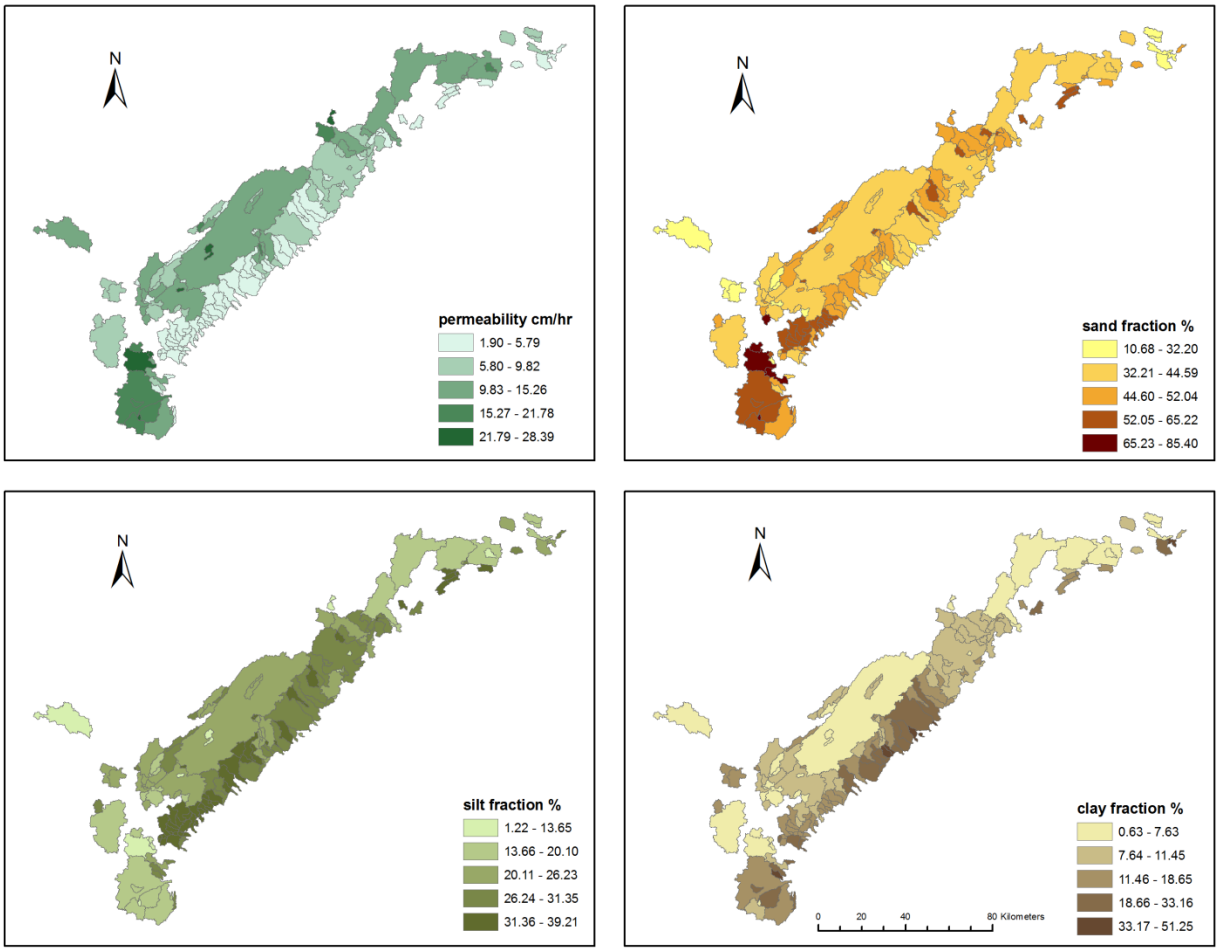

Appendix 8.5 Lithology map

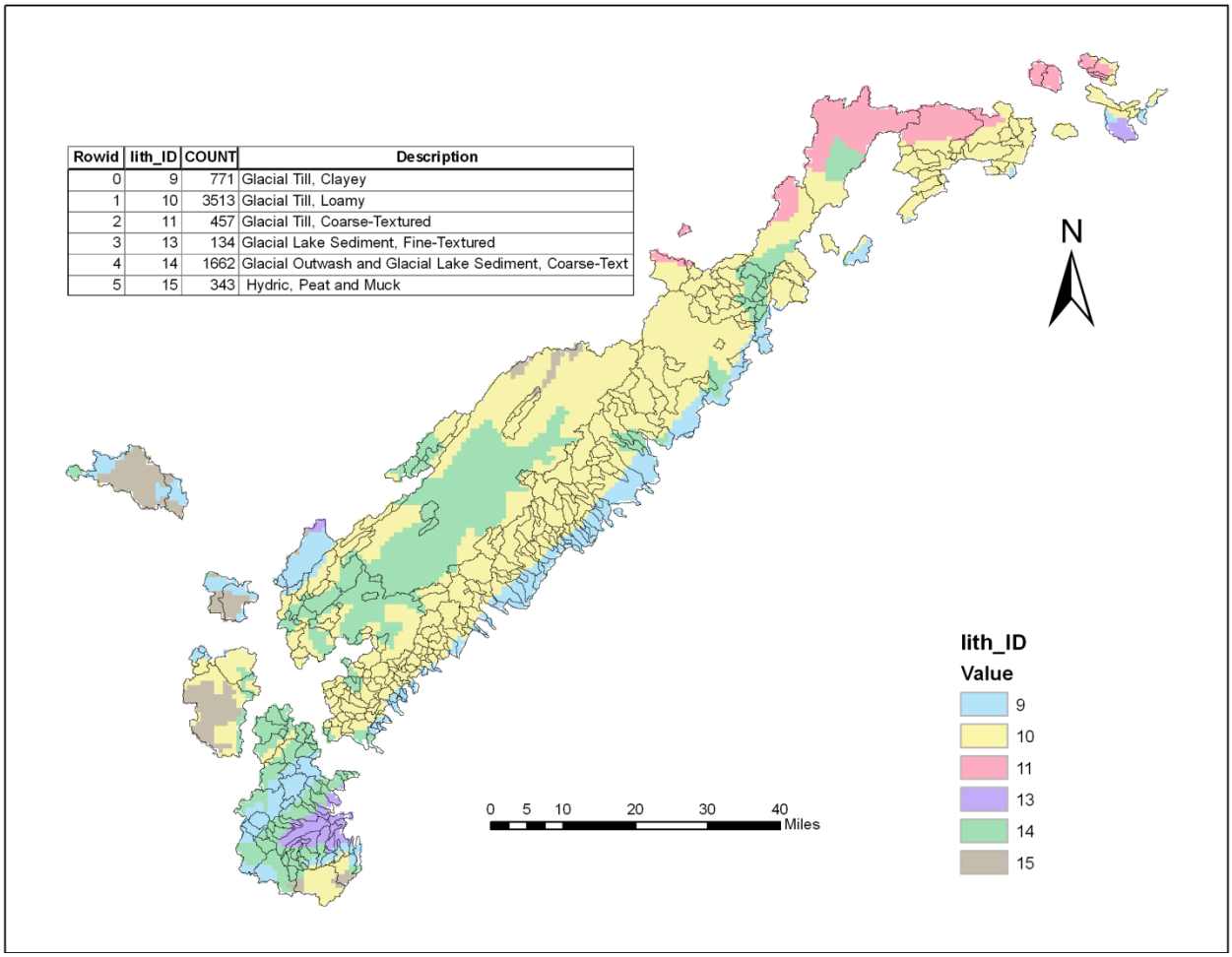

Rowid	lith_ID	COUNT	Description
0	9	771	Glacial Till, Clayey
1	10	3513	Glacial Till, Loamy
2	11	457	Glacial Till, Coarse-Textured
3	13	134	Glacial Lake Sediment, Fine-Textured
4	14	1662	Glacial Outwash and Glacial Lake Sediment, Coarse-Text
5	15	343	Hydric, Peat and Muck

Appendix 8.6 Model fit for July mean temperature, and leverage plots for independent variables

Whole Model

Actual by Predicted Plot

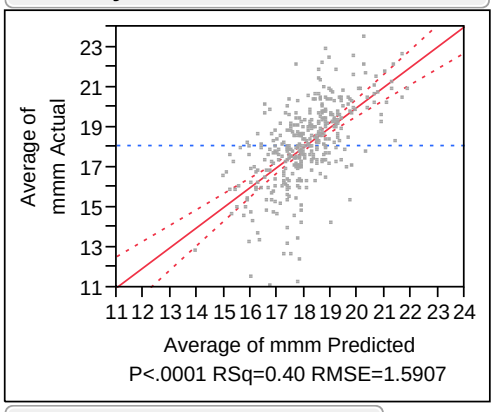

Summary of Fit

RSquare	0.397255
RSquare Adj	0.388953
Root Mean Square Error	1.590726
Mean of Response	18.07611
Observations (or Sum Wgts)	369

Analysis of Variance

Source	DF	Sum of Squares	Mean Square	F Ratio
Model	5	605.3881	121.078	47.8490
Error	363	918.5390	2.530	**Prob > F**
C. Total	368	1523.9271		<.0001*

Parameter Estimates

Term	Estimate	Std Error	t Ratio	Prob>|t|	VIF
Intercept	-33.35215	11.94053	-2.79	0.0055*	.
Average of Tave	0.6713968	0.067007	10.02	<.0001*	1.2538018
AREA_ha	1.5019059	0.156986	9.57	<.0001*	1.1834815
permeability for top 150 cm soil	-1.330613	0.29134	-4.57	<.0001*	1.1480687
latitude	6.5244e-6	2.184e-6	2.99	0.0030*	1.3894127
PCT_Woody Wetlands_150m	2.0454875	0.505299	4.05	<.0001*	1.3448019

Residual by Predicted Plot

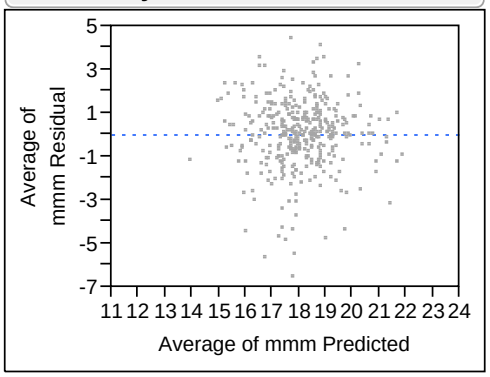

Leverage plots:

T_{ave_air}

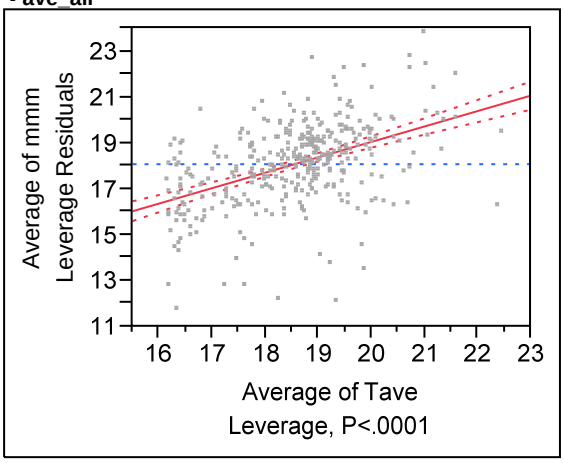

Permeability

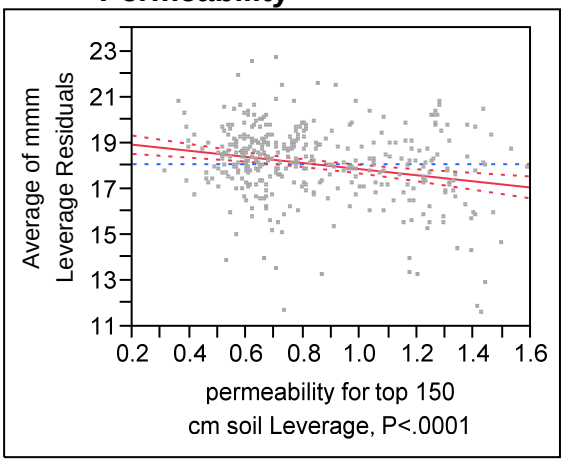

Area

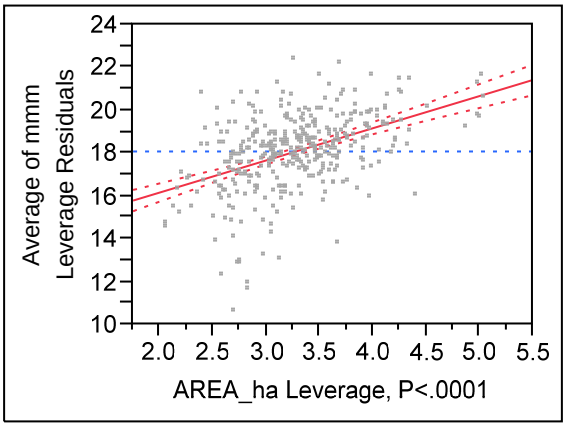

Latitude

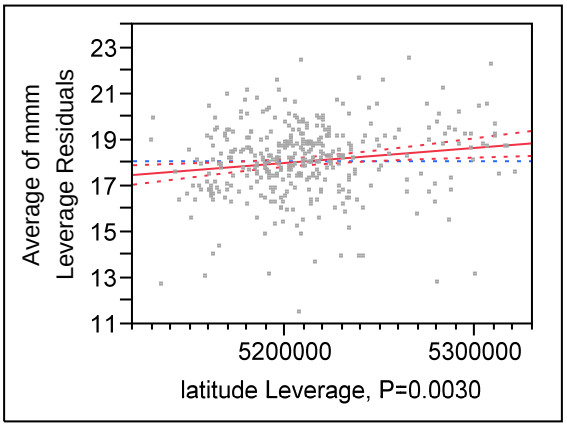

PCT_Woody Wetlands_150m

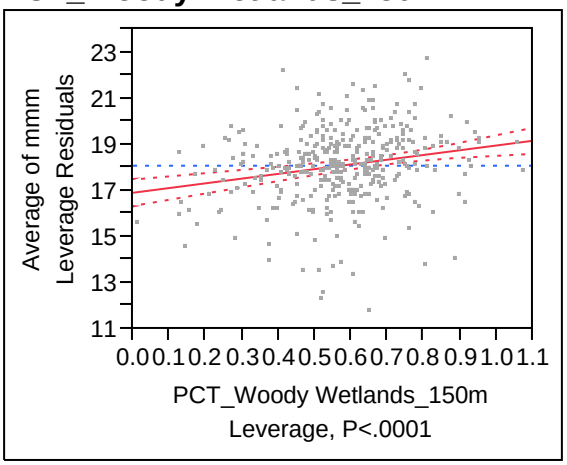

Appendix 8.7 Models for July maximum temperature, and leverage plots for independent variables

Appendix 8.7.1 the best fit model

Whole Model

Actual by Predicted Plot

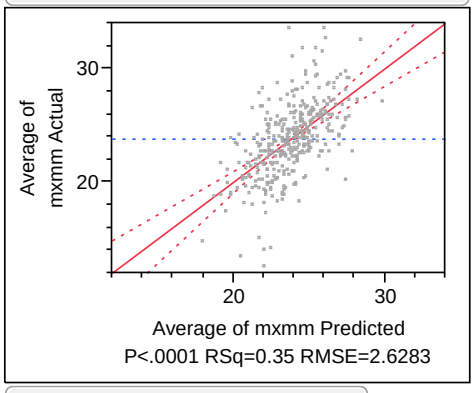

Summary of Fit

RSquare	0.347285
RSquare Adj	0.338294
Root Mean Square Error	2.628314
Mean of Response	23.80483
Observations (or Sum Wgts)	369

Analysis of Variance

Source	DF	Sum of Squares	Mean Square	F Ratio
Model	5	1334.2058	266.841	38.6276
Error	363	2507.6174	6.908	Prob > F
C. Total	368	3841.8232		<.0001*

Parameter Estimates

Term	Estimate	Std Error	t Ratio	Prob>|t|	VIF
Intercept	-79.12738	19.09853	-4.14	<.0001*	.
AREA_ha	2.2163772	0.259478	8.54	<.0001*	1.1843351
PCT_Woody Wetlands_150m	3.0972131	0.845627	3.66	0.0003*	1.3796084
permeability for top 150 cm soil	-1.210519	0.489425	-2.47	0.0138*	1.1868015
latitude	1.5769e-5	3.546e-6	4.45	<.0001*	1.3415643
Average of Tmin	1.0442544	0.112884	9.25	<.0001*	1.3131273

Residual by Predicted Plot

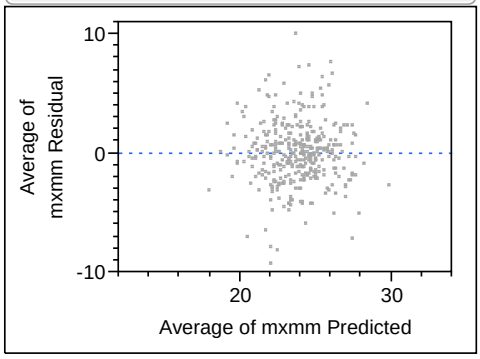

Leverage plots:

T_{min_air}

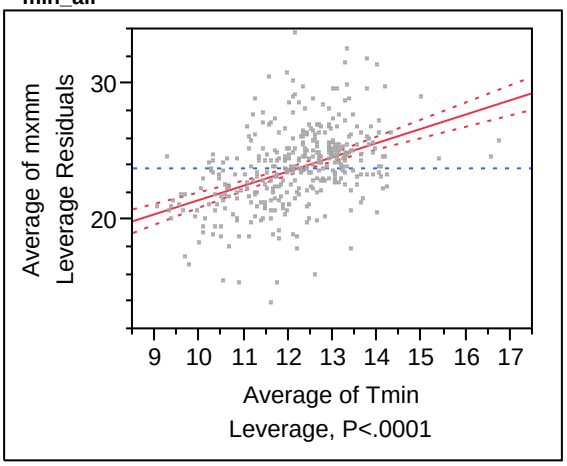

Permeability

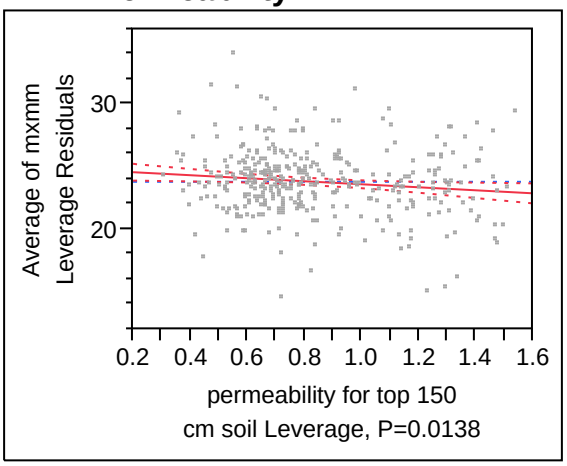

Area

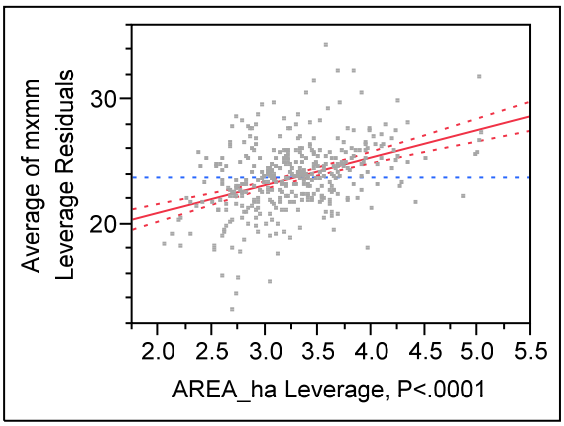

Latitude

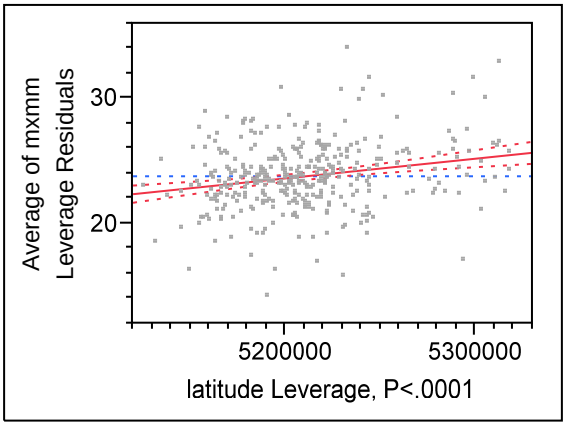

PCT_Woody Wetlands_150m

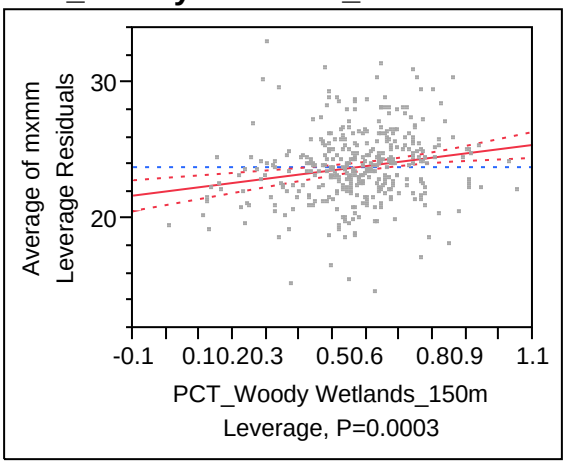

Appendix 8.7.2 The generalized model

Whole Model

Actual by Predicted Plot

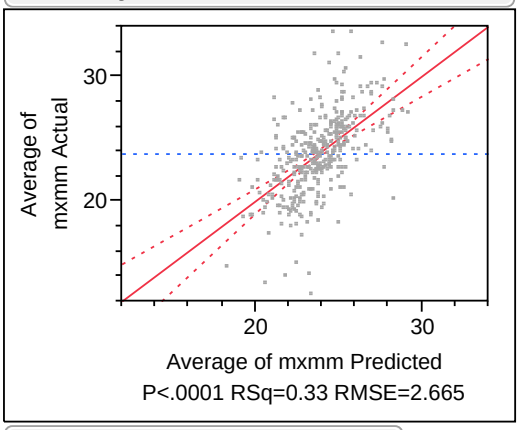

Summary of Fit

RSquare	0.328951
RSquare Adj	0.319708
Root Mean Square Error	2.664972
Mean of Response	23.80483
Observations (or Sum Wgts)	369

Analysis of Variance

Source	DF	Sum of Squares	Mean Square	F Ratio
Model	5	1263.7701	252.754	35.5888
Error	363	2578.0531	7.102	**Prob > F**
C. Total	368	3841.8232		<.0001*

Parameter Estimates

Term	Estimate	Std Error	t Ratio	Prob>|t|	VIF
Intercept	-86.62619	20.00418	-4.33	<.0001*	.
Average of Tave	0.9612294	0.112258	8.56	<.0001*	1.2538018
AREA_ha	2.2544596	0.263002	8.57	<.0001*	1.1834815
permeability for top 150 cm soil	-2.412566	0.488086	-4.94	<.0001*	1.1480687
latitude	0.0000165	3.658e-6	4.51	<.0001*	1.3894127
PCT_Woody Wetlands_150m	2.2124937	0.846536	2.61	0.0093*	1.3448019

Residual by Predicted Plot

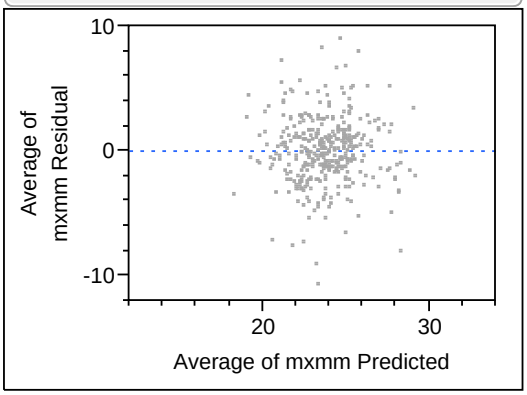

Leverage plots:

T_{ave_air}

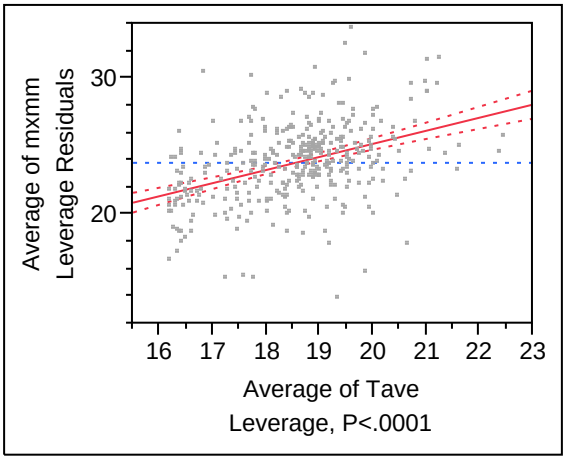

Permeability

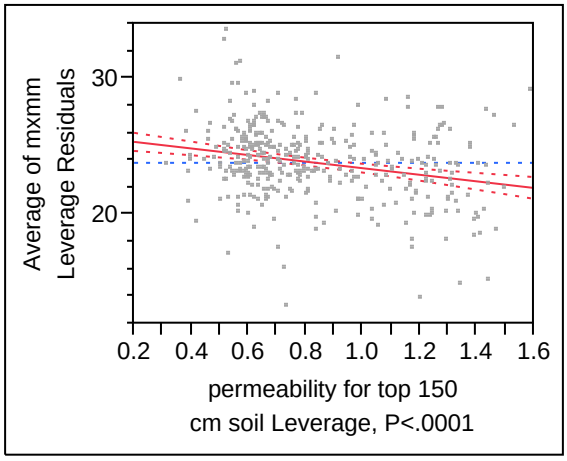

Area

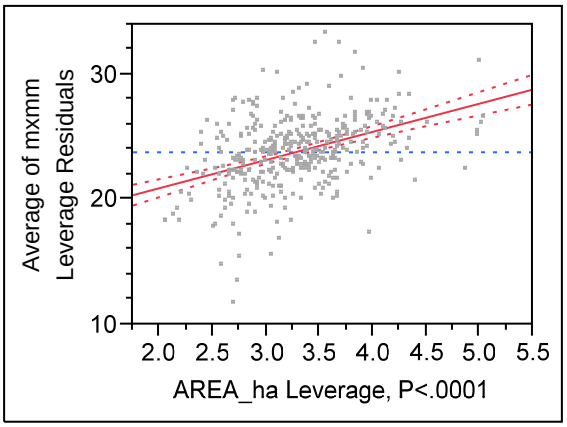

Latitude

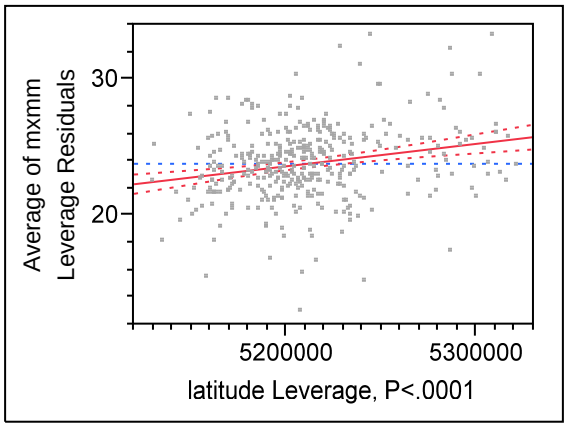

PCT_Woody Wetlands_150m

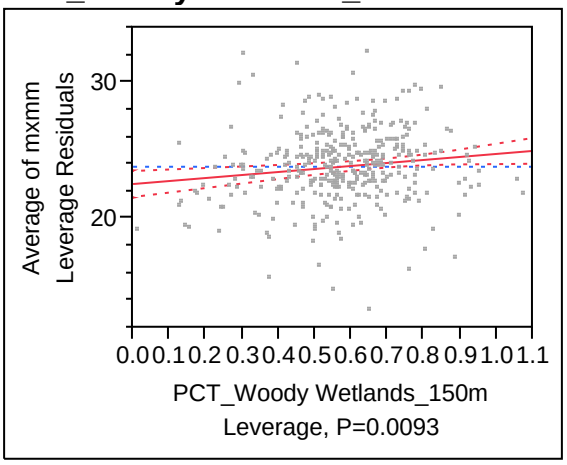

Appendix 10.1 Logistic regression model for brook trout presence/absence using July mean water temperature (Average of mmm) as predictor.

Generalized Linear Model Fit

Response: brook trout presence (1) or absence (0)
Distribution: Binomial
Link: Logit
Estimation Method: Maximum Likelihood
Observations (or Sum Wgts) = 79

Whole Model Test

Model	-LogLikelihood	L-R ChiSquare	DF	Prob>ChiSq
Difference	2.96629589	5.9326	1	0.0149*
Full	49.4849684			
Reduced	52.4512643			

Goodness Of Fit Statistic	ChiSquare	DF	Prob>ChiSq
Pearson	81.3097	77	0.3466
Deviance	98.9699	77	0.0467*

AICc
103.1278

Effect Tests

Source	DF	L-R ChiSquare	Prob>ChiSq
Average of mmm	1	5.9325918	0.0149*

Parameter Estimates

Term	Estimate	Std Error	L-R ChiSquare	Prob>ChiSq	Lower CL	Upper CL
Intercept	7.4765242	3.0083649	6.7754835	0.0092*	1.8011458	13.714275
Average of mmm	-0.373997	0.1599739	5.9325918	0.0149*	-0.705244	-0.071425

Studentized Deviance Residual by Predicted

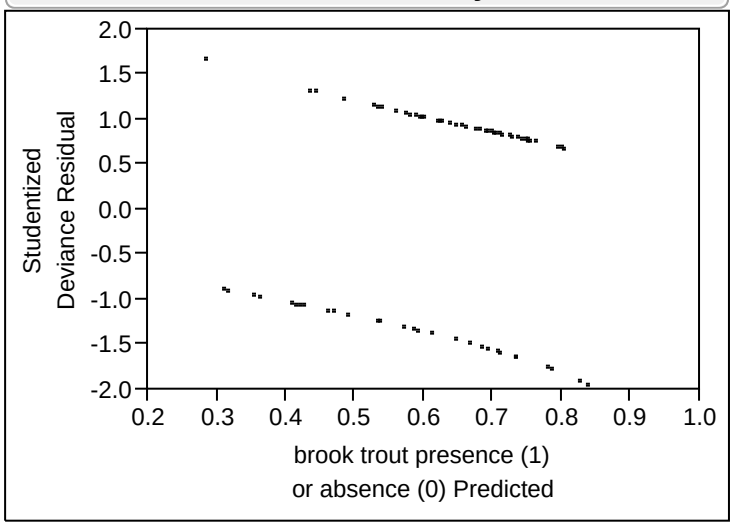

Appendix 10.2 Logistic regression model for brook trout presence/absence using July maximum water temperature (Average of mxmm) as sole predictor.

Generalized Linear Model Fit

Response: brook trout presence (1) or absence (0)
Distribution: Binomial
Link: Logit
Estimation Method: Maximum Likelihood
Observations (or Sum Wgts) = 79

Whole Model Test

Model	-LogLikelihood	L-R ChiSquare	DF	Prob>ChiSq
Difference	0.45776016	0.9155	1	0.3387
Full	51.9935041			
Reduced	52.4512643			

Goodness Of Fit Statistic	ChiSquare	DF	Prob>ChiSq
Pearson	79.2941	77	0.4065
Deviance	103.9870	77	0.0220*

AICc
108.1449

Effect Tests

Source	DF	L-R ChiSquare	Prob>ChiSq
Average of mxmm	1	0.9155203	0.3387

Parameter Estimates

Term	Estimate	Std Error	L-R ChiSquare	Prob>ChiSq	Lower CL	Upper CL
Intercept	2.5117865	2.144886	1.4004348	0.2367	-1.642815	6.8784522
Average of mxmm	-0.081495	0.0857572	0.9155203	0.3387	-0.255497	0.0855192

Studentized Deviance Residual by Predicted

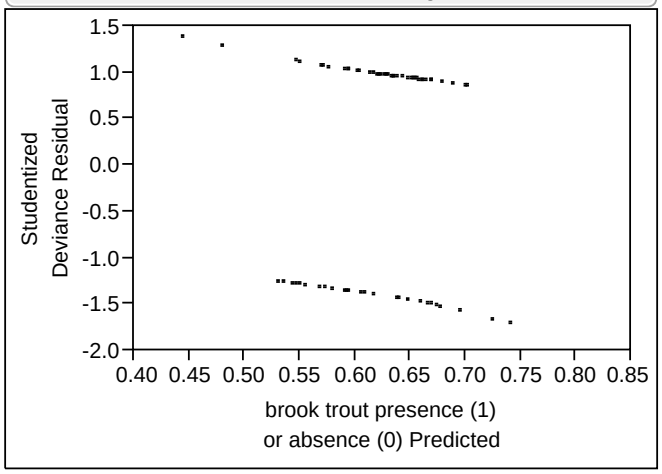

Appendix 10.3 Final logistic model to predict brook trout presence/absence

Generalized Linear Model Fit

Response: brook trout presence (1) or absence (0)
Distribution: Binomial
Link: Logit
Estimation Method: Maximum Likelihood
Observations (or Sum Wgts) = 79

Whole Model Test

Model	-LogLikelihood	L-R ChiSquare	DF	Prob>ChiSq
Difference	7.23363307	14.4673	3	0.0023*
Full	45.2176312			
Reduced	52.4512643			

Goodness Of Fit Statistic	ChiSquare	DF	Prob>ChiSq
Pearson	78.2399	75	0.3763
Deviance	90.4353	75	0.1081

AICc
98.9758

Effect Tests

Source	DF	L-R ChiSquare	Prob>ChiSq
Average of mmm	1	11.580875	0.0007*
log10(Q10)	1	3.2707068	0.0705
PCT_Deciduous Forest_150m	1	5.8481205	0.0156*

Parameter Estimates

Term	Estimate	Std Error	L-R ChiSquare	Prob>ChiSq	Lower CL	Upper CL
Intercept	15.186525	4.563041	14.294211	0.0002*	6.8922035	24.940912
Average of mmm	-0.630389	0.2061597	11.580875	0.0007*	-1.069431	-0.253415
log10(Q10)	0.3655378	0.2051139	3.2707068	0.0705	-0.030407	0.7811949
PCT_Deciduous Forest_150m	-5.28432	2.2883322	5.8481205	0.0156*	-10.04184	-0.97523

Studentized Deviance Residual by Predicted